The Psychophysical Characterisation of Dorsal and Ventral Stream Functions with Equivalent Noise Paradigm in Normal and Clinical Populations

Glasgow Caledonian University

Mahesh Raj Joshi

A thesis submitted in partial fulfilment of the requirements of

Glasgow Caledonian University for the degree of

Doctor of Philosophy

December 2016

Abstract

Global motion and global form are processed along the bifurcated visual processing pathways of dorsal and ventral stream. Global motion perception is reported to be affected more than the perception of global form in various developmental disorders, which has led to the suggestion of a dorsal stream vulnerability. However, a direct comparison of processing, deficits, or interaction between the two visual processing streams has remained difficult due to limitations in experimental design/stimulus.

In this current body of work, physically identical stimuli (random dot kinematograms for global motion and Glass patterns for global form) embedded in varying levels of noise were used to probe local/global processing in visually normal and clinical populations.

Our initial experiments revealed a higher sensitivity to global motion compared to global form perception in visually normal adults, which was due to an increased efficiency of the global integration mechanism in the motion domain. The results also showed that certain commonly used form stimuli may not target the global stage of form processing. The investigation of global motion and form interactions further revealed that such interactions may extend beyond local level processing at the primary visual cortex.

In order to evaluate complex visual processing effectively in the clinical arena, a more efficient paradigm is required. In the concluding chapters, a faster method was validated and employed to evaluate global motion and form perception in amblyopia a condition that has well documented global processing deficits.

Our results revealed motion and form processing deficits in strabismic amblyopia with relatively larger deficits found in the form processing mechanism – contradictory to the previously proposed dorsal stream deficiency in developmental disorders.

Overall our results showed that comparing motion and form processing is not a trivial task and careful consideration with regards to the experimental design/paradigms is required for an accurate comparison across the domains.

dedicated to my son Mevon

for the happiness he has brought to our lives

Acknowledgements

This thesis would not be completed without help, support, and encouragement from various people. I here take the opportunity to thank them for their support.

My heartfelt gratitude goes to my supervisor, Seong (Simon), for his excellent guidance. He was always available to help me; from solving my coding mistakes to providing quick feedbacks on my queries and write-ups. I am sure I will use the skills that I have learned from him time and again in the future.

I would like to thanks Anita, my second supervisor, for always being available from her busy schedule to guide and encourage me throughout this study period. Her enthusiasm and support for every project I undertook have made this body of work possible.

I would also like to thank all staffs and other PhD candidates at the Vision science department who were always helpful and encouraging. Special thanks go to Marianne for being there to chat through the everyday problems of completing research projects. To Abhishek and Rakesh, for the coffee sessions which provided much needed breaks from at times monotonous schedule.

This work would not have been completed without many hours of experimental time volunteered by the participants. I would like to thank them for their patience and commitment in spending their invaluable time for experimental works presented in this thesis.

Lastly, I would like to thank two most important people in my life. My wife Rashmini, who always supported me in every decision I made and always stood by me through many ups and downs during this period. I would not be nearing the completion of my PhD without her sacrifices to support our family financially. My mother, Jamuna Joshi, though away from us during this period, the values that she has instilled in me and her belief and support in whatever I do has made me the person that I am today.

Table of Contents

List of Figures

List of Tables

1.0 General Introduction

1.1 The Visual Pathways and Parallel Processing

The visual system is capable of processing a wide range of stimuli in the physical world including motion, orientation, texture, colour, and three-dimensional percept. The notion that these different attributes of vision may be processed along parallel streams has been prevalent as early as 1950's. The idea of parallel processing refers to the processing of different visual attributes through dedicated neural pathways, with cells within each pathway exhibiting functional specification. Within each pathway, visual information is processed in a hierarchical order with cells further along the pathway combining information from preceding visual areas to perform increasingly complex tasks.

Supporting evidence for such mechanisms have been proposed based on the anatomical studies in primates (Ungerleider and Mishkin, 1982; Morel and Bullier, 1990; Young, 1992) and humans (Goodale and Milner, 1992; Milner and Goodale, 1993; Milner and Goodale, 1996; Goodale and Westwood, 2004; Milner and Goodale, 2006; Milner and Goodale, 2008; Goodale, 2011). These studies propose two main subdivisions of the visual system, one from primary visual cortex to the dorsal area of parietal cortex – the dorsal stream and another extending from the primary visual cortex to the ventral area of inferotemporal cortex – the ventral stream (Figure 1.1). The dorsal stream is mostly responsive to the temporal properties of the stimulus and is implicated in motion perception and action generation. On the other hand, the ventral stream is responsive to the spatial properties, decoding complex form and colour (Goodale, 2011).

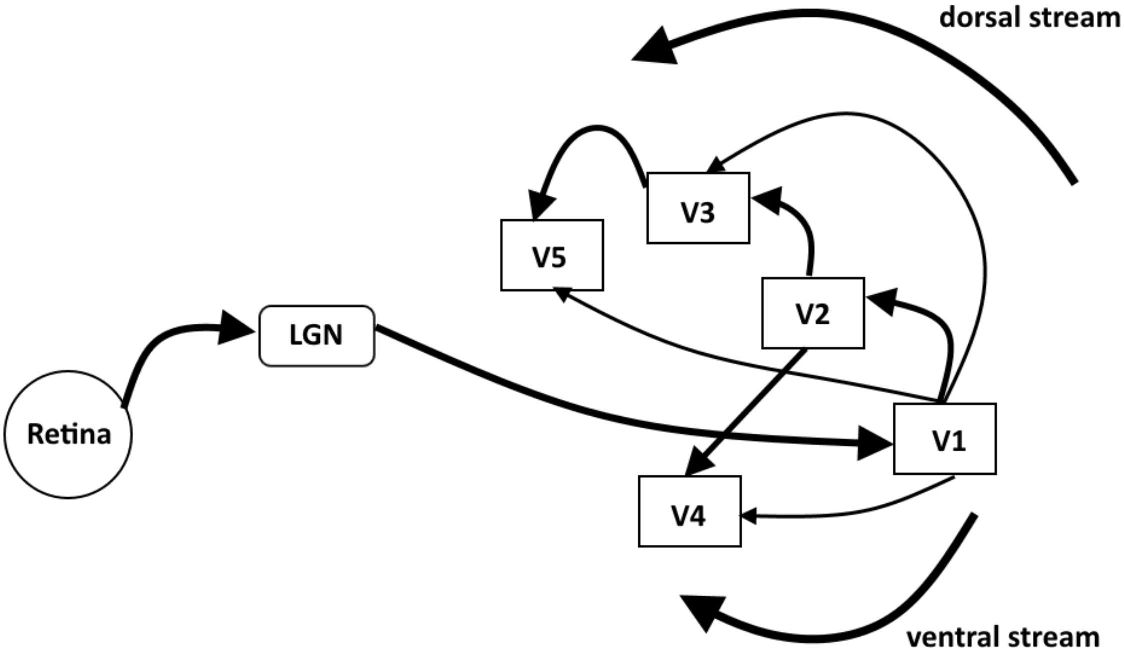

Figure 1.1: Schematic diagram of visual pathway.

The visual pathway originates from retina and proceeds through lateral geniculate nucleus (LGN) to primary visual cortex (V1). From V1, visual pathway bifurcates into two streams; dorsal stream and ventral stream. Dorsal stream projections end up at middle temporal cortex (V5) passing through areas V2 and V3. Ventral stream projections end up at area V4 through area V2. Major projections are represented by thick arrows, minor projections are represented by thin arrows. Adapted from Urbanski et al., (2014)

Subsequent findings of differences in the anatomical properties of cells and processing mechanisms in the retina, lateral geniculate nucleus (LGN), and various cortical areas along the visual pathway further reinforced the idea of parallel processing mechanism. In the following sections, the structural and functional properties of different structures along the visual pathway are described in relation to the parallel processing mechanisms of dorsal and ventral streams, followed by the evidence for and against each such mechanism.

1.1.1 Retina

The prospect of functional specialisation in visual processing was first proposed after the discovery of five different types of retinal cells in frogs (Lettvin *et al.*, 1959). Some of these cells responded to small black spots while others responded best to large moving stimuli. Later (Enroth-Cugell and Robson, 1966), cells with varying response to visual properties were detected in the mammalian visual system. The cat’s retinal cells, classified as the X and Y cells, differed in their responses to the spatial properties of the sine wave gratings.

The anatomical and functional differences were also observed in cells isolated from primate and human retina (De Valois *et al.*, 1974; Kaplan and Shapley, 1986). Retina contains two different types of light absorbing photoreceptors cells, rods and cones. The rods and cones differ in their structure, distribution, sensitivity, and photopigment content. These differences in properties of retinal photoreceptors translate to functional specialisation. Rods are mostly distributed towards the peripheral retina. They contain the photopigment known as rhodopsin which is very sensitive to light but has low spatial resolution. Cones are densely concentrated at the centre of the fovea. Cones consist of three different types of photopigments with different absorption properties, namely L-cone (peak sensitivity at 557nm), M-cone (peak sensitivity at 530nm) and S-cone (peak sensitivity at 426nm). Cones, therefore, have a high spatial resolution but lower sensitivity to light and are well suited to carry information on fine form and colour vision. The duplex nature and functional specialisation of photoreceptors indicate the presence of parallel processing mechanism from the earliest stage of visual processing.

The signals from photoreceptors are transmitted to bipolar cells either directly or via the lateral connections from horizontal and amacrine cells (Figure 1.2). A large number of rod photoreceptors synapse with a single rod bipolar cell while the cones, especially in the central retina, have almost 1:1 synapse with cone bipolar cell. This variation in the convergence of rod and cone photoreceptors onto bipolar cells helps in maintaining the functional specialisation. The larger numbers of rod photoreceptors synapsing with a single rod bipolar cells form a basis of spatial summation across retina in the expense of spatial resolution under scotopic conditions while a 1:1 synapse between cones and cone bipolar cells ensures that the information about fine structure and chromatic properties of the visual image are preserved under photopic condition. The bipolar cells then synapse to the retinal ganglion cells.

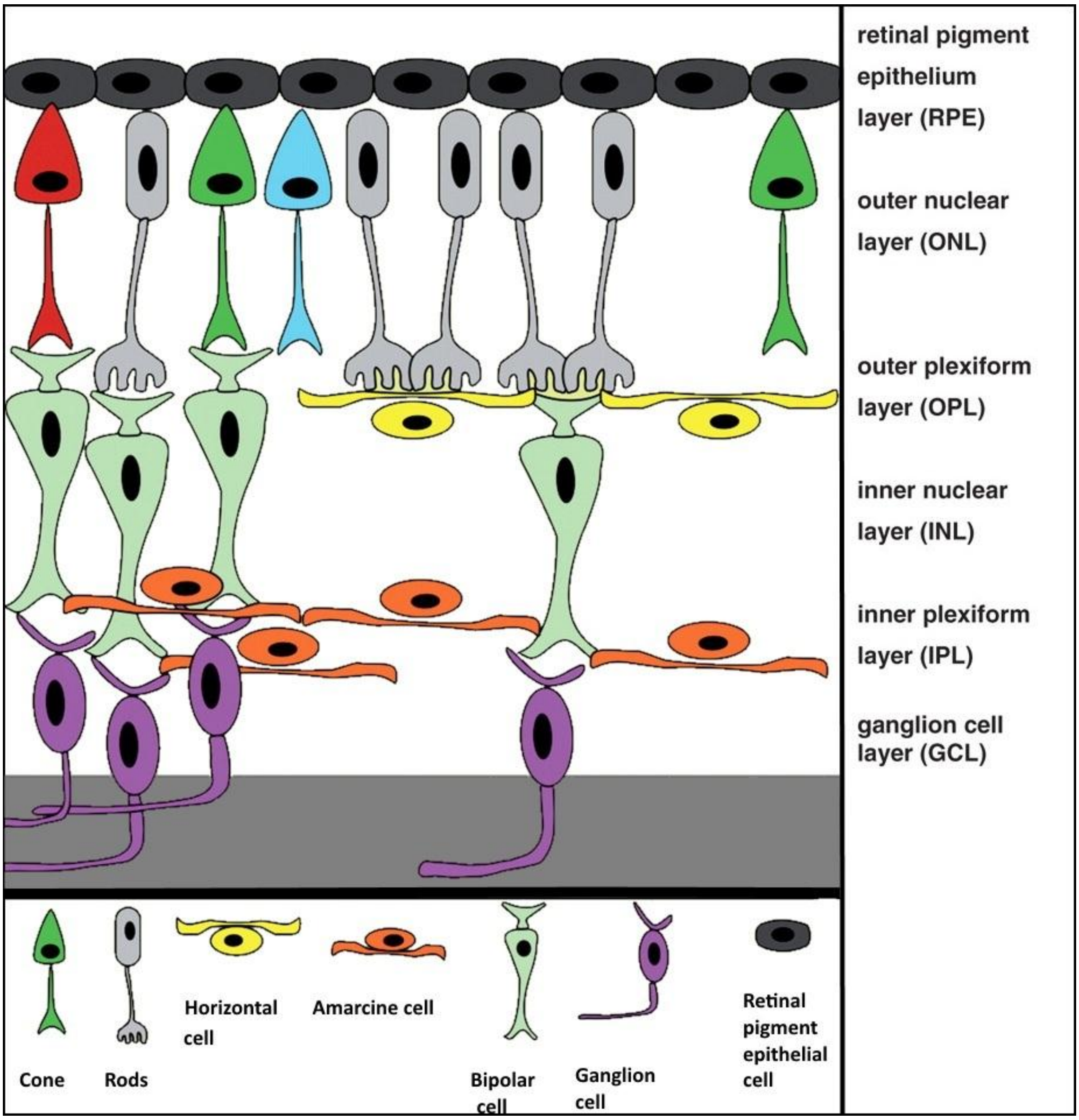

Figure 1.2: Schematic model of retinal layers.

Multiple rod photoreceptors synapse to a single bipolar cell while cones have almost 1:1 synapse. The bipolar cell in turn feeds the retinal ganglion cells. Adapted from Archibald et al., (*2009*)

The level of processing at the retinal ganglion cells combines inputs from preceding retinal cells. While photoreceptors only respond to presence or absence of light, the synapses between photoreceptors, horizontal, bipolar, and ganglion cells form the basis of complex circular on/off, centre/surround configuration of bipolar/ganglion cell's receptive fields (Figure 1.3). The on-centre cells are stimulated by centrally light and peripherally dark stimuli and inhibited by peripherally light and centrally dark stimuli. The off-centre cells exhibit an opposite pattern, responsive to peripherally light and centrally dark stimuli and inhibited by peripherally light and centrally dark stimuli. The diffuse light that covers the whole receptive field elicits a little response. The centre-surround receptive field results in lateral inhibition *i.e.,* the stimulation of centre results in inhibition of surrounding and vice versa. Such inhibition enhances the perception of edges and contours, forming the basis for contrast sensitivity.

The on-centre and off-centre receptive field characteristic is maintained as the information is passed onto the ganglion cells *i.e.,* the on-centre bipolar cells innervate the on-centre ganglion cells and off-centre bipolar cells innervate the off centre ganglion cells.

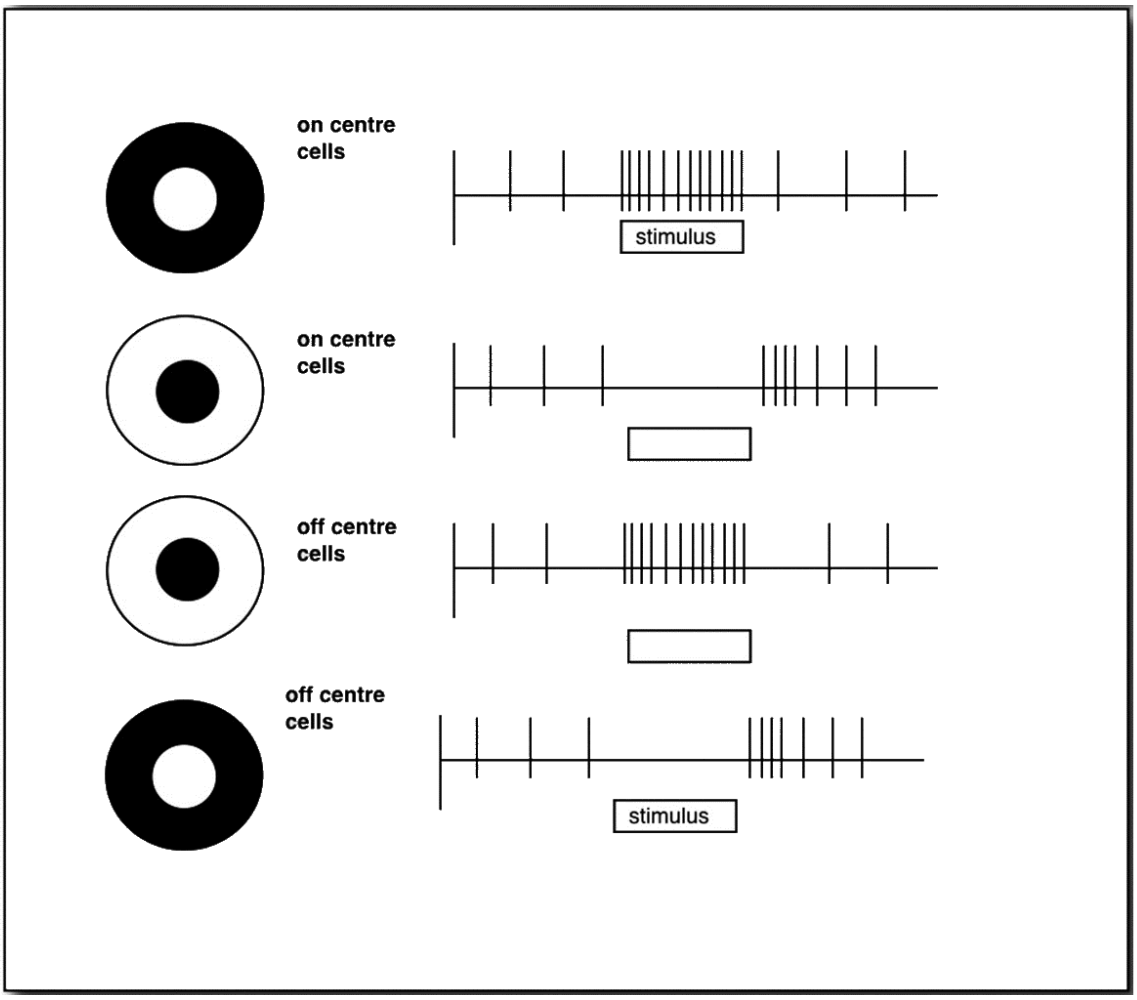

Figure 1.3: Receptive field of retinal cells and their response profiles.

The on-centre cells are only responsive to stimulus within their inner central receptive fields, as shown by increased action potentials to light (white areas) in the cells' central receptive fields. The off-centre cells are meanwhile responsive only to stimulus within the outer receptive fields. Adapted from Archibald et al., (*2009*)

The retinal ganglion cells are divided into three major types based on the specialised response to specific stimulus properties – parasol, midget and konio

(De Valois *et al.*, 1974). Subsequent studies have reported more than 20 different types of retinal ganglion cells (Dacey, 2000; Kaplan, 2004). The two major types of ganglion cells, midget and parasol, constitute almost 90% of the total ganglion cell population. The retinal ganglion cells also exhibit morphological and functional specialisation. Midget retinal ganglion cells, which constitute about 80% of all ganglion cells have smaller receptive fields and are responsive to higher spatial frequencies. Meanwhile, parasol ganglion cells, which constitute about 10% of ganglion cell population, are responsive to luminance (Kaplan and Shapley, 1986; Werner and Chalupa, 2004). Multiple photoreceptors/bipolar cells feeding a single parasol ganglion cell results in increased temporal summation and larger receptive fields (6 to 8 times larger than midget ganglion cells). These properties also lead to differences in temporal responses of the ganglion cells (Figure 1.4). The midget ganglion cells respond consistently to change in illumination (sustained response) while the parasol ganglion cells respond briefly and briskly at the onset and offset of stimuli (transient response). The transient response of the parasol ganglion cells makes them suitable to resolve fine temporal information. Another group of ganglion cells, known as the small bi-stratified cells (about 8% of total ganglion cells) receive input from the S-cone bipolar cells, carrying blue/yellow colour opponent signals (Dacey and Packer, 2003). The presence of these different types of cells in the retina with independent functionality provides the basis for specialised functioning within parallel systems of vision processing in higher visual areas.

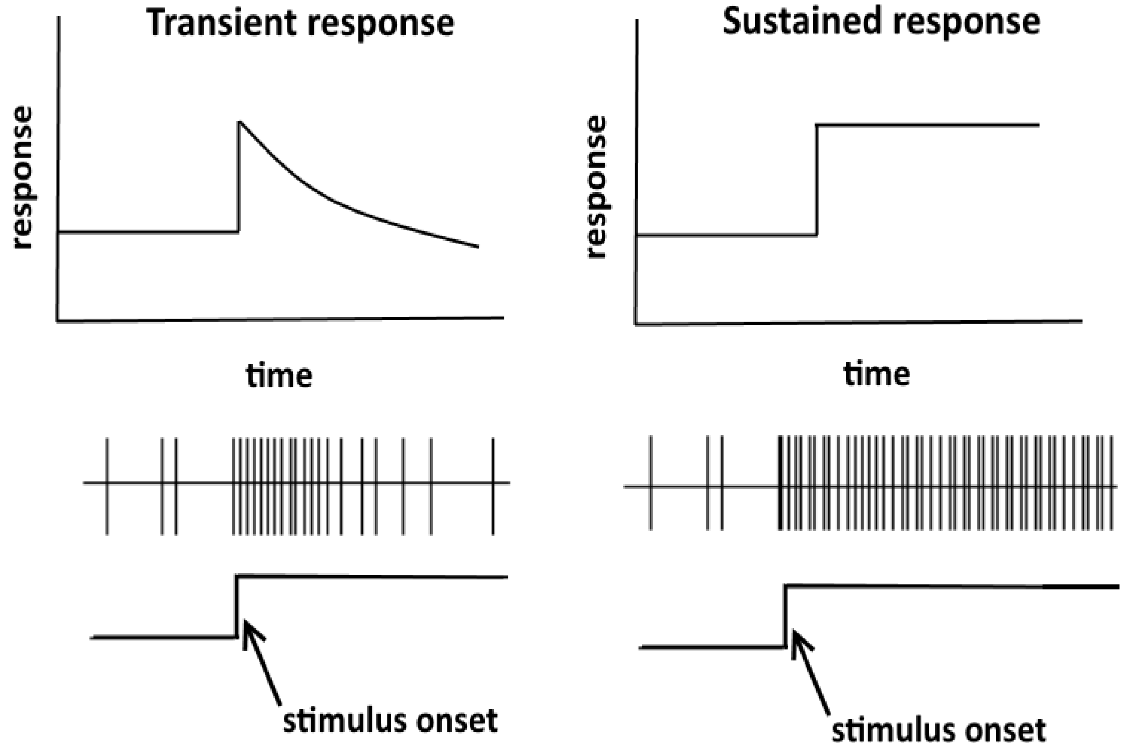

Figure 1.4: Temporal response of the retinal ganglion cells.

The parasol ganglion cells (left) exhibit a transient response with the highest response at the onset of stimuli with firing reverting back to the original level even in the continued presence of the stimuli. The midget ganglion cells (right) exhibit a sustained response with the firing rate being maintained throughout the stimulus presentation. Adapted from Wandell (1995)

1.1.2 Lateral Geniculate Nucleus

The output from retinal ganglion cells exits eye through the axons within the optic nerve. The optic nerves from two eyes undergo semi decussation at the optic chiasm with nasal retinal nerve fibres from each eye crossing over to the opposite side. The optic nerve carrying outputs of ipsilateral temporal retinal fibres and contralateral nasal retinal fibres finally project to the lateral geniculate nucleus (LGN) located in the thalamus of the brain.

The parallel projections inherited from retina remain segregated within distinct layers of LGN. The two magnocellular layers (layers 1 and 2) receive projections from the parasol retinal ganglion cells while the remaining four parvocellular layers (3 to 6) receive projections from the midget ganglion cells (Kaplan and Shapley, 1986). The projections from remaining small bistratified cells and other retinal ganglion cells end up at the inter-laminar region of the LGN (between the major magno and parvocellular layers) known as the koniocellular layer (Figure 1.5).

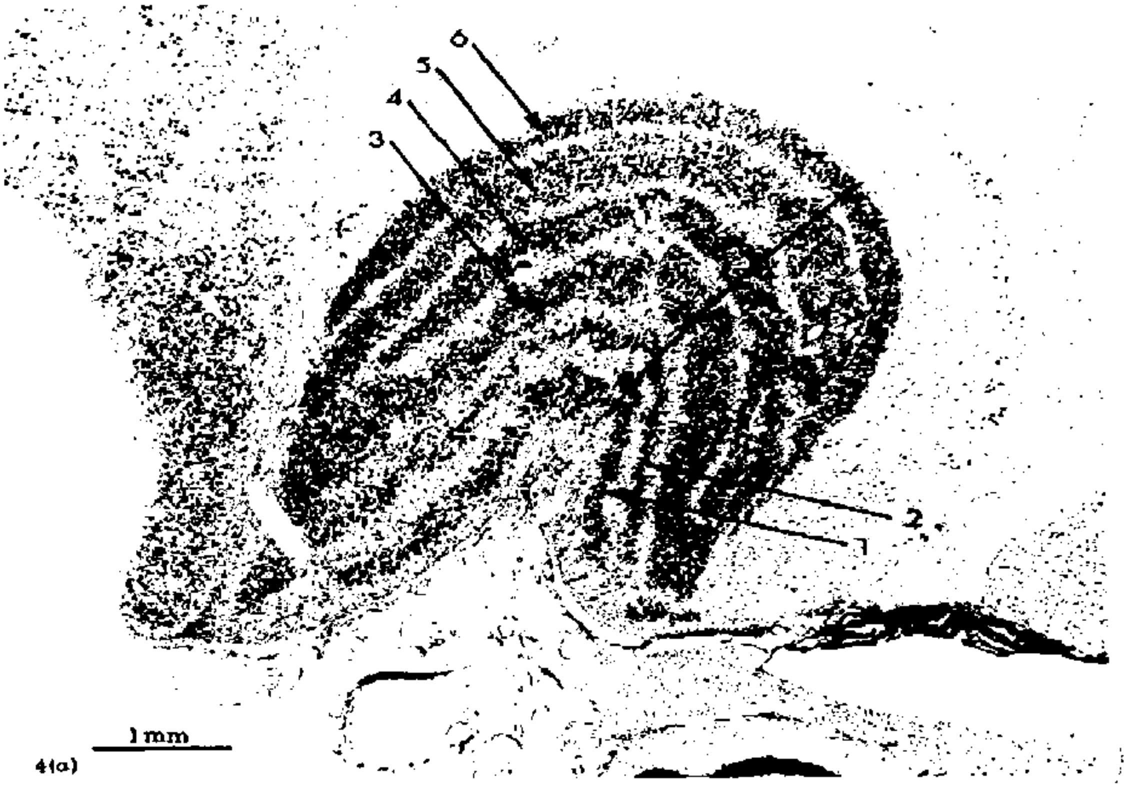

Figure 1.5: The architecture of lateral geniculate nucleus (LGN).

The lateral geniculate nucleus stained with Golgi material shows six distinct layers. The four superficial layers (3-6), the parvocellular layers, contain small cells. The two deep layers (1-2), the magnocellular layers, are composed of larger cells. Adapted from Wandell (1995) (Based on Hubel and Wiesel, 1977)

Each magno/parvocellular layer receives inputs from either left or right eye with the adjacent LGN cells receiving inputs from nearby retinal fields. Each LGN layer hence contains a complete monocular retinotopic map. While most of the projections from the retinal ganglion cells end up in LGN, around 10% of retinal projections synapse to the superior colliculus in the midbrain with mostly parasol (magno) inputs. The compartmentalised magnocellular and parvocellular layers of LGN also exhibit functional specialisation with each layer containing cells with similar properties to the retinal ganglion cells that they receive the input from. The LGN cells have somewhat larger circular on-off receptive fields and exhibit stronger inhibitory surround effect compared to the retinal ganglion cells (Hubel and Wiesel, 1961). The major functions and differences between the magnocellular and parvocellular layers are listed in Table 1.1. In addition to the inputs from the retina, LGN also receives feedback responses from the primary visual cortex which are also organised along the axes of the magnocellular, parvocellular, and koniocellular divisions (Briggs and Usrey, 2011).

Properties	**Magno/Parasol**	**Parvo/Midget**
Response to change in luminance	High	Low
Spatial resolution	Low	High
Temporal frequency	Higher (>60Hz)	Lower (>30Hz)
Colour coding	No or weak color opponency	Color opponency
Contrast sensitivity	High	Low
Conduction velocity	~15m/s	~6m/s
Projection		
Retinal Ganglion cells	LGN, Magnocellular	LGN, Parvocellular
LGN	V1, 4Cα	V1, 4Cβ

Table 1.1: Functional differences of parasol, midget retinal ganglion cells, and magno, parvo LGN cells.

The parasol retinal ganglion cells and magno cells in LGN are involved in the processing of high temporal frequency and luminance, the midget retinal ganglion cells and parvo cells in LGN are involved in the processing higher spatial frequency and colour.

The functional and anatomical characteristics of retina and LGN provide evidence of an early parallel system (Livingstone and Hubel, 1987; Briggs and Usrey, 2009). The magnocellular pathway with high sensitivity to temporal frequency, larger receptive fields, higher conduction velocity, and relative insensitivity to colour is well suited to the processing of rapidly changing stimuli such as flicker and motion. The parvocellular pathway with high sensitivity to higher spatial frequency and colour along with lower temporal frequency encode information about form and colour and respond to static stimuli. The koniocellular mechanism further aids the colour perception with its blue/yellow sensitivity.

1.1.3 Primary Visual Cortex (V1)

Lateral geniculate nucleus (LGN) projects to an area in occipital lobe called primary visual cortex (V1). The cells in V1 also exhibit structural and functional specialisation maintaining the parallel processing mechanism carried on from the preceding visual areas. The anatomical and functional segregation of processing various visual attributes continue with cells responsive to specific stimulus properties arranged in a more complex structure of layers and columns. Notably, the V1 cells are binocular while preceding retinal and LGN cells respond only to inputs from a specific eye. A general summary of structural and functional properties of V1 is discussed below.

The cells in V1 do not respond to a spot of light as observed in earlier areas of the visual pathway. Hubel and Wiesel (1962, 1968) discovered that V1 cells instead respond to elongated stimuli and exhibit orientation and direction selectivity. V1 cells are divided into simple, complex, and hypercomplex cells based on the complexity and functional hierarchy. The circular on- and off-centre LGN inputs are aligned to form an elongated receptive field of simple cells with excitatory and inhibitory sub regions separated by a straight line or parallel lines. The response of simple cells can be approximately predicted by the summation of its response to small circular spots of light (response from a particular area of the retina), the property also known as linearity. These simple cells carry the oriented arrangement of LGN inputs and hence best respond to stationary elongated bars or edges of a specific axis of orientation (Figure 1.6, A).

The complex cells make up almost 75% of V1cells and integrate information from simple cells. The receptive fields of complex cells are somewhat larger than that of the simple cells but retain the elongated shape of simple cells. Unlike the simple cells, complex cells do not respond to stationary images. Instead, these cells respond to a moving bar of preferred orientation making them powerful motion detectors. Around 20% of complex cells are direction selective, responding only to moving bars in a preferred direction (Figure 1.6, B). These complex cells are insensitive to stimulus position and respond to a moving bar anywhere within their receptive fields. Unlike the simple cells, complex cells are non-linear as their overall response cannot be predicted by a simple algebraic summation of responses from a particular area of the retina.

Unlike the simple and complex cells, hypercomplex cells contain inhibitory areas that are activated when a stimulus exceeds the diameter of its receptive fields – end stopping. The combined processing of these different V1 cells results in detection of edges, angles, and motion from a limited region of the retinal image (owing to the relatively small receptive fields of V1 cells), such processing from a limited area of the overall visual field is known as local processing.

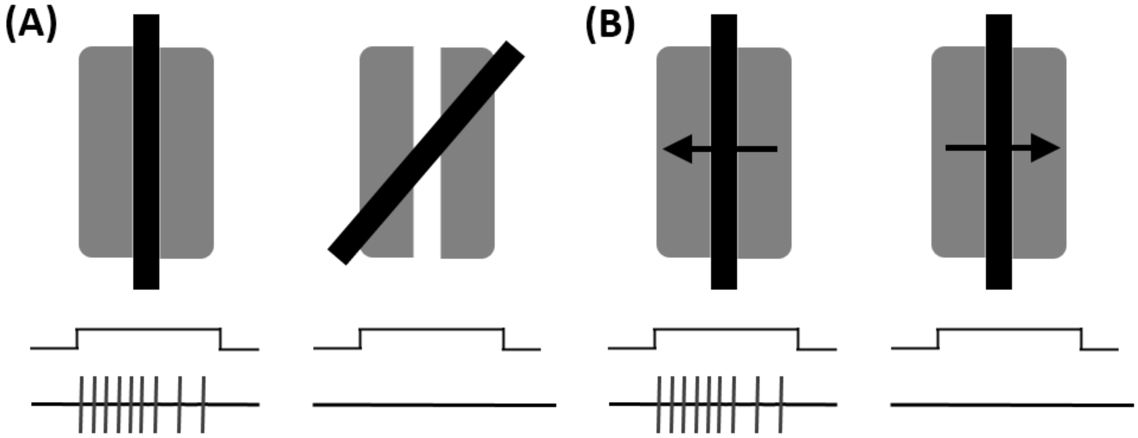

Figure 1.6: The responses of simple and complex cells of V1.

The bar with preferred orientation (vertical thick line on top left) within the receptive field of simple cells results in a maximum response (as shown by black lines in bottom) whereas the bar with non-preferred orientation (oblique here) results in no response (A). The bar with preferred orientation results in maximum response from direction selective complex cells only for the motion in the preferred direction (here leftward motion as indicated by the arrows) (B). Adapted from Hubel and Wiesel (1962, 1968)

V1 is the first area where motion selective cells are present. But the small receptive fields in V1 only allows for motion processing from a limited visual space resulting in a misrepresentation of the overall direction of motion, the phenomena known as the aperture problem (Adelson and Movshon, 1982; Adelson and Movshon, 1986) – Figure 1.7. Hence the motion processing in area V1 is only limited to the processing of local direction.

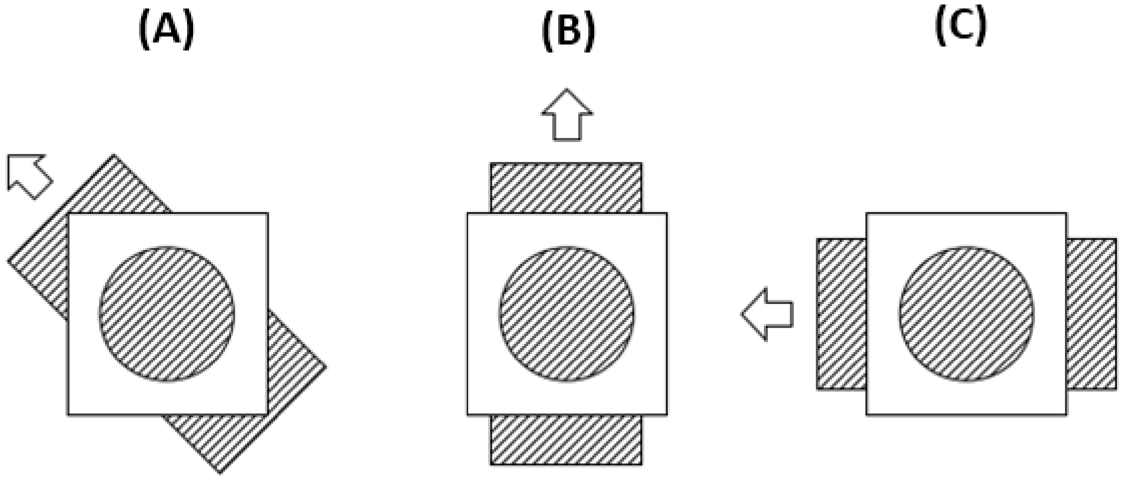

Figure 1.7: The aperture problem.

The direction of motion of a grating viewed through the centre aperture is identical (to the overall motion in A) irrespective of the overall motion of the grating; diagonal (A), vertical (B) and horizontal (C). Adapted from Adelson and Movshon (1986)

V1 also exhibits complex structural arrangement with cells responsive to similar properties lying nearby one another in a columnar structure. For example, the orientation selective neurones in V1 are arranged in a columnar fashion with neurones sensitive to a fixed orientation lying in a single column. V1 cells respond to binocular stimulation but with preference to inputs from one eye. The cells preferring right or left eye are arranged in an alternating columnar pattern, known as ocular dominance columns.

Hubel and Wiesel (1974) proposed that the retinotopic map of primary visual cortex is composed of many smaller units called hypercolumns that run perpendicular through the V1 layers (1 to 6). Each hyper column consists of ocular dominance and orientation columns arranged in an approximate grid structure. Figure 1.8 shows an example of such a hypercolumn from layer 4 of V1 which mostly consists of monocular cells (Hubel, 1982). Each hypercolumn consists of separate sub-columns from each eye (ocular dominance columns) with each sub-column further containing cells responsive to all possible orientations (orientation column).

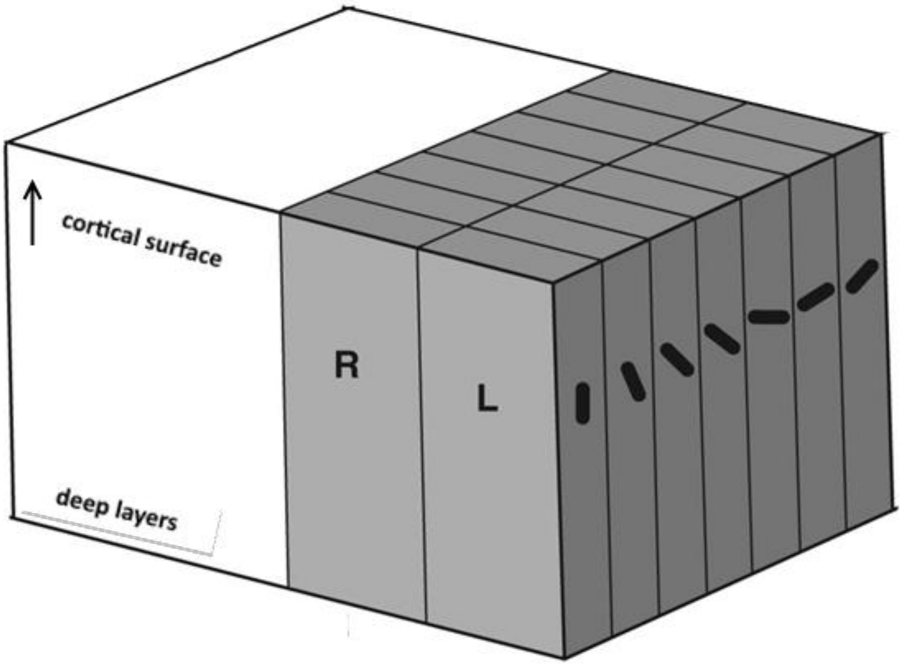

Figure 1.8: A primary visual cortex hypercolumn.

A hypercolumn containing ocular dominance columns (for each eye) and orientation columns (for orientation spanning 180˚) arranged in a grid structure. Adapted from Hubel (1982)

More recent studies, however, suggest that instead of the grid-like structure proposed by Hubel and Wiesel (1968), orientation preference changes systematically across different columns in a radial pinwheel configuration with the representation of all orientations converging towards the pinwheel centres (Bonhoeffer and Grinvald, 1991) – Figure 1.9.

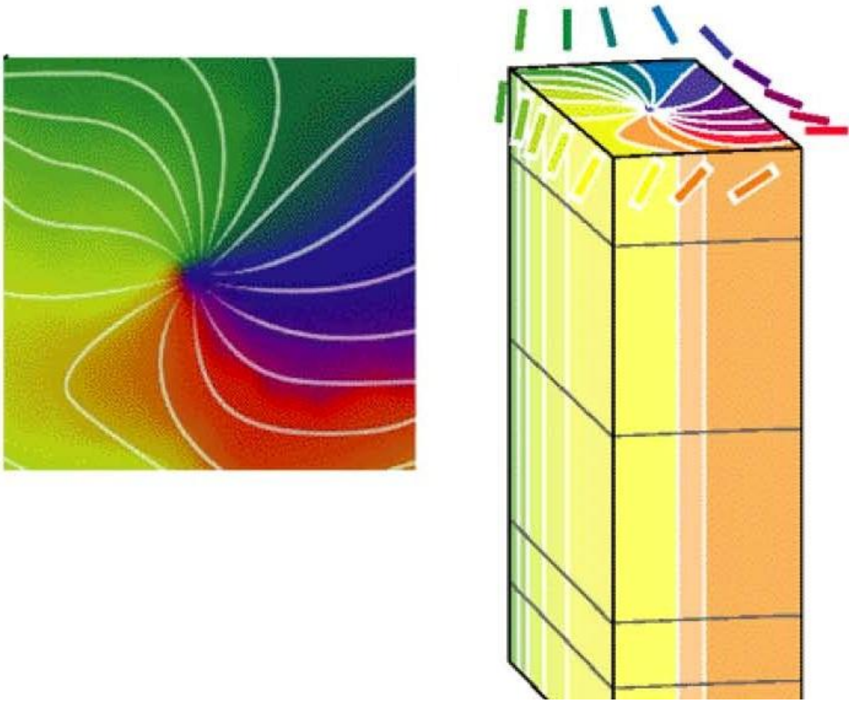

Figure 1.9: The pinwheel arrangement of the orientation columns in V1.

The colour codes in the pinwheel arrangement represent varying orientations. Adapted from Kandel (2013)

V1 cells are arranged in six layers with layer 4 further subdivided into 4A, 4B, 4Cα, and 4Cβ. These layers are arranged in line with the parallel inputs that V1 receive from the preceding visual areas. For example, layer 4Cα receives magnocellular input in turn projecting to layer 4B while layer 4Cβ receives parvocellular inputs with projections terminating at layer 2 and 3 (Figure 1.10). Layer 2 and 3 also receive inputs from the koniocellular layer. The segregation of V1 into areas receiving magnocellular and parvocellular inputs is also evidenced by the cytochrome oxidase (CO) staining which reveals dark stained patches, known as blobs and thin layer known as interblobs (Livingstone and Hubel, 1984; Lu and Roe, 2008). The interblobs receive input from the parvocellular layers of LGN while the remaining areas receive input from the magnocellular layers. Layer 4Cβ, 2, and 3 that receive the parvocellular and koniocellular inputs consist of cells that are highly orientation and colour selective. While layers 4Cα, 4A, 4B, and 6 which receive the majority of magnocellular inputs from LGN mostly contain direction selective complex cells (Hawken *et al.*, 1988). The functional and anatomical segregation of magnocellular and parvocellular inputs in V1 maintain the cortical continuation of the parallel retinogeniculate connection.

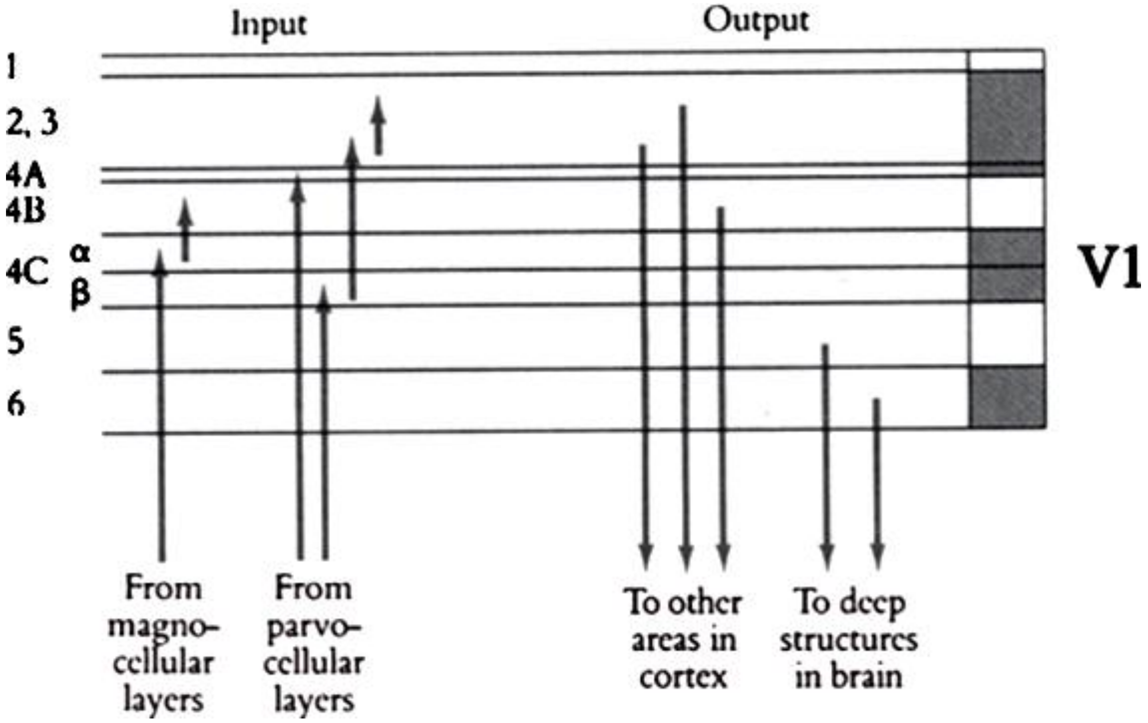

Figure 1.10: Magnocellular and parvocellular projections from LGN to primary visual cortex (V1)

The inputs from magnocellular and parvocellular layer are projected to separate areas of 4Cα and 4Cβ in V1. The projections are forwarded from 4Cα to layer 4B and from 4Cβ to layer 3. The outputs from these layers are projected to different extra-striate areas. Adapted from (Hubel, 1995)

To summarise, retinal photoreceptors respond to diffuse light, retinal ganglion cells respond to spots of light of specific diameter, simple cells in V1 to bar or edges with a specific orientation and complex cells to specific orientation and direction. In terms of the arrangement, photoreceptors/ganglion cells are dispersed in the retina, magno and parvo cells are arranged in monocular layers in LGN. V1 cells are arranged in columnar structures based on responses to stimulus feature and ocular preference. Such hierarchical increase in complexity along the visual pathway from the retina to V1 is an important characteristic of the parallel processing mechanism.

The inputs from LGN to V1 are segregated into different anatomical structures for processing of local orientation and direction of motion (Livingstone and Hubel, 1984). The studies discussed so far support the anatomical and functional segregation of magnocellular and parvocellular inputs in V1. Others, however, indicate a substantial intermixing of magnocellular and parvocellular inputs within V1. For example, Nealey and Maunsell (1994) found that the parvocellular inputs which are mostly directed to area 4Cβ also make numerous synapses into the magnocellular areas of 4Cα and 4B (Nealey and Maunsell, 1994; Sincich and Horton, 2005). Similarly, the CO stained areas of both blobs and interblobs in V1 receive the inputs from both magnocellular and parvocellular pathways (Lachica *et al.*, 1992).

1.1.4 Area V2

Most of the projections from area V1 end up in area V2 which is an elongated, narrow cortical area surrounding V1. The receptive fields of cells in area V2 are 2 to 3 times larger than that of V1 (Levitt *et al.*, 1994). The larger receptive fields allow V2 cells to integrate inputs from V1, resulting in the perception of curves and angles (Hegde and Van Essen, 2000; Ito and Komatsu, 2004). Almost all cells in V2 are binocularly driven with orientation, direction, and colour tuned neurones clustered in different areas (Hubel and Livingstone, 1987; Ts'o *et al.*, 2001).

The histological staining by cytochrome oxidase (CO) reveals organisation of V2 cells into different layers according to functional specification. The CO staining shows an arrangement of alternate thick and thin stripes separated by a thinner, lightly stained layer called pale stripes (Hubel and Livingstone, 1987). The thick stripes receive its projection from layer 4B of V1 with magnocellular inputs of motion and disparity. The thin and pale stripes are supplied by layers 2 and 3 of V1 with the parvocellular inputs of colour and orientation respectively.

These different V2 stripes form a three parallel visual processing pathways with orientation tuned cells in pale stripes, motion tuned cells in thick stripes, and colour tuned cells in thin stripes (Figure 1.11), thereby implicating different sub-compartments of V2 for form, motion, and colour processing (Livingstone and Hubel, 1984; Livingstone and Hubel, 1987; Shipp and Zeki, 2002; Lu and Roe, 2008; Lu *et al.*, 2010; Li *et al.*, 2013).

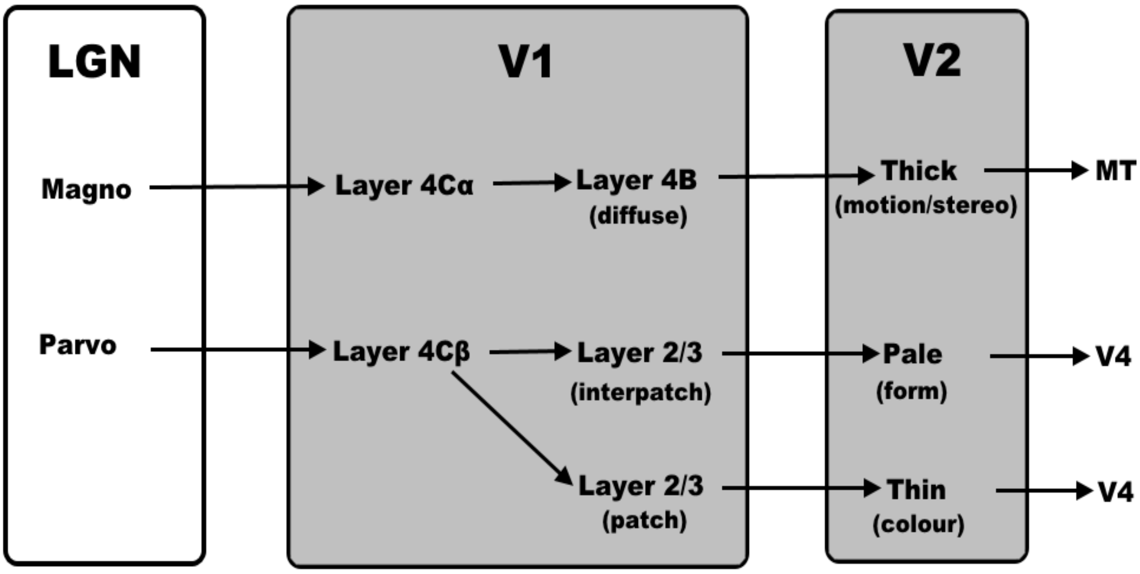

Figure 1.11: Projection of lateral geniculate nucleus outputs into V1, V2 and other extra striate areas.

V1 transforms parallel input streams from LGN into three output streams headed to area V2. The projections from V2 end up in different extra striate areas. Adapted from Sincich and Horton (2005)

While the proposed three way processing mechanism in V2 provides a strong basis for parallel processing along the visual pathways, various studies suggest that this differentiation may not be as independent as previously described. The direction selective cells in V2 only exhibit weak direction selectivity and are distributed in both thick and thin stripes (Gegenfurtner *et al.*, 1996; Roe and Ts'o, 1997). Others have reported that V2 cells are not specific to a single stimulus property but respond to a range of properties like disparity, orientation, and colour indicating that V2 acts as an area where different attributes of the visual inputs are intermixed and integrated (Ts'o *et al.*, 2001).

Even though the existence and independence of three parallel visual pathways have remained controversial, areas V1 and V2 are important for transmitting inputs to the higher cortical areas such as middle temporal (MT) area and area V4 that lie along the proposed dorsal stream and ventral stream respectively. The outputs of V1 and V2 to each proposed stream (dorsal and ventral) may carry mixed input from the parallel mechanism of magnocellular and parvocellular streams. One of the arguments forwarded to account for the significant intermixing of inputs along these early parallel processing pathways is that the inputs from the magnocellular and parvocellular systems are modulated in V1 and V2 to the requirements of the higher areas along the dorsal and ventral streams (Goodale, 2011). There is evidence which contradicts the presence of hierarchical processing along the proposed parallel streams as well. The early visual areas that were only thought to process simple stimulus attributes are also involved in processing complex tasks (Sincich and Horton, 2005; Kastner *et al.*, 2006). For example, area V2 is responsive to complex stimuli such as real and illusionary contours (von der Heydt *et al.*, 1984).

Having described the early visual processing mechanisms and their relative independence in regards to the parallel processing streams, some specialised areas proposed to be along the bifurcated dorsal and ventral pathways are discussed.

1.1.5 Area V4

Area V4 is the first specialised area along the ventral stream that contains cells with receptive fields that are 4 to 7 times larger than V1 (Desimone and Schein, 1987). V4 receives the projections from the thin and pale stripes of V2 carrying colour and form information respectively (DeYoe *et al.*, 1994). V4 also receives some direct projections from V1 (Nakamura *et al.*, 1993). The projections from thin and pale stripes of V2 innervate different subdivisions of V4 (Felleman *et al.*, 1997), maintaining the parallel processing pathway for form and colour information. The colour and orientation sensitive cells in V4 are arranged in multiple alternate bands in a structure similar to the thin and thick strips of V2 with linear and pinwheel arrangement as seen in V1 (Tanigawa *et al.*, 2010).

Area V4 consists of highly orientation selective cells, suggesting its role in shape processing (Schein *et al.*, 1982). The larger receptive fields of V4 cells allows for the integration of the local orientation information from preceding areas. The integrative property of V4 cells is reflected in their strong selectivity to angles and curvature of contours as well as complex shapes (Desimone and Schein, 1987; Pasupathy and Connor, 2001). V4 cells are more sensitive to circular and concentric shapes compared to parallel patterns (Dumoulin and Hess, 2007). The area is also responsive to other global form stimuli such as Glass patterns (Wilson and Wilkinson, 1998; Smith *et al.*, 2002; Tse *et al.*, 2002; Ohla *et al.*, 2005) and radial frequency patterns (Wilkinson *et al.*, 1998; Loffler, 2008) – Figure 1.12. Damage to area V4 results in a wide range of global form discrimination deficits including increased discrimination thresholds for Glass patterns and radial frequency patterns (Gallant *et al.*, 2000).

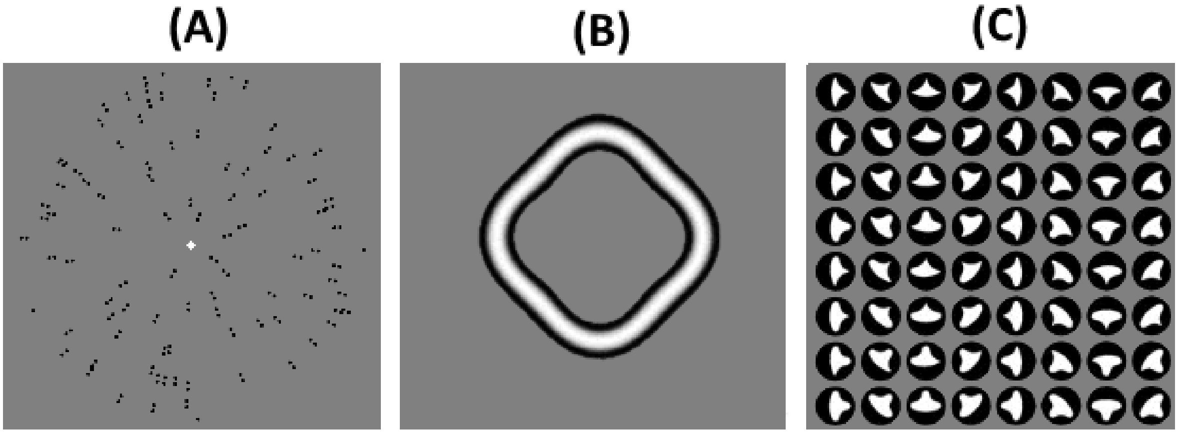

Figure 1.12: Commonly used stimuli to study area V4.

V4 is responsive to various global form stimuli including Glass pattern (A), radial frequency pattern (B) and various curvatures (C). C - adapted from Pasupathy and Connor (2001)

V4 is typically regarded as the ventral stream area that receives segregated parvocellular inputs. However, V4 also receives magnocellular inputs as suggested by a reduced response from V4 when the magnocellular areas in LGN are inactivated (Ferrera *et al.*, 1992; Ferrera *et al.*, 1994). In addition, V4 also contains direction selective cells (reported to range 13% to 33% of V4 cell population) which are believed to receive inputs from the magnocellular pathway (Desimone and Schein, 1987; Ferrera *et al.*, 1994). The direction selective cells in V4 are scattered and most probably are involved in decoding form from motion cues rather than real motion per se (Li *et al.*, 2013). However, it has also been reported that these direction selective cells are arranged in a columnar organisation according to the preferred direction of motion, indicating that V4 may be important for overall motion processing (Welberg, 2013).

The outputs from V4 are projected to the inferior temporal area (IT), which consists of highly specialised areas for complex form processing. The neurones in the more anterior parts of the IT are arranged in the columnar pattern similar to V1 but require more complex and complete object pattern for activation (Tanaka, 1993). Similarly, fusiform face area (FFA), lying on ventral surface of temporal lobe, specifically responds to human facial features (Kanwisher and Yovel, 2006).

1.1.6 MT+ (MT, MST)

Area MT is located at the lateral surface of the occipital lobe and contains a retinotopically organised representation of the contralateral hemifield of visual space (Huk *et al.*, 2002). The area is implicated in the processing of object motion and injury to MT is reported to result in a complete loss of motion perception in humans (Zihl *et al.*, 1983; Zihl and Heywood, 2015). The area receives magnocellular input directly through layer 4B of V1 with other minor indirect inputs from layer 6 of V1 and thick strips of V2 (Maunsell and Van Essen, 1983; Maunsell *et al.*, 1990; Nassi and Callaway, 2006). The major influence of magnocellular input to MT is evident as blocking the magnocellular input from LGN has a substantial effect on the responsiveness of MT cells while blocking the parvocellular inputs has a very small effect (Maunsell *et al.*, 1990).

Around 80 - 90% of MT cells are sensitive to the direction of motion (Maunsell and Van Essen, 1983; Snowden *et al.*, 1992). The receptive fields of MT cells are around 10x larger in linear diameter compared to overall V1 cells and 3x larger in linear diameter compared to complex direction selective V1 cells (Maunsell and Van Essen, 1983; Hawken *et al.*, 1988; Snowden *et al.*, 1992; Smith *et al.*, 1998). The direction selective cells in MT are arranged in a columnar fashion (Albright *et al.*, 1984). Each column contains cells whose preferred direction varies along the column with the nearby columns containing cells with a preference for opposite direction (Albright, 1993; Born and Bradley, 2005) (Figure 1.13).

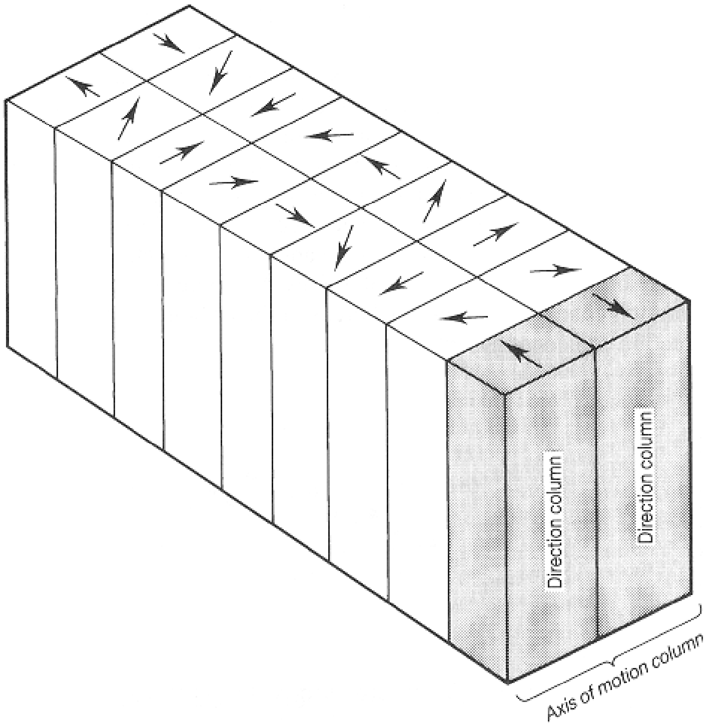

Figure 1.13: The columnar arrangement of direction selective cells in area MT.

The figure shows two adjacent columns of direction selective cells in area MT. The direction preference along the long axis of a column changes gradually. The adjacent column along the axis of motion (the direction of moving object) consists of cells with preference for opposite directions. Adapted from Albright et al., (1984)

Speed selectivity is also first encountered in the MT region (Liu and Newsome, 2003). MT cells respond to a range of speed but most cells are tuned to relatively faster speeds with mean tuning at 30˚/s (Zeki, 2015). The cells with a similar speed preference are localised in MT. However, these cells do not have the columnar organisation as with the direction selective cells (Liu and Newsome, 2003).

The larger receptive field and stronger centre surround organisation of MT cells summate and amplify the directional inputs from V1 (Born and Bradley, 2005), resolving the local uncertainties (aperture problem) observed in V1 to provide a global percept as illustrated by experiments employing plaid stimuli (Figure 1.14). Plaid stimuli consist of two gratings drifting in opposite directions, for example, one moving downwards and to the right and a second moving upwards and to the right. When superimposed, the two components form a plaid pattern that moves in a direction determined by the direction of the components (Adelson and Movshon, 1982), towards the right in the example illustrated here. V1 cells only respond to the direction of motion of the plaid components while about 75% of direction selective neurones in MT respond to the global motion of the whole pattern (Movshon *et al.*, 1995; Zeki, 2015) by pooling information from the spatially localised plaid components over a large receptive area (Majaj *et al.*, 2007).

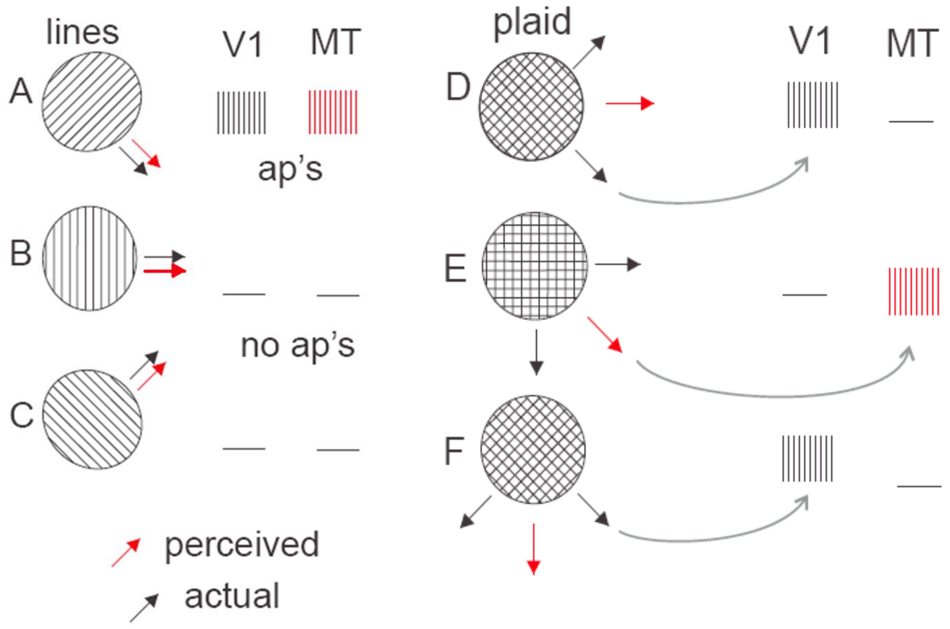

Figure 1.14: Responses of V1 and MT cells to simple gratings and plaids.

Both V1 and MT cells respond optimally to the motion of grating along its preferred direction – right down (A) but not to the motion along other directions (B and C). For plaid stimuli, V1 cells are responsive to motion of plaid component along the preferred direction (D and F) but not to overall perceived motion along the same direction (E) in contrast MT cells are not responsive to the direction of motion of the plaid component (D and F) but responds optimally when the overall perceived motion is along its preferred direction of motion (E).

Another commonly used stimulus to study global motion perception is the random dot kinematograms (RDK). The stimuli consist of randomly placed dots that are spatially displaced over time to produce motion signals. The local motion (direction of component dots) and global motion (direction of the overall pattern) can be manipulated independently in such displays. V1 cells can only process the local motion from individual dots in RDK. MT cells, however, integrate the local motion from the individual dots to provide a global motion perception of the overall pattern (Braddick *et al.*, 2001). The single cell response of macaque MT to motion signals in RDK show a significant correlation to the behavioural response (Britten *et al.*, 1992; Parker and Newsome, 1998). Similarly in humans, the response of area MT is correlated with the strength of the motion signals in RDK (Braddick *et al.*, 2001). The perceived motion direction in an RDK can also be influenced by micro stimulation to the area MT (Salzman *et al.*, 1990).

Motion opponency which refers to the suppression of a neuronal response by motion in an opposite direction to its preferred direction is also first observed in MT (Heeger *et al.*, 1999). Recent studies suggest that the direction and speed tuning of some complex V1 cells are similar to that of MT neurones (Born and Bradley, 2005; Priebe *et al.*, 2006). However, additional properties of MT such as a larger number of direction selective cells, larger receptive fields resulting in global processing, and motion opponency suggest a higher hierarchical role for MT in motion processing.

Middle superior temporal area (MST) that lies anterior to MT consists of cells with even larger receptive fields (Greenlee, 2000; Morrone *et al.*, 2000; Tohyama and Fukushima, 2005). The cells in the dorsal region of the middle superior temporal area (dMST) are involved in processing complex global motion pattern such as radial and rotational optic flow (Morrone *et al.*, 2000; Tohyama and Fukushima, 2005; Smith *et al.*, 2006). The ventral area of MST (vMST) is influential in the execution of smooth pursuit eye movement and generating action towards objects such as control of arm movements (Ilg and Schumann, 2007). In addition to the inputs from the retinogeniculate pathway, MT also receives retinal inputs (mostly magnocellular) from the superior colliculus via the pulvinar region (Rodman *et al.*, 1989; Rodman *et al.*, 1990). These inputs are influential in maintaining limited dorsal stream functionality even when area V1 is damaged (further discussed in section 1.2.1).

MT+ is an important area along the dorsal stream receiving the bulk of the magnocellular inputs. The area however also receives inputs from the parvocellular LGN through V1 and V2 (Nassi and Callaway, 2007). The parvocellular inputs to MT may be influential in processing motion from chromatic information (Nassi and Callaway, 2006). MT also sends a significant output to area V4. In view of the heavy inputs from MT to V4, it has been suggested that MT should be considered as an intermediary area between the dorsal and ventral stream (Milner and Goodale, 2006).

The dorsal stream inputs from MT/MST are projected to different areas of posterior parietal cortex (PPC). Area 7a in the PPC decodes the direction (such as expansion vs. contraction) and type (such as radial vs. rotation) of optic flow (Siegel and Read, 1997). PPC is also involved in the processing of more complex attributes of motion such as inferred motion from transiently disappearing moving visual targets (Assad and Maunsell, 1995). The PPC area is important for transforming the sensory inputs into motor outputs such as planning and execution of saccadic eye movements (Behrmann *et al.*, 2004). The neurones in lateral intra parietal (LIP) area are sensitive to reaching action generated in accordance to the saccadic eye movements (Dean *et al.*, 2012).

In summary, the segregation of complex visual processing into parallel processing mechanisms starts from retina, the first processing area of the visual pathway. Various types of retinal ganglion cells that process different stimulus properties transmit to the LGN where the inputs are arranged into different anatomical layers according to the stimulus properties they are responsive to. These early parallel streams in retina and LGN are segregated into magnocellular, parvocellular and koniocellular pathways. The early parallel pathways then innervate cortical areas in V1 and V2 forming an initial stage of dorsal and ventral stream processing with substantial intermixing of the magnocelluar, parvocellular, and koniocellular inputs. The differentiation is continued with dedicated extra striate areas (such as MT+ for motion and V4 for complex form) for each stream with final projection to the parietal cortex and inferior temporal cortex for the dorsal and ventral streams respectively. Along both streams the higher cortical cells exhibit increasingly larger receptive fields that pool cumulative information from the preceding areas. The cells responsive to specific properties (such as orientation, motion, and colour) become more segregated into anatomically defined areas of layers and columns. The visual processing also becomes increasingly complex at higher cortical areas. The information from a small area of visual field is initially processed in V1 and V2 – local processing followed by the integration of the local information at the intermediate areas of MT+, V4 – global processing. The processing of highly specialised features such as whole objects, faces occur further down the respective streams in areas of inferior temporal cortex and posterior parietal cortex.

Various anatomical studies discussed in this chapter support a classical view of a parallel processing mechanism. However, there is now a significant volume of literature that disputes the independence of each stream [for review (Kaplan and Shapley, 1986; Lennie, 1998; Goodale and Westwood, 2004; Milner and Goodale, 2008; Goodale, 2011)]. There is a consensus that the inputs from different pathways/streams are intermixed at some cortical level to provide a complete visual percept. The disagreements are on whether this occurs along the higher cortical areas after processing through the independent dorsal and ventral streams or if such intermixing is present from the early areas of processing within V1 and V2. The ever increasing evidence from different studies of greater cross-communication between the earlier stages of parallel pathways cannot be ignored. However, whether this intermixing only contributes to enhancing the processing along each channel or if it signifies the irrelevance/non-existence of the parallel processing streams is an issue yet to be resolved.

The next section discusses in more detail on how the theory of parallel processing along the dorsal and ventral streams has evolved and the relevance of a strict independence of parallel streams.

1.2 The Bifurcation of the Visual Pathway into Dorsal and Ventral Streams

The notion of division of labour in visual processing into bifurcated streams has been prevalent since the 1960s. Schneider (1969) suggested that the projections from the retina to the superior colliculus in rodents are influential in stimulus localisation while the retinogeniculate pathway is involved in object recognition. Later studies in primates showed that only minor projections from retina end up in the superior colliculus and these projections are not adequate to represent the range of visually derived localisation tasks [for review (Milner and Goodale, 2008)].

Ungerleider and Mishkin in 1982 proposed a cortical model for the bifurcation of visual perception based on lesion studies in primates (Ungerleider and Mishkin, 1982). Lesions of the inferior temporal cortex compromised the primates’ ability to identify object’s characteristics such as shape or pattern while lesions near the posterior parietal region rendered the primate unable to locate the object in space whilst maintaining object recognition. They proposed that the cortical pathway progressing ventrally from primary visual cortex to the temporal cortex forms an independent channel specialising in object recognition (the "What" pathway) and another pathway progressing dorsally towards the region of posterior parietal region specialises in localisation of objects in space (the "Where" pathway). Livingstone and Hubel (1987) suggested that different types of neurones in V1 and V2 that are selective to direction, orientation, and colour form the continuation of parallel stream of vision from the retina and LGN in the form of magno and parvocellular processing which ultimately converges to the dorsal and ventral streams respectively.

1.2.1 Evidence of functional bifurcation regarding the two-streams hypothesis in clinical population

In humans, Goodale and Milner (1992) observed that a lesion along the ventral stream in bilateral occipito-temporal cortex reduced the ability of object recognition (also called visual agnosia) as predicted by the "What and Where" theory. But these individuals could still accurately orient hand movements and scale the aperture size of their fingers according to the size of the object while performing a grasping action. This observation suggested that the intact dorsal system was influential in directing action towards the object. Based on these findings, they proposed an updated theory of double dissociation based on a broad functional organisation (Goodale and Milner, 1992; Milner and Goodale, 2008; Goodale, 2011), which defined dorsal stream as the vision for action and ventral stream as the vision for perception (Figure 1.15).

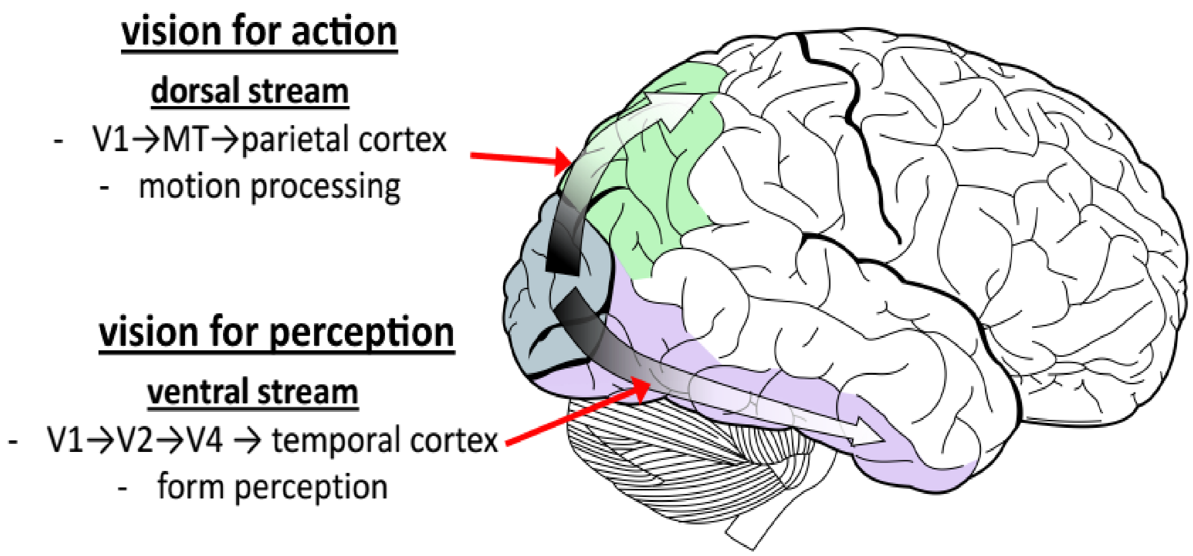

Figure 1.15: The hypothetical bifurcation of visual processing along the dorsal and ventral streams.

According to Goodale and Milner (1992), dorsal visual stream inputs from V1 are projected to middle temporal area (MT) and parietal cortex while the ventral stream inputs from V1 are projected to temporal cortex through area V2 and V4. Adapted from Goodale (2011)

The most widely studied patient DF with visual form agnosia due to carbon monoxide (CO) intoxication showed a range of perceptual problems that could not be explained by the low level changes in the visual system. She could detect spots of light in the central 30˚ of the visual field, could correctly detect gratings with high spatial frequency and had grossly preserved colour vision. The visual functions related to higher ventral cortical areas, however, were markedly compromised. She was unable to recognise line drawings and could not copy them. However, visual capabilities mediated by "vision for action" such as motion perception, grasping action, and scaling the finger aperture to the grasping target were normal (Milner *et al.*, 1991; Goodale, 2011). Another task commonly used to dissociate the vision for action and vision for perception involved either turning the card to match the orientation of the slot (perceptual task) or "posting" the card itself into the randomly oriented slot (action task) - Figure 1.16. In this task, DF could appropriately place the card into the slot but failed at matching the orientation. These results suggested that DF could accurately generate action towards objects in the environment without perceptual capacities (Goodale *et al.*, 1991). Similar dissociation in the tasks mediated by the vision for action and the vision for perception have been reported more recently in other patients suffering from visual form agnosia with more circumscribed brain lesion along the ventral stream (Dijkerman *et al.*, 2004; Karnath *et al.*, 2009) .

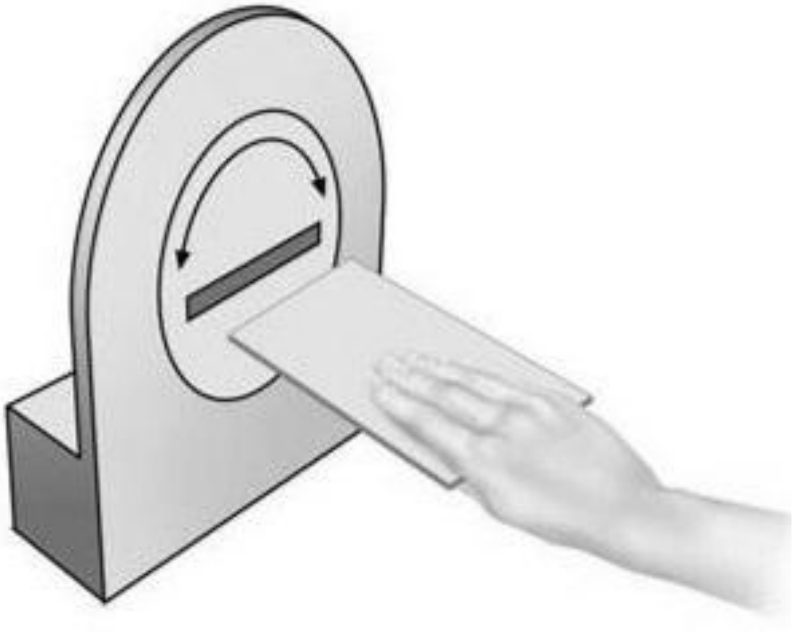

Figure 1.16: The card and slot test

In this test, patients are required to orient the card in space according to the orientation of the slot (vision for perception task) or place the card itself in the slot (vision for action task). Adapted from Milner and Goodale (1996)

The opposite pattern was observed in patient with optic ataxia who had lesions in the parietal cortex (dorsal stream). These patients could accurately describe object properties such as orientation, size, and shape but failed to properly orient the hand movements to grasp the object. Similarly, these patients could correctly match the orientation of the card according to the randomly presented slots but failed at placing the card in the slot [for review (Goodale, 2011)]. These observations led to a broad encapsulation of the functional bifurcation of the What and Where system into the vision for action and vision for perception. According to the updated theory, the ventral stream encodes the perceptual information including object characteristics and spatial relations such as size, orientation, shape, and texture – *vision for perception*. The dorsal stream meanwhile was proposed to be involved in the functions that encode actions towards the visual world such as motion perception, ocular movement, and other visually guided behaviour – *vision for action*.

Blindsight refers to a condition in which a patient with damaged primary visual cortex retains limited visual perception. It is reported that different cortical areas along the dorsal stream of blindsight patients respond to visual stimulation, implying that vision for action can be stimulated independently of vision for perception (Milner and Goodale, 1996; Cardoso-Leite and Gorea, 2010). These responses are proposed to be due to the projections from the superior colliculus to the dorsal stream areas (such as PPC). The ventral stream also receives input from the superior colliculus however these inputs do not have a similar influence as they do along the dorsal stream (Milner and Goodale, 2006).

Historically, the independence of dorsal and ventral visual streams in humans has been based around anatomical lesion studies. However, these studies are difficult to validate as it is often difficult to determine the localisation and true extent of such lesions. Indeed, patient DF whose results were widely presented as overwhelming evidence of the bifurcation of visual system into dorsal and ventral streams (Goodale and Milner, 1992; Milner and Goodale, 2008; Goodale, 2011) shows a diffuse, widespread cortical neuronal damage (Cardoso-Leite and Gorea, 2010). Furthermore, it is difficult to ascertain if the inability of the observer in a particular task is a direct result of the cortical lesion of a specific area. For example, a lesion in the area MT that results in difficulty in motion perception could be due to MT being an important area for motion but also there is a possibility that the damage in the area could result in the loss of the connections of area MT to other visual areas that may be equally important in motion processing. Additionally, some patients over time recover limited capabilities for visual functions attributed to the compromised area. This recovery is believed to be due to the reorganisation of the cortical connections by which the remaining healthy cortical areas take over the role of the compromised cortical areas (Payne *et al.*, 1996). Hence the visual cortical system appears to exhibit a tremendous amount of plasticity in comparison to the rigidity of functional segregation as suggested by the bifurcation of the visual pathway into dorsal and ventral processing streams. More recent lesion studies would also appear to contradict the original lesion studies on which the bifurcation of the dorsal and ventral stream was initially based. For example, anatomical lesions in the ventral pathway with intact dorsal pathway resulted in deterioration of motion processing capabilities in a wide range of tasks (Gilaie-Dotan *et al.*, 2013).

1.2.2 Evidence of functional bifurcation regarding the two-streams hypothesis in normal population

Behavioural evidence presented in support of the double dissociation in healthy individuals is based on the differences in response to various tasks purported to be processed along each stream. By definition vision for perception would be affected by perceptual illusions (such as size, tilt, or depth illusions). Assuming the streams are independent, the vision for action stream should remain unaffected. In size illusions such as Ebbinghaus/Titchener circles, the perceptual estimation of the size of the central circle is affected by the surrounding circles (Figure 1.17). However, dorsal stream remains unaffected by such illusions with the observer's grasp aperture accurately reflecting the actual size of the circle rather than the perceived one (Aglioti *et al.*, 1995). Similar findings from other size illusions such as the Ponzo illusion (Ganel *et al.*, 2008) and Muller-Lyer illusion (Otto-de Haart *et al.*, 1999) also support the dissociation of visual processing into the dorsal and ventral streams. Other studies, however, dispute the evidence from the illusion studies. Franz and colleagues (2000) reported that both vision for action and vision for perception are equally affected by size illusions if the stimuli are scaled properly for the task being evaluated (Franz *et al.*, 2000; Franz, 2001; Franz and Gegenfurtner, 2008). In defence of these inconsistent findings, Goodale (2011) suggests that such findings may merely represent the interaction between the two streams rather than a complete refutation of the two stream theory. It has also been reported that unless the illusions probe higher brain areas in the ventral stream, the illusory effect will be observable in both streams (Milner and Dyde, 2003). For example, the illusion that is processed in V1 may affect both dorsal and ventral stream functions but those which are perceptually processed along the higher ventral stream areas does not affect the tasks related to dorsal stream.

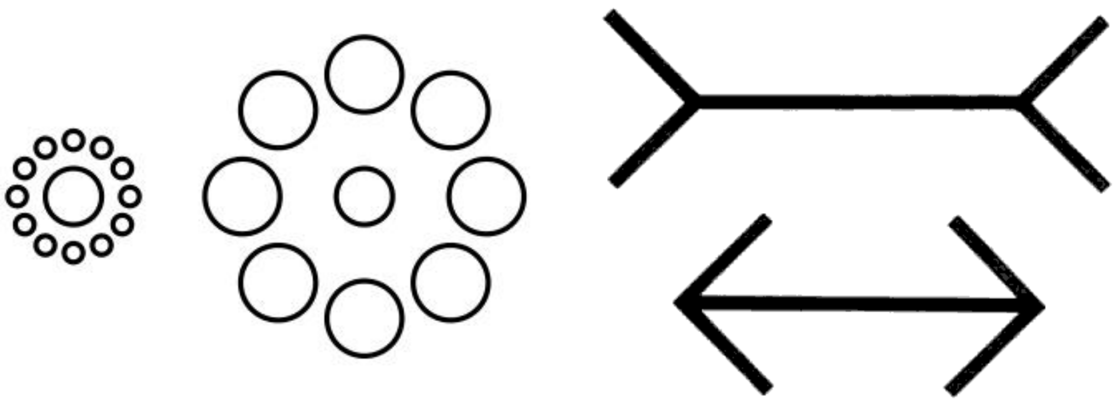

Figure 1.17: The size illusions: Ebbinghaus/Titchener circles and Muller-Lyer illusion.

In the Ebbinghaus/Titchener circles (left), the perceived size of the central circle is influenced by the size of the surrounding circles. In the Muller-Lyer illusion (right), the perceived length of the central line is influenced by the direction of the arrow heads (pointing inwards or outwards). The vision for action and vision for perception streams are affected differently by such illusions.

1.2.3 Imaging studies supporting the bifurcation theory

The development of better imaging techniques has enabled the study of different brain areas selective to various behavioural tasks in patients with different cortical lesions as well as healthy populations. fMRI evaluation of patient DF (with a lesion in the occipito-temporal cortex resulting in form agnosia) showed no activation in the lesion areas as well as in the early intact areas along the ventral stream while observing line drawings of common objects (James *et al.*, 2003). On the other hand, fMRI in normal individuals showed activation of ventral areas while the observer was discriminating the physical attributes of the object but no activation during grasping (Goodale, 2011). Other studies report findings from visual areas which are selectively activated by different stimulus properties such as complex form (Wilkinson *et al.*, 1998; Wilkinson *et al.*, 2000; Pasupathy and Connor, 2001), faces (Kanwisher and Yovel, 2006), and different objects (Malach *et al.*, 1995). These findings have further highlighted the fact that the human visual system does contain anatomically distinct areas dealing with different stimulus properties in accordance with the specialised channels hypothesised by Milner and Goodale (1996, 2006, 2008). Others have identified several regions with neurones responsive to the grasp-related activity along the proposed dorsal stream in the parietal cortex (Galletti *et al.*, 1997). These areas in the intra parietal sulcus have been named as the parietal reach region (PRR). In primates, PPR neurones are activated by the arm movements during grasping but not by the eye movements while lateral intraparietal cortex (area LIP) is activated by the eye movements and not by the arm movement (Snyder et al., 1997). Similarly in humans, the anterior intraparietal (AIP) area is shown to be more active during the reaching to grasp action compared to only reaching action or when judging the size and orientation of the 3-D objects.

A fMRI experiment (Ferber *et al.*, 2003) used the structure from motion stimuli (where a form is defined by motion boundary) to investigate dorsal and ventral stream activity. In such presentation, observers continue to perceive object's form for a brief time period (1-2 sec) even after the motion is stopped. The results showed that both motion area (MT+) along the dorsal stream and form area (lateral occipital region, LO) along the ventral stream are activated by such stimuli. However, it was observed that the activation of area LO continued even after the motion was stopped, with the period of activation of LO area correlating with the perceptual persistence (visibility of the post-motion form).

The evidence from the various physiological, behavioural, and imaging data provided here shows that it is highly unlikely that the bifurcation of visual processing into the dorsal and ventral streams is completely segregated and independent, both anatomically and functionally as Milner and Goodale (2006) have now conceded.

They suggest that both vision for action and vision for perception use the same visual inputs but the difference is in how each stream transforms these inputs for two different functions, one for perceptual judgement (ventral stream) and another for the generation of action (dorsal stream). In view of such arguments, it seems plausible to consider the dorsal and ventral streams as interactive, flexible channels which process the visual information from the early parallel processing in LGN (in terms of magno, parvo, and koniocellular processing) into the outputs suitable for the functionality of each stream.

1.3 Noise and Human Visual System

In the everyday environment, humans perceive hundreds of objects in clutter moving in different directions. Yet, they rarely have to decode motion or form information of an object in isolation. Selecting relevant signals in the presence of background clutter is an important function of any signal processing system. In addition to the variation in the input signal from the environment, the system has to deal with internal randomness generated within it during the signal processing. This random disturbance is collectively termed as "noise", which is an inherent feature of every mechanical as well as biological signal processing system. Noise present in the signal is called external noise while that generated within the processing system is called internal noise. To properly study how a signal is represented in any signal processing system, both external and internal noise should be considered.

During visual processing, photoreceptors convert light energy present in the stimulus to chemical signals which are subsequently amplified and converted into the electrical signal to be detected. Any external noise present in the signal is also amplified during this process. The action potential generated by a single neurone in response to the identical electrical signal varies over time. These fluctuations (noise) are a result of cellular and molecular variations within the neurones such as variability in membrane potential or variations in electrical discharges from different ion channels. At synaptic terminals, more noise is generated due to the fluctuations in diffusion or differences in calcium channel noise (Faisal *et al.*, 2008). At each step of signal processing, signals that are weaker than the accumulated noise are lost. Noise is hence ubiquitous in each processing component of the human visual system.

The noise generated within the visual system can be broadly divided into sensory noise and noise due to decision uncertainty (Faisal *et al.*, 2008). When the identical stimulus with the same visibility at threshold is presented twice to an observer, the response of the observer may differ (Burgess and Colborne, 1988) due to the variability in the response of different sensory mechanisms. This type of noise is called sensory noise (Faisal *et al.*, 2008). Another source of noise in the visual processing system is due to the decision uncertainty of the observer. The response of an observer to a same set of stimuli becomes more inaccurate when presented in the presence of other confounding stimuli (for example, when observers are asked to determine the relative size of two objects, the response is more inaccurate when these objects are presented with other similar objects compared to when they are presented in isolation).

Initial methods to characterise the noise in signal processing systems were developed by electrical engineers to measure the response of an electronic amplifier (North, 1942; Friis, 1944; Nagaraja, 1964). The underlying assumption of this method is that the output from any processing system is directly proportional to the sum of the noise present in the signal (external noise) and noise introduced by the components of the system itself (internal noise). When the added external noise is low, the output of an amplifier is governed by the internal noise and constant signal strength is required to maintain a constant signal to noise ratio over a range of external noise. When the external noise exceeds the internal noise of the system, output of the system is overwhelmed by the external noise and increasingly higher signal strength is required to maintain a constant signal to noise ratio. At the point where the external noise starts to take over the performance of the system, both external noise and internal noise have an equal effect on the performance and this level of external noise is equivalent to the internal noise of the system. The equivalent external noise method hence calculates the internal noise of the system in terms of the added external noise, which is described as "refereeing the internal noise of the system to the external noise" (Pelli, 1981).

In the early 1940s, vision scientists *e.g.,* (de Vries, 1943) began to explore the presence of noise in the visual system and its significance on visual processing. After a decade, Barlow (1956) introduced the term dark noise to represent the spontaneous activity of neurones in the absence of any physical stimuli. He proposed that for light to be detected in complete darkness, the absolute signal strength should be greater than the dark noise. In the 1970s, signal detection theory (Green and Swets, 1974), greatly advanced our understanding of the role of noise in signal processing and decision mechanism. The signal detection theory (SDT) evaluates variability in the decision making by an observer in different visual tasks. According to SDT, observer makes the decision of perceptual awareness (detection or discrimination of the object) based on a subjective criterion. If the accumulated signal strength is larger than this criterion, observer reports the presence of the signal. If the accumulated signal strength is weaker than the criteria, observer reports an absence of the signal. In some trials due to the effect of noise, an observer may report the presence of a signal even when the signal was absent. These trials are recorded as false alarms. Similarly on other trials, an observer may report an absence of signal even when the signal was present; these are recorded as the miss trials. In SDT, the observer's sensitivity is measured as the separation between the means of signal and noise distributions compared against the standard deviation of the noise distribution. SDT provides a bias free representation of the human performance (d') but does not deal with the nature of noise itself.

Barlow's concept of dark noise (Barlow, 1956) and the equivalent noise method used in electrical amplifier formed the basis of measuring equivalent internal noise in the visual domain. Barlow's proposal of the quantification of signal strength in terms of energy required to overcome dark noise and internal noise is only relevant in dark conditions. However, a similar concept can be adapted to the detection of different visual properties based on the equivalent noise method. Pelli (1981) proposed a black box model for the visual domain comparing the human observer to an electronic amplifier (Figure 1.18). In this model, the observer receives signal embedded in the external noise. The processing of this signal results in the addition of more noise (internal noise). The final perceptual decision is then made based on the resulting internal representation after the calculation. In such a model, different variability and fluctuations within the visual system are represented by a single component of internal noise. The model also assumes that the processing within the system is linear until the late decision stage and that the magnitude of the internal noise and the calculations are invariant with the strength of the stimulus.

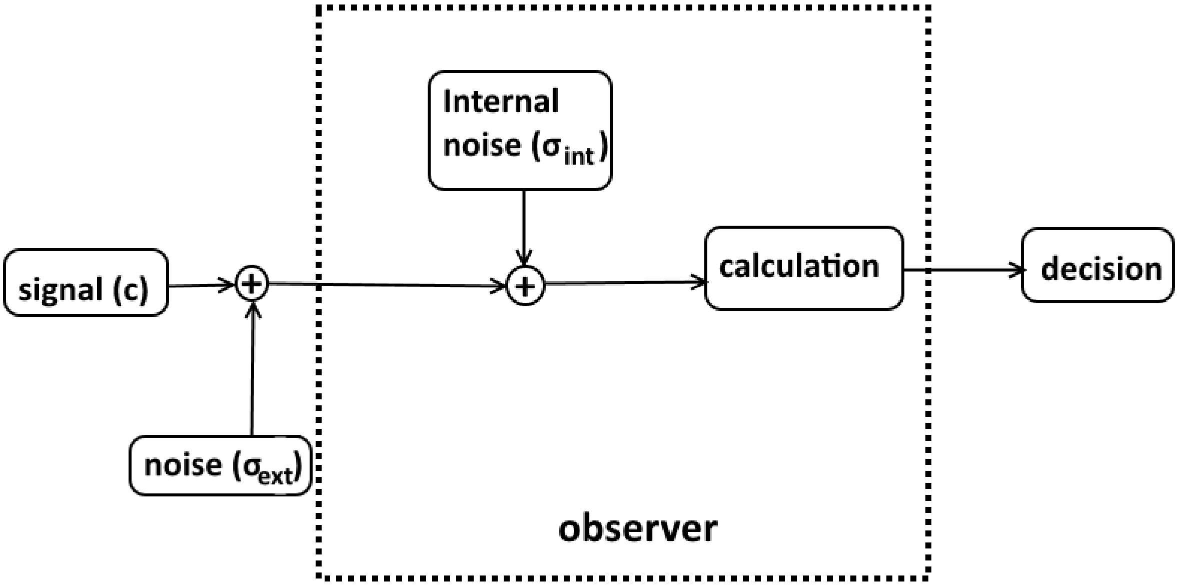

Figure 1.18: A black box model for human observer

The human observer is treated as a black box receiving the signal (c) embedded in noise (σ_{ext}*), the processing mechansim adds a fixed amount of variability (internal noise,* σ_{int}*) and the representation undergoes calculations to provide an internal response upon which the final decision is based. Adapted from Pelli (1981, 1999).*

For such a model, human response to varying contrast energy as input can be measured in terms of contrast energy threshold. Furthermore, external noise can be added by introducing luminance noise to the input display. Hence in such an arrangement with a contrast threshold experiment, the output of the processing system can be measured in terms of the input (signal plus noise) as required for the application of the equivalent noise method (Pelli, 1981; Ahumada and Watson, 1985). According to the prediction of the equivalent noise method when the contrast threshold is plotted against the added external noise, the threshold vs. noise curve (*TvN* curve) should remain flat and low at low levels of external noise and elevate proportionally to the added external noise at high noise levels. The knee point of the *TvN* curve then represents the internal equivalent noise of the system (Figure 1.19).

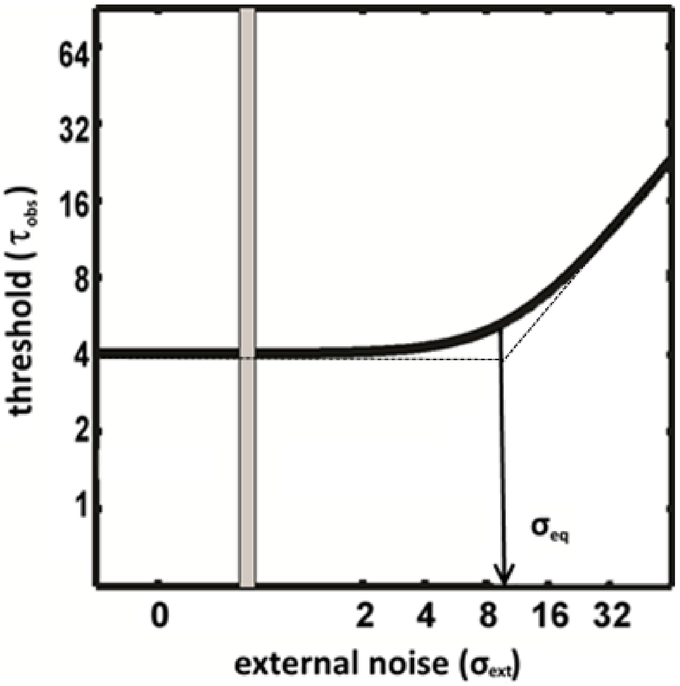

Figure 1.19: Schematic representation of the prediction from the equivalent noise model

The thresholds remains low and constant across a range of low external noise levels and increases exponentially at high noise levels with the knee point of the curve representing the internal equivalent noise of the system (σ_{eq}).

Pelli (1981) applied a simple linear model based on equivalent noise method to analyse the contrast threshold obtained at various external luminance noise levels. For a given stimulus with the contrast (*c*) embedded in random noise generated from the Gaussian distribution with standard deviation (σ_{ext}), the total energy is given by eq. 1.1.

$$S = \beta c \qquad \textbf{(\textit{eq.} 1.1)}$$

where, β is linear amplification by a noise-free amplifier

The total noise reaching the decision stage (*N*) is the sum of the external noise and internal noise (*eq*. 1.2).

$$N^2 = \sigma_{ext}^2 + \sigma_{int}^2 \qquad \textbf{(\textit{eq.} 1.2)}$$

The signal discriminability (*d'*) for such arrangement is given by the SDT as

$$d' = \frac{S}{N} \qquad \textbf{(\textit{eq.} 1.3)}$$

Substituting the values of eq. 1.1 and eq. 1.2 to eq. 1.3 gives

$$\boldsymbol{d' = \frac{\beta c}{\sqrt{\sigma_{ext}^2 + \sigma_{int}^2}}} \qquad \textbf{(\textit{eq.} 1.4)}$$

For the detectability (*d'*) at a contrast threshold (τ_{obs}), eq. 1.4 can be rearranged as

$$\boldsymbol{\tau_{obs}^2 = \left(\frac{d'}{\beta}\right)^2 \left(\sigma_{ext}^2 + \sigma_{int}^2\right)} \qquad \textbf{(\textit{eq.} 1.5)}$$

We can simplify the eq. 1.5 by replacing *d'/β* with *k* by considering *β* as a constant for *d'.* So,

$$\boldsymbol{\tau_{obs}^2 = (k)^2 \left(\sigma_{ext}^2 + \sigma_{int}^2\right)} \qquad \textbf{(\textit{eq.} 1.6)}$$

The factor *k* is inversely proportional to the calculation efficiency of the system, which is computed by comparing *k* for the human observer with an ideal observer and is regarded as an index of information available for the system (Pelli, 1981; Pelli and Farell, 1999). Hence the equation provides a model consisting of internal equivalent noise (σ_{int}) and sampling efficiency parameter (*Eff*) for fitting the threshold data (τ_{obs}) measured in the presence of varying levels of external noise (σ_{ext}) – eq. 1.7.

$$\boldsymbol{\tau_{obs} = \sqrt{\frac{\sigma_{ext}^2 + \sigma_{int}^2}{Eff}}} \qquad \textbf{(\textit{eq.} 1.7)}$$

where,

τ_{obs} = observed contrast threshold
σ_{int} = equivalent internal noise external noise
σ_{ext} = external noise
Eff = sampling efficiency

The model from equation 1.7, dubbed as the linear amplifier model (Lu and Dosher, 1999), predicts the observer's performance as a linear function of noise variance and efficiency (Figure 1.20). If the performance of an observer varies across two tasks due to the differences in the internal noise parameter, the *TvN* curves for two functions remain parallel at the lower levels of noise before converging at higher noise levels. If the variation in performance is due to the differences in the sampling efficiency parameter, *TvN* curves remain parallel across all external noise levels.

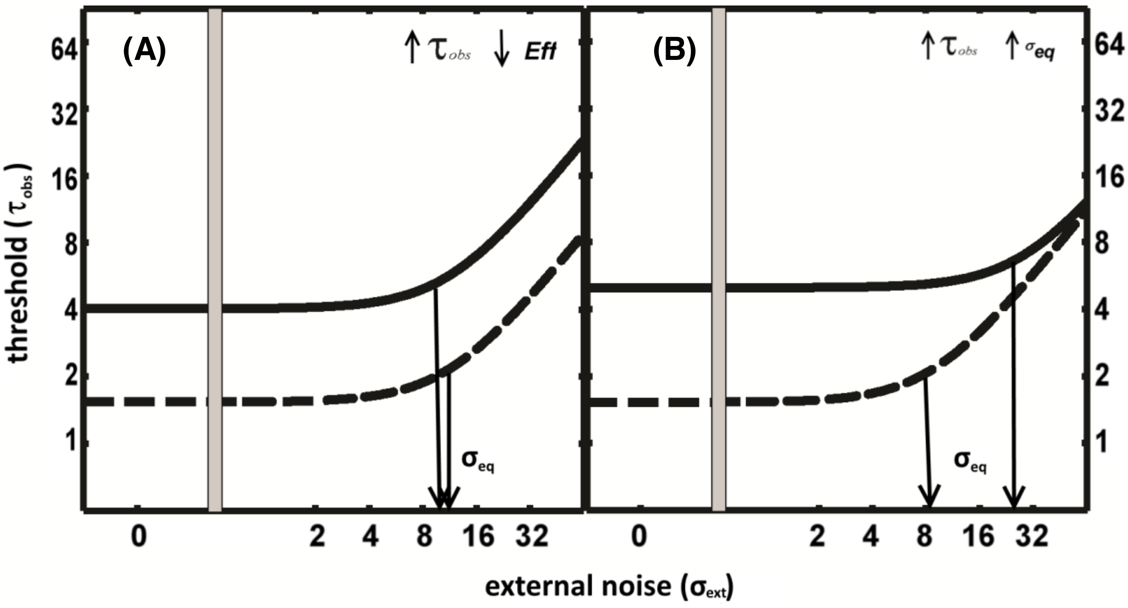

Figure 1.20: Schematic representation of the predictions of linear amplifier model (LAM).

If the thresholds for two functions differ due to changes in sampling efficiency (Eff), TvN curves remain parallel at all noise levels (A) but if the thresholds differ due to changes in the internal noise, TvN curves converge at higher noise levels (B).

Pelli (1990) adapted his model to study the effect of different visual attributes such as target size, background luminance, and the effect of eccentricities on contrast threshold. While contrast threshold was limited by internal noise or sampling efficiency, the underlying amount of internal noise remained similar. Pelli and Farell (1999) proposed that the efficiency of the visual system is largely independent of external viewing conditions and that the internal equivalent noise is dependent only upon the anatomical variance of the processing mechanism (Pelli and Farell, 1999).

Most of the works to date that have employed the equivalent noise (EN) paradigm in the visual processing system have been conducted in the contrast domain (Ahumada and Watson, 1985; Pardhan *et al.*, 1996; Bennett *et al.*, 1999; Radhakrishnan and Pardhan, 2006; Levi *et al.*, 2008). More recently the paradigm has been extended to various visual functions including visual acuity (Pelli *et al.*, 2004), stereo acuity (Wardle *et al.*, 2012), and perceptual learning (Gold *et al.*, 2004).

1.3.1 Noise in Dorsal and Ventral Stream

Previous research on motion and form processing in noise has most commonly used random noise to determine the sensitivity to coherent motion/form (Gunn *et al.*, 2002; Simmers *et al.*, 2003b; Lewis *et al.*, 2004; Simmers *et al.*, 2006b; Grinter *et al.*, 2010; Hadad *et al.*, 2015). More recent works have sought to quantify the nature of noise itself in these domains. The motion and form sensitivity measured at varying levels of noise have been used to unravel the processing limitations at different stages of visual processing. Normal visual processes (Watamaniuk and Sekuler, 1992; Watamaniuk, 1993; Dakin *et al.*, 2005; Mareschal *et al.*, 2008), visual development/ageing (Bogfjellmo *et al.*, 2013; Bogfjellmo *et al.*, 2014; Manning *et al.*, 2014), and abnormalities in visual functions in various clinical disorders (Mansouri *et al.*, 2004; Hess *et al.*, 2006; Falkenberg and Bex, 2007; Tibber *et al.*, 2014; Manning *et al.*, 2015) have been modelled with the consideration of noise in both the motion and form domains. However, due to the physical limitations in the stimuli employed, it is often difficult to directly compare the motion and form domains.

The influence of noise on global motion and global form visual processing mechanisms has been psychophysically evaluated to specifically target the processing along the dorsal and ventral streams. As described earlier (Section 1.1), the major areas for global motion and global form processing predominantly fall under the proposed dorsal and ventral stream respectively. Other studies, however, suggest that the processing of global motion and global form is not limited to the respective streams. For example, Braddick *et al.,* (2000) using fMRI reported that while motion and form stimulate independent pathways in the visual system, these pathways may not necessarily correspond to the gross segregation of the dorsal and ventral streams (Braddick *et al.*, 2000). They, however, do report a strong motion response in the area around MT and MST, while areas more responsive to form stimuli lay near the proposed ventral stream. Using similar techniques, other studies report increased responses from area MT along the dorsal stream (Braddick *et al.*, 2001) and area V4 along the ventral stream (Braddick *et al.*, 2002) with the increase in the global motion and form signals respectively. The notion that motion and form are processed by completely independent pathways is a debate that is closely mirrored by the dis/agreements on the independence of the parallel dorsal and ventral streams that have been discussed before (Section 1.2). However, even the staunch critics of the parallel processing mechanism agree that area MT has a special importance for motion processing (Lennie, 1998). Similarly, in the light of different studies showing V4 selectivity to complex form stimuli (Wilkinson *et al.*, 1998; Gallant *et al.*, 2000; Smith *et al.*, 2002; Tse *et al.*, 2002; Ohla *et al.*, 2005), it can be assumed that motion and complex form do stimulate at least limited independent mechanisms. The interaction between motion and form processing pathways is yet to be fully understood and such interaction will also be explored in this body of work. Despite the controversy surrounding the parallel processing of motion and complex form along the dorsal and ventral streams, motion and form stimuli have been widely used in behavioural studies in the vision science arena for the evaluation of dorsal and ventral processing streams in both normal and clinical populations [for review (Braddick *et al.*, 2003; Grinter *et al.*, 2010)].

The Random dot kinematogram (RDK) has been most commonly used to evaluate motion perception along the dorsal stream. Different stimuli including Glass patterns (Glass, 1969), Gabor patches, and objects of different shape and curvature have been used to probe ventral stream processing (further discussed in the methods section 2.3). The random dot kinematogram and Glass pattern are most suited for the concurrent investigation of motion and form processing as both stimuli share common physical properties and processing mechanisms. Random dot kinematograms (RDK) are based on the phenomenon of apparent motion. When two static images are spatially displaced in time at appropriate distance and interval, a smooth motion from one point to another is perceived. RDKs consist of patterns of dots which are temporally displaced to adjacent frames in a predefined direction. Glass pattern is named after Leon Glass who observed that when an identical set of random dot pattern (dipole) is superimposed upon another and rotated to a certain extent about its central axis, a compelling and readily observable swirling pattern is formed (Glass, 1969). Translational, radial and concentric structures can be created based on the angle of displacement by aligning the correlated pairs of dots to a desired geometric transformation (Figure 1.21).

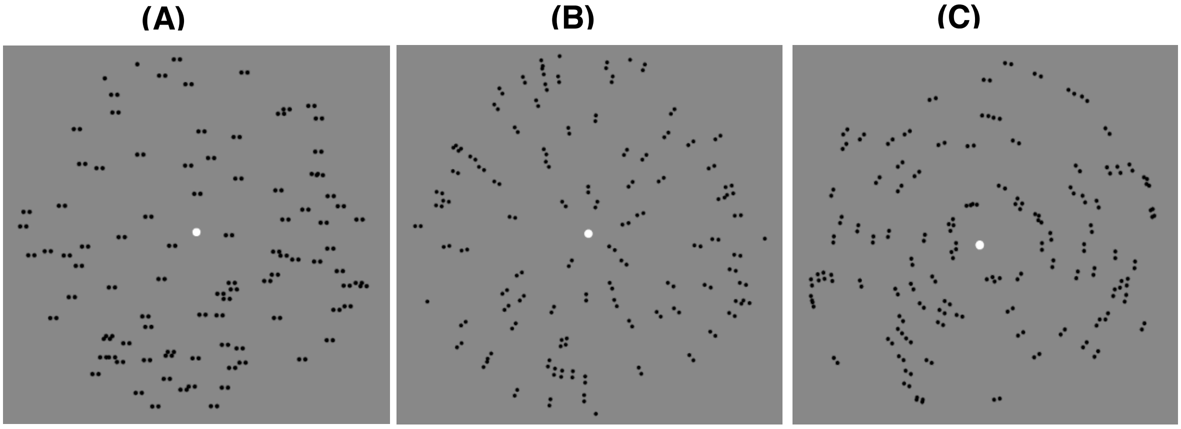

Figure 1.21: Schematic illustrations of different types of Glass patterns.

Horizontal translation (A), radial (B) and rotational (C)

RDKs and Glass patterns also share similar processing mechanisms. The local properties of RDKs are initially processed in the primary visual cortex followed by the global processing at higher extra striate areas of MT and MST. Similar to RDKs, the processing of Glass patterns also occurs in two distinct stages. In the first stage, local properties of dipole elements such as orientation and contrast are processed in primary visual cortex resulting in the integration of corresponding dots into dipoles. The global processing, integrating information from all dipole pairs to provide an overall orientation of Glass pattern, then occurs at higher extra striate areas along the ventral stream with area V4 being the most likely candidate (Wilson *et al.*, 1997; Wilson and Wilkinson, 1998; Tse *et al.*, 2002; Wilson and Wilkinson, 2003; Wilson *et al.*, 2004; Mandelli and Kiper, 2005; Dumoulin and Hess, 2007; Smith *et al.*, 2007).

Another important limitation in the evaluation of dorsal and ventral stream function thus far has been that the performance from each pathway is difficult to compare against each other as stimuli used are physically different (Grinter *et al.*, 2010). The Glass pattern is composed of dipole elements that are separated by a predefined distance in a specific direction. In RDK the dot elements are displaced by a predefined distance and direction over different frames. Hence a Glass pattern can be thought of as a snapshot of the RDK taken at two different times (two frames). Both stimuli can be created using dot patterns, which allows for the control of most of the physical parameters such as dot size, density, contrast etc.

Both RDKs and Glass patterns are also ideal to study of the influence of noise within the visual system. RDKs are most commonly used to study motion perception employing the motion coherence paradigm. In such a paradigm, dots carrying the motion signal in a defined direction are interspersed with dots carrying random motion (noise dots) (Newsome and Pare, 1988). The minimum proportion of the dots carrying signal direction required for detection of coherent motion is known as the motion coherence threshold (Figure 1.22). Even in the presence of different non-corresponding dot elements (noise) in the vicinity of an individual dot from one frame to another, visual system can easily perceive the apparent motion created by the displacement of individual dot pairs – referred to as overcoming the correspondence problem. The visual system is well adept at perceiving coherent motion from such display with thresholds as low as 5% for accurate judgement of motion direction.

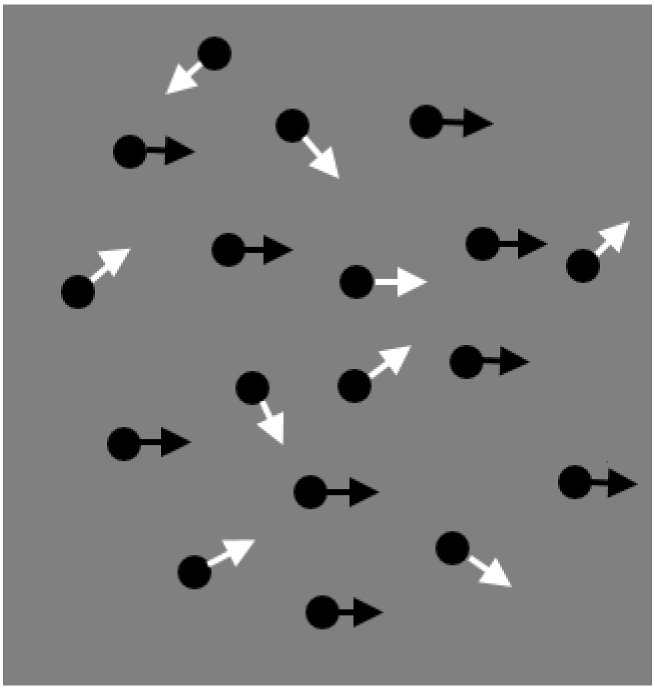

Figure 1.22: Schematic representation of motion coherence paradigm.

In the motion coherence threshold paradigm, the signal dots carry motion in a specified direction (represented by dots with black arrow, to right) interspersed with noise dots carrying random motion (represented by dots with white arrow).

Similar to the RDK, the addition of diploes with random orientation (noise) to Glass patterns reduces the ability of global detection and discrimination. Psychophysical experiments (Dakin and Bex, 2002; Lewis *et al.*, 2004; Spencer and O'Brien, 2006;

Nankoo *et al.*, 2012) have used this feature to evaluate the sensitivity of the visual system to global form in terms of form coherence thresholds, the minimum proportion of dipole pairs with coherent orientation required for the global detection (Figure 1.23).

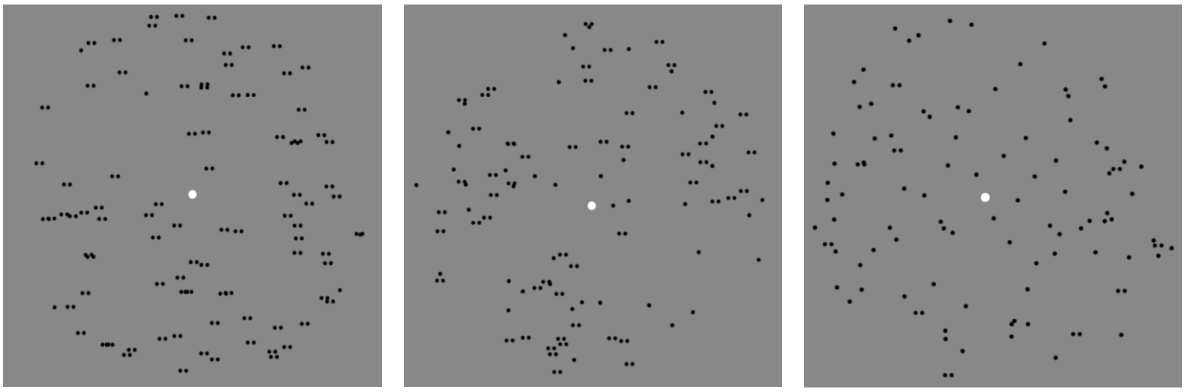

Figure 1.23: Schematic representation of coherence paradigm in translation Glass pattern.

The number of coherent dipoles in translation Glass pattern decreases from 100% to 60% to 10% from left to right.

The coherence threshold paradigm measures the influence of noise in terms of the number of elements (signal dots in a RDK, signal dipoles in a Glass pattern). As explained for the contrast domain, the pre-requisite for the equivalent noise paradigm is that the output of the signal processing system should be measured in terms of the input signal and added external noise. So the paradigm should be designed in order to "refer the system's internal noise to the external noise added to the input signal". The coherence threshold paradigm is hence unsuitable for the study of the external noise paradigm, as the observer's performance (output in terms of number of signal dots) cannot be directly referred to the property of added noise.

Another method for the evaluation of motion and form perception using RDKs and Glass patterns is with a task in which an observer has to determine the overall direction of motion or orientation of the RDK/Glass pattern from a reference direction/orientation (such as vertical) with the external noise being varied in the same parameter (direction/orientation from vertical). This method allows for the estimation of an observer's performance in terms of external noise added to the stimuli and hence is ideal for the adaptation of the equivalent noise paradigm (Figure 1.24).

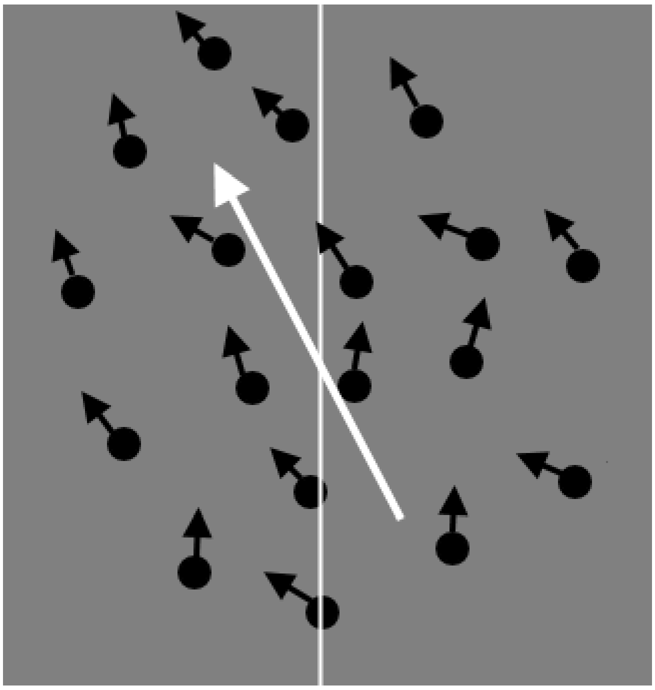

Figure 1.24: Schematic representation of fine direction discrimination paradigm.

In the fine direction discrimination task, the motion of individual dots (represented by black arrows) is derived from a Gaussian distribution with mean direction (represented by the white arrow) at predefined angle from vertical (here left from vertical).

In such tasks, the motion/orientation of individual elements is derived from a random distribution (usually a Gaussian distribution) with a prescribed mean and standard deviation. Hence all individual elements have independent local motion/orientation but when the motion/orientation cues from all dots are summated, the global motion/orientation representing the mean of the underlying distribution is perceived. All the dot/dipole elements in such arrangements act as signal elements as they represent the overall mean direction/orientation and the randomness (external noise) can be manipulated by changing the standard deviation of the distribution from which the direction/orientation of the elements are generated.

The linear model of the equivalent noise paradigm is based on the evaluation of threshold at different levels of external noise and separates the observer's performance into internal noise and sampling efficiency. For the RDK and Glass pattern, the internal noise derived from the equivalent noise paradigm experiment represents the local variance in direction of motion (RDK) and orientation (Glass pattern) of individual elements. The sampling efficiency meanwhile represents the number of elements the visual system summates to provide an overall global percept (Dakin *et al.*, 2005; Mareschal *et al.*, 2008) – Figure 1.25. The local properties of these stimuli are processed in the early visual areas (such as V1) and the global processing occurs at higher cortical areas (such as MT, MST and V4). Hence the equivalent noise paradigm can disambiguate the contribution of different cortical areas in visual processing.

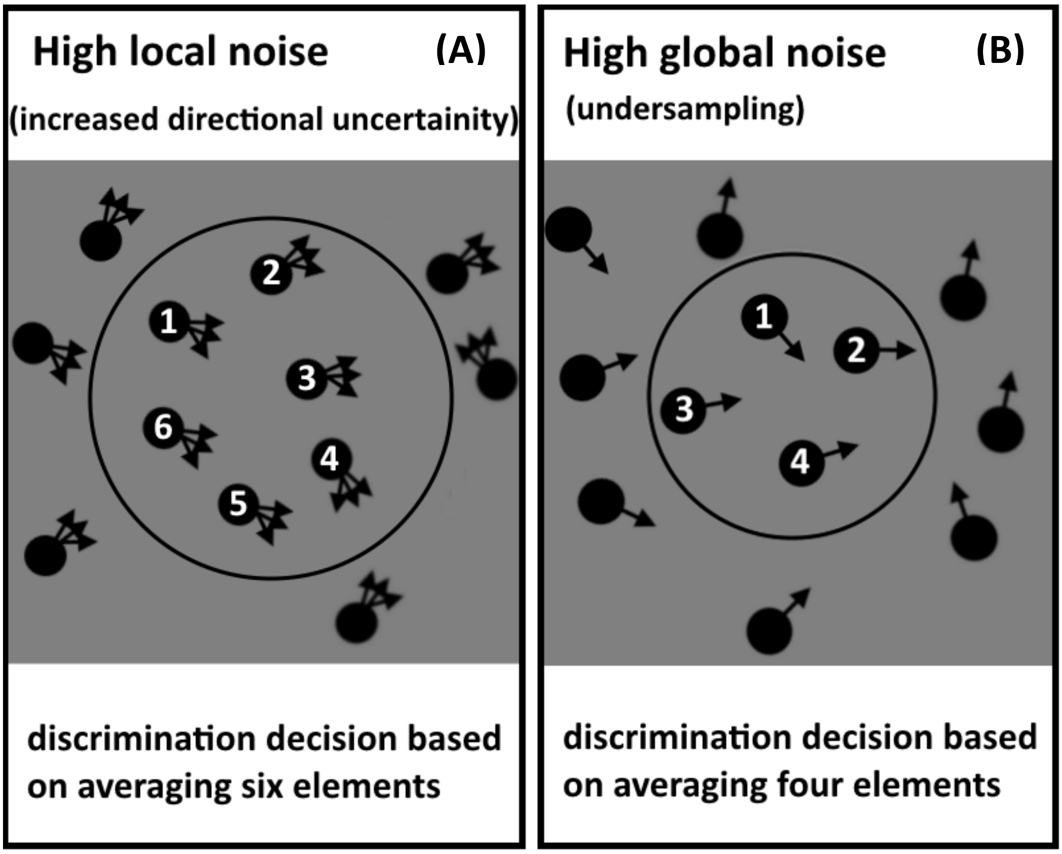

Figure 1.25: Local and global processing limitation on direction discrimination

The threshold for direction discrimination in RDK is limited by increased local directional uncertainty among the samples (A) or global undersampling of elements (B). Adapted from Mareschal et al., 2008

Summary

The visual system is proposed to be bifurcated into dorsal and ventral streams consisting of independent parallel pathways for processing various visual attributes (Goodale and Milner, 1992; Milner and Goodale, 1993; Goodale, 2011). Global motion and global form are predominantly processed along the proposed dorsal and ventral visual processing streams respectively (Braddick *et al.*, 1999; Gallant *et al.*, 2000; Wilkinson *et al.*, 2000; Braddick *et al.*, 2001). The motion and form information are initially processed along the areas shared by both dorsal and ventral streams such as lateral geniculate nucleus (LGN) and primary visual cortex (V1), where the processing from the limited area of the visual field occurs – local processing (Adelson and Movshon, 1982; Morrone *et al.*, 1995; Movshon *et al.*, 1995; Wilson and Wilkinson, 1998). These shared areas also consist of anatomically segregated units for processing motion and form attributes (Livingstone and Hubel, 1987). The local inputs from early shared areas are integrated to form a global percept at dedicated extra striate areas along each stream; for example, middle temporal (MT) and middle superior temporal (MST) areas for motion perception and area V4 for form perception (Morrone *et al.*, 1995; Wilson and Wilkinson, 1998). Motion perception is reported to be affected more than the form perception in various developmental disorders, leading to the assumption of dorsal stream dysfunction in these disorders [for review (Braddick *et al.*, 2003; Grinter *et al.*, 2010)].

Most of the previous studies have used motion and form stimuli that may not be compatible for the comparison of two processing streams (Grinter *et al.*, 2010). To compare the processing along each stream, the physical properties of the input stimuli have to be made as identical as possible to ensure that the outputs can then be attributed to the specific processing mechanism rather than the difference in the stimulus properties. In the current thesis, random dot kinematogram (RDK) and Glass pattern (Glass, 1969) were used to investigate motion and form processing. Both stimuli can be composed of random dot patterns allowing for the control of most physical parameters. Similarly, both stimuli share identical processing mechanisms within the dorsal and ventral streams; the local processing of motion (RDK) and orientation (Glass pattern) occurs in area V1 followed by the global processing within dedicated extra striate areas along dorsal

(MT) and ventral stream (V4) respectively (Morrone *et al.*, 1995; Wilson and Wilkinson, 1998). More recent studies suggest that visual processing including motion and form perception occurs through relatively flexible processing mechanisms with substantial interactions among two mechanisms (Kourtzi *et al.*, 2008; Mather *et al.*, 2012). Dynamic Glass pattern (Ross *et al.*, 2000), in which a perception of motion is induced by the underlying form cues of static Glass patterns, was used to explore interactions between motion and form perception in the current thesis.

Motion and form perceptions have most commonly been studied using the coherence threshold paradigm in which motion/form sensitivity is measured as the minimum number of signal elements required to make a correct motion/orientation judgement in the presence of random noise. The coherence threshold paradigm, using random noise, provides an overall estimate of the visual systems sensitivity without revealing the contributions from local and/or global processing stages. The quantification of noise can help to unravel the contribution of local and global processing mechanisms (Dakin *et al.*, 2005). This can be achieved by measuring sensitivity in the presence of varying levels of added external noise. In this thesis, we explore motion and form processing mechanisms and their interactions using physically similar stimuli embedded in noise to parse out the effects of the local and global processing in normal and clinical populations.

2.0 General Methods and Instrumentation

2.1 Psychophysical Methods

The psychophysical study of vision science deals with how changes in the physiological state in response to external stimuli result in a perceptual outcome. Sometimes the physiological process can be studied directly by recording responses from different areas of the visual system using electrophysiological and imaging methods. However, it is not always possible to make such measurements and studying the responses from isolated areas to provide an overall representation of the visual system has remained challenging even with the most recent advancements in the field of electrophysiology and neuroimaging.

Gustav Fechner was among the first scientists to recognise that the relative changes in mental sensation can be quantified as a function of changes in the physical stimuli strength and that these results can be inferred to the underlying physiological mechanism. His theories formed the basis for a new field of study in relation to physiological mechanisms – psychophysics (Fechner, 1860). Instead of studying each physiological component of the visual system independently, psychophysics considers the whole visual processing mechanism as a single system. This approach allows the investigator to capture the overall performance of the observer and speculate about the processing mechanism at component levels by building different theoretical models. Marks (1978) proposed a theoretical premise, the principle of nomination, to infer the psychophysical results to the physiological state (neuronal behaviour). The principle of nomination states that identical neural events give rise to identical psychological events *i.e.,* two stimuli that produce the same neural response will result in the same sensory experience (Marks, 1978). The reflexive form of the principle meanwhile suggests that the same sensory experience produced by two stimuli is a result of the same neural responses. Similarly, Teller (1984) proposed theoretical linking propositions (Table 2.1) to infer the overall responses of the visual system (perceptual experience, Ψ) to the underlying processing mechanism (physiological state,Φ) (Teller, 1984).

Contra positive identity	Non identical Ψ → Non identical Φ
Converse identity	Identical Ψ → Identical Φ
Identity	Identical Φ → Identical Ψ
Converse contra positive identity	Non identical Φ → Non identical Ψ

Table 2.1: The linking propositions for identity experiments.

The contra positive assumption states that if the perceptual states (Ψ) are different, the underlying physiological state (Φ) must also differ. The converse identity proposition states that identical perceptual experiences (Ψ) are a result of an identical physiological state (Φ). These propositions are used to generate conclusions about the physiological state from the psychophysical data while the remaining propositions deal with generating conclusions about the psychophysical state from the physiological data. Teller (1984) argued that the converse identity proposition may not be always accurate, as in some cases varying physiological states brought on by differences in external stimuli can still result in a similar perceptual experience. For example, perception of the colour yellow could be produced by yellow light with a wavelength of 570 - 590nm or similarly with a combination of red and green light. They suggest the consideration of the ''*bridge locus neural stage*'', a hypothetical intermediate substrate of visual perception up to which the neural signals remain indiscriminable and thereby result in a statistically indiscriminable perceptual experience. Different results drawn from this modified interpretation of propositions have remained widely accepted in the field of vision science. From these principles, any physiological hypothesis can be evaluated by testing a perceptual event. The results can then be used to build theoretical models that also incorporate findings from the conventional physiological studies (such as single cell recordings, imaging studies) to better understand the contribution of different visual areas.

In the present body of work different psychophysical methods were used to explore and compare the processing along the motion and form processing streams of the visual pathway. The modelling methods were also employed to unravel the limitations along each processing stream.

Before moving to the specific method used for each experiment a general description of threshold estimation and psychometric function fit and clinical instrumentation common to different studies within this thesis are discussed.

2.1.1 Methods for threshold estimation and psychometric function

In a typical psychophysical experiment, the property of the stimulus being evaluated is varied according to the responses of the observer over a number of trials to determine the sensory threshold. A threshold is the point of stimulus intensity at which the observer can just detect the presence of a stimulus (*i.e.,* minimum detectable stimulus strength - absolute threshold). In a psychophysical experiment, threshold is determined as stimulus intensities required to produce a given level of performance. In addition to the theoretical propositions which formed the basis for the field of psychophysics, Fechner also proposed comprehensive experimental methods for threshold determination (Fechner, 1860) – Table 2.2.

Method	**Procedure**	**Threshold calculation**
Method of limit	Investigator adjusts the stimulus strength till it becomes just noticeable or unnoticeable	The average value of two stimulus strength at which the reversal occurs
Method of constant stimuli	Observer responds to repeated, randomly-ordered trials with varying stimulus strength	The stimulus intensity for a certain judgement probability (e.g. 75%) from psychometric function fit.
Method of adjustment	Similar to method of limit but observer adjusts the stimuli strength	Same as the method of limit

Table 2.2: Fechner methods for threshold determination

The method of constant stimuli (MOCS) is the most reliable and commonly used method for psychophysical data collection. In a typical psychophysical experiment employing MOCS, a number of stimulus intensity levels (typically five to nine) are presented to the observer. The levels are chosen to represent the stimulus range from the lowest stimulus strengths that will elicit the chance probability of detection to the highest intensity level that will be detected 100% of the time. This range will span a psychometric function relating the stimulus strength to the observer's performance. When the correct responses are plotted against stimulus strength, the psychometric function can be a straight transition from no-detection (0% correct) to full detection (100% correct) - Figure 2.1, A. This model of performance is also called all or none concept of threshold (Lawless, 2013). When responses were collected in various psychophysical experiments, the psychometric function however resembled a smooth sigmoid-shaped curve representing a gradual progression from absence to the presence of the stimuli (Figure 2.1, B). This characteristic sigmoidal shape was due to the inconsistency in response of the observer for the same stimulus intensity presented multiple times. Such responses results in a lower proportion of correct responses for the stimulus strengths below the threshold and a higher level of proportion correct for the supra threshold stimulus strengths. The sigmoidal shape of the psychometric functions is remarkably consistent for different sensory functions. Threshold is then determined from such psychometric functions as the stimulus intensity at a certain performance criteria (such as 75% correct).

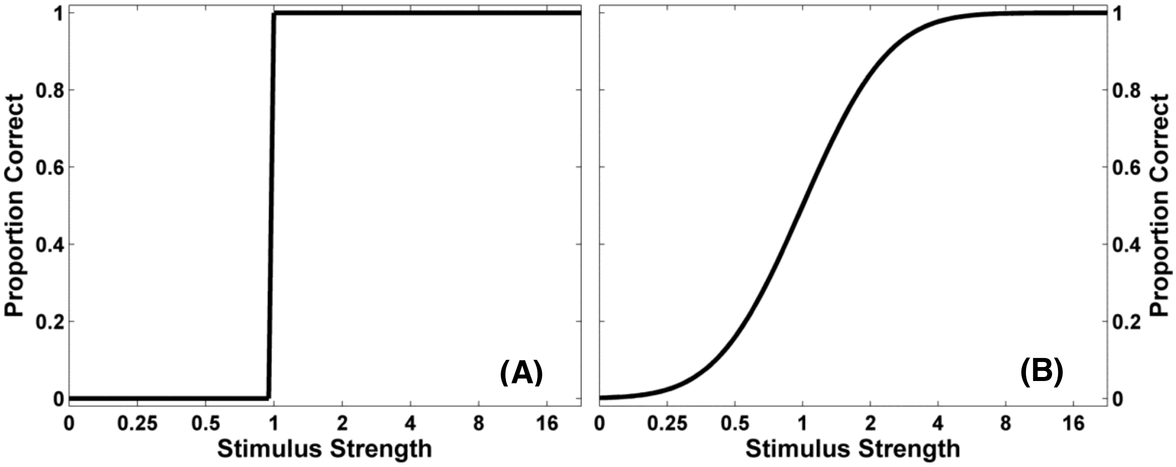

Figure 2.1: Psychometric function for a hypothetical observer on a yes/no task.

The psychometric function ranges from 0% correct to 100% correct with either straight transition from lower to upper asymptote (A) or a gradual transition following a characteristic sigmoidal shape (B).

2.1.1.1 Fitting the psychometric function

The psychometric function can be described by two variables, threshold and slope. Threshold (α) is calculated as the corresponding level of stimulus strength at a desired performance level (such as 75% correct) and the slope (β) represents the rate of change in performance with varying stimulus strength (Figure 2.2). The lower asymptote of the curve represents the chance probability called guessing rate (Υ) which is the reciprocal of the number of response choices in forced choice experiments (*e.g.,* 0.5 in 2AFC). The accurate responses to high stimulus strength result in the upper asymptote of the curve. In some trials, observers may respond to the stimulus independent of its intensity that results in incorrect responses even to highly perceivable stimulus strengths. These erroneous responses are called lapses (λ). The strength of the psychometric function fit can be improved by incorporating the lapse parameter to the fitting procedure which lowers the upper asymptote of the psychometric function as given by ($1-\lambda$).

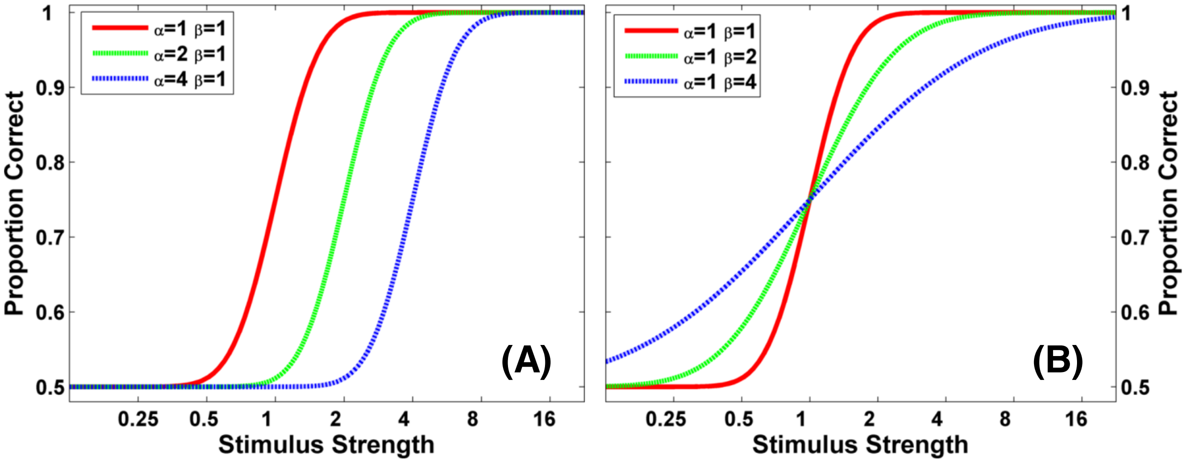

Figure 2.2 : Psychometric functions for a hypothetical observer in 2AFC task.

The figure shows that change in α is reflected along the X-axis (stimulus strength) while change in β represents the change in the slope of the function. The guess rate (ϒ) is 0.5 (for a 2AFC task). The threshold value (α) is at the detection criteria of 75%.

In a typical fitting procedure, a function that resembles the sigmoid shape such as a cumulative normal function, Weibull function, or Gumbell function is used to fit the observer's performance at different stimulus strengths. The parameters of interest (*α* and *β*) are allowed to vary (free parameters) while other two are fixed (*ϒ* and *λ*). Conventionally lapse rate is fixed at a small number, however it has been argued that the lapse rate should be treated as a free parameter for a better psychometric function fit (Wichmann and Hill, 2001). The general form of the psychometric function incorporating all four parameters is given by:

$$\boldsymbol{p(x) = \gamma + (1 - \gamma - \lambda)F(x)} \qquad \textbf{(\textit{eq.} 2.1)}$$

Where, $p(x)$ is the probability of a successful response at stimulus level x, the function *F* is a monotonic function of x, γ is the guess rate, and λ is the lapse rate (Treutwein and Strasburger, 1999).

2.2 Instrumentation

2.2.1 Clinical tests

The experiments described in this thesis used normal observers and those with amblyopia. Various clinical measures were used to assess the visual health of the observers.

2.2.1.1 Visual acuity

Visual acuity is the smallest detail that can be resolved and is the most commonly used measure of visual function. Visual acuity provides a measure of central macular function which in turn represents the state of overall ocular health.

Different charts are used to measure the visual acuity, all consisting of rows of letters with a progressive reduction in size in each row. The Snellen's chart is the most widely used method for the measurement of visual acuity, however the chart has several limitations such as an unequal number of letters in each line, varying legibility, disproportional spacing among letters, and ambiguity in recording acuity of partially resolved line. Bailey-Lovie chart (Bailey and Lovie, 1976) and its later modification, the ETDRS chart (Ferris *et al.*, 1982) addresses most of the limitations of the Snellen chart (Figure 2.3). The chart consists of Sloan letters (Sloan, 1959), which have similar legibility. Each row in the chart also consists of an equal number of letters. The progression in size of the letters in each row is also standardised into equal logarithmic intervals (0.1, equivalent to a ratio of 1.26X) so that letters double in size every three lines. Each letter resolved is assigned a log MAR value of 0.02, allowing for an accurate measurement of partially resolved lines. These modifications have established the Bailey-Lovie and ETDRS chart as the most preferred method of visual acuity evaluation.

Visual acuity in this study was measured with a modified Bailey-Lovie chart (Figure 2.3) displayed on a computer screen. The screen was placed at 4m from the observer. The chart consisted of five letters in each line with 0.1 logarithmic progressions in the size of the letters. The acuity was measured monocularly and recorded as the logarithmic value of minimum angle of resolution (log MAR value) of the letters correctly resolved.

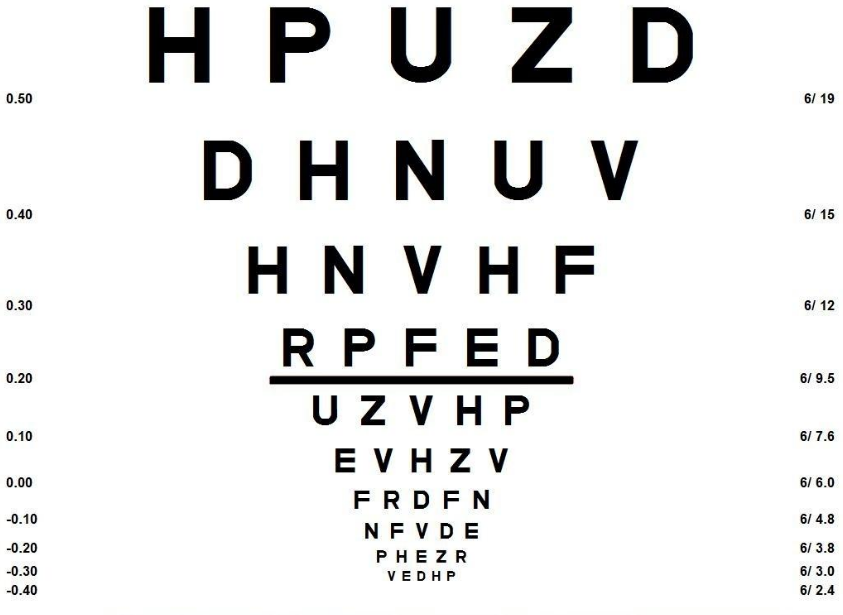

Figure 2.3: The modified Bailey-Lovie chart

2.2.1.2 Stereopsis

The lateral offset of an image due to the anatomical configuration of the human eyes results in a slightly different visual image being projected to the two retinae with a degree of overlapping in the central visual field. The single fused image from these disparate images provides a sense of depth, known as stereopsis. The measure of stereopsis, stereoacuity, is the smallest binocular disparity that can be reliably discriminated – usually measured in seconds of arc ("). The Frisby test (Frisby Stereotest, Sheffield, UK) was used to measure stereoacuity in the current body of work.

Frisby test

The Frisby test is a real depth test conducted in free space that does not require dissociation of eyes. The test plates consist of random elements printed onto four squared shapes, a circular portion in one of the squares is printed on the back surface of the plate, creating a real depth effect (Figure 2.4). The circular contour can be presented with either crossed or uncrossed disparity based on which side the plate is presented to the observer. The disparity is crossed if the plate is presented facing towards the observer, providing the effect of depth away from the observer and uncrossed if the plate is presented facing towards the experimenter, providing the effect of depth towards the observer. The Frisby test consists of three plates with varying thickness (6mm, 3mm and 1.5mm), producing different level of disparity. The disparity levels can also be varied by presenting the plates at different distance from the observer, over the ranges of plate thickness and presentation distance, the Frisby test can be used to assess the stereoacuity ranging from 20" to 600"of arc. Monocular cues (to depth perception) in the form of motion parallax can be easily elicited therefore it is advantageous to control for this by avoiding movement between the observer and the test plate. When the motion parallax is controlled for, Frisby test is least susceptible to monocular cues compared to other commonly used near stereo tests (Holmes and Leske, 1999).

Figure 2.4: The Frisby near stereotest

For the purpose of this study, the Frisby test was used to assess the stereoacuity up to 20". The test started with the thickest plate (60mm) presented against the white uniform background at a distance of 40cm, producing a disparity of 340". The plate thickness and test distance were then changed to achieve different levels of disparity. Participants were asked to identify the box containing the circular contour in a 4 AFC task. The disparity presented was reduced after two consecutive correct responses and increased after one incorrect response. The minimum disparity obtained from this method was recorded as the stereoacuity of the observer. Different studies have reported varying level of stereo-acuity in the normal adult population measured by this method ranging from 55" arc (Garnham and Sloper, 2006) to 30" of arc (Piano and O'Connor, 2013). For the purpose of this study normal stereo acuity was taken as 30" of arc.

2.2.1.3 Other measures

In addition to visual acuity and stereo acuity, other measures were also used to assess the ocular status. The cover test was used to determine the presence of any heterophoria/heterotropia. The Bagolini test was used to determine the presence of sensory fusion at distance and near. And finally ocular motility was assessed to rule out any abnormalities in the function of the extra ocular muscles.

2.2.2 Psychophysics setup

Image processing hardware and software

The psychophysical experiments were displayed on a 21" Sony FD Trinitron monitor with a pixel resolution of 1920 x 1440 and refresh rate of 75Hz connected to an Apple computer with OS X and ATI Radeon^{TM} HD 5770 1024 MB graphics card. The experimental stimuli were programmed in MATLAB 64 bit version, R2013a (MATLAB, 2013) with a Psychtoolbox-3 extension (Brainard, 1997b; Pelli, 1997). A switcher box (Li *et al.*, 2003) was used to increase the luminance depth of the monitor display from 8 bits to 12 bits and the monitor gamma corrected regularly using a spot photometer (Minolta LS 110).

2.3 Stimuli and procedure

A range of stimuli have been employed to study the global motion and global form perception processed along the dorsal and ventral streams respectively. To directly compare the functionality along the two streams, stimuli with similar physical properties and processing requirements should be employed. The studies that have sought to compare the performance along the two streams have most commonly used RDKs as the stimulus of choice for the motion pathway whereas various stimuli including Gabor patches, Glass patterns, and line segments have been used for the form pathway. These studies are summarised in Table 2.3.

Studies	**Motion stimuli**					**Form stimuli**				Task / Threshold
	Type	Display size/ time	Element no./ size/density	Lifetime (frames)	Speed (˚/s)	Type	Display diameter/ time	Element no. /size/density	Element separation	
Nankoo *et al.,* (2012)	RDK (translation, rotation, radial)	11.16˚/ 167ms	NG*/ 0.04˚x0.04˚/ 6%	10	15.67	Glass pattern (translation, rotation, radial)	11.16˚/ 167ms	NG/ 0.04˚ x0.04˚/ 6%	0.26˚	MCT†/ 2AFC, MOCS
Tsermentseli *et al.,* (2008)	Rotational RDK	6.6˚/ 250ms	NG/NG/ 4 dot/deg^2	3	5.8	Rotational Glass pattern (tripoles)	6.6˚/ 250ms	NG/NG/ 4 dot/deg^2	NG	MCT/ 2AFC, 2:1 staircase
Spencer and O'Brien (2006)	Rotational RDK	6.6˚/ 250ms	NG/NG/ 4 dot/deg^2	3	5.8	Rotational Glass pattern (tripoles)	6.6˚/ 250ms	NG/NG/ 4 dot/deg^2	NG	MCT/ 2AFC, 2:1 staircase
Simmers *et al.,* (2003, 2005)	Translational RDK	12˚/ 426.7ms	50 dots / 0.47˚/ 0.44 dot/deg^2	8	5.7	Translational line segments	12˚/ 426.7s	NG/ 50 line segments	NA#	MCT/ 2AFC,
Gunn *et al.,* (2002)	Translational RDK	NG/10s	NG/ NG/ 4 dot/deg^2	6	6	Rotational line segments	NG/10s	NG/NG/ 1.3 elements/ deg^2	NA	MCT/ 2AFC, 2:1 staircase
O'Brien *et al.,* (2002)	Translational RDK	12.1˚x 7.51˚	NG/NG/ 4 dot/deg^2	NG	5.8	Rotational line segments	13 ˚	0.41˚long/ 19 segment/ deg^2	NA	MCT/ 2AFC, 2:1 staircase
Hansen *et al.,* (2001)	Translational RDK	10˚x14˚/ 2.3s	300 dots	3	7	Rotational line segments	10˚x14˚/ 2.3s	600 lines, each 0.4˚	NA	MCT/ 2AFC, 1:1 staircase
Mansouri and Hess (2006)	Translation micropatterns	6˚/ 500ms	128	NA	10	Gabor micropatterns	6˚/ 500ms	64	NA	Eq. noise/ 2AFC, MOCS

Table 2.3: Compendium of studies that have used comparable stimuli along the motion and form pathway

** NG: not given, † MCT: Motion coherence threshold, #NA: Not applicable*

As can be observed from Table 2.3, the most common stimuli that have been used as an identical version of an RDK for the investigation of form perception are line segments and variants of Glass patterns. Most of these studies have used similar presentation parameters across the two stimuli types such as element size, display area, display duration, and psychophysical method for data collection. However, three studies used physically different stimulus for the motion and form domain; translational RDK for global motion but rotational line segment for global form perception (Hansen *et al.*, 2001; Gunn *et al.*, 2002; O'Brien *et al.*, 2002). On the other hand, Simmers *et al.,* (2005) spatially superimposed the motion trajectory of the translational RDKs to produce translational orientation streaks (line segments).

The physical structures as well as the processing mechanisms of the RDK and line segments are different. The processing of global RDK stimuli occurs in two stages; in the first stage, the position of a dot in one frame corresponds to the same dot in another spatial location over time to extract individual dot directions (local processing, occurring in V1), followed by averaging of the local inputs to provide a global percept (global processing in MT and higher areas) (further details section 1.3.1). However for the perception of a line segment, local correspondence does not appear necessary and instead these stimuli may be processed as extending contours under the influence of the long range lateral connections that occur between the columns with a similar orientation preference in V1 (Li and Gilbert, 2002; Field and Hayes, 2004; Grinter *et al.*, 2010). These long range horizontal connections may be involved in grouping/averaging the line segments with similar orientations in V1 itself, extracting at least in part the global information assumed to be processed at the higher cortical areas. Hence it has been suggested that line segment stimuli should be avoided for the study of global processing occurring in the higher areas of the ventral visual pathway such as V4 (Grinter *et al.*, 2010). The presumed processing differences are also observable behaviourally with lower discrimination thresholds for line segments compared to the Glass patterns (Dakin, 1997). The ability to discriminate a Glass pattern deteriorates if the dot displacement is increased beyond a certain limit (8 arc min, with the structure of the Glass pattern impossible to detect beyond 23 arc min). On the other hand, performance with line segment stimuli continues to improve with an increase in the line length up to 2˚ (Dakin, 1997).

Both Glass patterns and RDKs stimuli can be created using a random dot pattern that allows for the control of most of the physical parameters across the stimuli such as dot size, density, display aperture etc. These stimuli also share similar processing mechanisms along the dorsal and ventral streams; initial processing of local motion/orientation cues for both stimuli occurs in early visual areas such as V1/V2 followed by global pooling of local cues in the higher cortical areas of each stream, MT for RDK (Morrone *et al.*, 1995) and V4 for Glass pattern (Dakin, 1997; Wilson and Wilkinson, 1998). Unlike the line segment pattern, the perception of a Glass pattern is less affected by the long-range connections in V1. The random placement of a signal dot pair in the vicinity of other noisy dipoles results in the formation of few contours that are longer than the signal dipoles, hence the dipoles in Glass patterns are less likely to activate the long range connections among the orientation columns in V1 (Grinter *et al.*, 2010). Two studies (Spencer and O'Brien, 2006; Tsermentseli *et al.*, 2008) used triplet rotational Glass pattern with similar physical parameters as the RDK stimuli. The choice of the triplet Glass pattern seems to be motivated by an attempt to correspond the element’s length with the dot lifetime in the RDK stimuli (three frames). Another important factor to consider is the separation of the elements in each frame within a Glass pattern and RDK (in terms of distance travelled in one frame). For instance, the dipole separation in the Glass pattern employed by Nankoo *et al.,* (2012) was scaled to the distance travelled by the dots in each RDK frame.

All of the studies mentioned above used the RDK and Glass pattern/line segment to determine the motion/orientation coherence threshold. Although, Mansouri and Hess (2006) used an equivalent noise approach to study both motion and form perception, their stimuli were not physically similar. Therefore, it is difficult to attribute the differences in results to the processing mechanisms along each stream.

In the present thesis, the physical parameters of the stimuli which test both motion (RDK) and form (Glass pattern) processing were made as similar as possible to enable the concurrent investigation of each stream with the equivalent noise approach. The stimulus parameters of the translational RDK and Glass patterns, such as the dot size, display area, display duration, method of stimulus presentation were all made equivalent. The dipole distance in the Glass pattern was also matched to the distance travelled by the RDK dots in any two successive frames.

2.3.1 Random Dot Kinematograms (RDK)

The RDK stimulus comprised of 500 black dots (0.083° in diameter) presented in a circular aperture (10° in diameter at 50 cm) at the centre of the display monitor with a dot density of 12.81dots/deg^2. The mean background luminance of the display was 35cd/m^2 and the contrast of the dot elements was 95% Michelson contrast (Figure 2.8). The stimulus was displayed for 38 frames over a time of 0.5 sec. All dots followed a defined trajectory for 6 frames (0.08 sec) at a dot speed of 10°/sec after which they disappeared and were generated at a random location within the stimulus area. To ensure that all dots did not complete their lifetime on the same frame, the start of the lifetime (in frames) was randomly assigned to each dot.

The direction of motion of individual dots was generated from a standard Gaussian distribution with a prescribed mean and standard deviation. The increase in the standard deviation of the distribution increases the noise within the stimuli. In such stimuli, all dot elements act as signal and the best strategy to determine the overall direction of the RDK is proposed to be by integrating the direction information from all individual dot elements. The mean of the distribution was centred at different angles from the reference of the vertical (90°). The overall direction of motion of the RDK (right or left from vertical) was randomised.

Before the stimulus presentation, a white fixation dot of 0.2° diameter was presented at the centre of the stimuli which remained on the screen for the total duration of the stimulus presentation. After the observer pressed any key to indicate they were ready for the start of the experiment, the RDK stimulus was displayed for 0.5 sec. After the 0.5 sec stimulus display, a 10° diameter mask consisting of randomly generated texture was presented in the place of stimulus display for 0.25 sec.

2.3.2 Glass pattern

The Glass pattern stimuli (Glass, 1969) were generated by randomly placing 250 black dots (0.083° in diameter) at the centre of display within the display aperture of 10° diameter. Another identical set of 250 dots was then superimposed after linear geometrical transformation. The corresponding dot elements of the pattern were separated by a distance of 0.133°, which was scaled to the distance travelled by the dot in the RDK in two consecutive frames (dot speed of 10°/sec displayed for 0.5 sec with a monitor refresh rate of 75 frames per second). This arrangement of linear transformation at defined separation of dot pairs or dipoles created a translation Glass pattern (Figure 2.5).

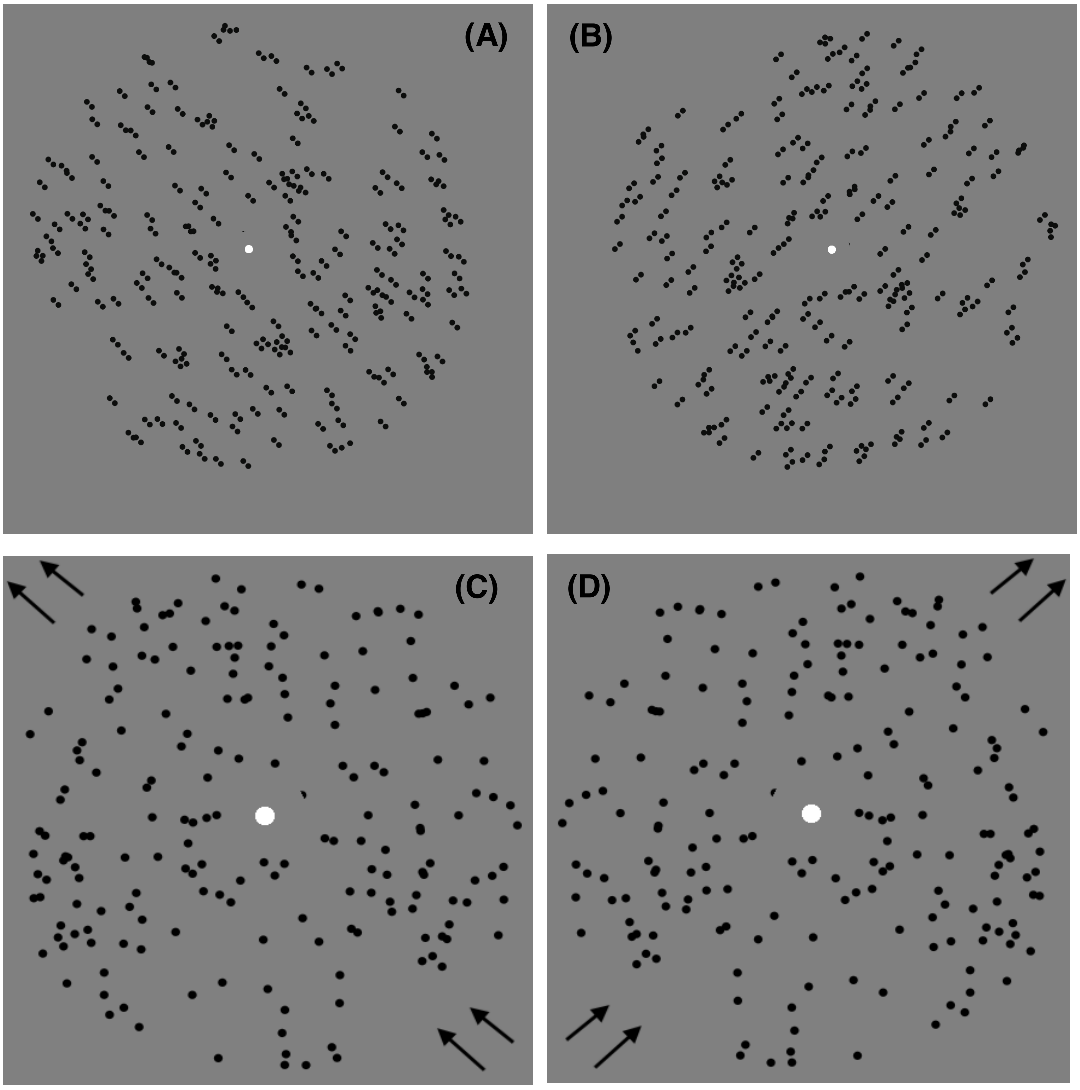

Figure 2.5: Random dot kinematogram and Glass pattern stimuli

Figure shows Glass pattern oriented to right (A) and left (B) and RDK patterns with right (C) and left motion (D). The arrows in RDK represent the direction of motion.

Simlar to the direction of individual dots in the RDK, the orientation of individual dipole elements in the Glass patterns were also derived from a Gaussian distribution with varying standard deviation (Figure 2.6). An increase in the standard deviation of the distribution increased the external noise with the mean of the distribution centred at different angles from the vertical reference (90°). The overall orientation of the Glass pattern (clockwise or anticlockwise from vertical) was randomised across trials. Other stimulus parameters such as background luminance and display duration were identical to that of the RDK stimulus.

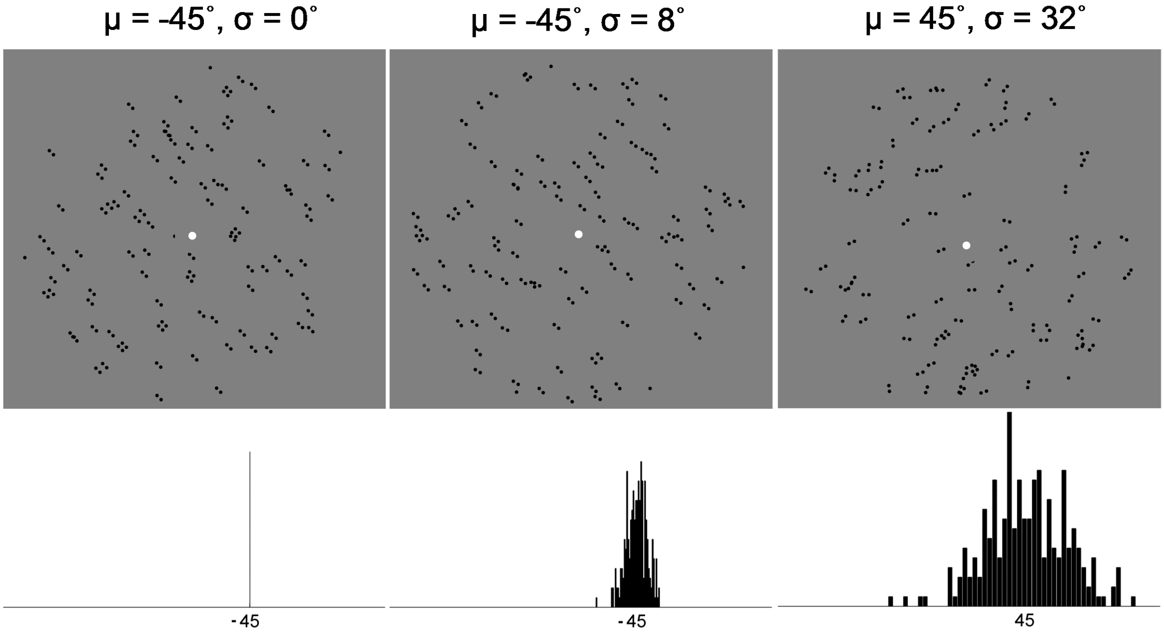

Figure 2.6: Orientation sampling of dipole elements from Gaussian distribution in Glass pattern

An example of Glass pattern showing how the orientations of dipoles were sampled from a Gaussian distribution with prescribed mean and different standard deviations, the increase in standard deviation represents the increased uncertainty of local properties in elements (external noise) with global overall orientation of pattern remaining constant.

2.3.3 General Procedure

The general procedure is described in relation to both RDK and Glass pattern stimuli. Written informed consent was obtained from each participant once the nature and possible consequences of the experiment had been explained (information sheet and consent forms, Appendix 9.1). All experiments in this body of work were carried out in accordance with The Code of Ethics of the World Medical Association, Declaration of Helsinki and approved by the Life Sciences Human Subjects Research Ethics Committee of Glasgow Caledonian University (Appendix 9.1). All participants underwent an optometric evaluation which included visual acuity and binocular vision assessment with tests described previously in section 2.2.1. Each participant completed the psychophysical experiment with the best refractive correction in place. The psychophysical experiments were conducted in a dark room with the computer monitor being the only source of light. Participants were seated comfortably and were allowed to adapt to the room environment, after which the experimental task was initiated. A white fixation dot of 0.2° diameter was presented at the centre of screen. After the observer pressed any key on the keyboard to indicate they were ready for the test, an experimental stimulus (RDK or Glass pattern) was displayed for 0.5 sec. This was followed by the presentation of a 10° diameter mask consisting of randomly generated texture for 0.25 sec. The mask was presented to eliminate any cue for response based on the afterimage of the displayed stimulus. A question mark was presented simultaneously on the screen to prompt the observer to register their response to the preceding stimuli. After the observer registered their response by pressing the right/left arrow on the keyboard, a response feedback was provided; a happy face for a correct response and a sad face for an incorrect response (Figure 2.7). The observer’s task in each trial was to discriminate the overall, not the individual, orientation (Glass) of dipoles or direction (RDK) of dots from the vertical reference.

2.3.3.1 Practice and main session

The practice session consisted of 10 trials of the experiment for each variance condition that was to be evaluated, while the main experiment consisted of 100 trials or ten reversals of the staircase for each condition. Each observer completed two practice sessions before being evaluated with the main experiment.

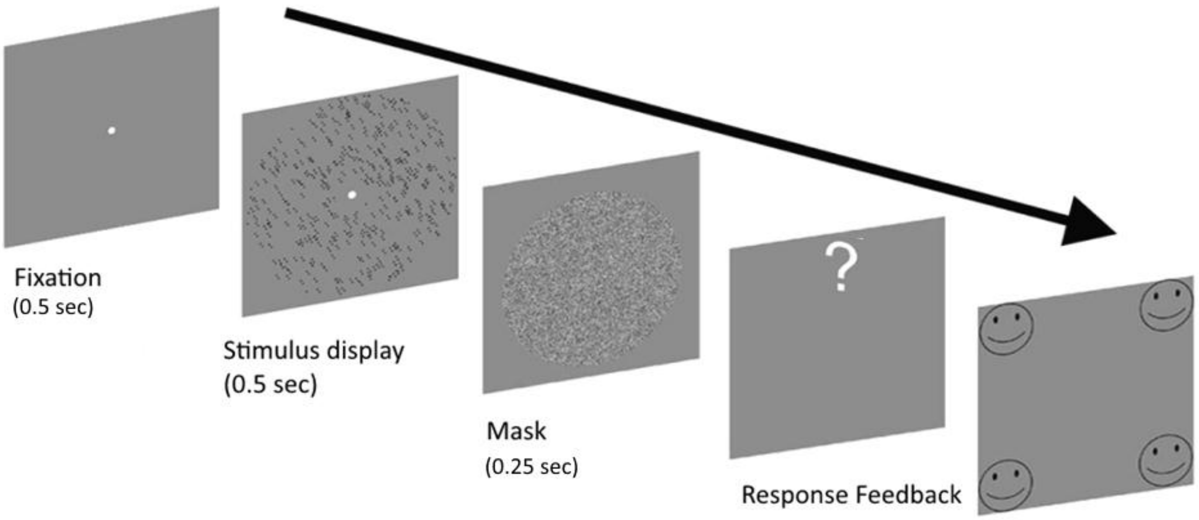

Figure 2.7: Schematic representation of one trial of experiment

Each trial of experiment started with the presentation of a fixation dot followed by stimulus display for 0.5s (here a Glass pattern is oriented anticlockwise from the vertical) and random mask. The feedback response was provided after the observer entered the response by pressing appropriate keys on a keyboard.

2.4 Psychophysical method for data collection and data analysis

The transformed staircase method (Wetherill and Levitt, 1965) in which the stimulus strength for the next trial is determined by the responses to the preceding trials was used for stimulus presentation and data collection. The staircase tracked the response of the observer, angular deviation of mean direction/orientation of RDK or Glass pattern from the vertical reference (90˚) for each level of variance evaluated. The staircase started with an overall mean orientation or direction of 30˚away from the vertical. Three consecutive correct trials reduced the orientation/direction disparity from the reference while an incorrect trial increased it by the same amount (3:1 staircase, targeting the performance to 79.73% correct). The initial step size by which the stimulus intensity were adjusted was an octave which was reduced to half an octave and further to quarter of an octave after three and six reversals respectively to increase the precision of the final threshold estimate (Figure 2.8). Each staircase terminated after the completion of ten reversals or 100 trials, whichever occurred first. Threshold was calculated as the geometrical mean of the last seven reversals.

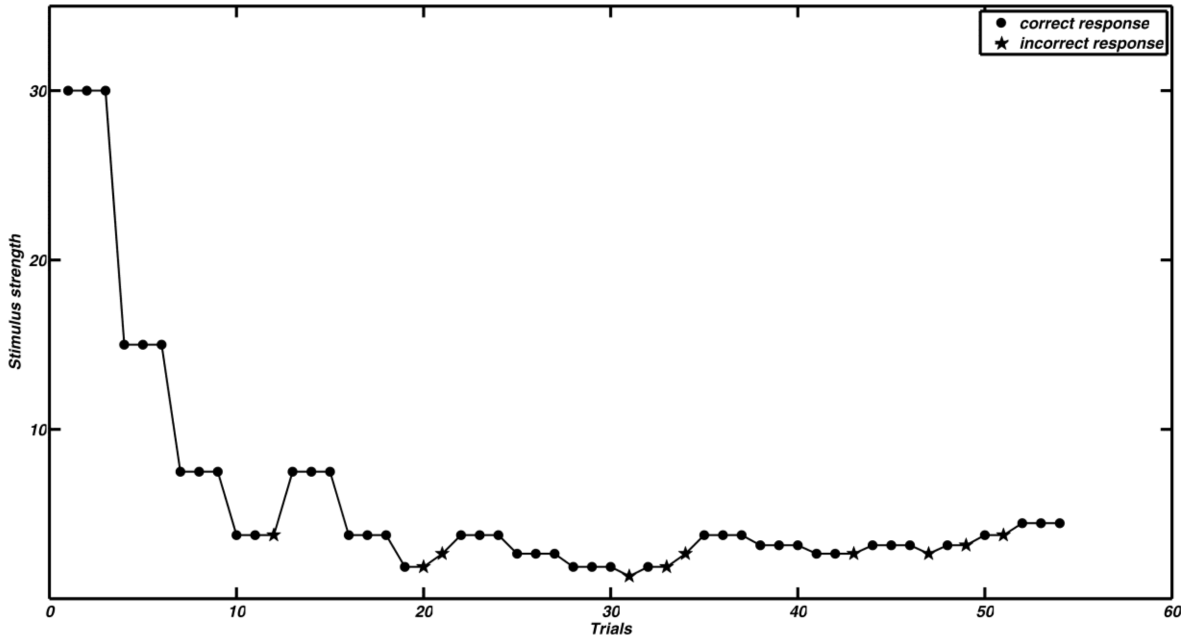

Figure 2.8: An example of a transformed 3:1 staircase with modified step size.

The stimulus strength reduced after three consecutive correct responses and increased with one incorrect response. The step size was larger at the start of the experiment (factor of 0.5) which was modified to 0.71 and 0.84 after third and sixth reversals respectively. The staircase terminated after completion of 10 reversals.

In the staircase method, a participant might be able to predict the stimulus strength of the next trial based on the direction of staircase, which may introduce bias in the final threshold estimate. To reduce the effect of anticipation, independent staircases for different variance conditions were interleaved and presented randomly. All responses were then aggregated by the signal levels presented for the session and a log-Weibull (eq. 2.2) function was fitted to generate the psychometric functions. The log-Weibull function was chosen as it is the most suitable for describing the response change along with the change in stimulus in logarithmic scale.

$$pC = \gamma + (1 - \gamma - \lambda)\ x\ (1 - exp(-exp((log(\varphi) - \alpha)/\beta))) \qquad \textbf{(\textit{eq.} 2.2)}$$

where,

pC = proportion correct (performance of the observer)
γ = chance performance level (0.5 for current 2AFC task)
λ = lapse rate
φ = signal strength tested (direction/orientation angle from vertical)

α = location parameter
β = shape (slope) parameter

In theory, a maximum-likelihood principle was applied to estimate the free parameters (*α*, *β*, and *λ*). In practice, we found the best fitting free parameters of the psychometric function that minimised the negative of log maximum-likelihood (eq. 2.3), assuming that the observers' responses come from the binomial distribution.

$$\boldsymbol{argmin}\left(-\log\left(\prod_{1}^{i} \boldsymbol{pC^{k}}\,(\mathbf{1}-\boldsymbol{pC})^{\boldsymbol{n-k}}\right)\right) \qquad \textbf{(\textit{eq.} 2.3)}$$

where, *pC* is defined by the eq. 2.2 with free parameters to be estimated, *k* is the number of correct responses at a given signal strength *i*, and *n* is the total number of aggregated trials tested at the signal strength *i*.

The fminsearch locates the minimum of a scalar function of different variables based on the Nelder-Mead minimisation algorithm which uses an unconstrained linear optimisation process after feeding the initial guess values. The geometrical mean threshold was used as an initial guess for the location parameter (*α*), while the initial guesses for the slope and lapse rate were fixed at 0.5 and 0.01 respectively. Thresholds were generated at the performance criterion of 79.73% – theoretical convergence level of 3:1 staircase. Thresholds from the psychometric function were compared with the thresholds from the 3:1 staircase. The results for each session were visually inspected with graphs for the staircase data presented as a function of stimulus strength and the psychometric function fitted to the data (Figure 2.9).

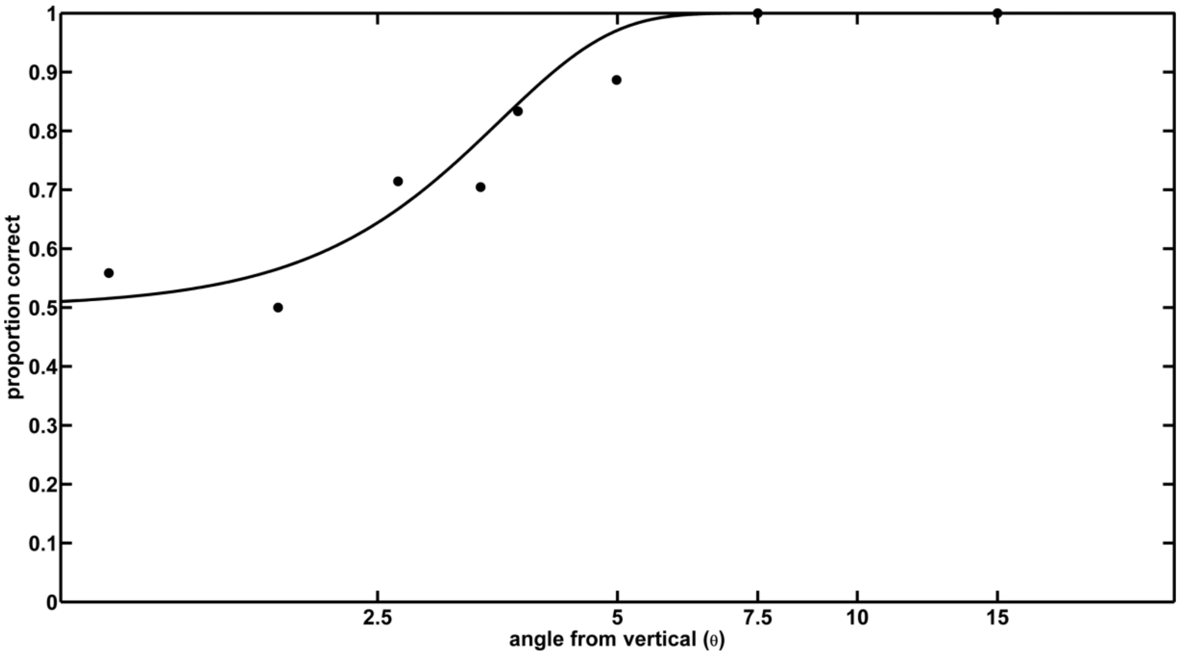

Figure 2.9: A sample psychometric function fit to the hypothetical staircase data

The round markers represent the observer's performance (proportion correct) plotted against the stimulus strength (angle from vertical). The curve represents the psychometric function fitted to observer's performance with equation 2.2. The best fitting parameters of the curve presented here are: $\alpha = 3.42$ *at performance criteria of 79% with* $\beta = 0.33$ *and no lapse* ($\lambda = 0$).

2.4.1 Equivalent Noise paradigm and data modelling

The linear amplifier model was used to fit the threshold (τ_{obs}) data at different external noise levels (σ_{ext}) to estimate the internal noise (σ_{eq}) and sampling efficiency (*Eff*) parameters – eq. 2.4.

$$\boldsymbol{\tau_{obs}} = \sqrt{\frac{\boldsymbol{\sigma^2_{eq}} + \boldsymbol{\sigma^2_{ext}}}{\boldsymbol{Eff}}} \qquad \textbf{(\textit{eq.} 2.4)}$$

The method of least squares was used to obtain the values of free parameters (σ_{eq} and *Eff*). In any modelling process, the experimental data varies from the theoretical model (Figure 2.10). The method of least squares assumes that the best fit to a given model is the model with parameters minimising the total sum of the squared difference (SSE in eq. 2.5) between the model and the data.

$$\boldsymbol{SSE} = \sum_{i=1}^{n}\left(y_i^{predicted} - y_i^{observed}\right)^2 \qquad \textbf{(\textit{eq.} 2.5)}$$

Throughout this body of work the fminsearch algorithm in MATLAB was used to determine the best fitting free parameters of the LAM.

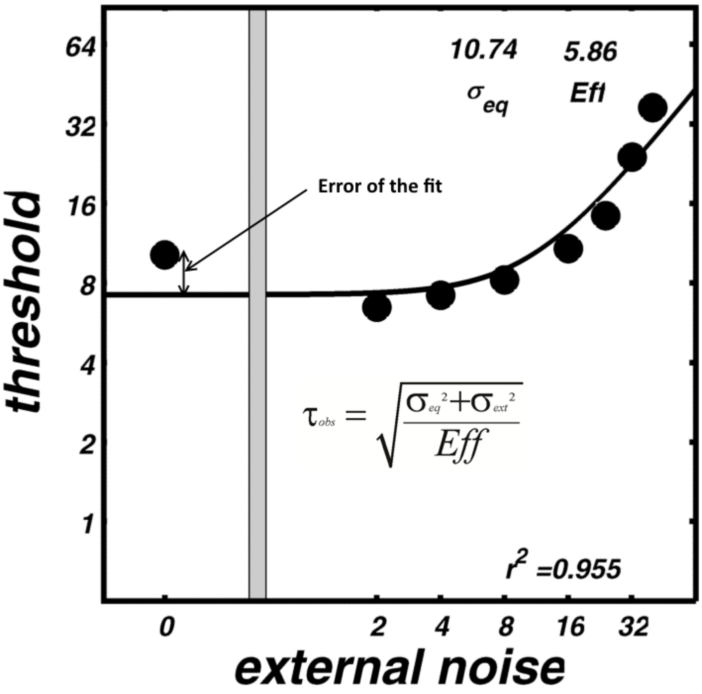

Figure 2.10: Hypothetical data at eight levels of external noise fitted to the linear amplifier model

The round markers represent the threshold measured at eight levels of external noise and the curve represents the LAM fitted to the data. The error of fit of the model on one data point is represented by the difference in the actual data and the predicted data as shown by the double arrow. Also shown are the model predictions for the free parameter of the LAM (σ_{eq} and Eff) and r^2 of the fit.

The measure of the goodness of fit of the data to the model provides a basis of estimation for how well the model explains the experimental data and thereby the strength of the model. The most commonly used measure of goodness of fit is the r^2 statistics, which represents the proportion of the data variance accounted for by the model. To calculate r^2, the total variance in the data (the total sum of square – SST, eq. 2.6) is first determined which is the difference between the observed data and mean of the observed data.

$$\boldsymbol{SST = \sum_{i=1}^{n}\left(y_i^{predicted} - \bar{y}_i^{observed}\right)^2} \qquad \textbf{(\textit{eq.} 2.6)}$$

The variance accounted by the model is provided by the sum of squared error (SSE). Hence r^2 is the given by:

$$\boldsymbol{r^2 = 1 - SSE/SST} \qquad \textbf{(\textit{eq.} 2.7)}$$

In the present body of work, the outputs from LAM fitted to data from the motion and form domains were compared. When comparing the two models quantitatively, the model with the higher r^2 value provides a better representation of the data. But this simple comparison does not take into account the relative strength of the models with different numbers of parameters used to explain the same data. In general, the model with the higher number of parameters will have a better fit (*i.e.,* higher r^2) than the model with a fewer number of parameters. Therefore, a statistical test between the models should consider the differences in the number of parameters as well as the differences in variance explained by the models. For that purpose, a nested *F*-test (eq. 2.8) was used to determine if the improvement in the goodness of fit of the model with an additional numbers of parameter(s) was statistically significant or not compared to the model with a fewer number of parameters.

$$\boldsymbol{F(df_1, df_2) = \frac{(r^2_{full} - r^2_{reduced})/df_1}{(1 - r^2_{full})/df_2}} \qquad \textbf{(\textit{eq.} 2.8)}$$

Where $\boldsymbol{df_1} = \boldsymbol{k_{full}} - \boldsymbol{k_{reduced}}$ and $\boldsymbol{df_2} = \boldsymbol{N} - \boldsymbol{k_{full}}$. $\boldsymbol{k}$ represent the number of parameters in each model, and $\boldsymbol{N}$ is the number of predicted data points.

3.0 Concurrent characterisation of dorsal and ventral stream function with the equivalent noise paradigm

3.1 Experiment 1: Comparison of global orientation thresholds in Glass patterns with global direction thresholds in RDK

3.1.1 Introduction

Global motion and form are processed under the anatomically and functionally bifurcated independent dorsal and ventral streams. These two processing mechanisms have been evaluated using various stimuli (refer to section 2.3) however comparing the results from two different processing mechanisms has remained difficult owing to the differences in the physical characteristics of the stimuli required for each domain. Few studies have used comparable stimuli to evaluate fine motion and orientation discrimination thresholds in the presence of variable noise (Mansouri and Hess, 2006) with most studies adopting the global coherence threshold paradigm (Simmers *et al.*, 2003b; Simmers *et al.*, 2005; Ditchfield *et al.*, 2006). The experimental stimuli used in these studies either differ physically or in the terms of the associated processing mechanism. Furthermore, the global coherence paradigm, the most commonly used method for evaluation of either domain, cannot differentiate if the performance is constrained by the local or the global processing mechanism. In this study, sensitivity to global motion (dorsal stream) and global form (ventral stream) were measured using physically similar stimuli embedded in varying levels of added external noise to disentangle the effects of local and global limitations along both domains in a normal adult population.

3.1.2 Methods

The stimuli parameters and general procedure have been described previously (refer to section 2.3).

A pilot experiment was first conducted to determine the appropriate levels of variance to be evaluated in the main experiment. Four observers (37.25 ±10.08 years) with normal or corrected to normal visual acuity participated to judge the overall direction of motion in a RDK and the orientation of a Glass pattern from vertical (90˚) at eight levels of variance (0˚, 1˚, 5˚, 10˚, 15˚, 20˚, 30˚, 40˚). Similarly, in the main experiment six visually normal observers (31.66 ±6.86 years) discriminated the overall direction of motion in a RDK and the overall orientation of a Glass pattern at eight levels of variance (0˚, 2˚, 4˚, 8˚, 16˚, 24˚, 32˚, 40˚). All observers in both pilot study and main experiment completed five experimental sessions for each stimulus (RDK and Glass pattern).

3.1.3 Results

3.1.3.1 Pilot experiment

The direction/orientation discrimination thresholds were low and similar at lower levels of variance and increased at the higher variance levels (Figure 3.1). The global orientation discrimination thresholds (Glass) were consistently higher than the global direction discrimination thresholds (RDK) irrespective of variance levels for all observers (with the exception of MP, for whom the thresholds were similar mostly at moderate variance levels).

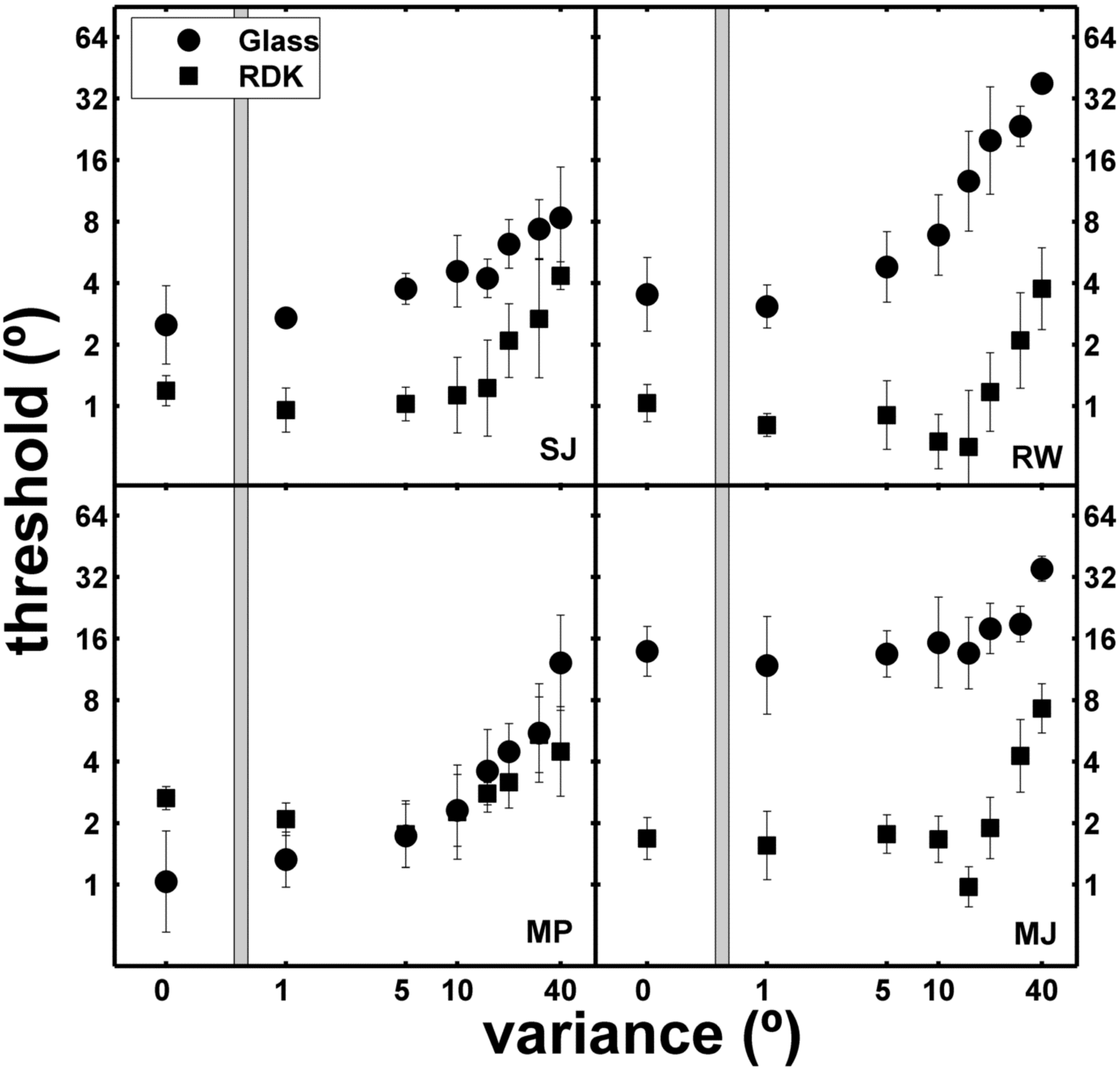

Figure 3.1: Mean direction and orientation discrimination thresholds for individual observers.

Each panel shows data for a single observer for RDK and Glass pattern at eight levels of variance. Each data point represents the mean from five experimental sessions and error bar represents ±1 standard deviation.

3.1.3.2 Main Experiment

The results showed a similar pattern as observed in the pilot experiment. The global orientation discrimination thresholds (Glass) were consistently higher than the global direction discrimination thresholds (RDK) at all noise levels for each observer (Figure 3.2) and the mean data (Figure 3.3). For both functions, when thresholds for individual observers and the mean data were plotted against the external noise in logarithmic scale, thresholds were low and similar at lower noise levels and started to increase at noise levels of 8˚ and 16˚.

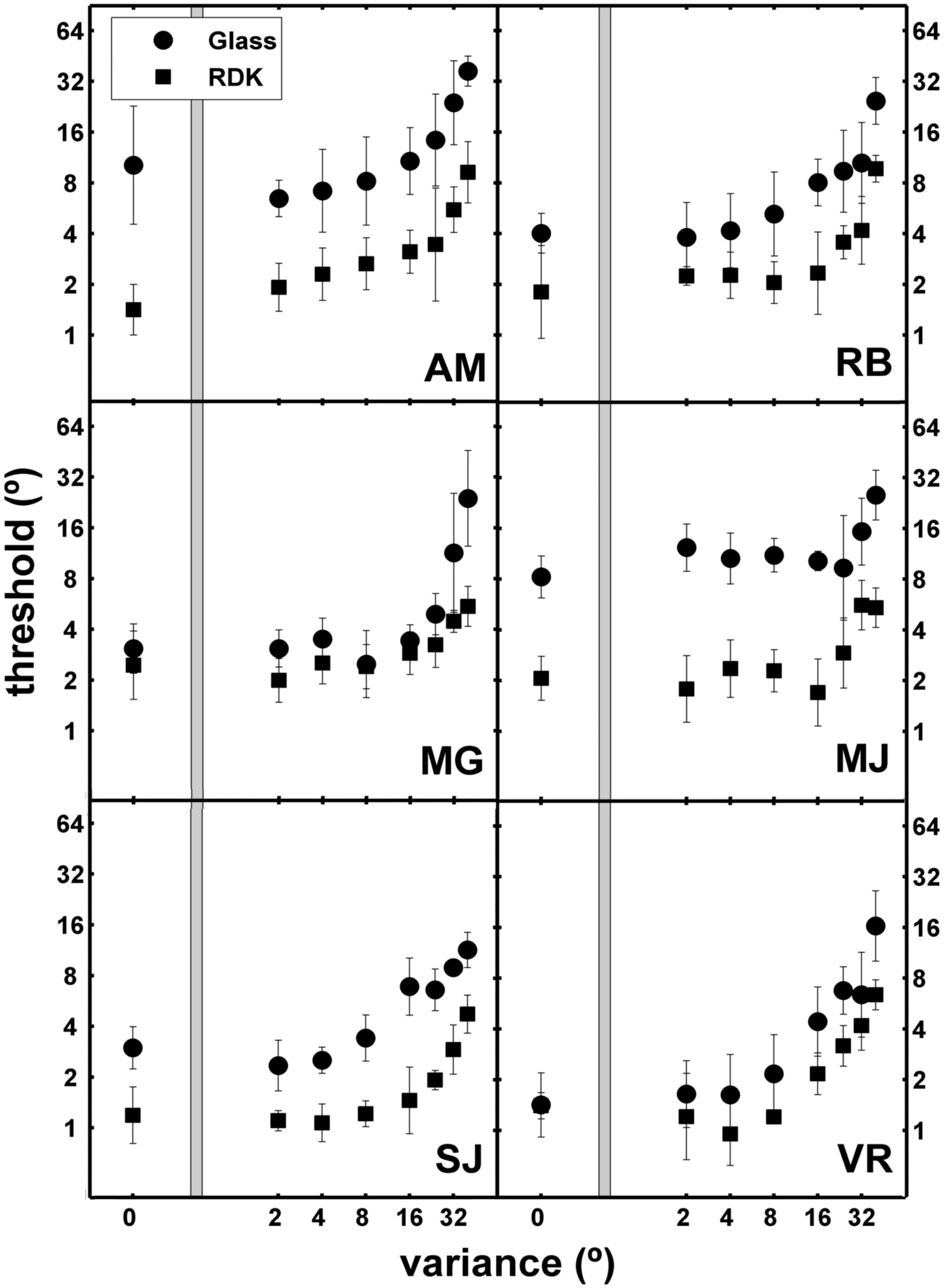

Figure 3.2: Mean direction and orientation discrimination thresholds for individual observers.

Each panel shows data for a single observer for RDK and Glass pattern at eight noise levels. Each data point represents the mean from five experimental sessions and error bar represents ±1 standard deviation.

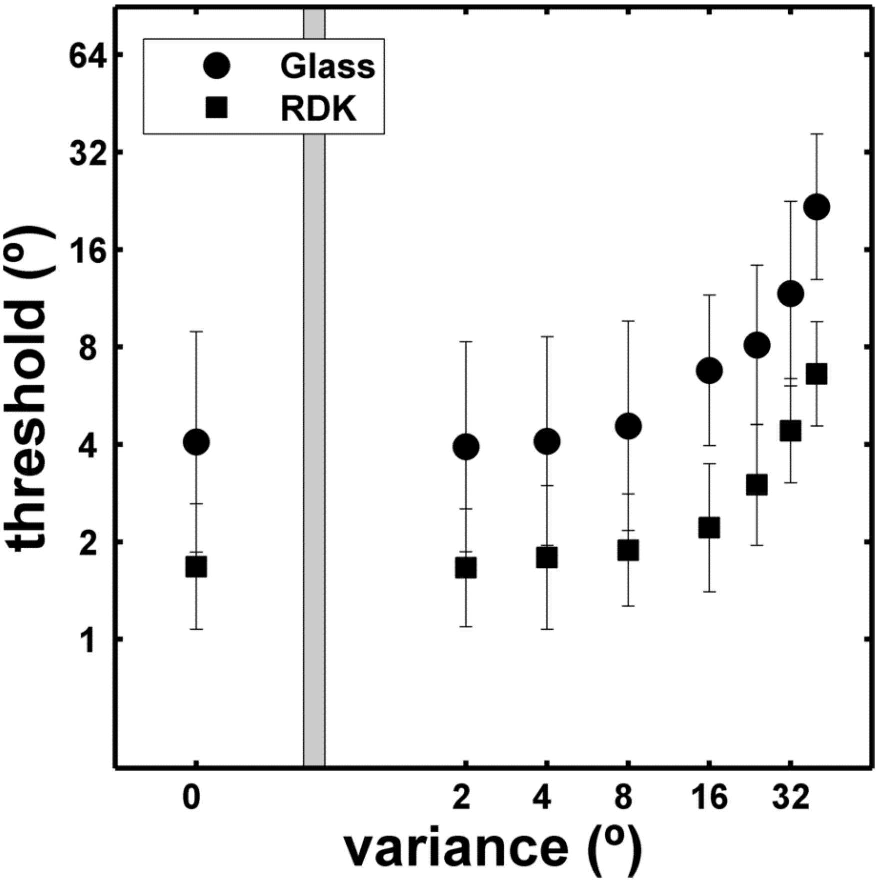

Figure 3.3: Mean direction/orientation discrimination thresholds at eight noise levels.

Each data point represents the mean thresholds for Glass pattern and RDK, the error bar represents ±1standard deviation.

The repeated measures ANOVA with *noise* (8 levels) and *stimuli type* (2 levels) as within subject factors was conducted to evaluate the effect of *noise* on discrimination thresholds for RDK and Glass pattern. The interaction between the two factors would suggest a differential effect of *noise* on performance according to the *stimuli type*. The Mauchly's test revealed that the log transformed data satisfied the assumption of sphericity for *noise* [$\chi^2(27) = 39.66$, $p > 0.05$] and *noise and stimuli type* interaction [$\chi^2(27) = 34.17$, $p > 0.05$]. The results revealed a significant effect of *noise* [$F(7, 203) = 99.64$, $p < 0.01$] and *stimuli type* [$F(1, 29) = 157.06$, $p<0.01$] but no interaction between the *stimuli type* and *noise* [$F(7, 203) = 1.82$, $p > 0.05$]. The pairwise comparisons for different *stimuli type* (RDK and Glass) revealed significantly lower thresholds for the RDK compared to the Glass pattern ($p < 0.01$).

Further analysis of the main effect of *noise* was conducted with an independent repeated measures ANOVA for each *stimuli type* (RDK and Glass) with *noise* as within subject factor. The Mauchly's test revealed that the log transformed data fulfilled the assumption of sphericity for both RDK [$\chi^2(27) = 25.47$, $p > 0.05$] and Glass pattern [$\chi^2(27) = 37.93$, $p > 0.05$]. The results showed a significant effect of *noise* for both RDK [$F(7,203) = 69.36$, $p < 0.01$] and Glass pattern [$F(7,203) = 52.77$ $p < 0.01$]. The post hoc analysis of the effect of *noise* after Bonferroni correction showed no significant difference in threshold for *noise* levels of 0˚ to 16˚ ($p > 0.05$) for RDK but the thresholds were lower than those at *noise* levels >24˚ ($p < 0.01$). For the Glass pattern, the thresholds for *noise* levels from 0˚ to 16˚ had no significant difference from each other ($p > 0.05$), the threshold at the *noise* level of 16˚ was not statistically different from that at 24˚ ($p > 0.05$) but higher than thresholds at *noise* levels >32˚ ($p < 0.05$).

3.1.3.2.1 Threshold fit to the equivalent noise paradigm

The mean threshold data from the main experiment were used to fit the equivalent noise paradigm (eq. 3.1) to separate the performance measured at different levels of external noise into internal equivalent noise and sampling efficiency (Pelli, 1981).

$$\sigma_{obs} = \sqrt{\frac{\sigma_{eq}^2 + \sigma_{ext}^2}{Eff}} \qquad \textbf{(\textit{eq.} 3.1)}$$

where,

σ_{obs} is the discrimination threshold,
σ_{eq} is the equivalent internal noise,
σ_{ext} is the added external noise,
Eff is the sampling efficiency

The best fitting parameters were determined using direct search technique, the Nelder-Meade algorithm featured as fminsearch function in MATLAB. The individual internal noise (σ_{eq}) varied from 8.65˚ to 19.44˚ for RDK and from 5.22˚ to 24.91˚ for Glass pattern. The mean equivalent internal noise (σ_{eq}) and sampling efficiency (*Eff*) parameters were 10.06˚ and 7.91 for RDK and 12.86˚ and 2.64 for Glass pattern (Table 3.1 and Figure 3.5). The values of σ_{eq} for both functions were more similar than the *Eff* factor for individual observers as well as the mean data.

The repeated measures ANOVA indicated that the thresholds for both patterns vary in a parallel fashion, which in terms of the linear model implies a similar internal noise with differences in performance reflected in changes in the sampling efficiency only. Nested modelling was then used to verify this finding. The full model of data fitting with the linear amplifier model had a total of four free parameters (σ_{eq} and *Eff* for RDK and Glass). The fitting model was reduced by restricting the number of free parameters by forcing both fits to use a single internal noise with independent sampling efficiency, single sampling efficiency with independent internal noise and a single internal noise and sampling efficiency. Figure 3.5 shows the mean data fitted to the equivalent noise paradigm for the full model and reduced models with different numbers of free parameters. The goodness of fit (r^2 statistics) for the model with one σ_{eq} and independent *Eff* ($r^2 = 0.96$) was more comparable to the full model (2 σ_{eq} and 2 *Eff*, $r^2 = 0.97$) than for the other two reduced models ($r^2 < 0.80$). This was confirmed by the nested hypothesis test (details methods section 2.4.1, Eqn. 2.8) which showed that the goodness of fit of the model with one σ_{eq} and two *Eff* fits were statistically similar to the full model [$F(1,12) = 1.64$, $p > 0.05$] while other reduced models resulted in a significantly poorer fit (*ps* < 0.01). Furthermore, to confirm the validity of the model, the model with one σ_{eq} and two *Eff* was treated as a full model and compared with the simplest model with both σ_{eq} and *Eff* restricted. The simplest model resulted in a poorer fit compared to the full model (1 σ_{eq} and 2 *Eff*), $p < 0.01$. The pattern of results was similar for individual observers (Table 3.1 and Figure 3.4).

Parameter /Subject	AM	MJ	RB	VR	MG	SJ	Average
σ_{eq} RDK	10.39	16.61	13.22	8.65	19.44	12.50	12.86
σ_{eq} Glass	11.05	24.91	9.24	5.22	9.51	8.95	10.06
Eff RDK	5.76	8.64	6.87	7.91	8.63	11.38	7.91
Eff Glass	1.51	2.56	2.40	3.75	3.46	3.37	2.64
r^2	0.95	0.94	0.92	0.95	0.82	0.97	0.97
Complicated reduced model-1 with σ_{eq} constrained							
σ_{eq}	10.74	20.14	11.13	6.79	12.85	10.67	11.36
Eff RDK	5.86	9.78	6.26	7.10	6.71	10.45	7.39
Eff Glass	1.49	2.21	2.63	4.16	4.05	3.68	2.81
r^2	0.95	0.93	0.91	0.93	0.77	0.96	0.96
$F(1,12)$	0.048*	1.22*	1.51*	3.79*	3.42*	2.63*	1.64*
Complicated reduced model-2 with *Eff* constrained							
σ_{eq} RDK	8.13	15.64	8.87	5.77	11.09	9.01	8.78
σ_{eq} Glass	50.61	95.33	24.55	8.87	16.34	33.55	28.78
Eff	4.76	8.21	4.90	5.59	5.38	8.64	5.75
r^2	0.82	0.90	0.75	0.84	0.65	0.78	0.79
$F(1,12)$	36.74	6.84	27.55	24.17	11.10	67.16	66.01
Simplest reduced model with both σ_{eq} *and Eff* constrained							
σ_{eq}	10.74	20.14	11.13	6.79	12.85	10.67	11.36
Eff	2.96	4.64	4.06	5.44	5.22	6.20	4.56
r^2	0.36	0.14	0.54	0.81	0.61	0.48	0.51
$F(2,12)^{\#}$	79.67	75.35	30.64	14.91	7.01	89.39	87.27
$F(1,13)^{\#\#}$	171.88	146.98	57.54	21.46	9.34	156.53	164.74

Table 3.1: The best fitting parameters and r^2 values for the LAM fits to the RDK and Glass pattern thresholds.

The values in the top section are the results of the fits with four free parameters (one σ_{eq} and Eff each for RDK and Glass). The second and third sections show the results with σ_{eq} and Eff constrained respectively across both RDK and Glass. The bottom section shows results with both σ_{eq} and Eff constrained across the conditions.

The F scores are the result of a nested hypothesis test between reduced models (3-parameter or 2-parameter models) and the full models (4-parameter or 3-parameter models).

** represents F scores which resulted in no significant difference ($p > 0.05$) in the goodness of the fit measure with reduced model (here 1 σ_{eq}, 2 Eff) compared to the full model (2 σ_{eq}, 2 Eff).*

$^{\#}$F score of reduced model (1 σ_{eq}, 1 Eff) compared to full model (2 σ_{eq}, 2 Eff).
$^{\#\#}$F score of reduced model (1 σ_{eq}, 1 Eff) compared to the statistically best model from first set of nested models (1 σ_{eq}, 2 Eff).

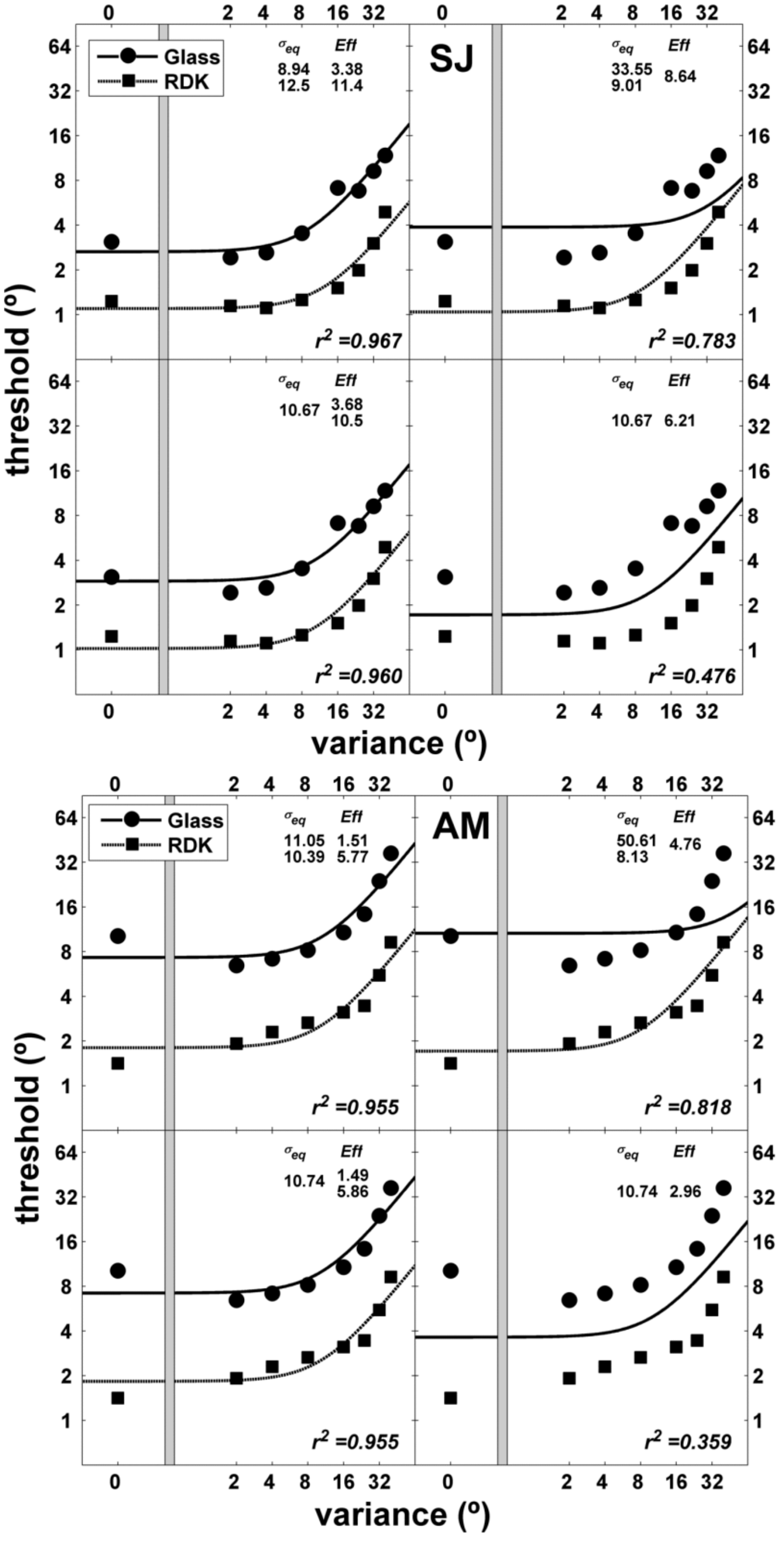

Figure 3.4: Nested modelling for individual direction discrimination and orientation discrimination threshold data.

For both psychophysically experienced observer (SJ) and naïve observer (AM), the reduced model with one σ_{eq} and two Eff (bottom left) resulted in no significant difference ($p > 0.05$) in the goodness of the fit measure (r^2) compared to the full model (top left). Error bars are omitted for a better presentation.

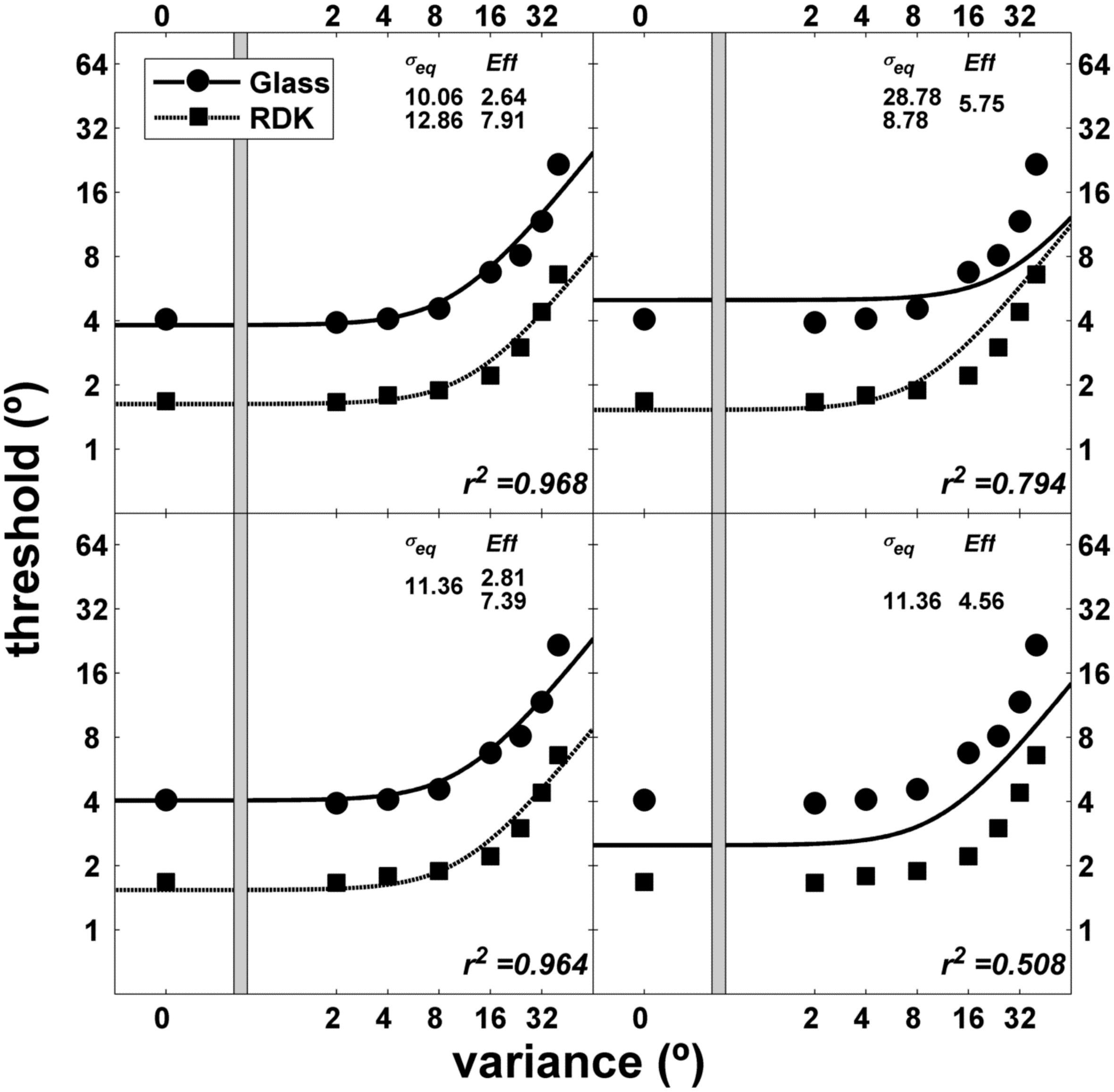

Figure 3.5: Nested modelling for mean direction discrimination and orientation discrimination threshold data.

The reduced model with one σ_{eq} and two Eff (bottom left) resulted in no significant difference ($p > 0.05$) in the goodness of the fit measure (r^2) compared to the full model (top left). Error bars are omitted for a better presentation.

3.2 Experiment 2: Comparison of global orientation thresholds in Glass patterns and line segments

3.2.1 Introduction

The random dot kinematograms (RDK) have remained the stimulus of choice for the study of global motion processing. A variety of stimuli has been used to study global form processing (refer to section 2.3). Some of the most commonly used form stimuli for the comparative study of motion and form processing are line segments (Dakin, 1997; Simmers *et al.*, 2005), Gabor patches (Simmers and Bex, 2004; Mansouri and Hess, 2006), and Glass patterns of varying dot lengths (Spencer *et al.*, 2000; O'Brien *et al.*, 2002; Tsermentseli *et al.*, 2008; Nankoo *et al.*, 2012).

The aim of the studies using these stimuli is to evaluate the global orientation processing which occurrs at the extra striate cortical areas of the visual system. However, at least some proportion of the global processing of Gabor patches and line segments occurs within the primary visual cortex (Grinter *et al.*, 2010). The orientation sensitive cells responsive to a particular orientation are arranged in a columnar fashion in V1 with adjacent columns responsive to contiguous orientation (Hubel and Wiesel, 1968). The orientation columns are interconnected forming a long range, lateral horizontal connections (Gilbert and Wiesel, 1983; Gilbert and Wiesel, 1989; Malach *et al.*, 1993; Field and Hayes, 2004). Such lateral connections are most prominent in the superficial layers of V1 (1 to 3) (Lund *et al.*, 1993) where most of the orientation selective cells are concentrated (Hawken *et al.*, 1988). These horizontal connections extend up to 6mm in length covering many V1 hypercolumns (Gilbert and Wiesel, 1983; Gilbert and Wiesel, 1989). Similar clustered horizontal connections are also present in area V2 (Lund *et al.*, 1993). The long range lateral connections in V1/V2 group visual scenes based on the orientation information such as the field of Gabor patches and line segments with similar orientations (Hess *et al.*, 2003; Field and Hayes, 2004; Grinter *et al.*, 2010) and may contribute in part to the global integration/averaging mechanism. Due to the influence of the local long range lateral interactions in the processing of such stimuli, it has been suggested that stimuli based on line segments and Gabor patches should be avoided if the aim is to evaluate the global orientation processing occurring at higher cortical areas such as V4 (Grinter *et al.*, 2010).

The detection of dipole Glass patterns is based on extracting orientation information from the dot to dot correspondence of dipole pairs. As the global structure of a Glass pattern is only perceivable within a dipole separation up to 23 arc min (Dakin, 1997), there is less likelihood of activation of the long range horizontal connections of V1 by the dipole Glass pattern (Grinter *et al.*, 2010). Hence the global orientation processing of Glass patterns most likely occurs at the higher extra striate cortical areas (*e.g.,* V4). The Glass patterns with multiple elements (> 2 dots) have a longer length than the dipole Glass pattern and in theory could activate the long range lateral connections. However, unlike in the line segment, the visual system also needs to solve the dot to dot correspondence problem in such Glass patterns. In this experiment, we evaluated how noise affects processing of these commonly used stimuli aimed at investigating global form processing.

3.2.2 Methods

The stimuli were "multipole" Glass patterns composed of different numbers of dots in a defined orientation axis and line segments of varying lengths. The "tripole" and "quadrapole" Glass patterns were created with three and four dot elements respectively in an orientation axis instead of two elements used in the dipole Glass pattern. The line segment stimuli were created by connecting the dot elements of the dipole and quadrapole Glass patterns.

The dipole Glass patterns were similar to what was explained in the general methods (section 2.0) and experiment 1, the only difference was that instead of 500 dot elements (250 dipoles), 480 dot elements (240 dipoles) were used. To create the tripole Glass pattern, a third dot element was added to the dipole Glass pattern on the same orientation axis. Each dot element (0.083˚ in diameter) was separated by the same dot to dot distance (0.133˚) as in a dipole Glass pattern. As the total number of dots (*i.e.*, 480) in the tripole Glass pattern was the same as in the dipole Glass pattern, the tripole Glass pattern contained 160 tripole elements (Figure 3.6, A). Similarly, for the quadrapole Glass pattern, four dots were aligned in the same orientation axis separated by the same dot to dot distance (Figure 3.6, B). The quadrapole Glass pattern hence contained 120 elements. Other physical properties of the tripole and quarapole Glass pattern were similar to the dipole Glass pattern.

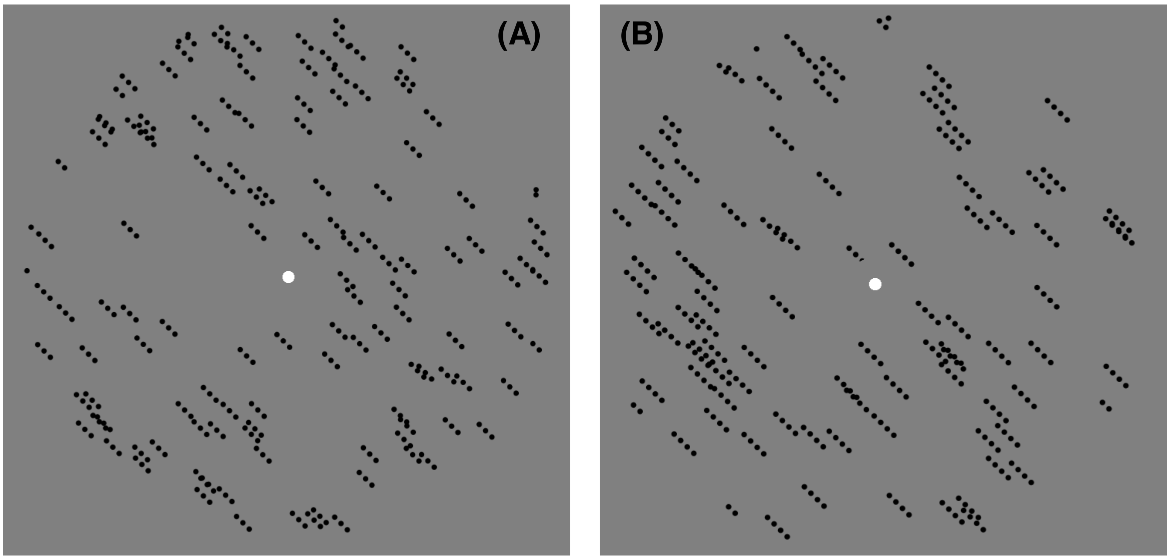

Figure 3.6: Schematic representation of the tripole and quadrapole Glass patterns.

The tripole (A) and quadrapole (B) Glass patterns with no added noise oriented 45˚ left from the vertical.

For the line segments, the dot to dot separation in the Glass pattern was connected with extra dots forming a line structure. The line width was hence equivalent to the dot diameter in the Glass pattern (0.083˚). Two line lengths were used; equivalent to the total length of the dipole Glass pattern (0.216˚) – Line2 and quadrapole Glass pattern (0.482˚) – Line4. The line segment stimulus that was equivalent to the dipole Glass pattern contained 240 line elements (Figure 3.7, A), while the line segment stimulus that was equivalent to the quadrapole Glass pattern contained 120 lines (Figure 3.7, B).

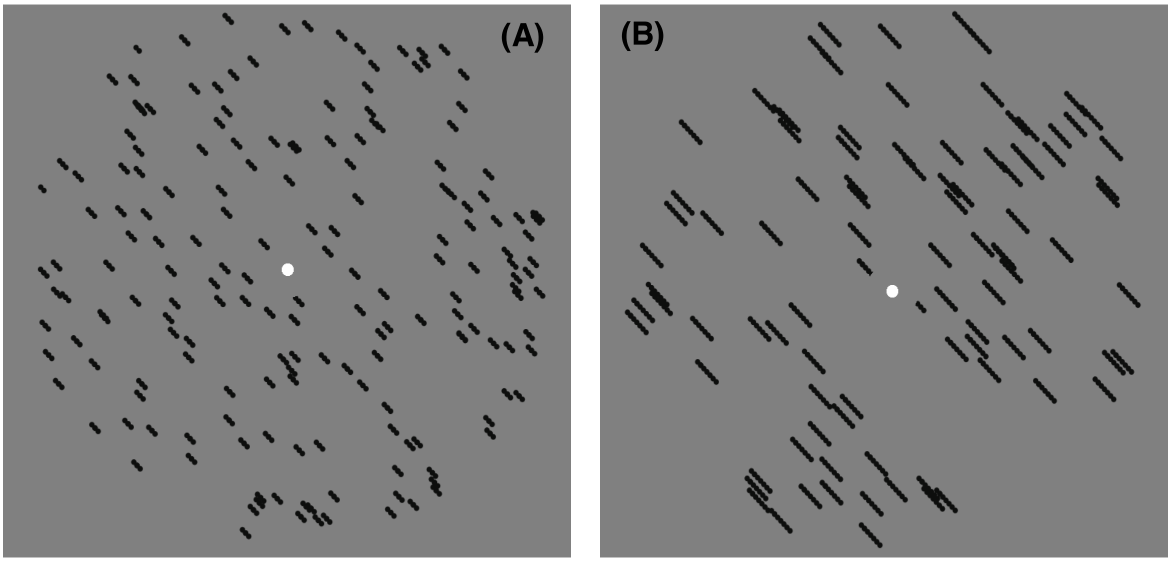

Figure 3.7: Schematic representation of the line segment stimuli.

The lengths of Line2, (A) and Line4, (B) are equivalent to dipole Glass pattern and quadrapole Glass pattern respectively and both are oriented 45˚ left from the vertical with no added noise.

The method of stimulus presentation, the procedure of data collection and analysis were the same as described previously in general methods (section 2.3). Five visually normal observers (35±5.7 years) participated in the experiments for the dipole Glass pattern, tripole Glass pattern, quadrapole Glass pattern, and line segments. All participants discriminated the overall orientation from the vertical reference (90˚) at five external noise levels (0˚, 5˚, 10˚, 20˚, and 45˚). Only five noise levels were used to reduce the time of the experimental sessions.

For the Glass patterns (described above), the number of dots forming each stimulus was kept constant (480 dots). This resulted in unequal numbers of signal elements in the different Glass patterns (240 in dipole, 160 in tripole and 120 in quadrapole). To rule out the influence of the number of signal providing elements on orientation discrimination thresholds, two psychophysically experienced observers also completed five experimental sessions for each stimulus in which the numbers of signal elements were kept constant by varying the total number of dots (240 dots for dipole, 360 for tripole and 480 for quadrapole). All three Glass patterns hence contained 120 signal elements. Similarly, the same observers also completed five sessions of experiments for line segment stimuli with equivalent length to the dipole and quadrapole Glass pattern containing an equal number of line elements (120 each).

3.2.3 Results

3.2.3.1 Orientation discrimination thresholds for dipole and other multipole Glass patterns

The orientation discrimination thresholds for the quadrapole Glass pattern were the lowest while the thresholds for the dipole Glass pattern were the highest at the no noise condition for both individual observers and the mean data (Figure 3.8). The thresholds for the tripole Glass pattern were mostly in between that of the quadrapole and dipole Glass patterns. The thresholds for all three Glass pattern types converged at higher noise levels.

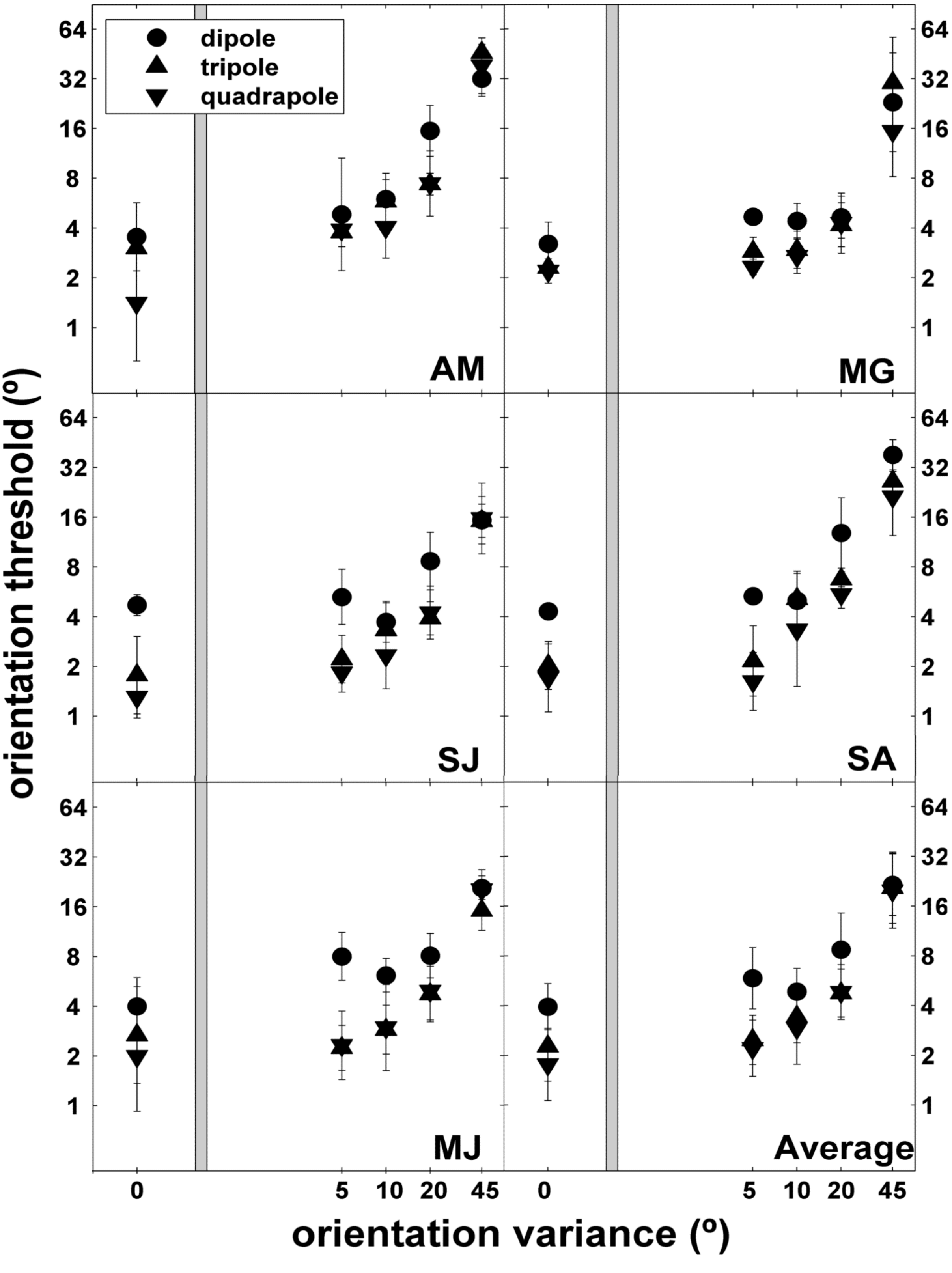

Figure 3.8: Orientation discrimination thresholds for Glass patterns with varying number of elements.

Each panel shows data for a single observer and average data (bottom right panel) for dipole, tripole, and quadrapole Glass patterns at five noise levels. Each data point for individual observer represents the mean from five experimental sessions for observers MJ and SJ and three sessions for the rest. The error bar represents ±1 standard deviation.

A repeated measures ANOVA was conducted with *noise* (5 levels) and *stimuli type* (3 levels; dipole, tripole and quadrapole) as within subject factors. The Mauchly's test revealed that the log transformed data conformed to the assumption of sphericity for *noise* [$\chi^2(9) = 7.36$, $p > 0.05$], *stimuli type* [$\chi^2(2) = 3.98$, $p > 0.05$], and *noise* and *stimuli type* interaction [$\chi^2(35) = 47.59$, $p > 0.05$]. The results showed a significant effect of *noise* [$F(4,68) = 207.52$, $p < 0.01$] and *stimuli type* [$F(2,34) = 35.45$, $p < 0.01$]. The interaction between *stimuli type* and *noise* was also significant [$F(8,136) = 5.16$, $p < 0.01$]. The comparison of *stimuli type* after Bonferroni correction revealed that the orientation thresholds for the dipole Glass pattern were significantly higher than both tripole and quadrapole Glass patterns (*ps* < 0.01) while the thresholds for the tripole and quadrapole were similar ($p > 0.05$).

The orientation discrimination thresholds from different stimulus types were then fitted to the linear amplifier model and the results were analysed with the nested modelling method (Figure 3.9). The goodness of fit (r^2 statistics) for the simplest model (with both σ_{eq} and *Eff* constrained across the stimulus types) was poorer than the full model [$F(4,9) = 4.20$, $p < 0.05$], while the other two reduced models resulted in a statistically similar fit to the full model; σ_{eq} constrained [$F(2,9) = 1.12$, $p > 0.1$] and *Eff* constrained [$F(2,9) = 0.82$, $p > 0.1$]. The model with the *Eff* constrained was chosen as the best model to represent the threshold data based on the higher r^2 value between the two models. The model (three σ_{eq} and one *Eff*) was then treated as the full model and compared to the simplest model (both σ_{eq} and *Eff* constrained). The results showed that the simplest model resulted in a poorer fit than the model with *Eff* constrained across the stimuli type [$F(2,11) = 9.26$, $p < 0.01$].

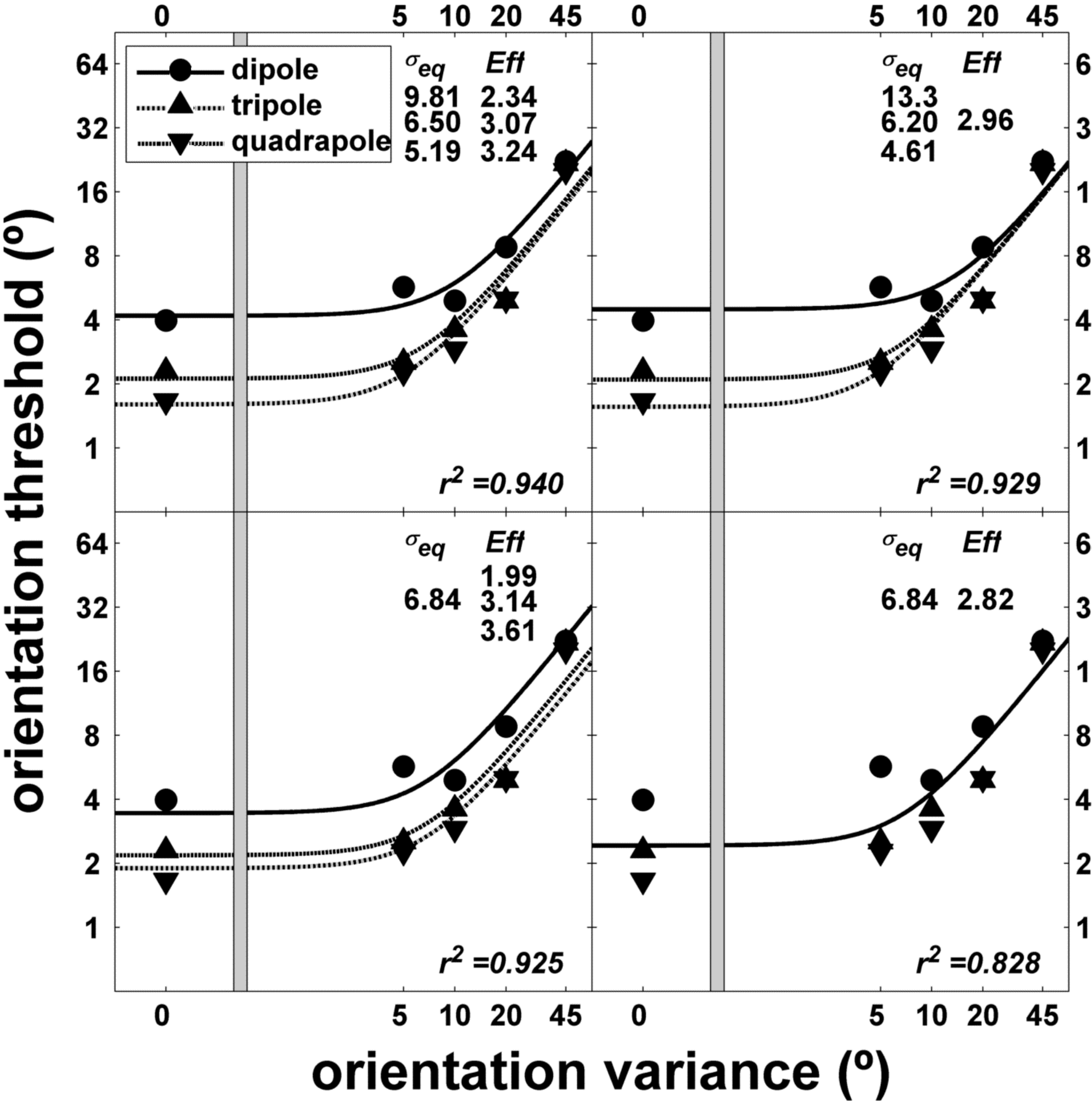

Figure 3.9: Nested modelling for mean orientation discrimination thresholds from dipole, tripole and quadrapole Glass patterns.

The reduced model with three σ_{eq} and one Eff (top right) was statistically chosen as the best model to represent the threshold data. Error bars are omitted for a better presentation.

The pattern of results was similar for two psychophysically experienced observers when the signal elements in all three stimuli were kept constant (120 dipole, tripole, and quadrapole). The thresholds for the dipole Glass pattern were highest followed by the tripole and qudrapole Glass patterns at the lower noise levels while the thresholds for different Glass patterns converged at higher noise levels for both observers (Figure 3.10).

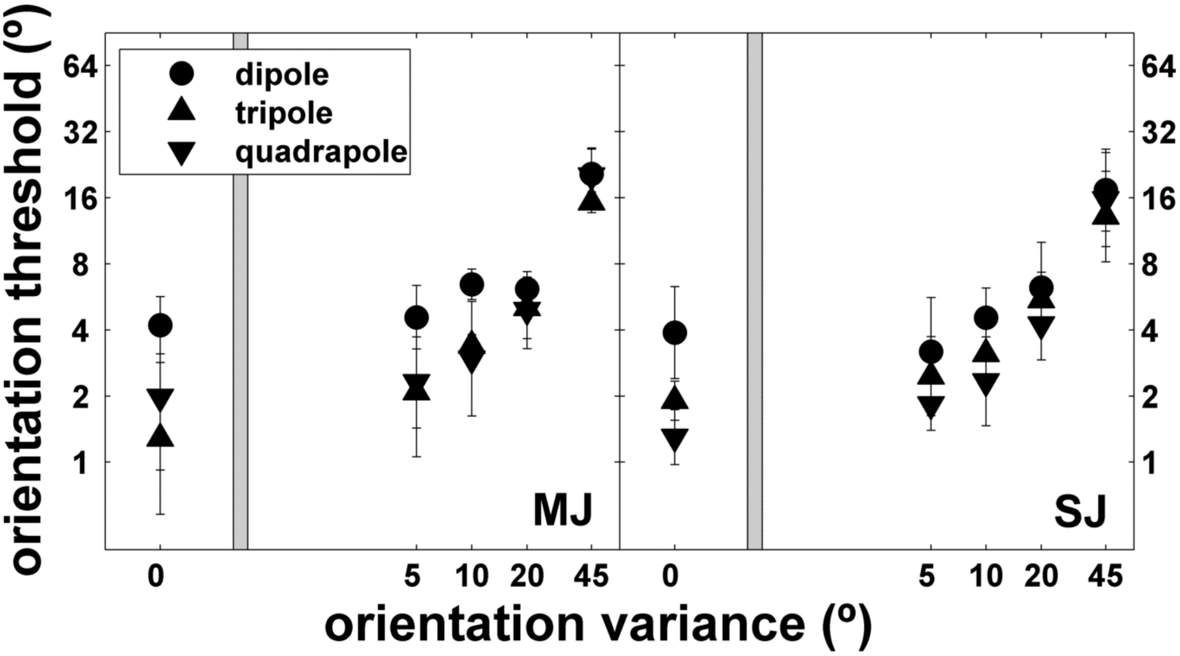

Figure 3.10: Orientation discrimination thresholds for Glass patterns with equal number of signal elements.

Each panel shows data for a psychophysically experienced observer for dipole, tripole and quadrapole Glass pattern containing equal number of signal elements (120) with different number of dot elements (240, 360, 480 dots for dipole, tripole and quadrapole respectively). Each data point represents the mean from five experimental sessions and the error bar represents ±1 standard deviation.

3.2.3.2 Orientation discrimination in line segments

The orientation discrimination thresholds for the line segments with varying lengths were then compared to the thresholds from the dipole Glass pattern. The threshold for the line segment with length equivalent to the quadrapole Glass pattern – Line4 was the lowest at the low noise condition. The thresholds for the line segment with equivalent length to that of dipole Glass pattern – Line2 and dipole Glass pattern were similar at all noise levels (Figure 3.11). However, at the high noise condition, orientation discrimination thresholds for all three stimuli converged.

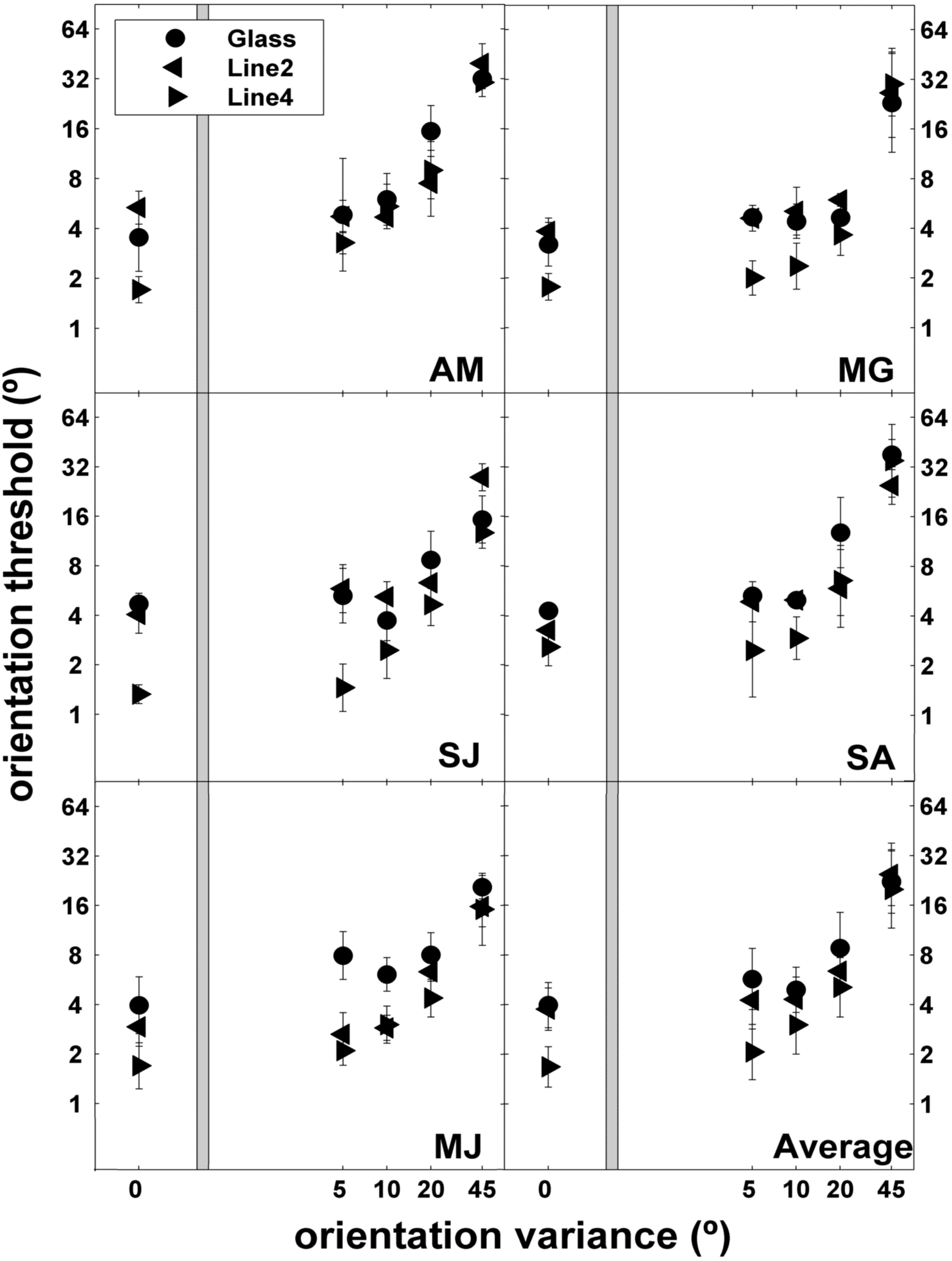

Figure 3.11: Orientation discrimination thresholds for line segments and dipole Glass pattern.

Each panel shows data for a single observer and average data (bottom right panel) for dipole Glass pattern, Line2 and Line4 at five noise levels. Each data point represents the mean from five experimental sessions for observers MJ and SJ and three sessions for the rest. The error bar represents ±1 standard deviation.

The repeated measures ANOVA was then conducted with *noise* (5 levels) and *stimuli type* (three levels; dipole Glass pattern, Line2 and Line4) as within subject variables. The Mauchly's test revealed that the log transformed data confirmed to the assumption of sphericity for *noise* [$\chi^2(9) = 12.49$, $p > 0.05$], *stimuli type* [$\chi^2(2) = 1.65$, $p > 0.05$], and the *noise* and *stimuli type* interaction [$\chi^2(35) = 32.80$, $p > 0.05$]. The results showed significant effect of *noise* [$F(4,68) = 283.75$, $p < 0.01$] and *stimuli type* [F (2,34) = 33.80, $p < 0.01$]. The interaction between *stimuli type* and *noise* was also significant [$F(8,136) = 7.17$, $p < 0.01$]. The comparison of *stimuli type* after Bonferroni correction revealed that the thresholds for the dipole Glass pattern and Line2 were significantly higher than Line4 (*ps* < 0.01) with no statistical difference between the thresholds for the Line2 and dipole Glass pattern ($p > 0.1$).

The nested modelling analysis (Figure 3.12) showed that the simplest model (with both σ_{eq} and *Eff* constrained across the stimulus types) resulted in a poorer fit compared to the full model [$F(4,9) = 5.08$, $p < 0.05$]. The goodness of fit of the other two reduced models were meanwhile statistically similar fit to the full model; σ_{eq} constrained [$F(2,9) = 1.64$, $p > 0.1$] and *Eff* constrained [$F(2,9) = 1.09$, $p > 0.1$]. The model with the *Eff* constrained was chosen as the best model based on the higher r^2 value among the two models. Further, the model with *Eff* constrained was treated as the full model and compared to the simplest model (both σ_{eq} and *Eff* constrained). The result showed that the simplest model resulted in a poorer fit compared to the model with *Eff* constrained across the stimuli types [$F(2,11) = 11.09$, $p < 0.01$].

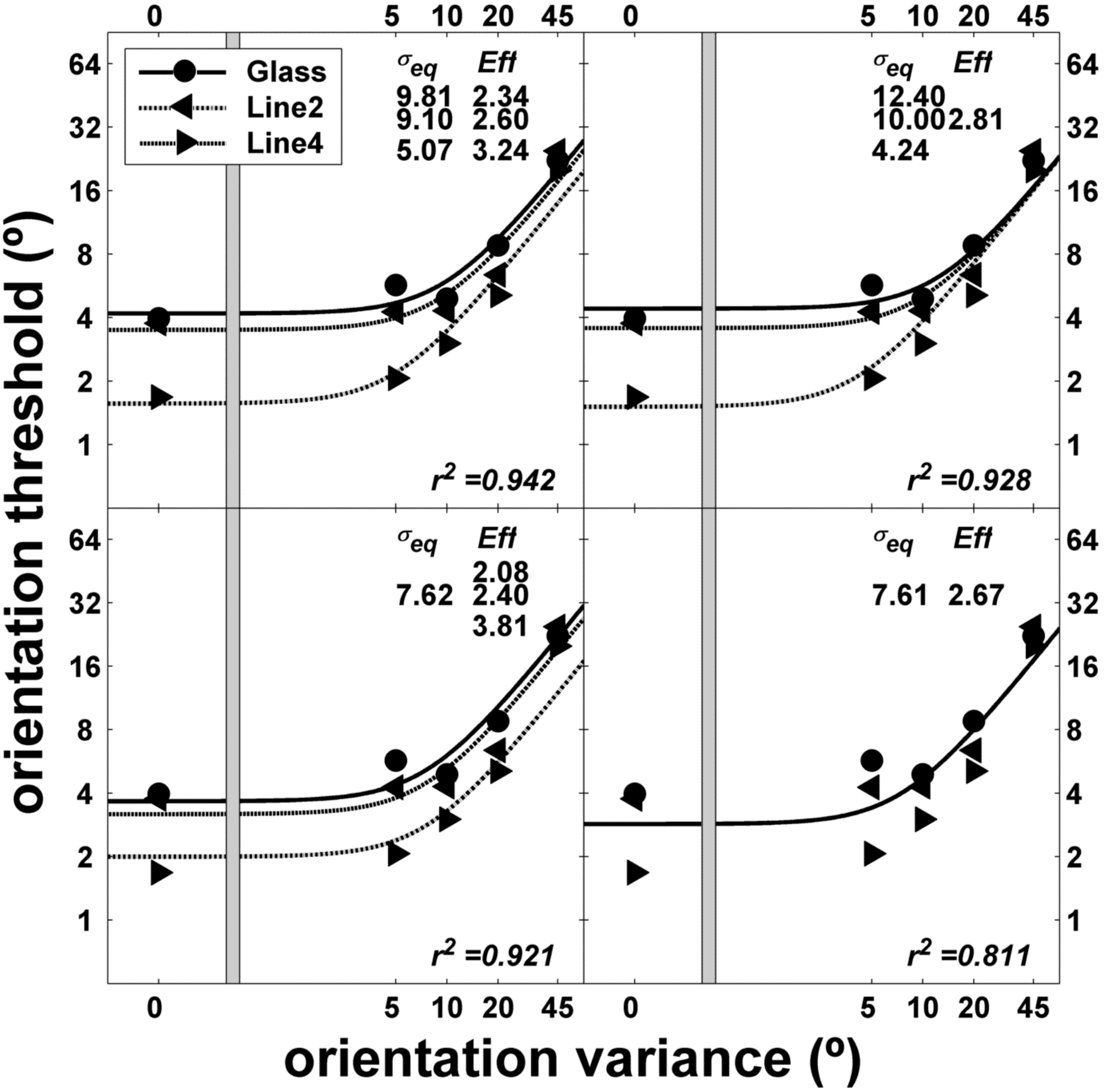

Figure 3.12: Nested modelling for mean orientation discrimination thresholds from dipole Glass pattern, and line segments of varying lengths.

The reduced model with three σ_{eq} and one Eff (top right) was statistically chosen as the best model to represent the threshold data. Error bars are omitted for a better presentation.

When the orientation discrimination thresholds for the line segments with 120 line elements were compared to dipole Glass patterns with the same number of dipole elements, the thresholds for the dipole Glass pattern and Line2 were higher than the Line4 at low noise levels (Figure 3.13). The thresholds for all three stimuli were similar at the higher noise levels, following the pattern of results seen in the previous experiment.

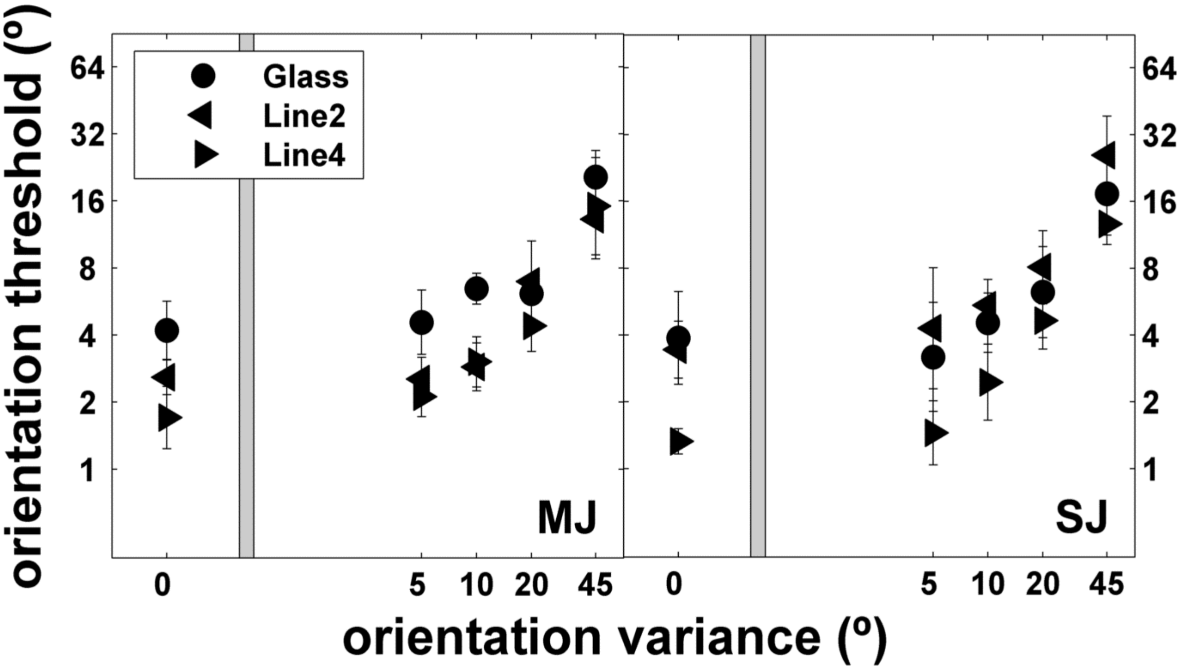

Figure 3.13: Orientation discrimination thresholds for dipole Glass patterns and Line2 and Line4 with equal number of signal elements.

Each panel shows data for a single psychophysically experienced observer for dipole Glass pattern, Line2 and Line4 with equal number of signal elements (n = 120) at five noise levels. Each data point represents the mean from five experimental sessions and the error bar represents ±1 standard deviation.

3.2.3.3 Comparison of orientation discrimination thresholds between Glass patterns, line segments and direction discrimination thresholds in RDK

We then compared thresholds across all stimuli (Glass patterns with 480 dots and their equivalent length line segments) aimed at evaluating global orientation discrimination. At low and moderate noise levels, mean orientation discrimination thresholds for the quadrapole Glass pattern, and Line4 were similar and the lowest, followed by the tripole Glass pattern while the thresholds for the dipole Glass pattern and Line2 were mostly similar and the highest (Figure 3.14). The orientation discrimination thresholds for all stimuli converged at the highest noise level evaluated.

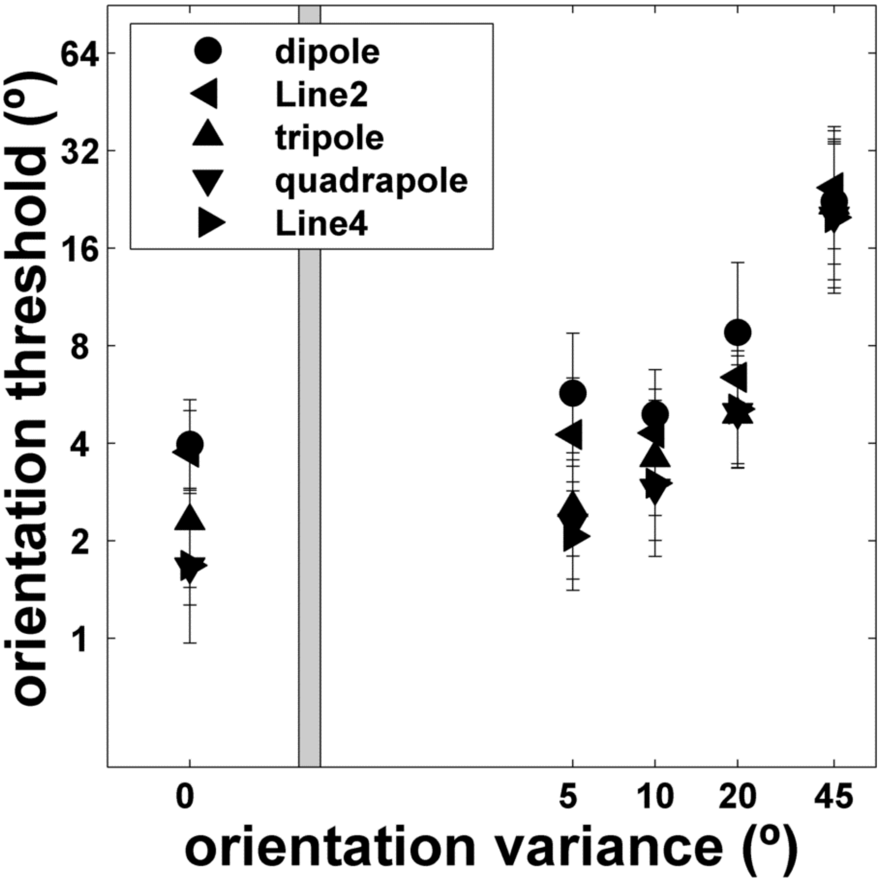

Figure 3.14: Comparison of mean orientation discrimination thresholds for Glass patterns and line segments.

To compare the orientation thresholds (Glass patterns and line segments) with the direction of motion (RDK), four out of five observers (except SA) also completed the evaluation for the RDK stimuli with similar stimulus parameters (*i.e.*, number of dots = 480 and evaluation at five noise levels). The results showed that the direction discrimination threshold for the RDK were similar to the orientation discrimination thresholds for the quadrapole Glass pattern and Line4 in the no noise condition. However, the direction discrimination thresholds (RDK) remained lowest at all other noise levels compared to orientation discrimination thresholds for Glass patterns and line segments, even at the highest noise level (Figure 3.15).

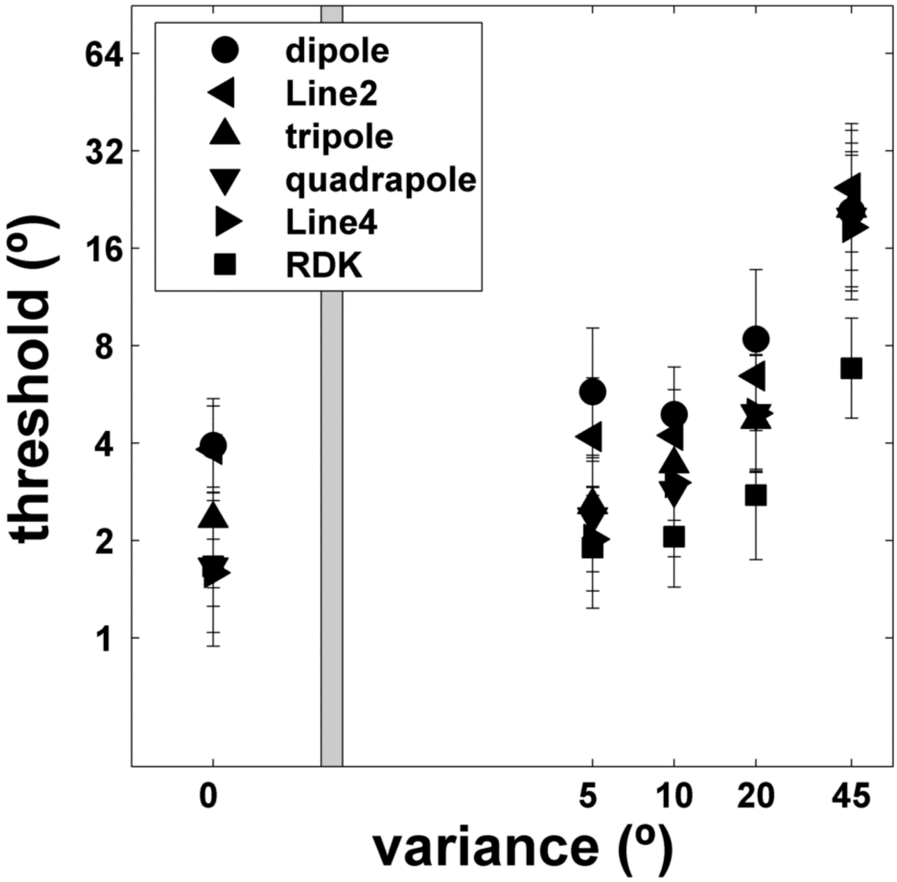

Figure 3.15: Comparison of mean orientation discrimination thresholds for Glass patterns and line segments with the direction discrimination for RDK.

3.3 Discussion

3.3.1 Comparison of orientation discrimination (Glass pattern) with direction of motion discrimination (RDK)

The mean fine discrimination thresholds (*i.e.*, thresholds at no noise condition) for the direction of motion in the RDKs and the orientation of the dipole Glass patterns were 1.85° (±0.89°) and 5.62° (±5.76°) respectively. Our results are in agreement with previous studies that showed similar fine direction discrimination thresholds for young adults (Bocheva *et al.*, 2013; Bogfjellmo *et al.*, 2014). There are no reports on fine orientation discrimination thresholds with Glass pattern.

The orientation discrimination thresholds (Glass pattern) were consistently higher than that for the direction of motion (RDK) at all levels of added external noise. This shows that the human visual system is more sensitive to motion cues than form cues. The global orientation coherence thresholds for the physically comparable Glass pattern were also reported to be higher than that for the direction of motion discrimination in RDK in a visually normal population (Ditchfield *et al.*, 2006; Nankoo *et al.*, 2012). Another study that used the motion path of a RDK converted to line streaks to simultaneously study motion and form perception also reported higher coherence thresholds along the form pathway than the motion pathway for normal individuals (Simmers *et al.*, 2003b; Simmers *et al.*, 2005; Simmers *et al.*, 2006b). Even though these studies used a different global task, the pattern of results is similar to our findings.

The better motion discrimination threshold compared to the orientation discrimination threshold could be due to the differences in processing mechanisms. The direction of motion in the RDK is computed from the direction vectors created by the correspondence of each dot from one frame to the next. The motion streak system (Geisler, 1999) suggests that the direction as well as orientation selective cells in V1 and higher cortical areas both respond to the motion and motion trail left behind by stimuli such as a RDK. The responses are then combined to accentuate the perception of motion. The influence of such a mechanism could have resulted in the better direction discrimination thresholds for RDKs. Edwards and Crane (2007) also reported that direction discrimination is accentuated by the motion streak mechanism. They measured direction discrimination thresholds in a RDK stimuli in which the coherent motion signal was carried by either the same dot over the frames (creating longer motion streak) or different dots. They report lower thresholds when the motion signal was carried by same dots at high speed.

The local and global processing of both stimuli that could have resulted in the observed differences is further discussed in relation to the internal equivalent noise and sampling efficiency.

We further probed better performance for motion processing with the equivalent noise paradigm to parse out the effects of local and global processing mechanisms. The threshold vs. noise (*TvN*) curve for both motion and form perception showed that the performance remained constant at low noise levels and increased at higher levels of external noise. Similar findings have been reported in the motion domain using RDK stimuli (Watamaniuk and Sekuler, 1992; Watamaniuk and Heinen, 1999; Dakin *et al.*, 2005; Mareschal *et al.*, 2008; Bocheva *et al.*, 2013; Bogfjellmo *et al.*, 2013; Bogfjellmo *et al.*, 2014) and in the form domain using Gabor elements (Dakin, 2001).

Internal equivalent noise and sampling efficiency from a linear model fit for the mean direction discrimination thresholds were 12.86˚ and 8 elements. Watamaniuk and Sekuler (1992) reported that the threshold for direction discrimination in RDKs starts to increase when the external noise in the stimuli exceeds 25˚. In the present study the results of the repeated measures ANOVA suggested that the direction discrimination threshold starts to increase between an external noise of 8˚ and 16˚. The difference in the level of equivalent internal noise could be due to the different stimulus parameters such as the number of elements (163 dots), element size (0.05˚), element density (2.56 dots/deg^2) and display duration (0.4s) used. In the current study, 500 dot elements of 0.083˚ diameter with the dot density of 12.81dots/deg^2 were displayed for 0.5s. Similarly, Bocheva *et al.,* (2013) reported the internal noise and sampling efficiency of 2.97˚ and 15 elements at the dot speed of 6.75˚/s with stimulus containing 128 Gabor micro-pattern elements (Bocheva *et al.*, 2013). In another study using similar micro-patterns with 256 elements, Dakin *et al.,* (2005) reported an equivalent internal noise of 4.4 - 5.9˚ and a sampling efficiency of 10 - 22.7 elements. They also reported that both internal noise and sampling efficiency increases with an increase in the number of elements in the display, with minimal influence of other stimulus parameters such as dot density or display aperture (Dakin *et al.*, 2005). The pattern of results from these different studies seems to reaffirm the finding that internal equivalent noise increases with the increase in the number of dot elements. Bocheva *et al.,* (2013) used 128 elements to report an equivalent internal noise of 2.97˚, Dakin *et al.,* (2005) reported an equivalent internal noise of 5.5˚ with 256 elements while the current study finds an equivalent internal noise of 12.86˚ with 500 elements display. However, Dakin *et al.,* (2005) also reported an internal equivalent noise of 4.8˚ for a stimulus display with 64 elements, which is higher than that reported by Bocheva *et al.,* (2013) for a 128 element display. Hence such comparisons across different studies might only be reflective of the differences in the stimulus and parameters used.

The mean equivalent internal noise and sampling efficiency for the orientation discrimination was 10.06˚ and 3 elements respectively. The sampling efficiency is proposed to represent the number of elements that are integrated to provide a global percept (here dipole pairs). The low values of sampling efficiency (ranging from 1.51 to 3.75 for individual observers) observed here is due to the log values used for the fitting purpose. The reported values hence represent the index of information available for the global judgement. There are no previous reports on the internal noise and sampling efficiency employing Glass pattern stimuli. A study that investigated fine orientation discrimination with stimuli containing 256 Gabor patches reported equivalent internal noise in the range of 4.4˚- 7.8˚ (Dakin, 2001). Dakin (2001) evaluated the effect of different stimulus parameters such as area and radius of the display using a completely different stimulus from the one used in the current study and hence the results are not directly comparable.

Comparison of the *TvN* curves along the motion and form domain analysed by the repeated measures ANOVA and nested modelling showed that the equivalent internal noise remained constant across two processing pathways with the difference in threshold best described by the changes in the sampling efficiency. The difference in equivalent internal noise is reflective of changes in the local directional/orientation uncertainty of the elements while sampling efficiency reflects the number of elements that the system can pool to reach the overall direction/orientation judgement (Dakin *et al.*, 2005). Our result of similar internal equivalent noise suggests that both pathways might share similar local processing limitations with differences in the performance due to a better efficiency in the global processing mechanism along the motion pathway. Various studies suggest that the local processing of dot motion in RDKs (Morrone *et al.*, 1995; Nishida, 2011) and dipole orientation in Glass patterns (Wilson *et al.*, 1997; Smith *et al.*, 2002; Wilson *et al.*, 2004; Smith *et al.*, 2007) occurs in area V1/V2 with global processing occurring in areas of MT and V4. The direction and orientation sensitive neurones in V1 share common processing limitations such as aperture problem (Wuerger *et al.*, 1996). These common physiological limitations could have resulted in the similar internal equivalent noise observed in both domains.

The better sampling efficiency along the motion pathway reported here is in line with the previous findings of a larger global pooling for motion processing than form processing. The global pooling of motion (Morrone *et al.*, 1995) and form (Wilson and Wilkinson, 1998) has been studied using a similar methodology of restricting the coherent signals in the RDK and Glass pattern to wedge shaped areas of varying size within the stimulus. The discrimination threshold for a translating RDK pattern improved linearly with the increase in the size of the signal area, implying global spatial summation of almost 100% (Morrone *et al.*, 1995). However, for the translating Glass pattern, the global summation was only about 25-33% (Wilson and Wilkinson, 1998).

Using identical stimulus, the current study showed that the human visual system is more sensitive to motion cues which are processed along the dorsal stream compared to the orientation processing along the ventral stream. Our results showed that local processing of information in the early processing areas are similar for both motion and form processing however global pooling of information is more efficient for motion processing compared to that of form processing.

3.3.2 Global orientation processing in the Glass pattern and line segments

3.3.2.1 Glass patterns

The orientation discrimination thresholds were lower for tripole and quadrapole Glass patterns compared to the dipole Glass pattern at the lower noise levels before converging at the highest noise condition. Further, the thresholds for the tripole and quadrapole Glass patterns were similar at all noise levels. This suggests that the advantage of facilitating the orientation discrimination by strengthening the axis of orientation with more dot elements is present at low and mid noise levels only. The detection of the dipole Glass pattern is based on one to one correspondence of two dipole elements (Glass, 1969). However for the tripole and quadrapole Glass pattern, such correspondence does not seem necessary as the multiple elements along the same orientation axis form a structure similar to a line segment. The similar threshold between the quadrapole Glass pattern and its equivalent Line4 stimuli at all noise levels further suggests that this indeed may be the case. The line segments activate the local lateral connections in V1 and are processed more as an extended contour (Field and Hayes, 2004) (details in line segment section 3.3.2.2). This difference in processing mechanism may have resulted in lower orientation discrimination thresholds for both tripole and quadrapole Glass patterns. Our results, therefore, suggest that the processing of the dipole Glass pattern is different from that of the Glass patterns with more than two elements defining the orientation axis.

Upon fitting the threshold data to the linear amplifier model, the reduced models with internal noise constrained and sampling efficiency constrained across the stimulus were similar to the full model. We selected the model with sampling efficiency constrained as best model based of better goodness of fit. The difference in the internal equivalent noise is related to the local level processing, which occurs at the early cortical areas of V1 and V2 (Wilson *et al.*, 1997; Wilson *et al.*, 2004). The processing of dipole Glass patterns is relatively immune to the influence of the lateral horizontal connections of V1 due to the length of the dipoles being inadequate to activate such a mechanism (Grinter *et al.*, 2010). However, little is known about the influence of the lateral connections in the Glass pattern composed of more than two dipole elements. The lower internal equivalent noise for tripole/quadrapole Glass pattern compared to dipole Glass pattern could be due to the differences in the local orientation processing mechanisms from the influence of local horizontal connections. The influence of local lateral connections in the processing of line segments is further discussed in section 3.3.2.2.

The similar pattern of results in the experiment employing an equal number of signal elements showed that the differences in the performance between dipole, tripole, and quadrapole Glass pattern is robust to the variation in the number of constituent elements in the display, at least in the range tested here. Dakin (1997) reported that a change in the number of dipole elements in the Glass pattern has no effect on the performance when the number of dipoles exceeds 64. Our results showed that this may be true for the tripole and the quadrapole Glass patterns as well. However, a study with larger variation in the number of signal elements is needed to substantiate such a claim beyond the number of elements evaluated here.

3.3.2.2 Line segments

The orientation discrimination thresholds for the longer line segment (Line4) were lower than that of the smaller line segment (Line2) and its equivalent dipole Glass pattern at the lower noise levels. The thresholds for different patterns converged at higher noise levels. The results were also similar with stimuli containing an equal number of line elements of varying lengths. This pattern of result is similar to that of the Glass patterns with multiple elements. Dakin (1997) also reported lower thresholds for line segments (of length 1.23˚) compared to Glass patterns of equivalent length at all noise levels. In the current study, the length of line stimuli Line2 (0.216˚) and Line4 (0.482˚) were shorter than that of the line segments used in the Dakin (1997) study. Our result of lower thresholds for the Line4 is in line with the findings from Dakin (1997). However, we find similar thresholds for Line2 and the dipole Glass pattern irrespective of noise levels. This suggests that the facilitation of orientation discrimination with line segments as opposed to the dipole Glass pattern is only activated after the length of the line exceeds a certain limit (beyond 0.216˚ here for the Line2). Aspell *et al.,* (2006) also reported lower coherence thresholds for the parallel line segments compared to the Glass pattern. They suggested that the elevated coherence thresholds for the Glass pattern could be due to the increase in correspondence noise during matching of the dipole pair to extract the local orientation information (Aspell *et al.*, 2006), which could also be the case for the dipole Glass pattern here.

The result of the nested modelling showed that the difference in thresholds between the dipole Glass pattern and the line segment (Line4) could be explained by both changes in internal noise or sampling efficiency with the model with difference in internal noise showing marginally better goodness of fit measure. In a similar study, Dakin (1997) reported lower orientation discrimination thresholds for line segments compared to dipole Glass patterns at all noise levels. They suggested that the internal noise remained constant between the dipole Glass pattern and the line segment, with differences in the performance related to the effect of the multiplicative noise, a parameter similar to the sampling efficiency reported here (Dakin, 1997). However, the study evaluated noise levels up to 32˚. We also find that the mean orientation discrimination thresholds for the dipole Glass pattern and Line4 were generally parallel until the noise levels reached 20˚ before converging at the highest noise levels (45˚).

The difference in the internal noise between dipole Glass pattern and line segments could be related to the presence of correspondence noise in the dipole Glass pattern stimuli as suggested by Aspell *et al.,* (2006). However, we find that the orientation discrimination thresholds for Line2, in which dot-to-dot correspondence is not required, were also similar to the dipole Glass pattern at all noise levels. Hence the higher internal noise for the Glass pattern compared to Line4 does not seem to be related to the correspondence noise. Another reason for the differences in the internal noise could be due to the influence of the local horizontal connections in the early cortical areas of V1/V2. The length of the dipole pairs in the dipole Glass patterns is inadequate to activate the local lateral connections in V1 and V2, and our results suggested that this was the same when the dipole elements are connected to create a line. The lower internal noise for longer line segments, however, suggests that processing at early cortical areas of V1/V2 may be different for such stimuli. The lateral connections in V1/V2, group the line segments with similar orientation within up to 2˚ of visual space (Li and Gilbert, 2002). Such a process contributes to the global averaging process in the line segment reserved for the higher extra striate cortical areas for Glass pattern stimuli. Our modelling results showed that both models with changes in internal noise and sampling efficiency could explain the difference in performance across the stimuli, suggesting that at least some part of global processing could occur under the influence of the local lateral connections at early cortical areas of V1/V2 How such differences in processing might have resulted in the differences in internal equivalent noise is open to investigation. If we assume that local orientation processing occurs after the grouping of the line segment by local lateral connections at V1/V2, this would effectively lead to a smaller number of local orientation samples being processed. The smaller iterations of the local processing would lead to a lower internal noise for the longer line segment observed here.

When the orientation discrimination thresholds for different Glass patterns and line segments were compared to the direction discrimination thresholds for the RDK, the thresholds for the dipole Glass pattern and Line2 were higher at all noise levels (reflecting differences in sampling efficiency with constant internal equivalent noise), as observed in the previous experiment. The orientation discrimination thresholds for the quadrapole and Line4 were similar to the thresholds for the direction discrimination in RDK in the no noise condition with thresholds being significantly higher at the high noise. Various studies have used the Glass patterns composed of more than two elements and line segments as a comparable form stimulus to the motion discrimination in RDKs when measuring coherence thresholds in different clinical disorders such as autism (Spencer *et al.*, 2000), dyslexia (Tsermentseli *et al.*, 2008). In the coherence threshold paradigm, added noise is in a random direction/orientation. The implication of the interaction of direction and orientation thresholds in RDK and quadrapole/ Line4 stimuli observed at the lower noise levels in the current study to the coherence threshold paradigm needs more investigation.

Our findings suggest that the processing of line segments and Glass patterns with more than two elements may be influenced by the local processing mechanism and careful consideration needs to be made on attributing such results to the local/global stage of orientation processing or indeed comparing the results to RDK.

The results of this chapter were presented at the 36th European Conference on Visual Perception, Bremen, Germany, 25 – 29, August 2013.

Joshi M, Jeon S T, 2013; "Characterisation of the Dorsal and Ventral Pathways Using External Noise Paradigm" Perception, 42 ECVP Abstract Supplement, page 210

4.0 The processing of implied motion in a normal population

4.1 Introduction

Our environment contains numerous visual cues including motion and form. Stable visual perception requires interaction and integration of information from a range of visual attributes. As discussed earlier (Introduction section 1.1 and 1.2), numerous studies (Ross *et al.*, 2000; Ross, 2004; Sincich and Horton, 2005; Nassi and Callaway, 2007; Goodale, 2011; Mather *et al.*, 2012) suggest significant interactions along the proposed parallel processing mechanisms of dorsal and ventral streams, including along the motion and form processing pathways. Motion cues are known to influence perceived form. Similarly, form information also affects motion perception. The most dramatic example of how motion influences form perception is the demonstration of biological motion (Johansson, 1973). The "point lights" placed along the key joints and extremities of a human body in dark are perceived as a human shape only when motion is introduced. Similarly, form information also facilitates motion perception. For example, blurred static lines are frequently used by artists to infer the direction of motion in still images. The static lines that induce or accentuate the sense of motion are called motion streaks. Geisler (1999) proposed that fast moving objects also create motion streaks and that these streaks provide important information in resolving directional ambiguities.

Similarly, when an independent random sequence of sets of static Glass patterns with the same general orientation (such as left translation) are displayed over time, the perception is of induced motion along the global orientation of static Glass patterns (Ross *et al.*, 2000). Such displays of static Glass patterns that induce a perception motion are known as a dynamic Glass pattern (Ross *et al.*, 2000). In motion stimuli such as random dot kinematograms (RDK), the coherent motion is perceived due to the motion vectors created by an apparent motion of corresponding dots from one frame to the next. The positions of individual dots and dipole elements in a dynamic Glass pattern do not correspond from one frame to the next. However, despite the absence of coherent motion vectors, a sense of motion is readily perceived. The source of such perceived motion could only be from the underlying dipole orientation of static Glass pattern structures. The dipoles in the dynamic Glass pattern are believed to "approximate a small line segment" which forms motion streaks that stimulate the local orientation selective detectors in V1 (Burr and Ross, 2002; Ross, 2004). The motion sensitive V1 cells are responsive to motion in an orthogonal direction to the preferred spatial orientation of their receptive fields. The motion streaks thereby stimulate V1 neurones that are sensitive to the orientation parallel to the overall motion direction (Geisler, 1999). Geisler (1999) proposed that outputs of both orientation and motion selective cells in V1 are combined to form spatial motion direction (SMD) sensors that are sensitive to both the direction of motion as well as the orientation of the motion streak (Figure 4.1). Furthermore, Geisler suggested that the combination of direction and orientation cues by SMD sensors overcomes the aperture problem observed in V1 to provide an overall percept of global motion. According to this model, motion streaks that are parallel to the overall motion would accentuate the perceived motion while the streaks along the orthogonal direction would inhibit the perceived motion.

The involvement of a motion streak mechanism in dynamic Glass processing is based on the assumption that the dipole pairs in a dynamic Glass pattern approximate small line segments. Increasing the length of dipole pairs in a dynamic Glass pattern should result in an approximation of longer line segments. The longer segments should, therefore, leave behind a stronger motion streak resulting in better discrimination thresholds. However, increasing the dipole separation in a Glass pattern beyond 8 arc min makes the detection of the structure difficult with complete abolishment of Glass pattern structure beyond 23 arc min (Dakin, 1997). Ross (2004) employed dynamic patterns composed of static line segments (as used in Chapter 3.0) to study the impact of increasing the line length on the perceived speed of a radial dynamic pattern. Indeed, the perceived speed of the radial dynamic pattern composed of line segments increased with the increase in line length (Ross, 2004).

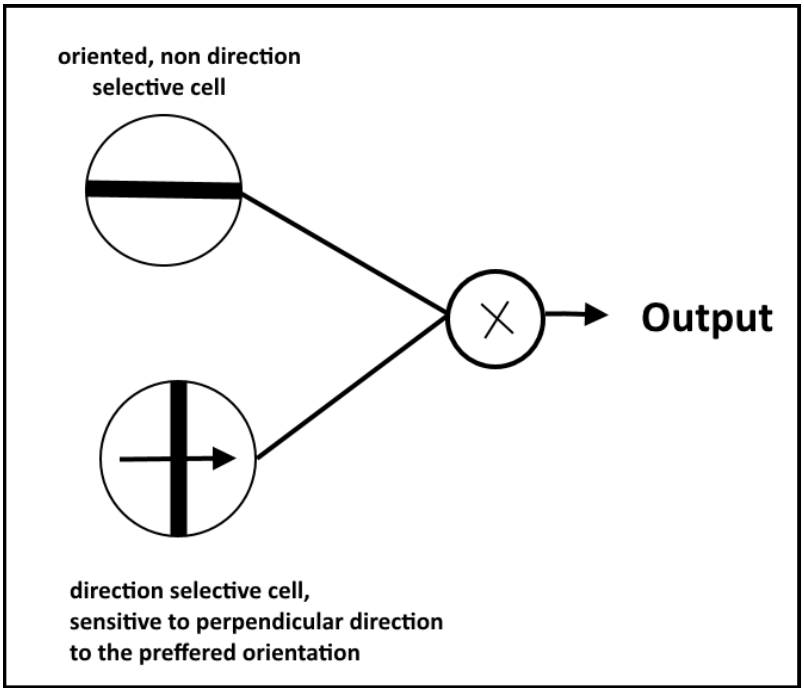

Figure 4.1: Geisler's model for motion streak processing.

The model shows a response from the orientation (non-direction) selective cell is combined multiplicatively with a response from the perpendicularly oriented direction-selective cell to provide the final output of direction of motion of motion streaks. Adapted from Geisler (1999)

The involvement of V1 neurones in decoding motion streaks is further supported by the finding of motion sensitive cells that are responsive to parallel motion (*i.e.,* in the direction of their preferred orientation) instead of regularly encountered cells which are responsive to an orthogonal motion. Such cells have been isolated from the primary visual cortex of both cats and primates (Geisler *et al.*, 2001). A fMRI study in humans also reported the presence of cells that are sensitive to motion streaks in area V2 (Apthorp *et al.*, 2013).

More recent studies suggest that processing at V1 level through SMD sensors alone cannot decode the overall global direction of implied motion. The spatial motion direction (SMD) sensors of V1 (Geisler, 1999) may only be involved in the local processing that is, the dipole orientations in a dynamic Glass pattern (Ross *et al.*, 2000). A fMRI study in humans also reported that only a small part of the implied motion from dynamic Glass patterns can be accounted for by processing at V1 and V2 levels (Krekelberg et al., 2005). Kourtzi *et al.* (2008) suggested that neurones with larger receptive fields that are present along the higher extra striate areas are required for overall global processing of dynamic Glass pattern (Kourtzi *et al.*, 2008).

More recent behavioural studies have provided evidence of motion and form interaction within higher extra striate areas. Mather *et al.,* (2012) measured the strengths of the motion aftereffect (MAE) to an adapting stimulus that contained two fields of transparent bi-directionally moving dots (one 45˚above the horizontal and the other 45˚ below horizontal) in the presence of static gratings of varying orientations. The adaptation to such moving dot fields produces an aftereffect in the direction opposite to the vector average of the two adapting directions. The MAE was stronger when the gratings were placed parallel to the resultant MAE direction compared to when the gratings were orthogonal. These findings reflected the predictions of SMD sensors which were proposed by Geisler (1999) to be present at the level of V1. The integration of multiple directions of motion occurs in extra striate areas of MT and beyond (Albright, 1993; Blake *et al.*, 2003). Therefore, the results of the MAE experiments reported by Mather *et al.,* (2012) demonstrated that the interactions of motion and orientation cues are also present at a global processing stage. Similarly, when the adapting stimulus was presented with radial or rotational (orthogonal to radial) static gratings, the strength of the MAE for the radial optic flow was facilitated by the adapting stimuli that contained the radial grating and was suppressed by the adapting stimuli containing rotational grating (Pavan *et al.*, 2013). These results from behavioural studies imply that motion and form interactions are present from early visual areas (V1) extending up to the areas of global motion processing (MT and MST).

The interactions between the extra striate areas involved in both global motion and global form processing have also been reported by imaging and electrophysiological studies (Braddick *et al.*, 1999; Li *et al.*, 2013). Ross *et al.* (2000) suggested that the processing of dynamic Glass patterns may well be influenced by such interconnections between a motion processing area (e.g. MT) and a form processing area (*e.g.,* V4). Imaging studies (Krekelberg *et al.*, 2003; Krekelberg *et al.*, 2005) in monkeys and humans report that the motion selective cells in MT/MST respond similarly to the real motion in RDKs and the implied motion in dynamic Glass patterns. In contrast, the motion sensitive cells along the ventral stream areas (such as V4 and LOC) did not respond to the implied motion (Krekelberg *et al.*, 2003; Krekelberg *et al.*, 2005). Krekelberg *et al.* (2005) suggested that the inability of the MT/MST cells to differentiate between the real and implied motion is why humans perceive motion in dynamic Glass patterns.

Behavioural studies have employed the coherence threshold paradigm to evaluate human detection sensitivity to implied motion in dynamic Glass patterns (Or *et al.*, 2007; Nankoo *et al.*, 2012). These studies reported a better detection of dynamic Glass patterns compared to the static Glass patterns, but the detection sensitivity was lower than that for the real motion in RDKs (Nankoo *et al.*, 2012). A recent study that evaluated the effect of speed on dynamic Glass pattern perception suggested that the improvement in implied motion thresholds compared to the orientation thresholds in static Glass patterns was due to the temporal summation of multiple Glass patterns present in a dynamic Glass pattern (Day and Palomares, 2014). The motion streak mechanism is more active at faster speeds (Geisler, 1999; Edwards and Crane, 2007) and the improved thresholds for the implied motion at higher temporal frequencies was due to the facilitation of such a mechanism (Day and Palomares, 2014). However, Nankoo *et al.,* (2015) argued that with an increase in temporal frequency the number of unique static Glass pattern frames within a dynamic Glass pattern also increases. They reported that the improved sensitivity was related to the number of unique static Glass pattern frames rather than the temporal frequency per se (Nankoo *et al.*, 2015). The results from behavioural studies employing the coherence threshold paradigm hence seem unclear about the mechanism underlying the dynamic Glass pattern processing.

Another behavioural method to evaluate dynamic Glass pattern processing in relation to motion (RDK) and form (Glass pattern) processing is with the equivalent noise paradigm. The equivalent noise paradigm can provide a better insight into the interaction of motion and form processing at both local and global levels. In this study, we evaluated the sensitivity to implied motion in normal adults at varying levels of added external noise. In the first experiment, we evaluated how noise affects the perception of dynamic Glass patterns and whether the local and global limitations on dynamic Glass pattern processing are di/similar to that of RDKs and/or Glass patterns. In the second experiment, we investigated how implied motion sensitivity varies for dynamic patterns composed of varying line lengths.

4.2 Experiment 1: The processing of dynamic Glass pattern in relation to the RDK and static Glass pattern

4.2.1 Methods

Dynamic Glass pattern stimuli were composed of nine independently generated static Glass patterns with the same mean direction and variance. The physical properties of stimuli such as dot size (0.083˚), display diameter (10˚), dipole separation (0.133˚ or 8 arc min) were similar to what was described for the static Glass pattern in the general methods (section 2.3.2). Each independently generated static Glass pattern was displayed for 55.55ms (equivalent to four frames), with a total stimulus duration of 0.5s. Ross *et al.,* (2000) suggest that a dipole separation of 6 to 15 arc min and frame duration between 16 and 128ms are the most optimal for the perception of dynamic Glass patterns. The stimulus parameters of the current study are within this range and are similar to that of other studies employing translational dynamic Glass patterns (Krekelberg *et al.*, 2005; Nankoo *et al.*, 2012; Day and Palomares, 2014; Nankoo *et al.*, 2015).

Six visually normal participants from previous experiment (Chapter 3.0, experiment 1) completed five sessions of threshold evaluation at eight variance levels (0˚, 2˚, 4˚, 8˚, 16˚, 24˚, 32˚, and 40˚). The procedure was as described in the general methods (section 2.3.3) where observers judged the mean implied motion from the vertical reference (90˚). The thresholds for dynamic Glass patterns were compared to the thresholds for RDK's and Glass pattern stimuli (from Chapter 3) with repeated measures ANOVA and nested modelling methods.

4.2.2 Results

For each individual observer (Figure 4.2) and the mean data (Figure 4.3), thresholds were low and similar at the lower noise levels (0 - 8°) before increasing at higher noise levels (>16°). Repeated measures ANOVA with eight levels of *noise* as the within subject factor was conducted. The Mauchly's test revealed that the log transformed data satisfied the assumption of sphericity, [$\chi^2(27) = 29.31$, $p > 0.05$]. The results showed a significant effect of *noise* [$F(7,203) = 71.29$, $p < 0.01$]. Further analysis of the main effect after Bonferroni correction showed no statistical difference between the thresholds at noise levels from 0˚ to 8˚ ($p > 0.05$) while the thresholds at noise levels of 0˚ to 16˚ were lower than those at noise levels >24˚ ($p < 0.05$).

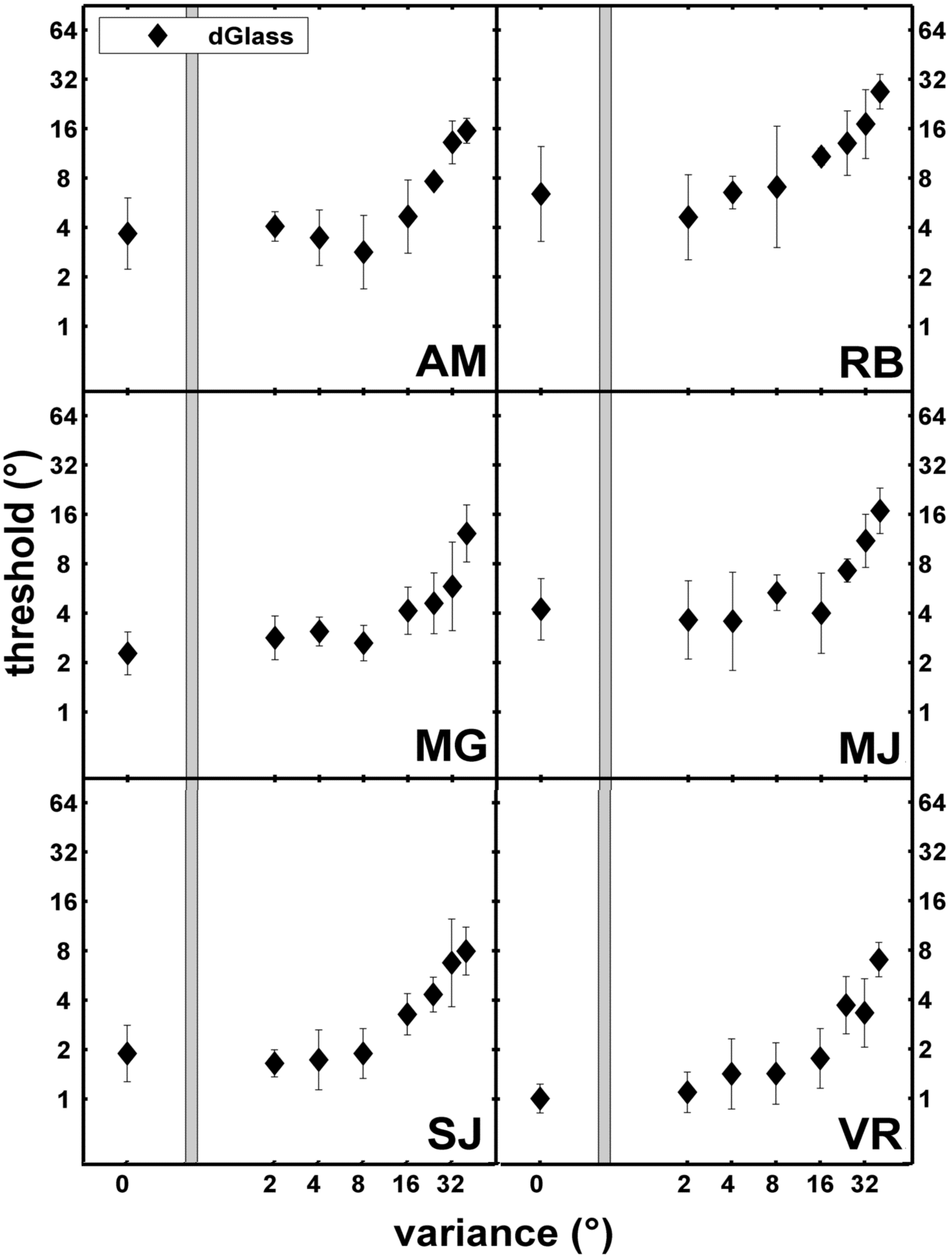

Figure 4.2: Mean implied motion discrimination thresholds for individual observers.

Each panel shows data for a single observer for a dynamic Glass pattern at eight noise levels. Each data point represents the mean from five experimental sessions and error bar represents ±1 standard deviation.

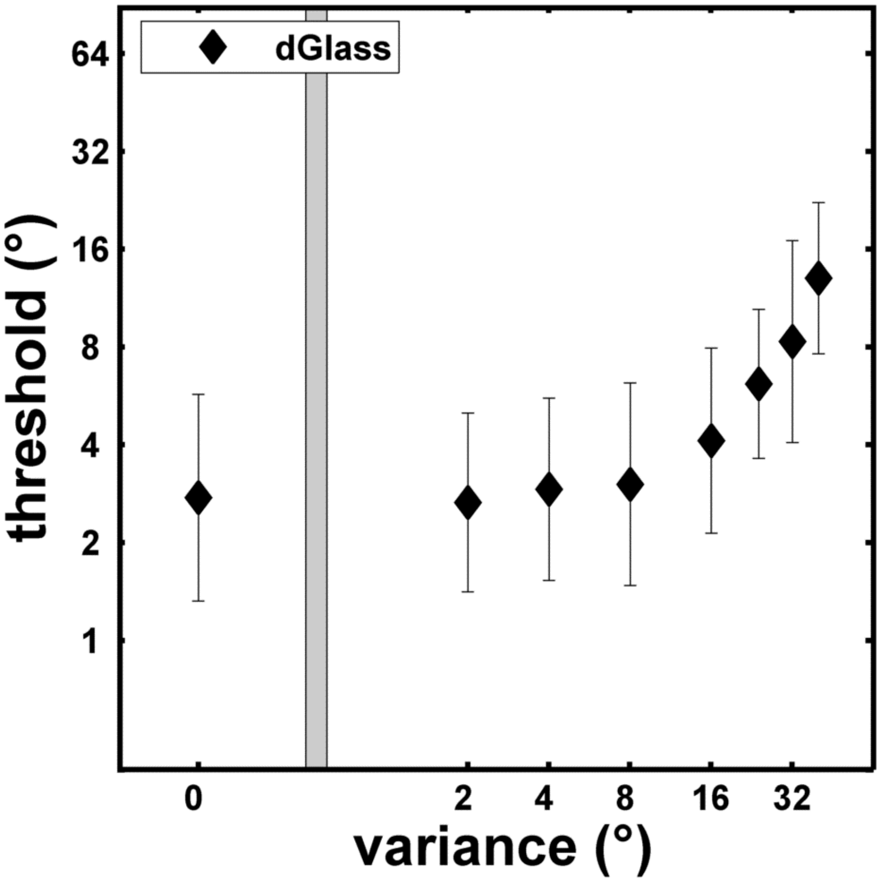

Figure 4.3: Mean implied motion thresholds at eight noise levels.

Each data point represents the mean (n = 6) thresholds for a dynamic Glass pattern, the error bar represents ±1 standard deviation.

The thresholds for dynamic Glass patterns (dGlass) at different noise levels were then compared to those of the RDK and Glass patterns (refer to Chapter 3). The mean thresholds for dGlass were higher than the thresholds for the RDK but lower than those for the Glass patterns at all variance levels (Figure 4.5). The trend was similar for all individual observers (Figure 4.4), except for the observer RB who showed higher thresholds for dynamic Glass pattern compared to both Glass pattern and RDK.

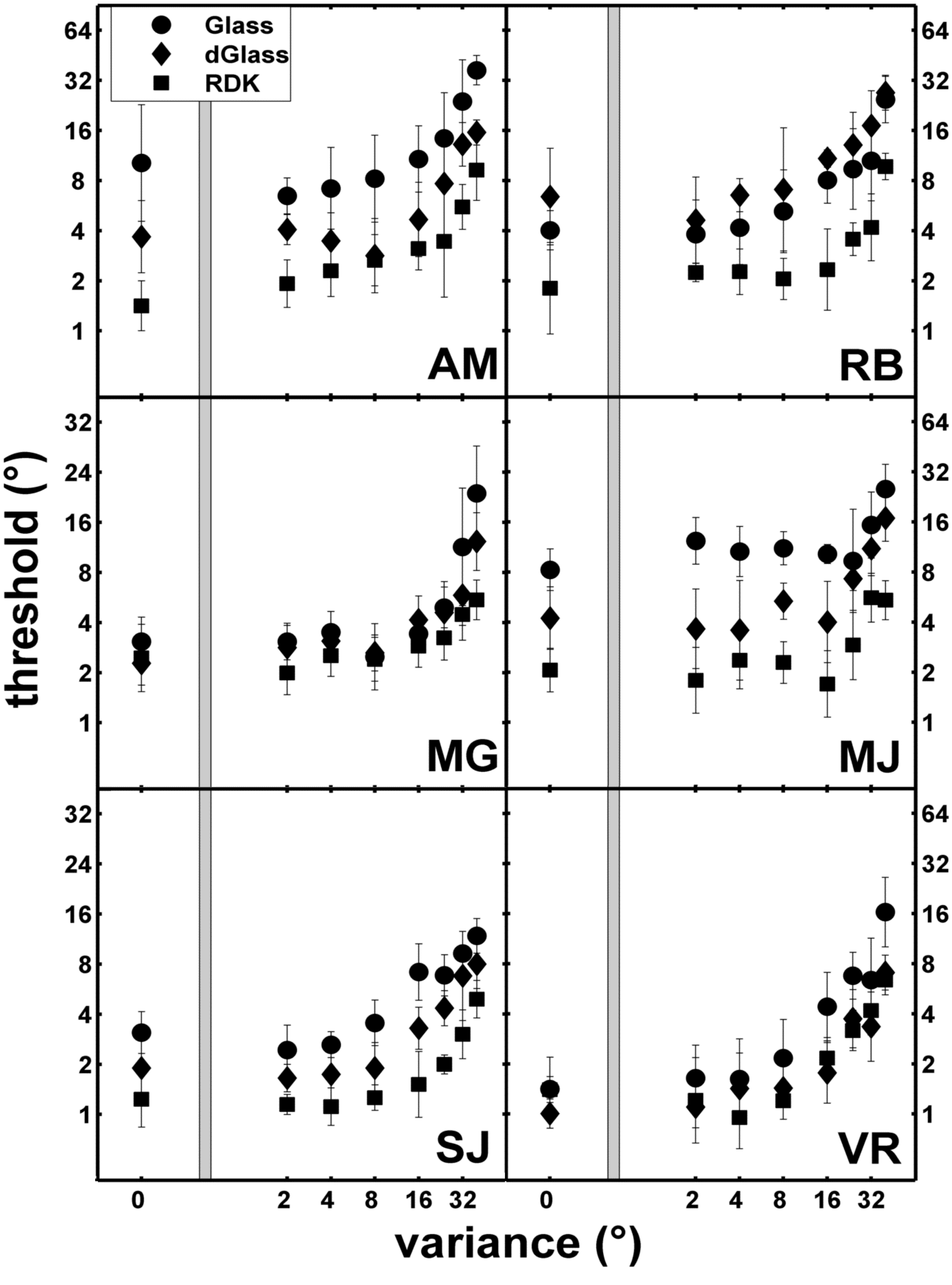

Figure 4.4: Comparison of implied motion thresholds with motion direction and orientation discrimination thresholds for individual observers.

Each panel shows data for a single observer for Glass pattern, dynamic Glass pattern and RDK at eight noise levels. Each data point represents the mean from five experimental sessions and error bar represents ±1 standard deviation.

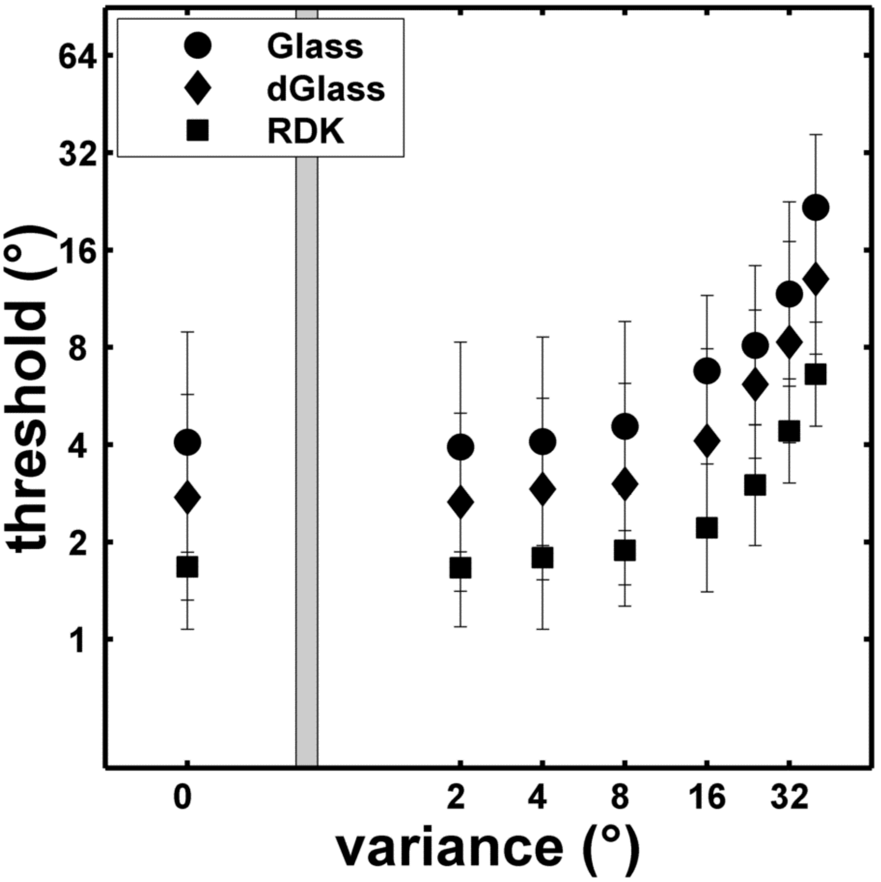

Figure 4.5: Comparison of mean implied motion thresholds with direction and orientation discrimination thresholds.

Each data point represents the mean from six observers for RDK, Glass pattern, and dynamic Glass pattern and error bar represents ±1 standard deviation.

A repeated measure ANOVA with *noise* (8 levels) and *stimuli type* (3 levels; Glass, dGlass and RDK) as within subject factors was conducted. The Mauchly's test revealed that the log transformed data satisfied the assumption of sphericity for *noise* [$\chi^2(27) = 38.44$, $p > 0.05$], *stimuli type* [$\chi^2(2) = 0.05$, $p > 0.05$] and *noise* and *stimuli type* interaction [$\chi^2(104) = 126.19$, $p > 0.05$]. The results showed a significant effect of *noise* [$F(7, 203) = 158.52$, $p < 0.01$] and *stimulus type* [$F(2, 58) = 76.69$, $p < 0.01$]. The interaction between *stimulus type* and *noise* was not significant [$F(14, 4.6) = 1.15$, $p > 0.05$]. The comparison between stimulus types after Bonferroni correction revealed that the thresholds for the three *stimulus type* were significantly different; with the highest threshold for Glass pattern followed by that for dynamic Glass pattern and RDK (*ps* < 0.01).

No interaction between *stimulus type* and *noise* suggested that the differences in the performance were possibly due to changes in the sampling efficiency. To confirm this result, the thresholds were used to fit the linear equivalent noise model hierarchically (Figure 4.6 and 4.7). Among the reduced models, the goodness of fit (r^2) with one σ_{eq} and three *Eff* was equivalent to the full model (three σ_{eq} and three *Eff*) [$F(2,18) = 1.10$, $p > 0.1$] while the fits with three σ_{eq} and one *Eff* [$F(2,18) = 42.92$, $p < 0.01$] and one σ_{eq} and one *Eff* [$F(2,18) = 49.07$, $p < 0.01$] resulted in poorer fits compared to the full model (Table 4.1 and Figure 4.7). The pattern of the result was similar for each individual observer (Table 4.1 and Figure 4.6). A further test with one σ_{eq} and three *Eff* as a full model and one σ_{eq} and one *Eff* as reduced model showed that the reduced model resulted in a significantly poorer fit [$F(2,20) = 107.83$, $p < 0.01$]. The result confirmed that the model with one σ_{eq} and three *Eff* best described the performance of the observers across the three stimulus types.

Subject	AM	MJ	RB	VR	MG	SJ	Average
The full model							
σ_{eq} RDK	10.39°	16.61°	13.22°	8.65°	19.45°	12.50°	12.86°
σ_{eq} Glass	11.05°	24.91°	9.24°	5.22°	9.51°	8.95°	10.06°
σ_{eq} dGlass	10.45°	12.24°	10.01°	8.44°	12.38°	9.01°	10.32°
Eff RDK	5.77	8.64	6.87	7.92	8.63	11.40	7.91
Eff Glass	1.51	2.56	2.40	3.75	3.46	3.38	2.64
Eff dGlass	3.19	3.30	1.80	7.83	4.90	5.48	3.97
r^2	0.94	0.94	0.95	0.94	0.83	0.97	0.97
Complicated reduced model-1 with σ_{eq} constrained							
σ_{eq}	10.63°	16.91°	10.75°	7.27°	12.70°	10.06°	11.00°
Eff RDK	5.83	8.74	6.15	7.31	6.67	10.10	7.27
Eff Glass	1.48	1.97	2.58	4.29	4.03	3.58	2.76
Eff dGlass	3.22	3.99	1.86	7.32	4.97	5.78	4.10
r^2	0.94	0.90	0.94	0.92	0.80	0.96	0.96
$F(2,18)$	0.03*	2.12*	1.06*	2.30*	1.92*	2.19*	1.10*
Complicated reduced model-2 with *Eff* constrained							
σ_{eq} RDK	6.316°	10.83°	6.92°	6.60°	10.69°	7.06°	7.33°
σ_{eq} Glass	38.95°	67.54°	17.98°	10.51°	15.68°	24.73°	23.10°
σ_{eq} dGlass	13.33°	26.51°	26.22°	6.42°	13.38°	12.30°	13.55°
Eff	3.89	5.99	3.94	6.29	5.21	6.99	4.92
r^2	0.81	0.83	0.75	0.84	0.71	0.80	0.81
$F(2,18)$	19.32	11.13	33.32	14.89	6.85	48.84	42.92
Simplest reduced model with both σ_{eq} and *Eff* constrained							
σ_{eq}	10.63°	16.91°	10.75°	7.27°	12.70°	10.06°	11.00°
Eff	3.03	4.10	3.09	6.12	5.11	5.94	4.35
r^2	0.45	0.25	0.49	0.81	0.67	0.59	0.61
$F(2,18)^{\#}$	37.34	39.20	38.74	9.73	4.31	55.22	49.07
$F(2,20)^{\#\#}$	82.96	84.75	84.91	19.06	7.44	120.28	107.83

Table 4.1: The best fitting parameters and r^2 values for LAM fits to the threshold data for RDK, Glass and dGlass.

The values in the top section are the results of the fits with six free parameters (one σ_{eq} *and Eff each for RDK, Glass and dGlass). The second and third sections show the results with* σ_{eq} *and Eff fixed respectively across RDK, Glass and dGlass. The bottom section shows results with both* σ_{eq} *and Eff fixed across the conditions. The F scores are the result of a nested hypothesis test between restricted models (4-parameter or 2-parameter models) and the full models (6-parameter or 4-parameter models).*

** represents F scores which resulted in no significant difference (p>0.05) in the goodness of the fit measure with reduced model (here 1* σ_{eq}*, 3 Eff) compared to the full model (3* σ_{eq}*, 3 Eff). Rest of the F scores in the table represent a poorer fit (p < 0.05) compared to the full model (1* σ_{eq}*, 3 Eff)*

 # F statistics of the simplest model (1 σ_{eq}*, 1 Eff) compared to full model (3* σ_{eq}*, 3 Eff)*

F statistics of the simplest model (1 σ_{eq}*, 1 Eff) compared to the simpler model (1* σ_{eq}*, 3 Eff)*

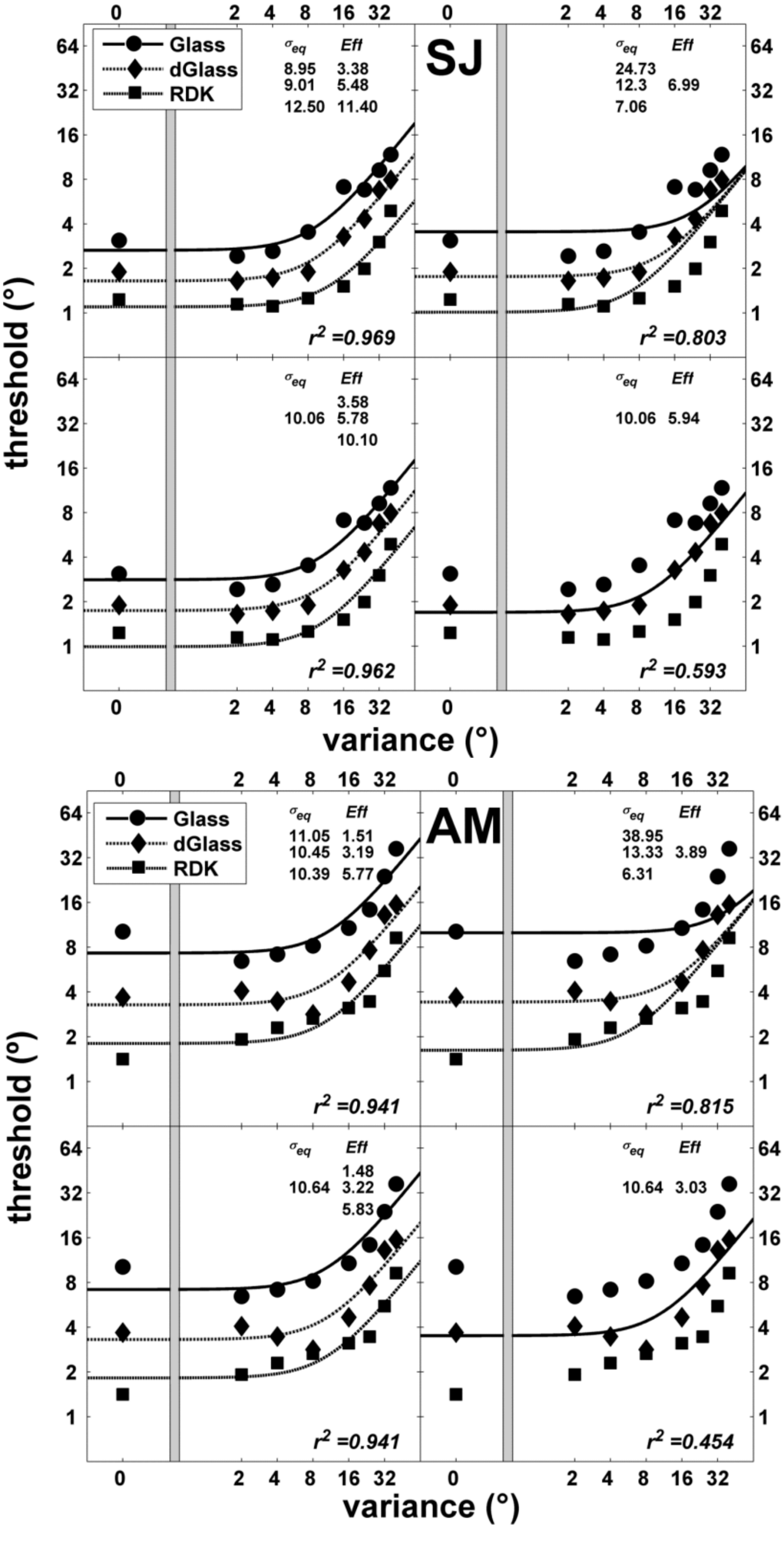

Figure 4.6: Nested modelling for individual observers relating the threshold data to different values of internal noise and sampling efficiency for Glass pattern, dGlass, and RDK.

The figure shows results for psychophysically experienced observer (SJ) and naïve observer (AM). The reduced model with one σ_{eq} *and two Eff (bottom left panels) resulted in no significant difference* ($p > 0.05$) *in the goodness of the fit measure* (r^2) *compared to the full model for each observer. Error bars are omitted for a better presentation.*

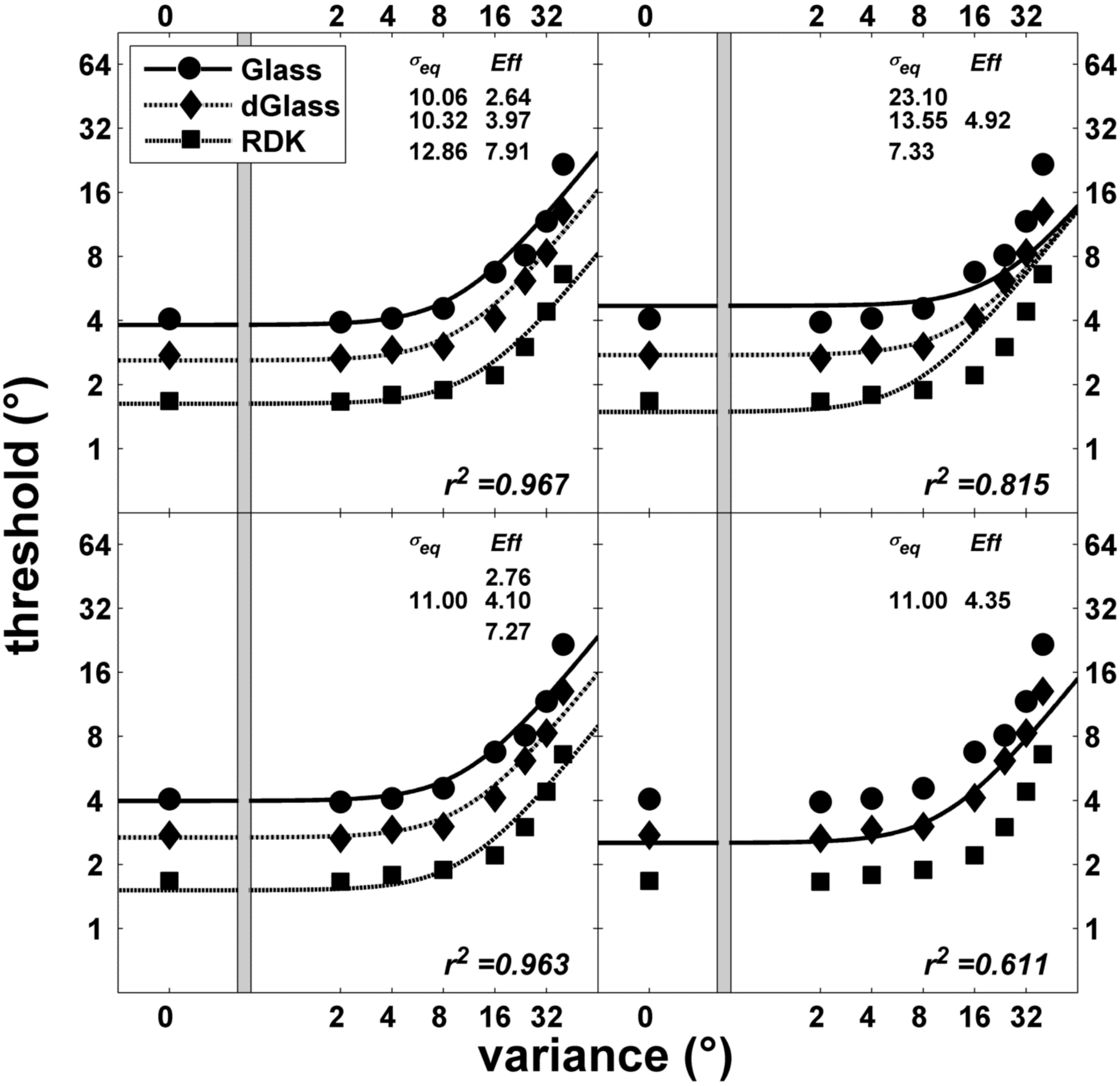

Figure 4.7: Nested modelling relating the mean thresholds to different values of internal noise and sampling efficiency for Glass pattern, dGlass, and RDK.

The reduced model with one σ_{eq} and three Eff (bottom left) resulted in no significant difference ($p > 0.05$) in the goodness of the fit measure (r^2) compared to the full model. Error bars are omitted for a better presentation.

4.3 Experiment 2: A comparison of processing dynamic Glass patterns with dynamic line patterns

4.3.1 Methods

The stimuli were dynamic Glass patterns (dGlass) and dynamic patterns created with line segments (dynamic line pattern). The dynamic Glass pattern stimulus was the same as described for the first experiment but composed of only 480 dot elements (240 dipole pairs). The dynamic line patterns were created by filling the space between the dipole pairs of the dynamic Glass pattern with extra dots as described for static line patterns in Chapter 3.0. Two line lengths were used; equivalent to the length of the dipole Glass pattern (0.216˚) – dLine1 and two times the length of dLine1 (0.432˚) – dLine2.

The method of stimulus presentation, the procedure of data collection and analysis were the same as for the first experiment. Four visually normal observers (33 ± 6.22 years) participated in the experiments for dynamic Glass/line patterns. All participants discriminated the overall implied motion from the vertical reference (90˚) at five external noise levels (0˚, 5˚, 10˚, 20˚, and 45˚).

4.3.2 Results

The thresholds for dLine2 were the lowest compared to the dGlass and dLine1 at no noise to mid noise levels (5˚ and 10˚) for all individual observers (Figure 4.8) and the mean data (Figure 4.9). However, at the highest noise (45°), the thresholds for all three patterns converged.

The repeated measures ANOVA was conducted with *noise* (five levels) and *stimuli type* (3 levels; dGlass, dLine1 and dLine2) as within subject variable. The Mauchly's test revealed that the log transformed data confirmed to the assumption of sphericity for *noise* [χ^2 (9) = 6.88, $p > 0.05$], *stimuli type* [χ^2 (2) = 5.63, $p > 0.05$] and *noise* and *stimuli type* interaction [χ^2 (35) = 37.20, $p > 0.05$]. The results showed a significant effect of *noise* [$F(4,64) = 173.21$, $p < 0.01$] and *stimuli type* [$F(2,32) = 16.37$, $p < 0.01$]. The interaction between *stimuli type* and *noise* was also significant [$F(8,128) = 2.30$, $p < 0.05$]. The comparison of *stimuli type* after Bonferroni correction revealed that the implied motion thresholds for the dGlass and dLine1 were similar ($p > 0.05$). The thresholds for dLine2 meanwhile were lower than both dGlass ($p < 0.01$) and dLine1 ($p < 0.05$).

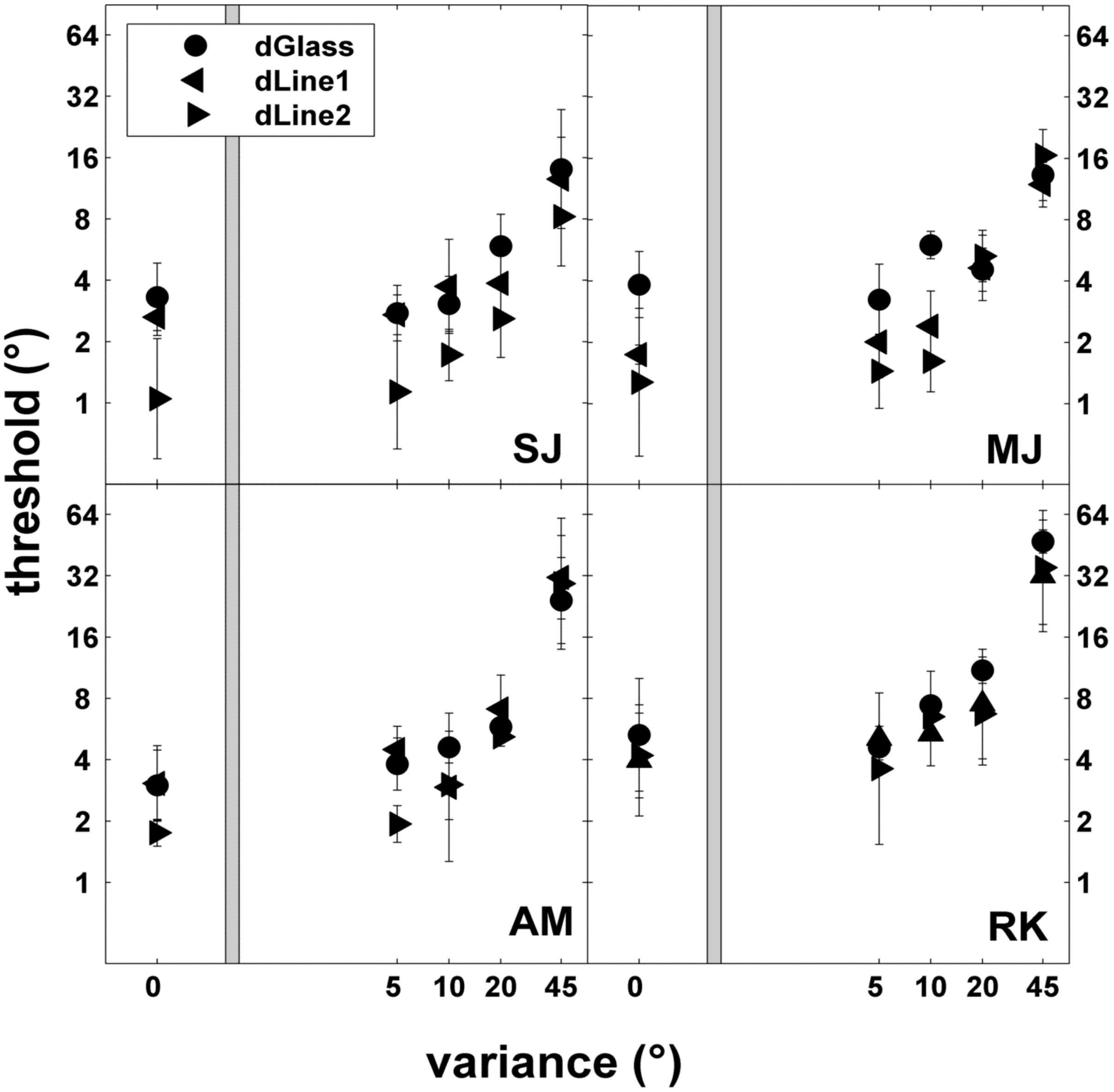

Figure 4.8: Mean implied motion thresholds for dynamic Glass patterns and dynamic line patterns for individual observers.

Each panel shows data for a single observer for dGlass, dLine1 and dLine2 at five noise levels. Each data point represents the mean from five experimental sessions and error bar represents ±1 standard deviation.

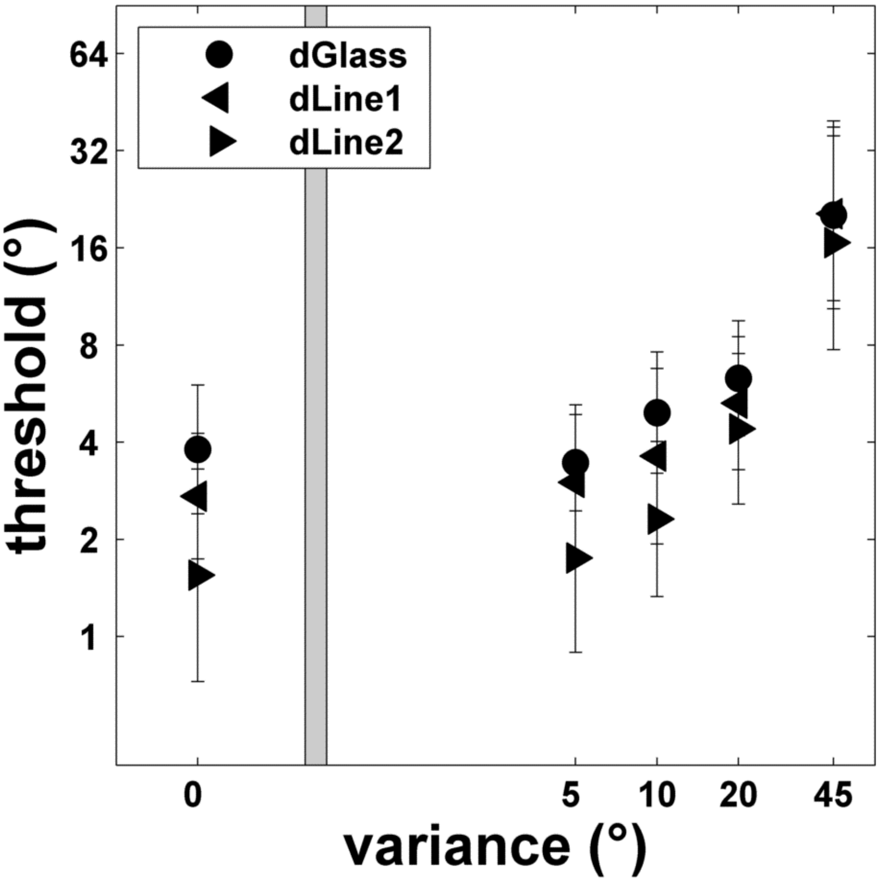

Figure 4.9: Mean implied motion thresholds for dynamic Glass pattern and dynamic line patterns at five noise levels.

Each data point represents the mean (n = 4) thresholds for dGlass, dLine1 and dLine2, the error bar represents ±1 standard deviation.

The nested modelling for the mean thresholds data fitted to the LAM (Figure 4.10) showed that the simplest model (with both σ_{eq} and *Eff* constrained) resulted in a statistically poorer fit compared to the full model [$F(4,9) = 3.97$, $p < 0.05$]. The other two reduced models with σ_{eq} constrained with independent *Eff* [$F(2,9) = 0.91$, $p > 0.1$] and *Eff* constrained with independent σ_{eq} [$F(2,9) = 1.14$, $p > 0.1$] resulted in a statistically similar fit to the full model.

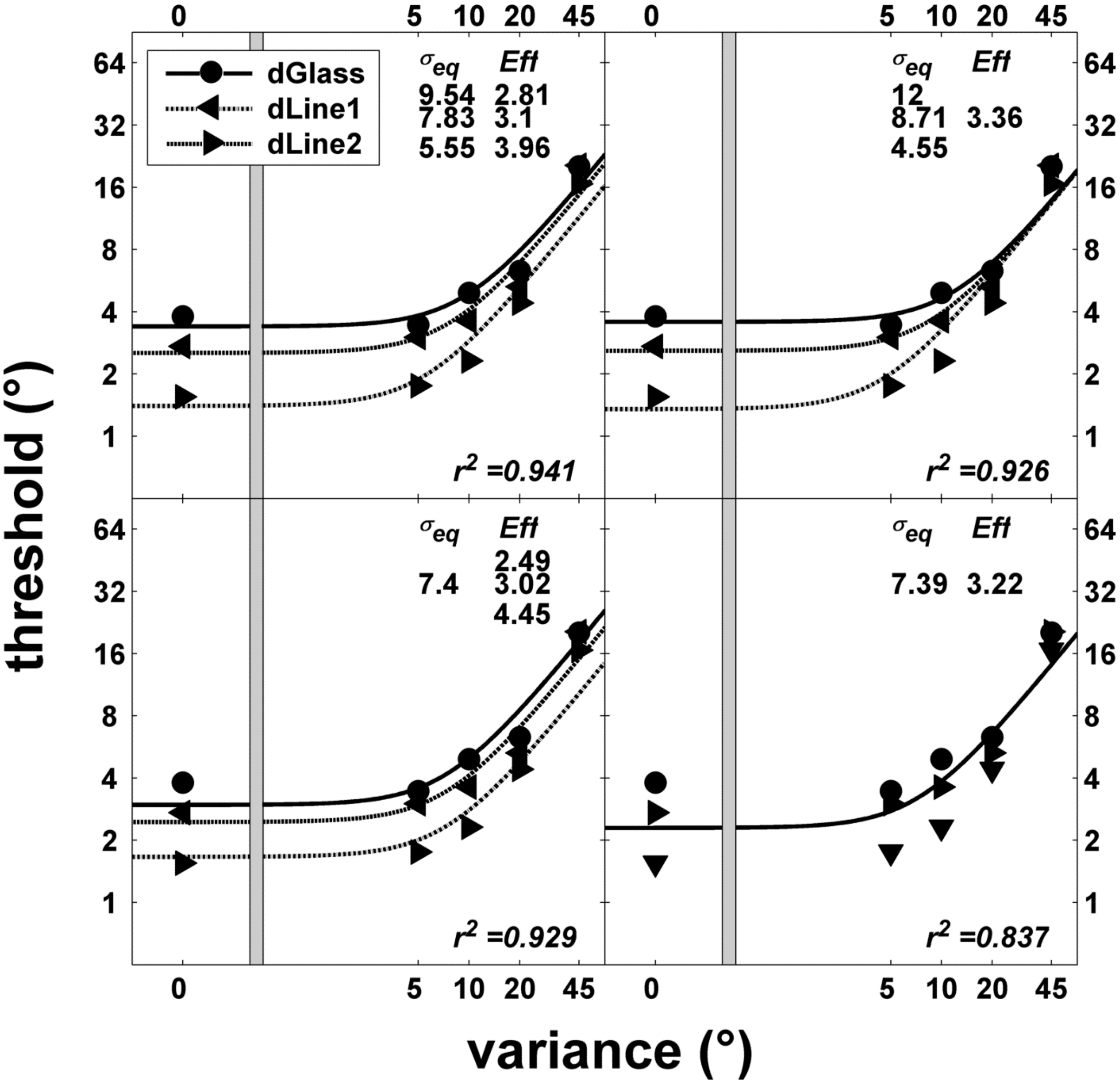

Figure 4.10: Nested modelling for mean implied motion thresholds from dynamic Glass pattern (dGlass) and dynamic line patterns of varying lengths.

The reduced models with three σ_{eq} and one Eff (top right) and one σ_{eq} and three Eff (bottom left) resulted in no significant difference ($p > 0.05$) in the goodness of the fit measure (r^2) compared to the full model (top left). Error bars are omitted for a better presentation.

4.4 Discussion

The perception of implied motion in a dynamic Glass pattern relies on both form and motion cues. The thresholds for the dynamic Glass patterns were lower than those for the static Glass patterns but higher than the RDKs at all levels of external noise. As far as we know, no study has evaluated the sensitivity to dynamic Glass patterns using the equivalent noise paradigm. Our results suggest that dynamic Glass patterns are processed differently from both static form (Glass pattern) and motion (RDK) irrespective of noise levels. If the implied motion in Glass patterns were processed as the real motion in RDKs, thresholds would be expected to be similar to those for the RDK. On the other hand, if the implied motion was processed exclusively along the channels processing static form, the thresholds would be closer to that of the static Glass patterns. These results are in line with a previous study where the coherence thresholds for implied motion in dynamic Glass patterns were higher than the thresholds for motion (RDK) but lower than the orientation coherence thresholds (static Glass patterns) (Nankoo *et al.*, 2012).

The reduced thresholds for the dynamic Glass pattern compared to the static Glass pattern could be due to the activation of the motion streak mechanism (Ross *et al.*, 2000; Ross, 2004) that may be present from the early cortical visual areas of V1 and V2 (Burr and Ross, 2002; Apthorp *et al.*, 2013) up to the later global processing areas of MT and MST (Krekelberg *et al.*, 2005; Mather *et al.*, 2012; Pavan *et al.*, 2013). The motion streak theory for dynamic Glass patterns is based on the assumption that the dipole pairs in a Glass pattern approximate the ends of line segments. This assumption seems supported by our finding of similar thresholds at all noise levels for dynamic Glass patterns and dynamic line patterns containing line segments of equivalent length (dLine1). Similarly, the improved threshold for the dynamic line pattern with a longer length (dLine2) at low to mid noise levels is in line with the prediction from the motion streak mechanism that a longer line segment would create a longer motion streak, which subsequently improves the discrimination thresholds. Similar results have been reported for radial dynamic Glass/line patterns as well (Ross, 2004).

Another possible reason for better sensitivity to implied motion in dynamic Glass patterns compared to the static Glass pattern could be due to the summation of information from multiple independent static Glass patterns over time (Nankoo *et* *al.*, 2015). Two factors are involved in such improvement; the accumulation of form information from multiple static Glass patterns (Nankoo *et al.*, 2012; Nankoo *et al.*, 2015) and the influence of the temporal frequency of the presentation (Day and Palomares, 2014). Though both of these factors are interlinked, studies have sought to separate the effect of each entity. Nankoo *et al.,* (2012) reported that the coherence thresholds for the dynamic Glass pattern varied according to the pattern types (translation, radial, and rotation) as observed for the static Glass pattern (higher threshold for translation compared to other types) while the motion coherence thresholds were similar for all three motion types. Based on these findings, Nankoo *et al.,* (2012) proposed that the higher sensitivity to dynamic Glass patterns were due to the accumulation of information from multiple static Glass patterns. They suggested that the dynamic Glass patterns are processed mainly as static Glass patterns, thereby emphasising a larger role for the form processing mechanism along the ventral stream. However, other studies have reported that the motion coherence threshold in the RDK also varies depending upon the pattern types with higher thresholds for translation compared to radial and rotation, especially at slower speeds (Freeman and Harris, 1992; Lee and Lu, 2010). In the current study, the thresholds for the dynamic Glass patterns and dynamic line patterns of longer length (dLine2) remained separated at low and mid noise levels before converging at the higher noise levels. This pattern of result is similar to the results comparing static Glass pattern and line patterns (refer to chapter 3). Our results hence seem to support the assumption made by Nankoo *et al.,* (2012, 2015) that the dynamic Glass patterns could share more properties with static Glass patterns than with RDKs.

In another study, Day and Palomares (2014) measured the coherence thresholds for dynamic Glass patterns at different temporal frequencies ranging from 2 to 36HZ. The coherence threshold reduced linearly with the increase in temporal frequency. They suggested that the processing mechanism for dynamic Glass patterns relies more on the temporal properties. They also reported that their findings are explained well by the motion streak mechanism (Day and Palomares, 2014) as faster speeds are known to leave longer motion streaks and accentuate motion perception (Edwards and Crane, 2007). In response, Nankoo *et al.,* (2015) argued that with an increase in the temporal frequency of the dynamic Glass presentation, the number of unique frames of the static Glass pattern presented also increases. They then independently varied the temporal frequency and the number of unique frames in a dynamic Glass pattern and reported that the number of unique frames presented is more influential in the reduction of the coherence threshold than the temporal frequency. They proposed that these findings add further support to their claim that the processing of dynamic Glass patterns is in fact more similar to static Glass patterns (Nankoo *et al.*, 2015). The similar pattern of result with dynamic Glass pattern vs. dynamic line pattern and static Glass pattern vs. static line pattern observed in our studies also suggests that dynamic Glass patterns may indeed share more properties with the static Glass pattern than the RDK.

4.4.1 The local and global limitations in the dynamic Glass pattern processing

The parallel shift of thresholds and results from the nested modelling revealed that the internal equivalent noise remained similar for dynamic Glass patterns compared to both RDK and Glass patterns. The difference in performance among different stimuli was due to the change in the efficiency parameter. The similar levels of internal noise for different stimuli (Glass pattern, dynamic Glass pattern and RDK) documented in the current study suggests that all local cues (in both the motion and form domain) may share a common local level processing mechanism before global processing along a more efficient channel for processing motion cues. The finding that the perception of both static and dynamic Glass patterns are lost when the dipoles are of opposite polarity (Or *et al.*, 2007) further suggests that both patterns share similar local level processing.

Geisler (1999) proposed that the motion streak detectors present in the primary visual cortex are responsible for the processing of implied motion in line streaks. The similar internal noise observed here, which reflects the local level processing occurring at V1, suggests that the motion streak detectors in V1 have a minimal influence on the processing of dynamic Glass patterns. If the perception of implied motion in the dynamic Glass pattern was facilitated only by the local level streak detectors in V1, the internal noise for the dynamic Glass pattern should have differed from that of both static Glass pattern (which does not stimulate the motion streak mechanism) and RDK (in which the direction discrimination will be facilitated by the motion streak mechanism). Whether the constant internal noise observed in the current study across all domains (motion, form and implied motion) relates to the processing of different motion/orientation cues in area V1 or whether it reflects an overall processing of local cues along different areas of the processing pathways is open to interpretation.

The differences in the performance for three stimulus types (RDK, static Glass pattern, and dynamic Glass pattern) were best represented by the changes in the global processing parameter, the sampling efficiency. Global processing is proposed to occur in the extra striate areas of MT, MST and beyond for the direction of motion in RDK (Morrone *et al.*, 1995) and V4 for the global orientation in Glass patterns (Wilson and Wilkinson, 1998). The area responsible for the global processing of implied motion is still not well established. The motion sensitive cells in MT/MST respond to both real motion and implied motion (Krekelberg *et al.*, 2003; Krekelberg *et al.*, 2005) and may well be involved in the global processing of the implied motion in a dynamic Glass pattern. The motion-form interactions similar to that proposed for motion streak mechanism are also present at the global processing levels of MT (Mather *et al.*, 2012) and MST (Pavan *et al.*, 2013), and such interactions could have influenced the differences in the sampling efficiency observed here. Furthermore, some MT cells responsive to the orthogonal motion, change their preference over time (Pack and Born, 2001). The preferred direction of these MT cells changes from the orthogonal direction to that of parallel motion (in the direction of the motion streak) starting from around 75ms of the stimulus onset. This change in sensitivity could be influential in processing the motion streaks left behind by the fast moving objects (Burr and Ross, 2002). Our results show that any facilitation of the implied motion processing due to the interaction of motion and form processing streams in line with motion streak mechanism may well extend to the global processing level.

From our results and previous literature, we speculate that the local processing of dipole orientation in a dynamic Glass pattern is similar to the processing of a static Glass pattern with further global processing most likely occurring along the motion processing areas of MT/MST. The assumption that the processing of the dynamic Glass pattern initially involves orientation processing along the ventral stream followed by the subsequent processing of implied motion in the dorsal stream is also supported by a series of imaging studies (Krekelberg *et al.*, 2003; Krekelberg *et al.*, 2005). The motion responsive neurones along the ventral stream are not responsive to the implied motion in dynamic Glass patterns suggesting that any contribution from the ventral stream to the processing of the dynamic Glass pattern is mostly limited to the processing of local form cues in earlier cortical areas. Similarly, a recent behavioural study that evaluated tilt after effects (TAE) showed that adaptation to a wide range of static orientations affects the perceived direction of motion streaks (Tang *et al.*, 2015). This range was broader than what would have been predicted by the Geisler model, which assumes that the neuronal properties of V1 are adequate to account for the motion streak mechanism. Furthermore, this range closely approximated the broad bandwidths of motion selective cells in area MT. Based on these findings Tang *et al.,* (2015) proposed an alternate model to that of Geisler, where the orientation cues are initially processed at the V1 level with the second stage of motion processing occurring at area MT. The model predictions are in line with our findings of similar internal equivalent noise and differences in sampling efficiency for dynamic Glass patterns compared to both RDK and static Glass patterns.

Our results further suggest that even if the global processing of implied motion occurs in regions similar to that of real motion (MT), the underlying mechanism may not be as efficient as that for real motion and may well involve more interaction with the form processing pathways.

The results of this chapter were presented at the 14th Annual Vision Sciences Society Meeting, Florida, USA, 16-21 May 2014 and the British Congress of Optometry and Vision Science, Cardiff, UK, 8-9 Sep 2014.

Joshi M R, Simmers A J, Jeon S T; Limiting Factors in Form and Motion Perception: Shared locally, Differentiated Globally. Journal of Vision 2014;14(10):1418.

5.0 Modification of the data collection method for the faster application of the equivalent noise paradigm

5.1 Introduction

The equivalent noise paradigm is based on measuring sensory thresholds at various levels of added external noise. The method has most commonly been used to study the visual function in normal populations (Pelli, 1981; Watamaniuk and Sekuler, 1992; Lu and Dosher, 1998; Pelli and Farell, 1999; Dakin *et al.*, 2005; Bocheva *et al.*, 2013; Bogfjellmo *et al.*, 2014; Manning *et al.*, 2014). More recently it has been applied to clinical populations with a range of different ocular and neurological disorders, such as amblyopia (Pelli *et al.*, 2004; Hess *et al.*, 2006; Husk and Hess, 2013), autism (Manning et al., 2015), migraine (Ditchfield *et al.*, 2006; Wagner *et al.*, 2010; Tibber *et al.*, 2014), glaucoma (Falkenberg and Bex, 2007). The threshold data obtained from the equivalent noise paradigm shows a remarkable similarity across different domains, with the threshold vs. noise (*TvN*) curve remaining low and constant at low noise levels before increasing linearly at the higher noise levels. The linear amplifier model (Pelli, 1981) is the most commonly used model to analyse the results from the equivalent noise paradigm. The linear amplifier model differentiates the observer's performance from the *TvN* curve into equivalent internal noise and sampling efficiency parameters. Generally, thresholds from six to eight levels of external noise are used to fit such curve. However, obtaining reliable thresholds at up to eight noise levels, with independent staircase/psychometric function fits, requires substantial time and effort. This has remained the major obstacle when implementing this method in special populations such as children or those with various cognitive disorders.

Modifications to the data collection and analysis process have been developed to reduce the experimental time in the contrast domain (Lesmes *et al.*, 2006; Jeon *et al.*, 2009). For the current study, we were interested in adapting the equivalent noise paradigm to discrimination of both direction of motion and orientation. Recently faster methods for the implementation of the equivalent noise paradigm have been explored in the motion domain (Bogfjellmo *et al.*, 2013; Bogfjellmo *et al.*, 2014; Manning *et al.*, 2014; Tibber *et al.*, 2014). Bogfjellmo *et al.,* (2013,2014) used the FAST method (Vul *et al.*, 2010) to determine the appropriate level of external noise and direction offset from vertical based on the observer's response from a series of previous trials while other studies have used the method of measuring variance thresholds at a predefined directional offset (Manning *et al.*, 2014; Tibber *et al.*, 2014).

Our previous experiments have shown that the *TvN* curve in both the motion and form domains remains flat and low at lower noise levels before increasing in threshold with added noise at the higher noise levels. Such a *TvN* curve is constrained by two points; the low noise levels where thresholds remain constant and low and the high noise levels where discrimination thresholds are raised. The knee point of the curve where threshold starts to increase with the added noise represents the internal equivalent noise of the system. The regularity of the curve suggests that the equivalent noise paradigm can be reliably established based on these two points. If the data collection can be limited to only two points, it would avoid the need for evaluating different mid-level noises that have minimal contribution to the overall structure of the *TvN* curve. This would result in a significant reduction in the experimental time.

The first point of this curve can be determined by obtaining the motion direction/orientation discrimination thresholds at the no noise condition. For the high noise condition, a modification to the method described in previous experiments can be used. Instead of measuring the motion direction/orientation discrimination thresholds at different levels of external noise, noise thresholds can be measured at a predefined motion direction/orientation offset angles. Recent studies have used a similar method to estimate the internal noise and sampling efficiency parameters along the motion domain in children (Manning *et al.*, 2014) and migraineurs (Tibber *et al.*, 2014). In the current study, a similar technique was used to facilitate data collection and the results were validated with the previously established method of measuring thresholds at different external noise levels.

5.2 Pilot study

5.2.1 Methods

The physical parameters of the stimuli such as display diameter, dot size, dot speed, dipole distance were the same as described in the general methods (section 2.3). The stimulus for the *no noise* condition contained dots/dipoles whose direction/orientation were generated from a normal distribution with no added variance (*i.e.*, standard deviation = 0). The initial mean direction/orientation was lowered to ±10˚ from vertical (instead of ±30˚ used in Chapter 3) as the direction/orientation discrimination threshold at the no noise condition was found to be around 2˚– 8˚. The mean direction/orientation offset was manipulated based on the 3:1 staircase as in the previous experiments (Figure 5.1). In *high noise* conditions, the variable was the added external noise instead of the direction offset from vertical as in the no *noise* condition. The external noise was manipulated by changing the standard deviation of the normal distribution based on a 3:1 staircase, with the mean remaining constant at a defined offset from the vertical. As the aim was to measure the maximum tolerable variance at the predetermined direction/orientation offset angles, the variance of the distribution which was initially set at 10˚ was increased with three consecutive correct responses to make the task more difficult and decreased with an incorrect response to make the task easier (the direction of the staircase was, therefore, opposite to the *no noise* condition) - Figure 5.1. The range of added external noise (variance) could vary between 0.01˚ to 120˚ in the pilot study and between 0.01˚ to 64˚ in the main validation study.

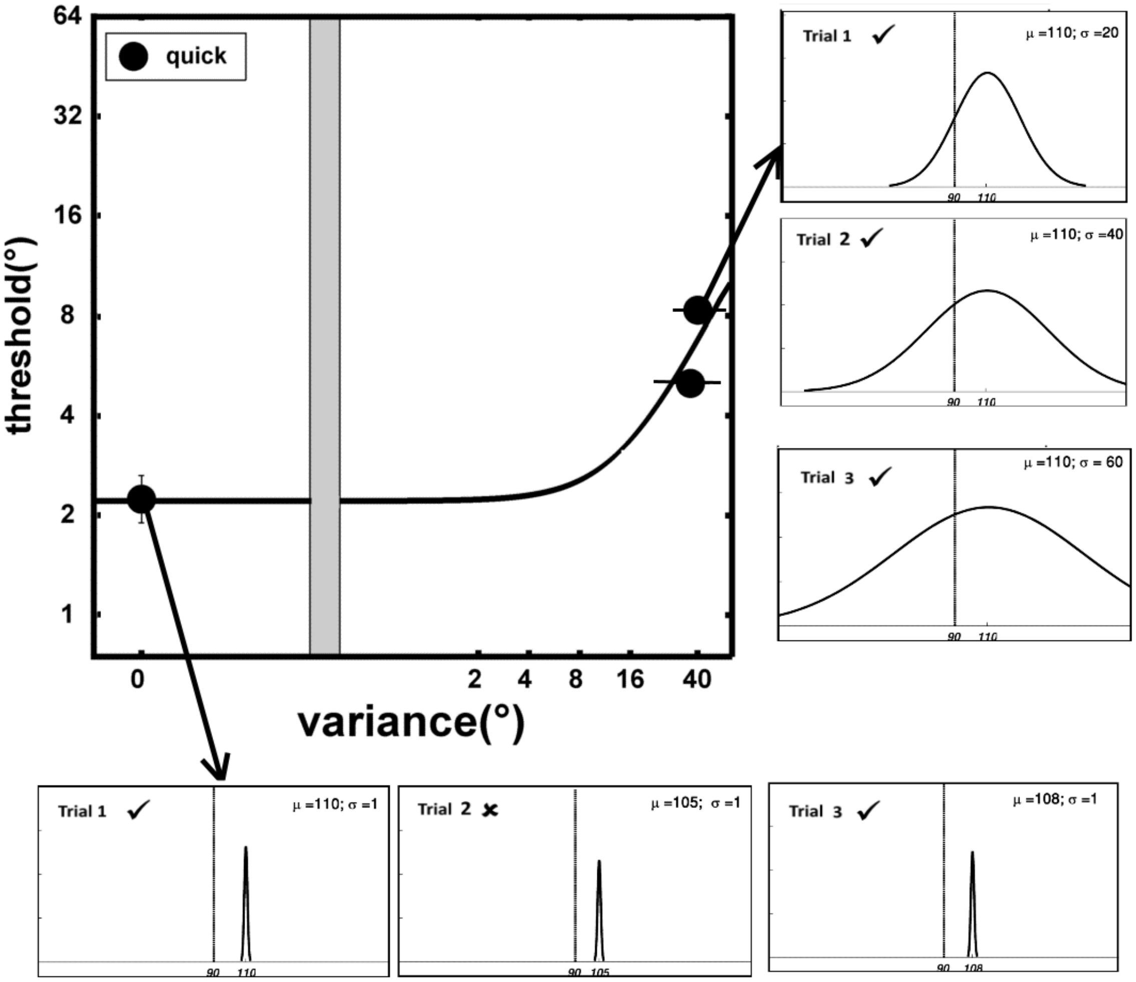

Figure 5.1: Schematic representation of the quick method.

At the no noise condition (here the distribution of standard deviation of one is used for illustrative purpose) the variance of the distribution from which direction/orientation of the RDK/Glass pattern was generated was fixed at zero with the offset from vertical (mean of the distribution) changing between the trials depending on the participant's response. At the high noise condition, the offset from the vertical is fixed (8° for the highest noise condition here) and the variance is changed based on the participant's response.

For the pilot study, six observers (33.5 ± 8.04 years) with normal or corrected to normal visual acuity participated to complete three experimental sessions for both RDK and Glass patterns. The variance thresholds were measured (*high noise*) at the offset angles (from vertical) of 5° and 10° for the direction of motion in RDK while the offset angles of 15° and 20° were used for the orientation discrimination in the Glass pattern. These values were selected based on the results of the previous experiments that showed that the discrimination thresholds at high noise ranged between 5° and 10° for the direction of motion in an RDK and between 15° to 20° for the orientation in a Glass pattern (section 3.1). Three conditions (one *no* *noise* and two *high noise* conditions) were then evaluated with interleaved 3:1 staircases. The properties of staircases were as defined in the general methods (Section 2.4). Two runs of practice sessions with ten trials for each condition were carried out before the main experiment. In the main experiment, each staircase terminated after ten reversals or 100 trials whichever came first. Discrimination thresholds were then determined as the geometrical mean of the last seven reversals and the reliability of the results was assessed with psychometric function fits of the raw data.

5.2.2 Results

The results showed that measuring the variance thresholds at pre-determined direction/orientation angles was a viable method. The measured direction/orientation variance thresholds at fixed discrimination angles showed the expected result of an increase in tolerable variance at larger direction/orientation offset (Figure 5.2 and 5.3). There were individual differences among the observers for variance thresholds at the *high noise* condition. For the direction discrimination, the tolerable variance at a 5˚ offset angle ranged from 28˚ (RB and MA) to 67˚ (RW). Similarly, for the orientation discrimination the tolerable variance at 15˚ was between 10˚ (MA) to 44˚ (MP). At the larger offset (10˚ for direction discrimination, 20˚ for the orientation discrimination), the variance thresholds were mostly similar to the lower offset angles (5˚ and 10˚ for direction and orientation respectively). When the angular offset from the vertical was set at 45˚ as used in other studies (Manning *et al.*, 2014; Tibber *et al.*, 2014), the task no longer seemed to resemble that of discriminating direction/orientation angle from the vertical.

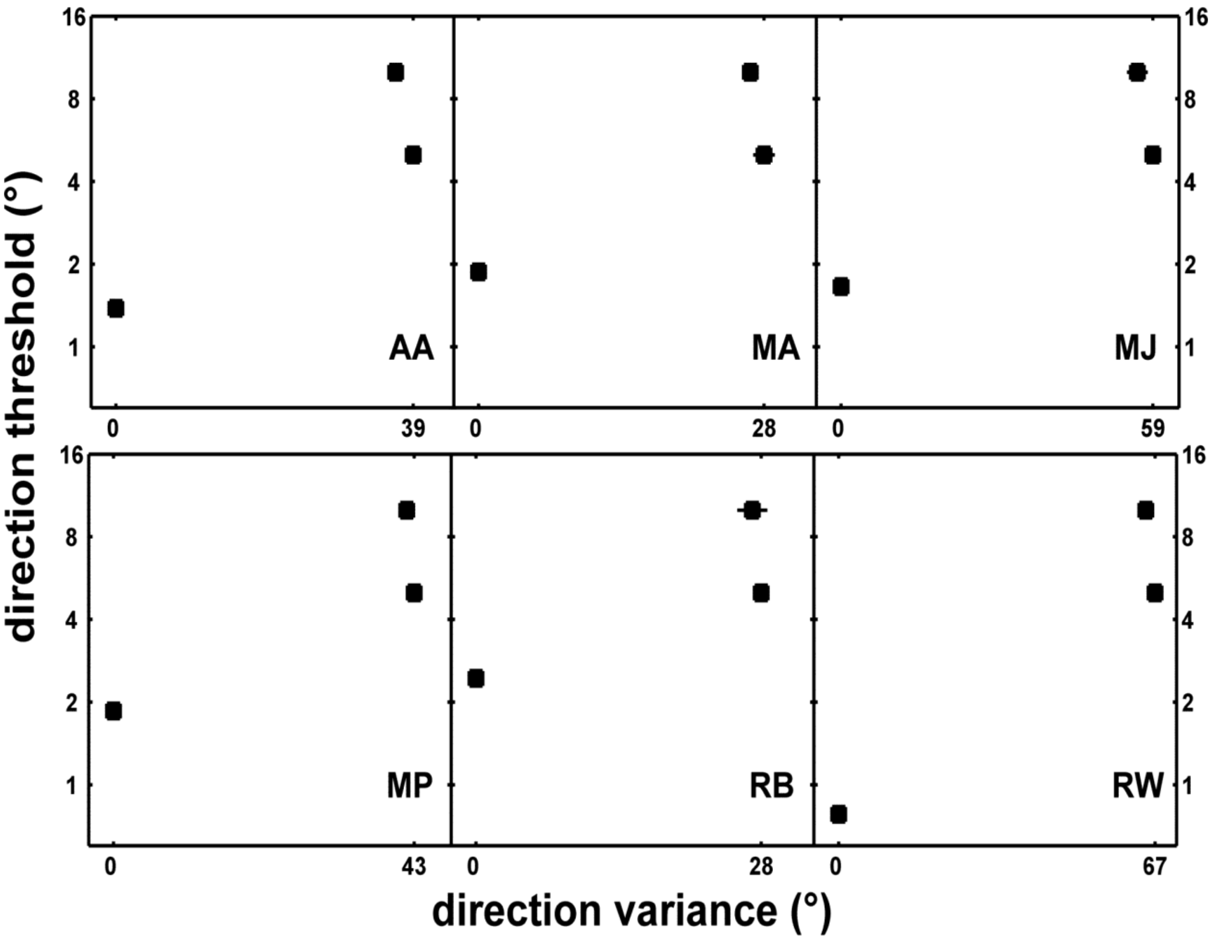

Figure 5.2: The mean direction discrimination threshold at *no noise* condition and variance threshold at *high noise* conditions.

The offset from vertical for high noise conditions were set at 5˚ and 10˚ angles. The vertical (for no noise condition) and horizontal (for high noise condition) error bars represent ± 1standard deviation.

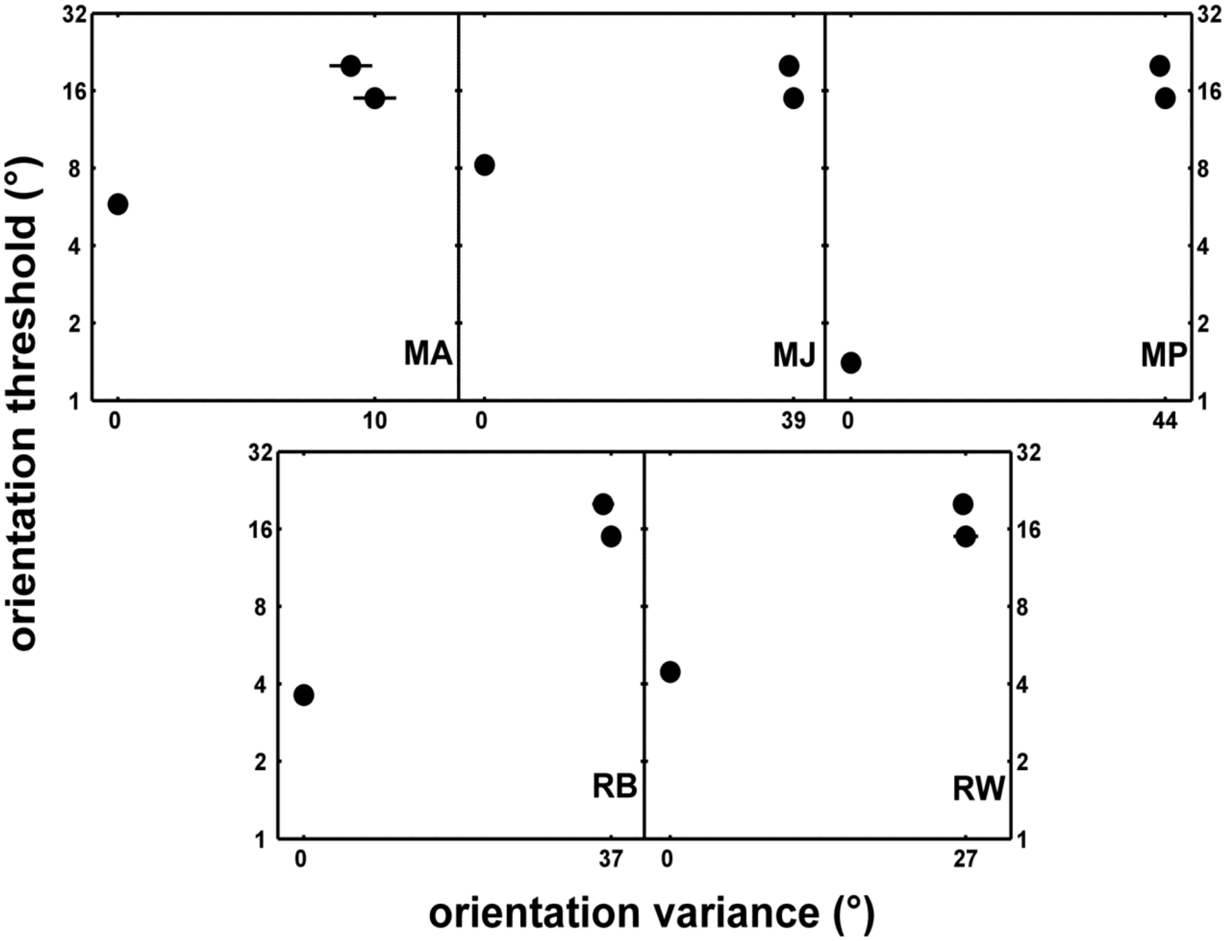

Figure 5.3: The mean orientation discrimination threshold at *no noise* condition and variance threshold at *high noise* conditions.

The offset from vertical for high noise conditions were set at 15˚ and 20˚ angles. The vertical (for no noise condition) and horizontal (for high noise condition) error bars represent ± 1standard deviation.

5.3 Main validation study

5.3.1 Methods

The stimulus parameters were the same as described for the pilot study. The validation experiment was carried out to compare the results from the quick method with the established method of measuring thresholds at different levels of added external noise. The results from the pilot study showed that the tolerable variance for both functions varied among observers and evaluating the variance threshold at a fixed direction/orientation angles may not target the desired *high noise* levels. Hence the direction/orientation angles for the evaluation of the tolerable variance threshold for this experiment were set at two times (*high noise I*) and four times (*high noise II*) of the threshold measured for the *no noise* condition.

Five observers (35.8±9.31 years) with normal or corrected to normal visual acuity completed five sessions of the experiment each for the direction of motion discrimination (RDK) and orientation discrimination (Glass pattern). The validation experiment included two designs; recording the direction/orientation discrimination thresholds at five levels of variable external noise (*TvN* method) and determining the tolerable external noise at two different direction/orientation discrimination angles (quick method). For the *TvN* method, the external noise (variance) of 0˚, 15˚, 20˚, 30˚ and 40˚ were used. For the quick method, the direction/orientation discrimination threshold for the *no noise* condition was initially determined in a separate experiment. The 2x (*high noise I*) and 4x (*high noise II*) multiples of this threshold were then used as the direction/orientation offset angles to determine the tolerable variance thresholds. A total of seven conditions, five *TvN* and two quick, were evaluated with interleaved 3:1 staircases with similar parameters as described for the pilot experiment. Observers first completed two practice sessions with ten trials for each condition before the main experiment in which the staircase terminated after ten reversals or 100 trials whichever came first. Thresholds were then determined as the geometrical mean of the last seven reversals.

5.3.2 Results

The results from the five sessions of *TvN* experiment showed that the discrimination thresholds were constant at lower levels of external noise and increased at higher noise levels for both RDK and Glass pattern. The thresholds from the quick method also showed a similar trend. Figure 5.4 and 5.5 shows the results from five individual observers and the mean data for RDK and Glass patterns respectively. As can be seen from figure 5.4, the variance thresholds (targeting *high noise*) from the quick method at the predefined direction/orientation angles were similar to that of the thresholds from the conventional *TvN* method for all observers for both the RDK and Glass patterns.

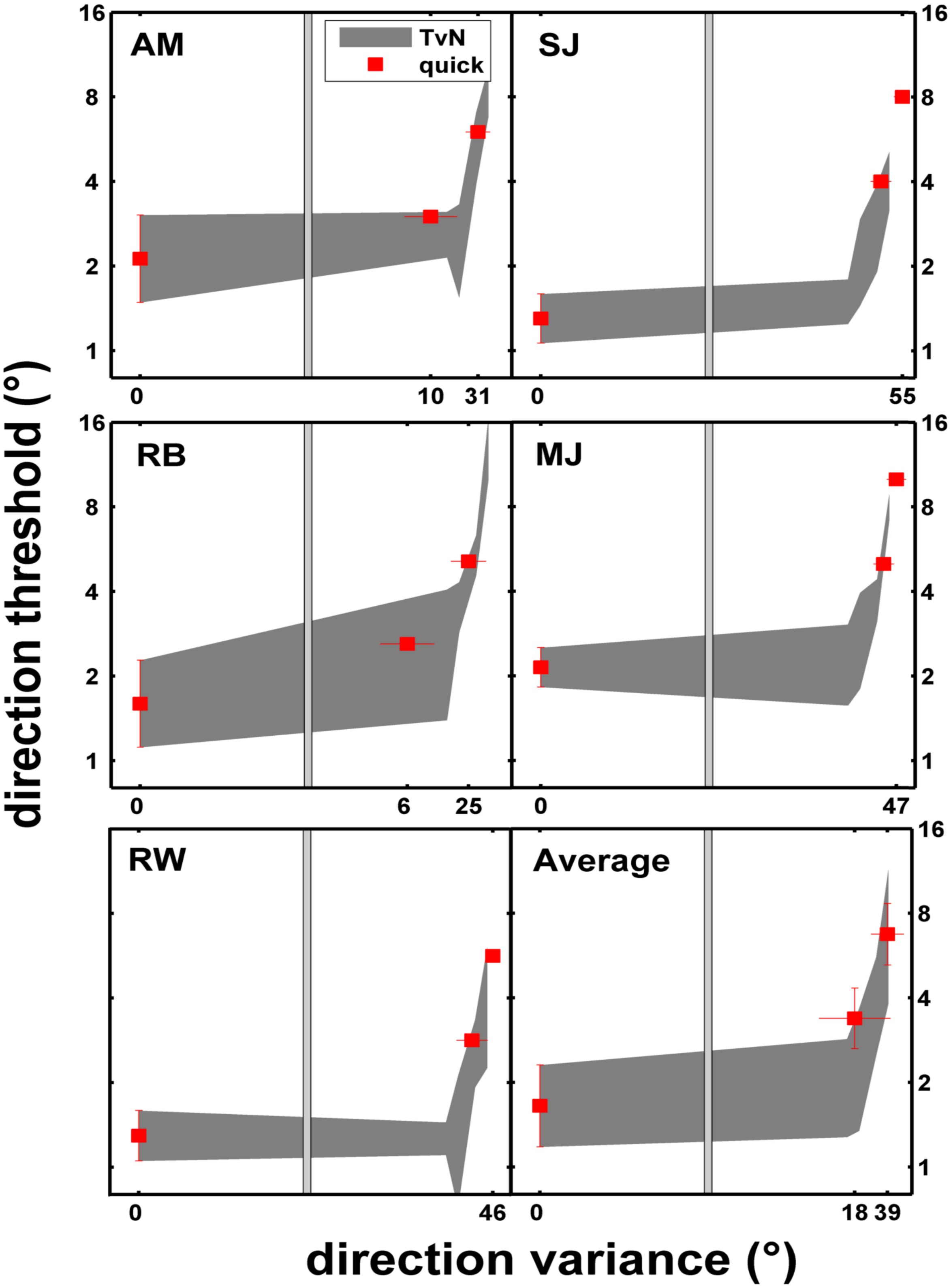

Figure 5.4: The direction discrimination thresholds from threshold vs noise method (*TvN*) and quick method (quick) for five observers and average data.

The shaded area represents one standard deviation from mean of the TvN thresholds and the error bar represents ± 1standard deviation for thresholds measured from the quick method.

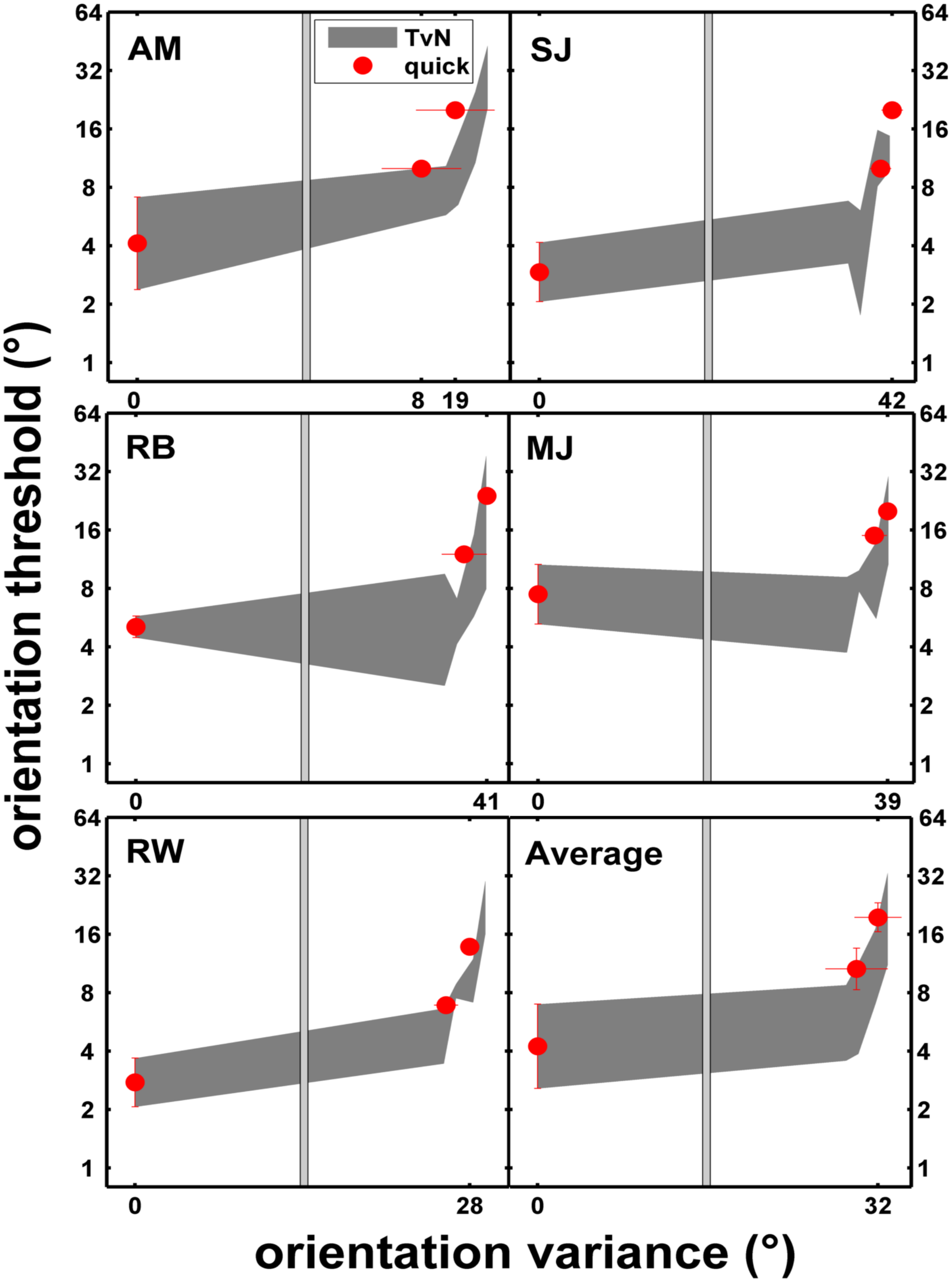

Figure 5.5: The orientation discrimination thresholds from threshold vs. noise method (*TvN*) and quick method (quick) for five observers and average data.

The shaded area represents one standard deviation from mean of the TvN thresholds and the error bar represents ±1standard deviation for thresholds measured from the quick method.

The external noise levels and direction/orientation discrimination thresholds from each method were then used to fit the linear model of the equivalent noise paradigm. We further evaluated the validity of the quick method with nested modelling on the mean data. The full model was fitted with independent internal equivalent noise (σ_{eq}) and sampling efficiency (*Eff*) parameters for *TvN* and quick methods while the simplest model consisted of one internal equivalent noise and sampling efficiency for both methods (Figure 5.6 and 5.7). The statistical analysis on the goodness of fit showed no significant difference in the reliability of the fit with the simplest model as compared to the full model for both the direction discrimination [$F(2,3) = 1.43$, $p > 0.1$] and orientation discrimination [$F(2,3) = 3.08$, $p > 0.1$] thresholds.

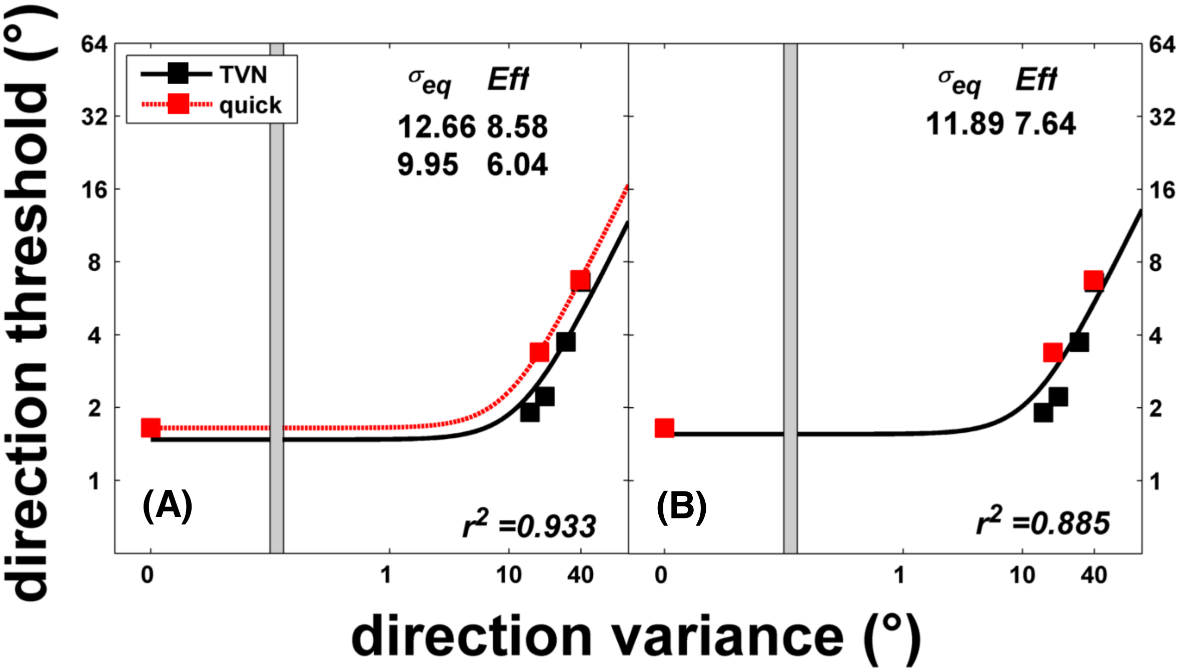

Figure 5.6: Nested models for the mean direction discrimination thresholds for *TvN* and quick methods.

The panels represent the full model (A) and simplest reduced model (B). The TvN curves in each panel relate the offset thresholds and variance thresholds to independent values of internal noise (σ_{eq}) and sampling efficiency (Eff). The best fitting parameters and the goodness of fit (r^2) of each model is also provided. Error bars are omitted for a better presentation.

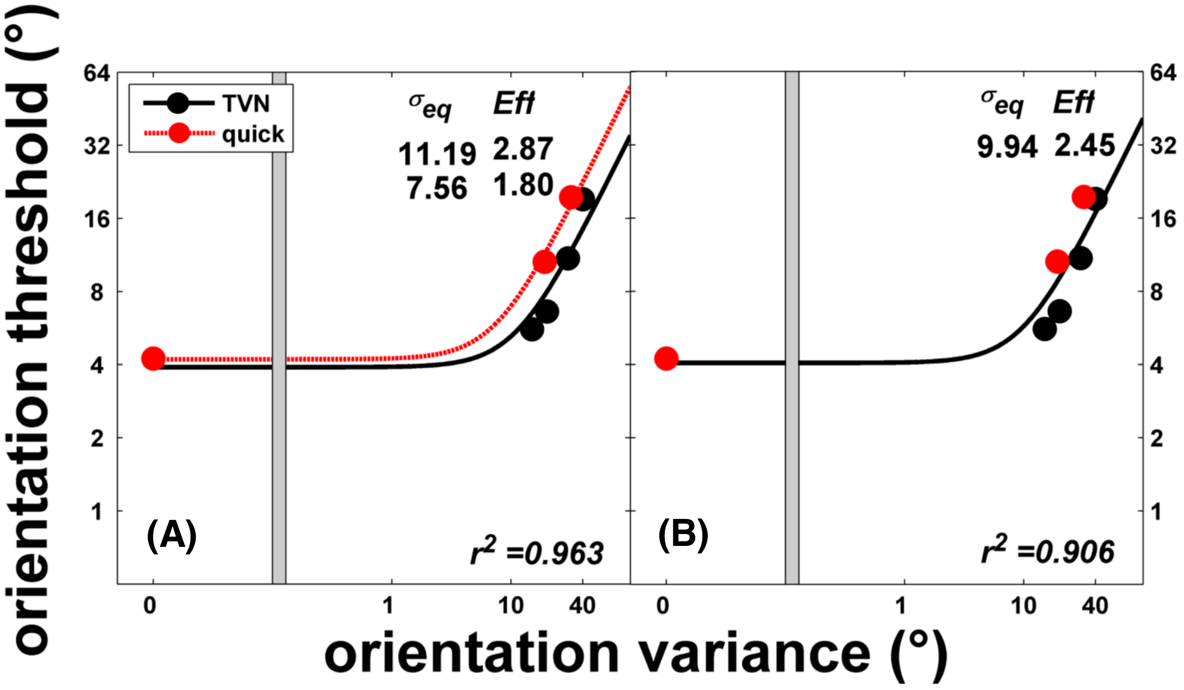

Figure 5.7: Nested models for the mean orientation discrimination thresholds for *TvN* and quick methods.

The panels represent the full model (A) and simplest reduced model (B). The TvN curves in each panel relate the offset thresholds and variance thresholds to independent values of internal noise (σ_{eq}) and sampling efficiency (Eff). The best fitting parameters and the goodness of fit (r^2) of each model is also provided. Error bars are omitted for a better presentation.

5.4 Discussion

In this study, we provided evidence of equivalence in the quality of data obtained from the simplified data collection method in the motion and form domain. We simplified the data collection procedure to estimate the *TvN* curve by measuring thresholds at three levels of noise (one no noise and two high noises) instead of 7-8 noise levels in the classical method. This effectively reduced the experiment time by more than half. Observers were able to complete a session within 4 - 5 minutes without sacrificing the precision of threshold estimation, while it would have taken 10 to 15 minutes with the conventional method employed in previous experiments (Chapter 3 and 4).

The main modification was to measure the variance thresholds at two direction/orientation offsets to target the high noise points. In the current task discriminating the mean direction/orientation becomes easier as the directional offset from the vertical is increased. Hence for a larger directional/orientation offset, observers should be able to tolerate higher levels of external noise. Therefore, measuring the maximum tolerable noise threshold at larger directional offsets should theoretically provide a similar result as measuring the directional/orientation offset thresholds at high noise levels. Our results showed that both methods predict similar results in the motion and orientation domains.

A similar method has been proposed to expedite the measurement of the *TvN* curve by measuring the directional threshold at a no noise condition and a tolerable variance threshold at a directional offset of 45˚ (Manning *et al.*, 2014; Tibber *et al.*, 2014). When the direction variance threshold is measured at a large directional offset such as 45˚, the stimulus wrap (for example, the direction of 0˚ and 360˚ is same with regard to motion) and the variance threshold obtained may not be accurate (Manning *et al.*, 2014; Tibber *et al.*, 2014). The study then used Monte Carlo simulation of a model observer's performance over a range of external noise to overcome stimulus wrapping. The simulation predicted the relationship to determine the sampling efficiency parameter using only the maximum tolerable noise obtained at the directional offset of 45˚. The internal noise factor was subsequently determined with the discrimination thresholds at the no noise condition and the efficiency parameter. The method was also adapted to the orientation domain using stimuli composed of multiple Gabor patches with the high noise point investigated at an orientation offset of 22.5˚ from vertical (Tibber *et al.*, 2014). When we evaluated the direction variance threshold at the high directional offset of 45˚ the task no longer resembled that of direction offset discrimination from the vertical instead it seemed more akin to a task which differentiated motion along the horizontal plane. Hence we used lower directional offset based on the observer's threshold at the no noise condition. The direction/orientation thresholds in the no noise condition ranged from 2˚ - 6˚ in our previous experiments (Chapter 3), hence we used 2*x* and 4*x* the threshold in the no noise condition to evaluate the variance threshold. At these levels of direction/orientation offset (range of 4˚ - 24˚ from vertical), the effect of stimulus wrap would be minimal and the threshold obtained can be used to fit the *TvN* curve using traditional modelling methods. Our validation results employing the nested modelling further demonstrated that the LAM parameters generated from both the quick and *TvN* methods are similar for both direction and orientation discrimination.

In the current study, we evaluated a method to minimise data collection without sacrificing the quality of the data when estimating the *TvN* curve in the both motion and form domains. This was achieved by measuring the variance threshold at pre-determined direction/orientation offsets from vertical and the direction/orientation offset threshold in a no noise condition. The method provided equivalent results in less than half the time that would be required when employing conventional methods. This faster method can, therefore, be applied more readily to clinical populations to help establish the role of local and global processing limits in our understanding of the neural basis of coherent visual perception. The ready application of an equivalent noise paradigm in a clinical population will subsequently shed light on the mechanisms by which an abnormal visual system then integrates local information to form the global percept in our cluttered everyday visual environment.

The results of this chapter were presented at the 14th Annual Vision Sciences Society Meeting, Florida, USA, 16-21 May 2014 and the British Congress of optometry and Vision Science, Cardiff, UK, 8-9 Sep 2014.

Joshi M R, Simmers A J, Jeon S T; Limiting Factors in Form and Motion Perception: Shared locally, Differentiated Globally. Journal of Vision 2014; 14(10):1418.

6.0 Concurrent investigation of dorsal and ventral stream visual processing in amblyopia: an equivalent noise approach

6.1 Introduction

Amblyopia is a neurodevelopmental disorder manifested as a monocular/binocular reduction in vision in the absence of any organic cause. The condition is most commonly associated with strabismus, anisometropia or visual deprivation during the early developmental years. The decorrelated inputs from misaligned visual axes in strabismus or a blurred image from one eye in anisometropia result in inadequate stimulation of the affected eye that hinders the normal development of the visual system.

Early animal models reported abnormal retinal ganglion cells in amblyopic cats (Ikeda, 1980). The functional receptive fields of cats' central fovea were enlarged mimicking that of a normal retinal periphery (Ikeda, 1980). However, subsequent study ruled out such deficits in retinal ganglion cells (Cleland *et al.*, 1982). The retinotopic representation of the central visual field from the amblyopic eye in humans is reported to be only minimally altered at V1 and extra striate areas (Li *et al.*, 2007). The LGN responses are also reduced in amblyopia, however, these reductions are in part modulated by the feedback responses from the striate cortex (Barnes *et al.*, 2010). Hence the contribution of retinal and LGN abnormalities to the functional deficit in amblyopia has remained controversial (Hess, 2001).

The primary site of the deficit in amblyopia appears to be the striate cortex (Wiesel and Hubel, 1963b; Wiesel and Hubel, 1965; Movshon *et al.*, 1987; Kiorpes and Movshon, 1996; Hess, 2001; Kiorpes, 2006). The abnormalities in striate cortex (V1) which include the disruption of the ocular dominance columns and a reduced number of neurones driven by amblyopic eye was first reported by Hubel and Wiesel in cats with surgically induced strabismus (Wiesel and Hubel, 1963b; Wiesel and Hubel, 1965), similar results have also been reported in macaques (Movshon *et al.*, 1987; Kiorpes, 2006). These changes lead to a shift of the ocular dominance columns to the fellow eye resulting in an inhibition of the amblyopic eye (Joly and Frankó, 2014). The neurones in area V2 also show similar changes to that of V1 (Bi *et al.*, 2011).

The magnitude of the physiological visual deficit measured from the neurones driven by amblyopic eyes in primary visual cortex of amblyopic monkeys is lower than the behavioural deficit (Kiorpes *et al.*, 1998; Kiorpes and Movshon, 2004; Kiorpes, 2006; Levi, 2006; Bi *et al.*, 2011). Subsequent studies have reported neuronal abnormalities across a range of extra striate cortical areas along both dorsal (El-Shamayleh *et al.*, 2010; Thompson *et al.*, 2012) and ventral streams (Movshon *et al.*, 1987; Lerner *et al.*, 2003; Muckli *et al.*, 2006). Area MT along the dorsal stream is appears mostly activated by the fellow eye with a behavioural loss in global motion perception closely resembling the pooled loss from the neurones driven by the amblyopic eye in the macaques (El-Shamayleh *et al.*, 2010). Similarly, the responses from the motion areas MT and MST in response to plaid stimuli are reported to be reduced in amblyopia (Thompson *et al.*, 2012) and during the visual tracking of moving targets (Secen *et al.*, 2011). El-Shamayleh *et al.* (2010) also reported that the neuronal response in area MT was inadequate to account for the behavioural loss of motion sensitivity and that the amblyopic deficits could extend to even higher areas along the dorsal stream. Similarly along the ventral stream, the activation of V4 neurones from the amblyopic eye is reduced with responses mostly driven by the fellow eye (Movshon *et al.*, 1987). fMRI stimulation from the amblyopic eye in response to simple sinusoidal grating is progressively reduced along the higher ventral stream areas of V4 and LO complex compared to V1/V2 (Muckli *et al.*, 2006). The responses from these higher ventral stream areas are also reduced when evaluated with complex form stimuli such as line drawings (Lerner *et al.*, 2006) and faces (Lerner *et al.*, 2003). The deficits in the higher extra striate areas are associated with V1/V2 abnormalities suggesting that the deficits might only be an upstream manifestation of changes at lower levels. However, more recent studies have found that the extra striate deficits in amblyopia are independent of (Li *et al.*, 2012) or even occur in the absence (Muckli *et al.*, 2006) of the more traditional lower level deficits at V1 and V2.

Behavioural studies in humans have also reported reduced sensitivity to various visual functions in amblyopia. While the clinical diagnosis of amblyopia is made mostly based on the loss of visual acuity and contrast sensitivity, other functions such as stereoacuity (Wallace *et al.*, 2011), vernier acuity (Levi and Klein, 1985) are also reduced in varying degree depending upon the type of amblyopia (Hamm *et al.*, 2014). The sensitivity to global perceptual tasks processed at higher cortical areas of the dorsal and ventral streams are also reduced in amblyopia (Ellemberg *et al.*, 2002; Simmers *et al.*, 2003b; Simmers and Bex, 2004; Simmers *et al.*, 2005; Mansouri and Hess, 2006; Simmers *et al.*, 2006b; Husk and Hess, 2013).

Different neural theories have been proposed for the multitude of visual deficits observed in amblyopia. The under sampling theory suggests that the receptive field size of the neurones processing the central visual field in amblyopia resembles that of the normal peripheral retina containing cells with a larger receptive field (Levi and Klein, 1985). This results in under sampling of information from the central field leading to positional uncertainties and temporal instabilities. Instead of the under sampling, the neural disarray theory suggests that the amblyopic deficits are a result of topographical disorganisation of the retinotopic map due to the stimulation of non-corresponding areas of visual space by two disparate images (Hess and Field, 1994). More recently the amblyopic deficits are being explored with the consideration of noise in contrast (Levi *et al.*, 2008) as well as motion and form domains (Hess *et al.*, 2006; Mansouri and Hess, 2006; Husk and Hess, 2013).

The dorsal stream in amblyopia has been investigated frequently with RDKs by measuring motion coherence thresholds as an index of global motion sensitivity (Figure 4.1). These studies report reduced sensitivities to global translation, rotation and radial motion that persist even after the contributions from V1/V2 are accounted for in terms of loss of sensitivity to spatial frequencies and contrast in anisometropic and strabismic amblyopia (Simmers *et al.*, 2003b; Simmers *et al.*, 2006b; Aaen-Stockdale *et al.*, 2007; Aaen-Stockdale and Hess, 2008). These motion coherence deficits appear to extend to the higher extrastriate areas of the dorsal stream (MT, MST and beyond) for the amblyopic as well as fellow eye (Simmers *et al.*, 2003b; Simmers *et al.*, 2006b). Another method to study global motion is with a task in which directions of individual dots in a translational RDK are derived from a standard Gaussian distribution with a varying degree of variance to manipulate the level of noise in the overall direction – an equivalent noise task. In such a task, the most efficient way to calculate the overall direction is suggested to be by integrating the individual directions of motion dots. Studies that have used this task have reported normal direction discrimination threshold for amblyopes (Mansouri and Hess, 2006). Amblyopes also performed normally in a task that required integration of direction of the motion of plaid components (Thompson *et al.*, 2008a). These studies suggested that the normal findings on global fine motion discrimination tasks (using equivalent noise method) was due to the global integration ability being normal in amblyopes while the abnormal global motion sensitivity from the coherence threshold paradigm was due to the inability of the amblyopes to segregate the noise dots from the signal dots (Hess *et al.*, 2006; Mansouri and Hess, 2006).

Global form processing along the ventral stream in amblyopia has also been extensively evaluated with different stimuli such as line segments (Simmers *et al.*, 2005), radial frequency patterns (Dallala *et al.*, 2010), Gabor elements (Mansouri and Hess, 2006; Husk and Hess, 2013) and Glass patterns (Lewis *et al.*, 2002; Rislove *et al.*, 2010) - Figure 4.1. The studies that employed the coherence threshold paradigm using line segments and Glass patterns reported abnormal global form coherence thresholds for translational and rotational patterns (Lewis *et al.*, 2002; Simmers *et al.*, 2005; Rislove *et al.*, 2010). These deficits were observed for both amblyopic and fellow eyes in anisometropic (Simmers *et al.*, 2005), strabismic (Rislove *et al.*, 2010) and deprivation (Lewis *et al.*, 2002) amblyopia.

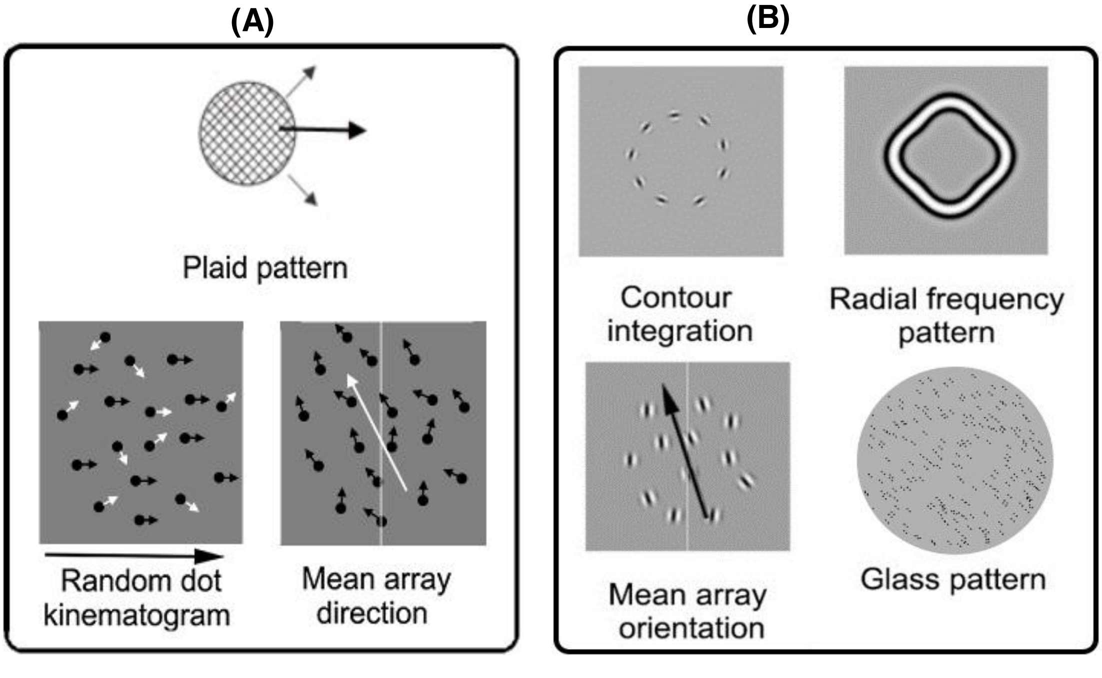

Figure 6.1: Common stimuli used to evaluate global motion (A) and global form (B) perception in amblyopia.

Adapted from Hamm et al., (2014)

However, for a fine global orientation task that relies on the integration of elements, the results are varied. The mean global orientation offset threshold from the array of Gabor patches is reported to be normal (Mansouri and Hess, 2006), slightly reduced (Husk and Hess, 2013) or abnormal (Simmers and Bex, 2004) in the amblyopic and fellow eyes of anisometropic and strabismic amblyopes. In other studies using radial frequency patterns, the subsumed integration performance is reported to be abnormal (Dallala *et al.*, 2010; Subramanian *et al.*, 2012). Moreover, some of the strabismic amblyopes were unable to reliably detect the coherent translational Glass pattern (Anderson and Swettenham, 2006; Rislove *et al.*, 2010), where the fundamental task is integration in the absence of noise elements. Other global integrative tasks that use inputs from both the motion and form domain such as structure from motion is reported to be abnormal in amblyopia (Hayward *et al.*, 2011; Husk *et al.*, 2012); while biological motion perception, which also relies on the inputs from both domains is mostly preserved (Hamm *et al.*, 2014). Therefore the reported abnormalities in the global processing of motion and form along the higher extra striate areas vary significantly depending upon the task and stimulus.

Several reviews of global motion and form perception in a range of developmental disorders (Braddick *et al.*, 2003; Grinter *et al.*, 2010) including amblyopia (Simmers *et al.*, 2003b; Simmers *et al.*, 2005) indicate that dorsal stream functions are more affected than those of the ventral stream. The direct comparison of the two streams, however, can only be made using a common experimental stimulus that shares the same parameters except for the domain specific outputs of interest. For example, Simmers *et al.,* (2003, 2005) used a stimulus set to measure global coherence thresholds in motion and form where the motion stimulus was translational RDKs and the form stimulus was a still image of oriented streaks captured frame by frame from a respective translational RDK. Using this stimulus set, they reported deficits along both streams, with a relatively larger deficit in the dorsal stream compared to the ventral stream. Similarly, Mansouri and Hess (2006) employed moving micro patterns and static Gabor patches in direction and orientation integration tasks respectively. The task was to determine the mean direction/orientation offset from the vertical in the presence of direction and orientation noise. They reported no difference in the performance of amblyopes compared to the normal but their results were not directly comparable.

As described earlier (General Methods, Chapter 2), there are limitations in the stimuli used by these studies (Simmers *et al.*, 2003b; Simmers *et al.*, 2005; Mansouri and Hess, 2006) for the concurrent evaluation of motion and form perception. Briefly, the orientation streaks used by Simmers *et al.,* (2003, 2005) looked no different from line segments where the global integration of local elements does not seem necessary to do the task. The stimuli used by Mansouri and Hess (2006) were physically different making it difficult to directly compare the results from two streams.

In the current study, we measure similar outputs, which are thought to share common processing mechanisms along the early, shared areas in the dorsal and ventral streams and probe differences (or commonalities) in global processing assumed in the higher regions of the respective streams. The findings from the studies employing the global coherence threshold paradigm almost unanimously report deficits in both motion and form perception in amblyopia. However, the findings for global motion and form processing using fine direction/orientation discrimination tasks are not very clear. What is evident is that measuring coherence thresholds cannot separate the local and global limitations of the processing mechanisms occurring at the early visual areas (V1 and V2) and the extra striate areas. However, measuring the direction/orientation thresholds at varying levels of noise, using the equivalent noise paradigm, can separate the effects of local and global processing mechanisms. Hence we propose evaluating the global motion and form processing in amblyopia using identical stimuli based on the equivalent noise paradigm. The results will provide comparable data along the two streams and parse out the influence of local and global processing mechanisms in each stream.

6.2 Experiment 1: Fine direction and orientation discrimination in anisometropic amblyopia

6.2.1 Methods

6.2.1.1 Stimuli and procedure

The quick method (Chapter 5) was used for the evaluation of motion and form processing in amblyopia. The RDK and Glass pattern stimuli were similar to that used in the previous study (Chapter 5). The dot size was increased from 0.083° to

0.166° to facilitate the viewing of the dot elements for the amblyopic participants. The dipole distance for the Glass pattern was also altered accordingly, increased from 0.133˚ to 0.266˚. Other physical parameters, stimulus presentation and data collection methods were the same as that used for the quick method (Chapter 5).

Briefly, the direction/orientation of the RDK/Glass pattern elements were derived from a standard Gaussian distribution with prescribed mean and standard deviation. The means of the distribution were set at defined angles from the vertical (90˚) with varying standard deviation introducing external noise to the stimulus. The fine direction/orientation discrimination thresholds (offset from vertical) were first determined at *no noise* condition (zero variance) in a separate experiment. The multiples (2x, *high noise I* and 4x, *high noise II*) of this direction/orientation offset threshold were then used to evaluate the variance (noise) threshold targeting the *high noise* conditions in the main experiment. The experiment hence contained a staircase for the direction/orientation offset threshold at the *no noise* condition that was interleaved with two staircases for the variance threshold (*high Noise I and II*) at the pre-determined direction/orientation offsets. The staircase for the *no noise* condition started with the mean direction of ±10˚ away from the vertical while the staircases for the variance threshold (*high noise I and II*) at predetermined offset angles started with a variance of 10˚. The directional offset from vertical decreased for the *no noise* condition with three correct responses and increased with an incorrect response. The variance for the other two staircases in the *high noise* conditions increased after three correct responses as the aim was to determine maximum tolerable noise at a fixed direction/orientation offset. All staircases terminated after ten reversals or 100 trials, whichever was reached first. The thresholds were then calculated as the geometrical mean of the last seven reversals. The raw thresholds were also used to fit the psychometric function for each observer to analyse the reliability of participant's responses. All participants completed two practice runs of the experiment containing only 15 trials for each condition (*no noise, high noise I and II*). Upon the satisfactory completion of the practice session, the full experiment was conducted.

6.2.1.2 Participants

The criterion for the diagnosis of amblyopia was an interocular difference in acuity (IOD) of ≥ 0.2 log MAR units or a past history of amblyopia treatment. All participants underwent the following screening tests (details in General Methods, 2.2.1).

- Visual acuity with modified log MAR chart
- Stereoacuity with Frisby near stereo test
- Sensory fusion with Bagolini Glasses
- Cover test

Eight anisometropic amblyopes (mean age = 19.38 ±2.00 years) and six visually normal participants (mean age = 29.00 ±2.75 years) were recruited for experiment 1 (Table 6.1). Both groups of participants completed the experiments monocularly with the best refractive correction in place; amblyopic eye and fellow eye for amblyopes, non-dominant and dominant eye for the normal controls. The eye dominance in normal controls was determined with the hole in a card test.

ID	Age (yr.)	Visual Acuity		Refraction		Binocularity	Cover Test	Stereo (sec of arc)	Treatment History
Amblyopes		**RE**	**LE**	**RE**	**LE**				
KW	18	0.1	0	-6.25/-1.25*170	-6.50/-1.50*180	Present	Exophoria	20	Patching
RK	19	0.2	-0.02	+1.75/-1.00*180	0	Present	Exophoria	85	None
LC	18	-0.2	-0.06	+3.75/-1.00*170	+5.25/-1.25*180	Present	Exophoria	36	Patching
HM	18	0.18	0	-2.75/-3.00*180	-2.25/-1.75*10	Present	Exophoria	75	None
MR	20	0.26	0.1	+6.00/-3.75*10	+5.25/-3.25*180	Present	Esophoria	100	Patching
LS	19	0.2	-0.2	+5.25/-0.50*105	+3.50/-0.50*105	Present	Esophoria	No	Patching
MI	19	0	0.2	-3.50/-.050*60	-8.50/-1.50*140	Present	Exophoria	40	Patching
HMc	24	-0.14	0.12	-0.25	+1.00/-1.00*90	Present	Exophoria	20	None
Normal									
AM	28	0	0	-0.50/-0.50*180	-0.50/-0.75*120	Present	Exophoria	30	
MA	31	0	0	-0.25	-0.25*180	Present	Orthophoria	20	
MP	27	0.06	0.06	-2.75/-0.75*166	-3.00/-2.25*178	Present	Exophoria	20	
SA	32	-0.1	-0.1	-0.50	-0.50	Present	Exophoria	30	
AL	25	-0.06	-0.1	-3.25/-0.50*90	-3.50/-0.75*5	Present	Exophoria	20	
MJ	31	0	0	-1.00	-1.00	Present	Exophoria	30	

Table 6.1: The clinical details of the anisometropic amblyopes and normal participants.

6.2.2 Results:

6.2.2.1 Direction/orientation discrimination in normal controls

The mean direction offset and direction variance thresholds for dominant eye and non-dominant eye were similar across all noise levels for normal participants (Figure 6.2). The orientation discrimination thresholds also followed a similar pattern (Figure 6.3). Overall the orientation discrimination thresholds (Glass) were consistently higher compared to the direction discrimination thresholds (RDK) irrespective of the noise levels; Figure 6.4 shows the results from both eyes combined.

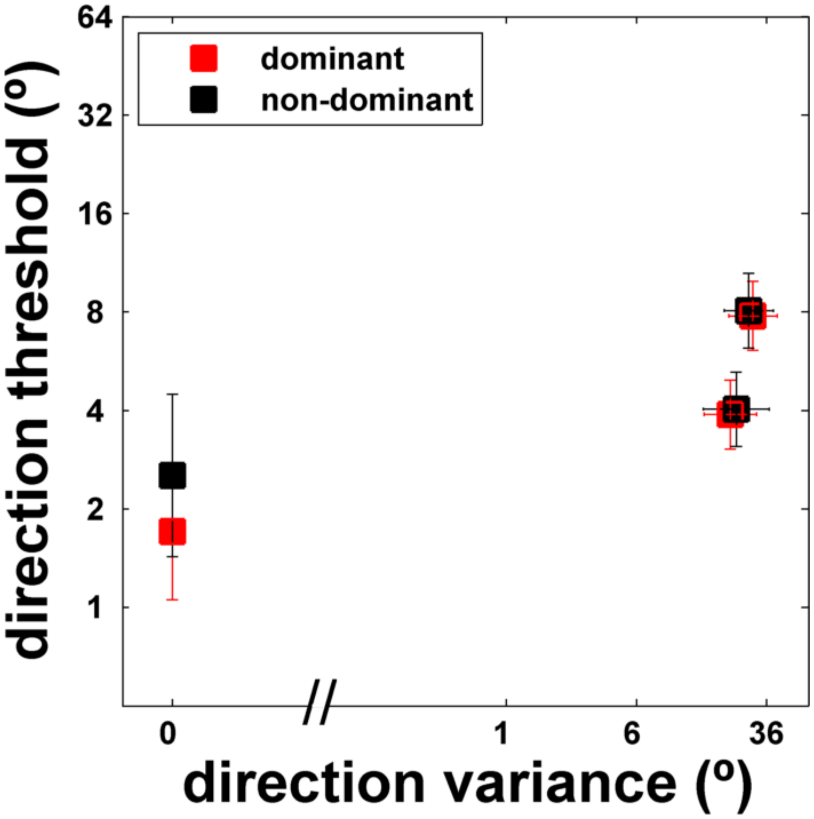

	No Noise	*High Noise I (x at y)*	*High Noise II (x at y)*
dominant	**1.71˚ (1.02˚)**	**21.71˚ (8.61˚) at 3.88˚ (1.04˚)**	**29.65˚ (9.94˚) at 7.78˚ (2.09˚)**
non-dominant	**2.53˚ (2.19˚)**	**23.58˚ (9.64˚) at 4.03˚ (1.11˚)**	**27.98˚ (8.80˚) at 8.07˚ (2.23˚)**

Figure 6.2: The mean direction offset/variance threshold for normal controls.

The thresholds are presented for dominant eye (red squares) and non-dominant eye (black squares), the error bars represent ± 1standard deviation. The attached table shows the mean direction/variance thresholds for no noise, high noise I and high noise II. The values in parenthesis represent the standard deviation.

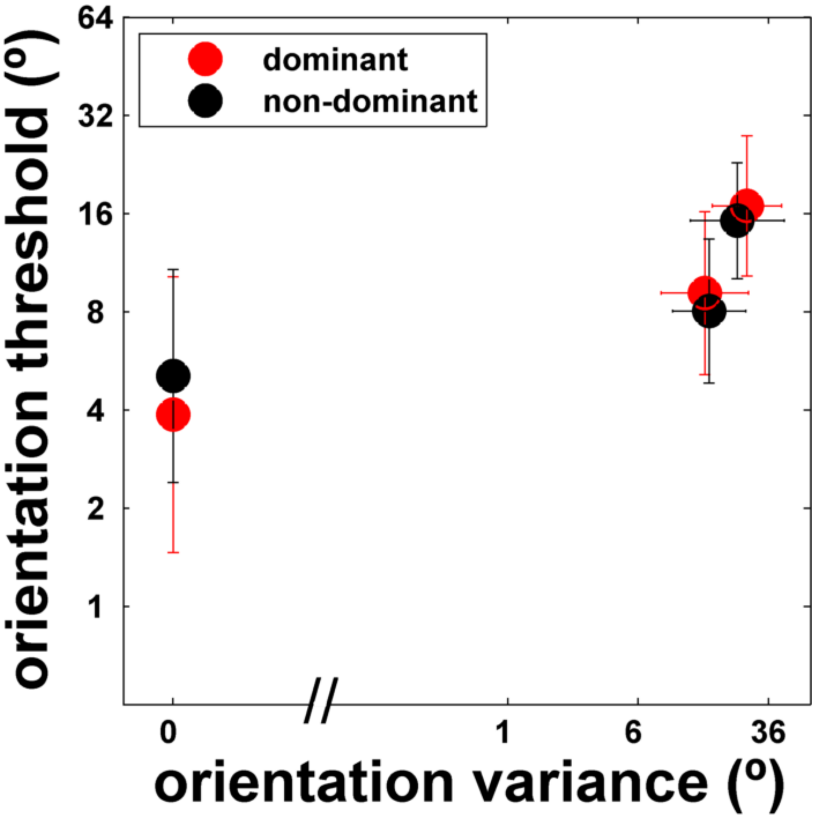

	No Noise	*High Noise I (x at y)*	*High Noise II (x at y)*
Dominant	**3.87˚ (5.21˚)**	**14.92˚ (7.96˚) at 9.12˚ (5.52˚)**	**26.58˚ (10.13˚) at 16.87˚ (7.97)**
Non-dominant	**5.08˚ (3.99˚)**	**15.83˚ (9.70˚) at 8.03˚ (4.35˚)**	**23.29˚ (12.22˚) at 15.20˚(6.11˚)**

Figure 6.3: The mean orientation offset/variance threshold for normal controls.

The thresholds are presented for dominant eye (red circles) and non-dominant eye (black circles), the error bars represent ± 1standard deviation. The attached table shows the mean direction/variance thresholds for no noise, high noise I and high noise II. The values in parenthesis represent the standard deviation.

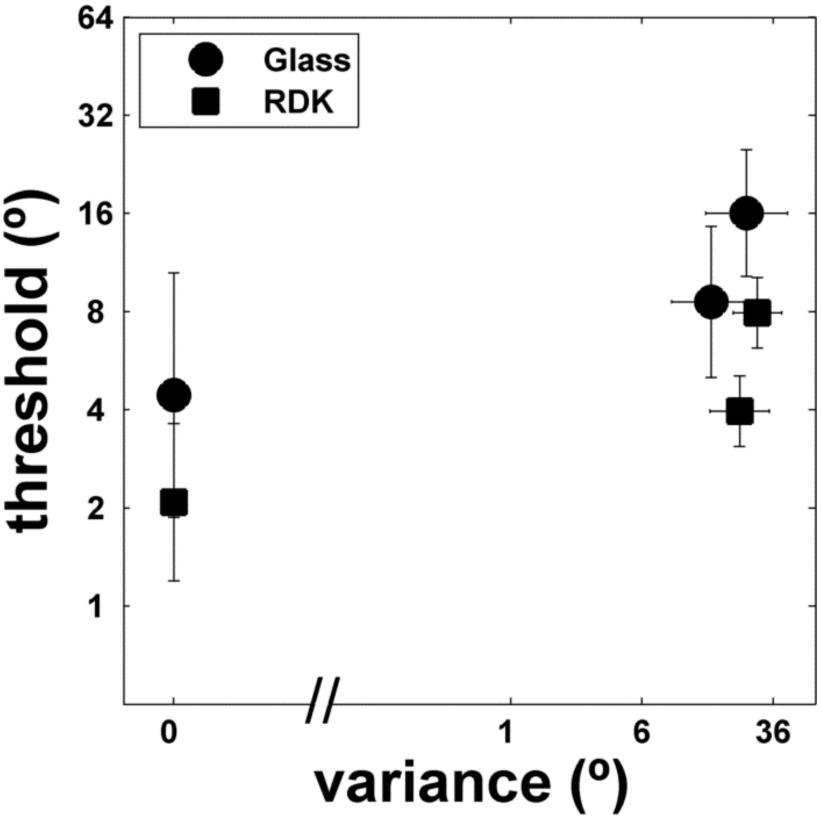

Figure 6.4: The mean orientation discrimination (Glass) and direction discrimination (RDK) thresholds for the normal participants.

The data points for Glass and RDK are mean data with dominant and non-dominant eyes collapsed. The error bars represent ± 1standard deviation.

6.2.2.2 Direction/orientation discrimination in anisometropic amblyopes

The thresholds for dominant and non-dominant eyes were collapsed (normal eye here forward) and compared to the thresholds from amblyopic participants. The mean direction offset/variance thresholds were similar for the fellow eye, amblyopic eye and normal eye at all noise levels (Figure 6.5). The average orientation discrimination thresholds also followed a similar pattern with no difference between the fellow, amblyopic and normal eyes (Figure 6.6).

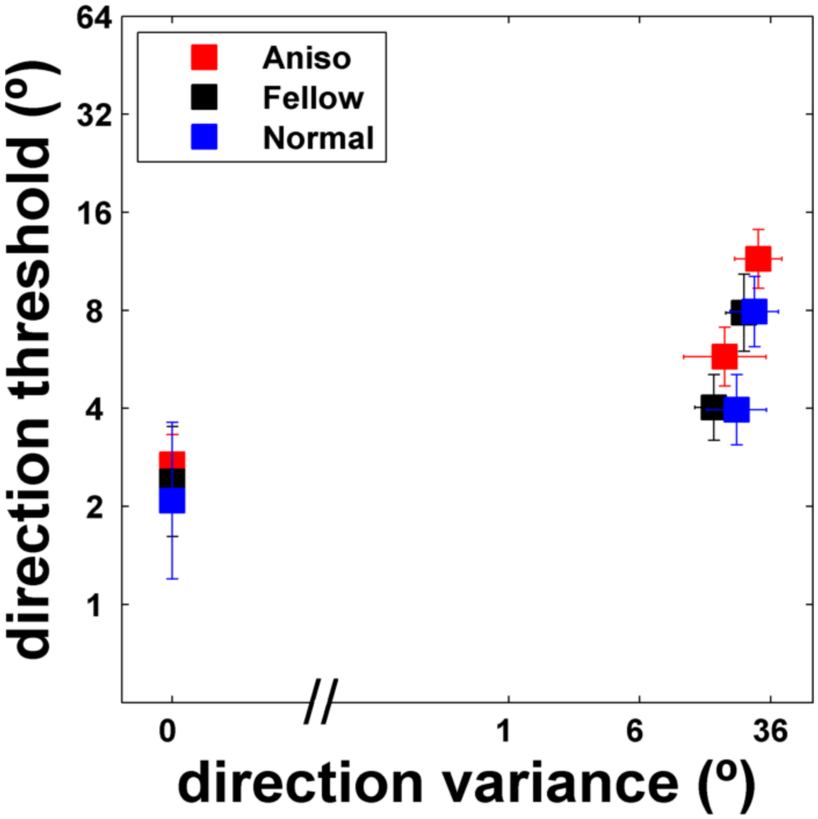

	No Noise	*High Noise I (x at y)*	*High Noise II (x at y)*
Aniso	**2.69˚ (0.58˚)**	**19.20˚ (8.80˚) at 5.76˚ (1.20˚)**	**30.38˚ (10.04˚) at 11.52˚ (2.41˚)**
Fellow	**2.55˚ (1.59˚)**	**15.88˚ (4.70˚) at 4.03˚ (0.96˚)**	**24.68˚ (6.37˚) at 7.87˚ (2.09˚)**
Normal	**2.12 (1.61)**	**22.65 (9.13) at 3.97 (1.08)**	**28.82 (9.37) at 7.92 (2.16)**

Figure 6.5: The mean direction offset/variance threshold for anisometropic amblyopic and normal participants.

The thresholds are presented for anisometropic amblyopic eye (red squares), fellow eye (black squares) and normal eye (blue squares), the error bars represent ± 1standard deviation. The attached table shows the mean direction/variance thresholds for no noise, high noise I and high noise II. The values in parenthesis represent the standard deviation.

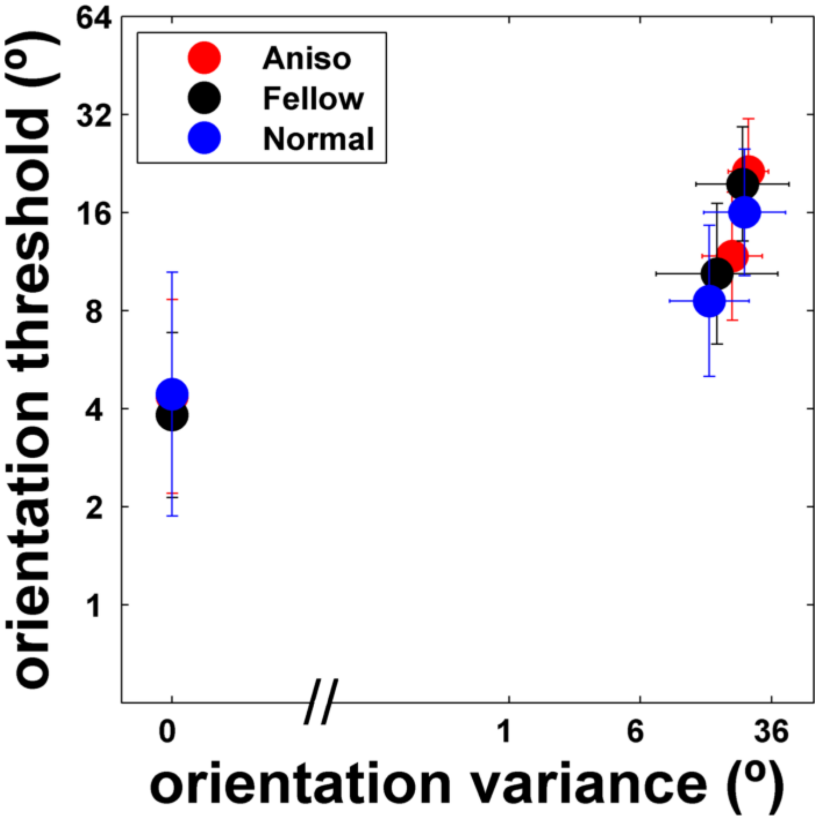

	No Noise	*High Noise I (x at y)*	*High Noise II (x at y)*
Aniso	**4.35 (3.50)**	**21.04 (9.76) at 11.74 (6.61)**	**26.21 (8.06) at 21.36 (8.11)**
Fellow	**3.82 (2.62)**	**17.09 (13.06) at 10.38 (6.53)**	**24.21 (11.13) at 19.55 (8.27)**
Normal	**4.47 (4.60)**	**15.38 (8.83) at 8.58 (4.93)**	**24.93 (11.17) at 16.03 (7.04)**

Figure 6.6: The mean orientation offset/variance threshold for anisometropic amblyopic and normal participants.

The thresholds are presented for anisometropic amblyopic eye (red circles), fellow eye (black circles) and normal eye (blue circles), the error bars represent ± 1standard deviation. The attached table shows the mean orientation/variance thresholds for no noise, high noise I and high noise II. The values in parenthesis represent the standard deviation.

The direction/orientation offset thresholds were measured at a fixed no noise condition but the variance thresholds for high noise conditions were measured at varying direction/orientation offset angles based on the initial direction/orientation thresholds with the no noise condition. As both direction/orientation offset thresholds and direction/orientation variance thresholds differed with the *eye* being evaluated and *type of stimuli*, both were treated as dependent variables. The performance of normal and amblyopic participants was then evaluated with the MANOVA.

The log direction/orientation offset and noise (levels of variance) were treated as dependent variables while *eyes* (four levels; dominant, non-dominant, fellow and amblyopic) and *stimulus type* (two levels; RDK and Glass) were considered as between subject factors. Box's test of equality of covariance matrices showed that covariance of the dependent variable was significantly different between the groups ($M = 63.98$, $F = 2.98$, $p < 0.001$). However, when the sample size across different groups are similar, the Pillai's trace (V) is robust against the violation of equality of covariance matrices assumption for MANOVA analysis (Tabachnick and Fidell, 2001).

Levene's test of equality of variance showed that the variance of dependent variables was similar across the groups for both noise [$F(7,325) = 0.07$, $p > 0.05$] and direction/orientation offsets [$F(7,325) = 1.99$, $p > 0.05$]. The between subject tests revealed a significant effect of *stimulus type* on the direction/orientation offset [$F(1, 332) = 75.94$, $p < 0.001$] but not on the noise [$F(1,332) = 0.04$, $p > 0.05$]. The effect of *eye* on noise [$F(3,332) = 0.01$, $p > 0.05$] was not significant while the effect of eye on direction/orientation offsets [$F(3,332) = 2.68$, $p = 0.05$] were borderline. The interaction of *eye* and *stimulus type* on noise [$F(3,332) = 0.016$, $p > 0.05$] and direction/orientation offsets [$F(3,332) = 0.33$, $p > 0.05$] were not significant.

Pairwise comparison of *eye* after Bonferroni correction showed no significant difference between the fellow, amblyopic, dominant and non-dominant eye on both noise and direction/orientation offset ($p > 0.05$), with the comparison between the amblyopic eye and dominant eye for direction/orientation offset being borderline ($p = 0.05$). The pairwise analysis of *stimulus type* showed significantly high orientation offset thresholds for Glass pattern compared to the direction offset threshold for RDK ($p < 0.001$) with no significant difference between the noise levels ($p > 0.05$).

As the thresholds between the fellow eye and amblyopic eye were similar, the data were collapsed over the eyes to compare the thresholds for direction discrimination (RDK) with orientation discrimination (Glass). The results showed that the thresholds for Glass were higher than the RDK at all noise levels (Figure 6.7).

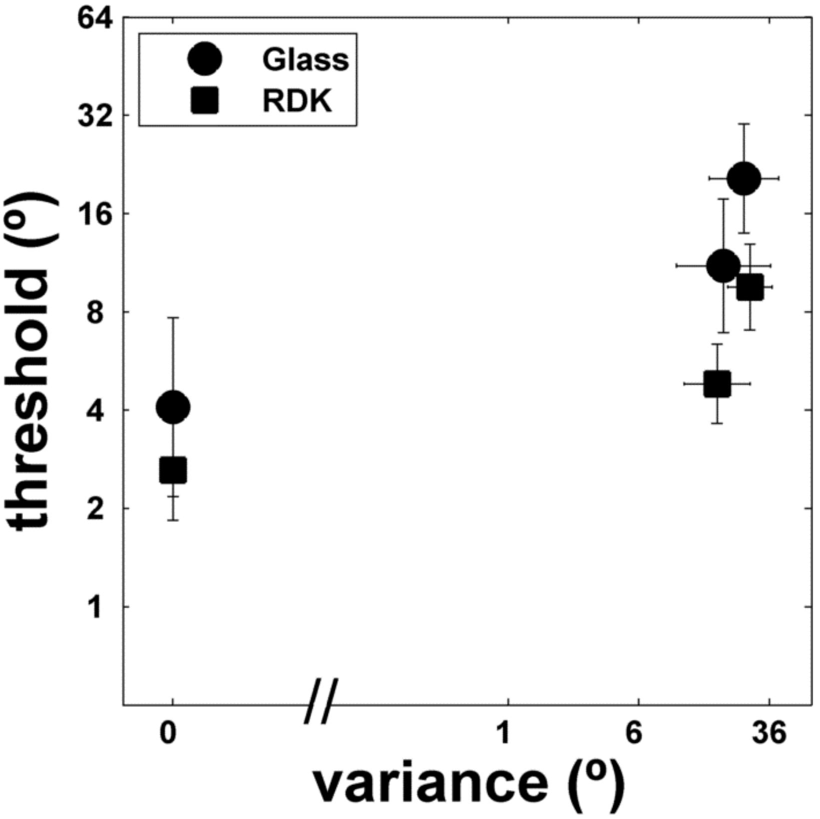

Figure 6.7: The mean orientation discrimination (Glass) and direction discrimination (RDK) thresholds for the amblyopic participants.

The data points for Glass and RDK are mean data with the amblyopic and fellow eyes collapsed. The error bars represent ± 1standard deviation.

6.2.2.3 Equivalent noise fit analysis with nested modelling in anisometropic amblyopes

The direction/orientation offset thresholds and the noise (levels of variance) thresholds were then used to fit the linear equivalent noise model for each group of participants to evaluate if no difference in thresholds was related to internal equivalent noise or sampling efficiency parameters. The thresholds (normal, fellow and amblyopic eyes) were fitted with nested models containing different numbers of parameters, and the goodness-of-fits were statistically evaluated. Figure 6.8 shows the mean direction offset and direction noise data fitted to the equivalent noise paradigm for full and reduced models with different numbers of free parameters. The goodness of fit (r^2) for all reduced models ($r^2 > 0.85$) were similar to the full-model ($r^2 = 0.93$); one σ_{eq} and three *Eff* [$F(2,3) = 0.06$, $p > 0.1$], three σ_{eq} and one *Eff* [$F(2,3) = 1.03$, $p > 0.1$], and one σ_{eq} and one *Eff* [$F(4,3) = 0.74$, $p > 0.1$]. The fit with the least number of parameters was then chosen as the statistically the best model to represent the threshold data, *i.e.,* the model with both σ_{eq} and *Eff* constrained across the *eyes*.

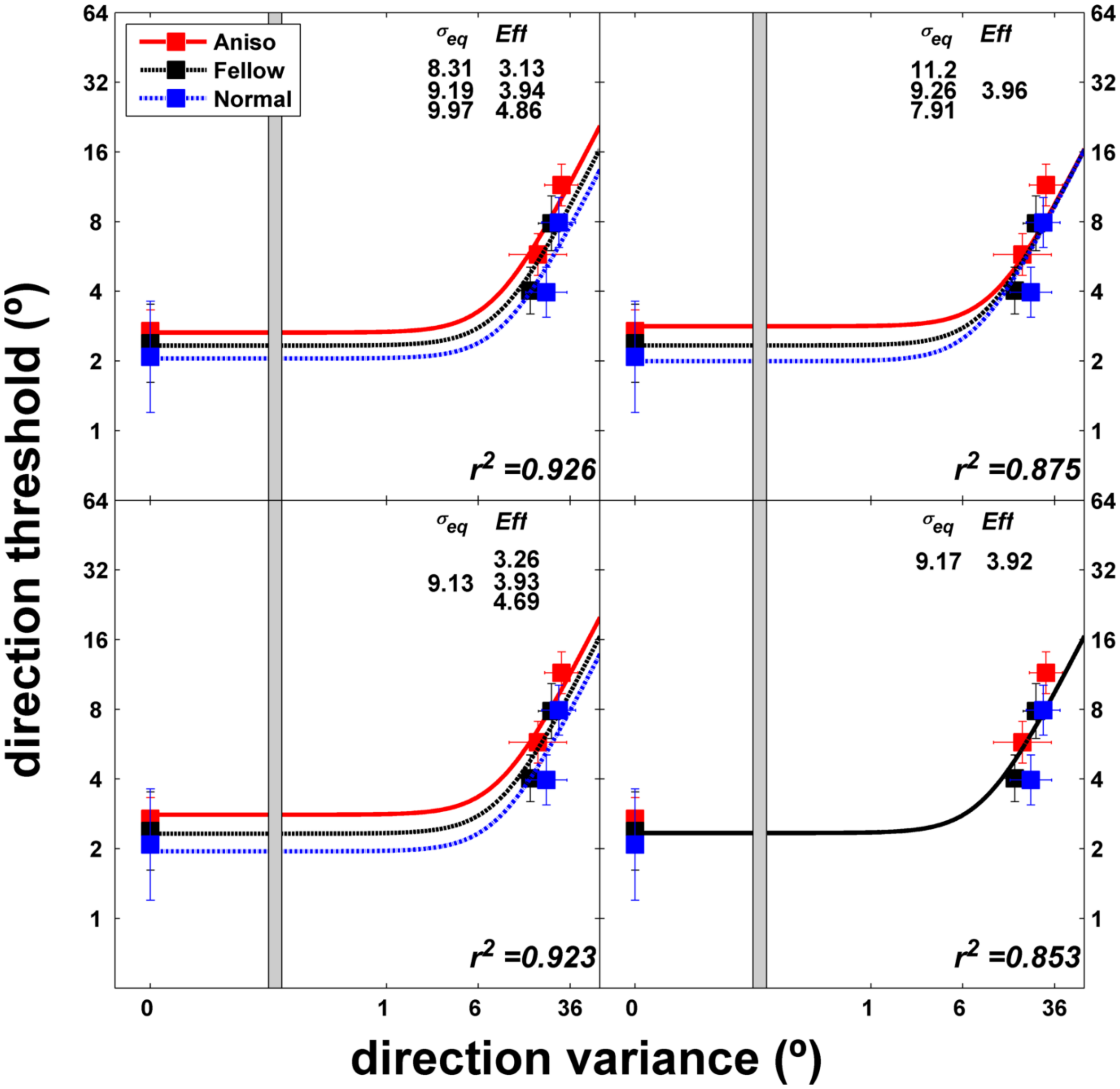

Figure 6.8: Nested models for the mean direction discrimination threshold data for the normal and anisometropic amblyopic participants.

The models relate the direction offset thresholds and variance to different values of internal noise and sampling efficiency. The model with both parameters constrained across normal, fellow and amblyopic eyes (bottom right section) was statistically the best model to represent the threshold data. The best fitting parameters (σ_{eq} and Eff) and the goodness of fit (r^2) of each model is also provided.

Similarly, figure 6.9 shows the mean orientation offset and orientation noise data fitted to the equivalent noise paradigm for full models and reduced models with different numbers of free parameters. The goodness of fit (r^2) for all reduced models ($r^2 > 0.94$) were similar to the full-model ($r^2 = 0.96$); one σ_{eq} and three *Eff*

[$F(2,3) = 0.32$, $p > 0.1$], three σ_{eq} and one *Eff* [$F(2,3) = 0.36$, $p > 0.1$], and one σ_{eq} and one *Eff* [$F(4,3) = 0.90$, $p > 0.1$]. The model with both σ_{eq} and *Eff* constrained across both groups of participants was hence chosen as statistically the best model to represent the threshold data.

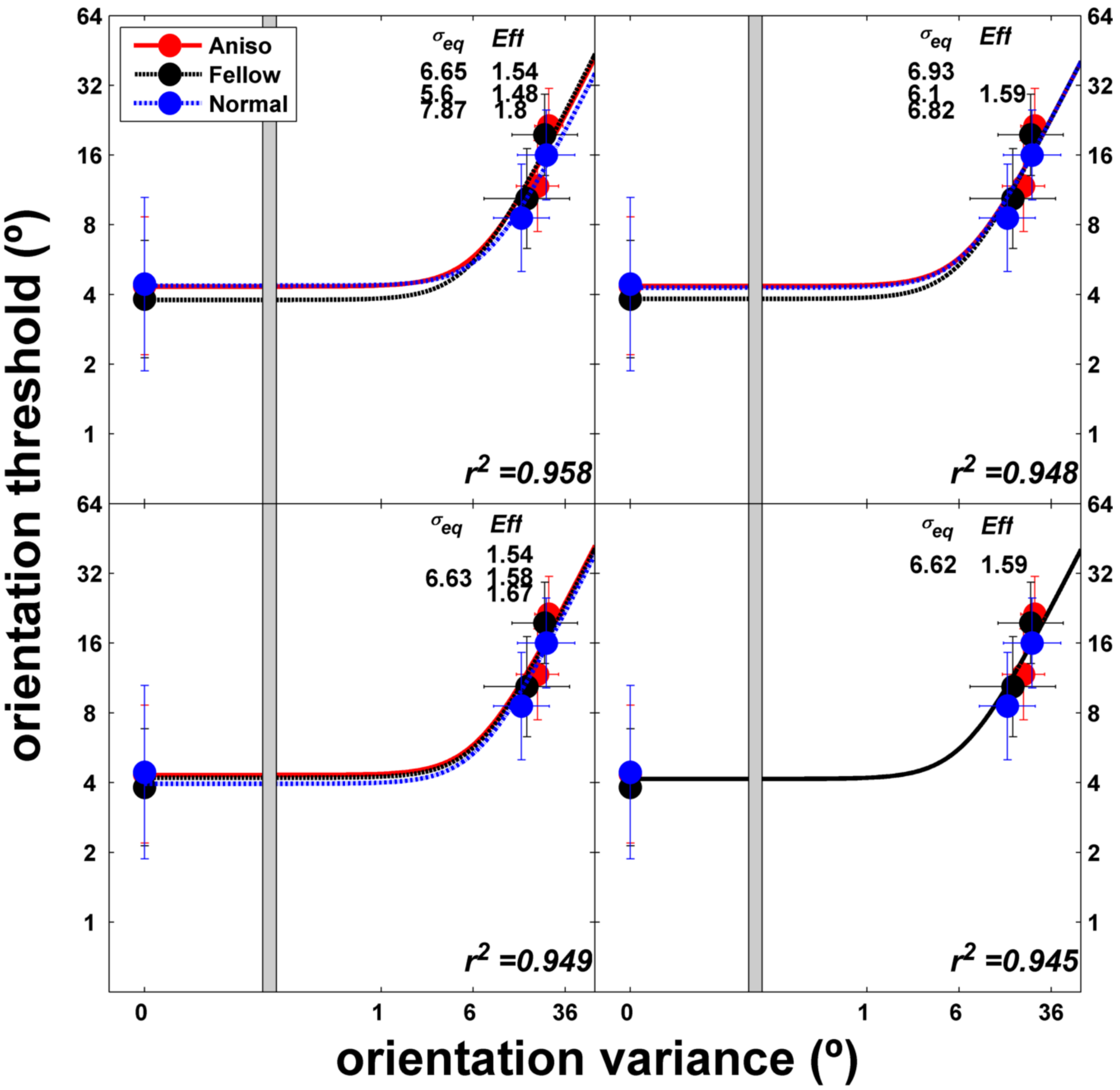

Figure 6.9: Nested models for the mean orientation discrimination threshold data for the normal and anisometropic amblyopic participants.

The models relate the direction offset thresholds and variance to different values of internal noise and sampling efficiency. The model with both parameters constrained across the normal and amblyopic participants (bottom right section) was statistically the best model to represent the threshold data. The best fitting parameters (σ_{eq} and Eff) and the goodness of fit (r^2) of each model is also provided.

6.3 Experiment 2: Fine direction and orientation discrimination in strabismic amblyopia

In the second experiment, direction and orientation discrimination thresholds were evaluated in strabismic amblyopes. Initially, two strabismic amblyopes (JR and SS. Table 6.2) were evaluated for both motion and orientation with the stimulus set (RDK and Glass pattern) described in the first experiment. However, both participants could not complete the evaluation for the Glass pattern. One of the two strabismic amblyopes (JR) could not detect the structure of the Glass pattern with both eyes even in the no noise condition while the other (SS) could detect the structure with the fellow eye but not with the amblyopic eye. Other studies have also reported an inability of strabismic amblyopes to detect the structure of translational Glass patterns (Anderson and Swettenham, 2006; Kiorpes, 2006; Rislove *et al.*, 2010). The detection of a Glass pattern is based on extracting local orientation information from dipoles followed by integration of the local information to provide a global percept. The mismatch of a dot element from one dipole pair with another dipole pair results in an increase in noise reducing the percept of the Glass pattern structure. The noise due to the mismatching of the dipole element to a non-corresponding dipole is called correspondence noise (Dakin, 1997). Therefore an increase in the number of dipoles could potentially increase the correspondence noise. In normal participants, change in the number of dipoles has a minimal effect on the perception of a translational Glass pattern (Dakin, 1997; Wilson and Wilkinson, 1998). Although the effect of correspondence noise is not well known in amblyopia, reduction in orientation discrimination ability has been reported with an overall increase in noise (Mansouri and Hess, 2006; Husk and Hess, 2013). A study evaluating the effect of stimulus parameters on mean orientation discrimination of Gabor patches in amblyopia did report that it is the number of elements, not the density or stimuli diameter which determines the performance in such a task (Mansouri *et al.*, 2004). Similarly, Rislove *et al.,* (2010) also reported an inability of some strabismic amblyopes to reliably detect the translational Glass pattern containing a relatively large number of elements (1024 dots) within 5.7˚ diameter display. Therefore, we modified the stimulus parameters for the strabismic amblyopes in this experiment to facilitate the detection of the dipole Glass pattern.

Our previous experiment (Chapter 3) showed that normal observers have a better sensitivity to Glass patterns containing more than two elements defining the orientation axis. In a tripole Glass pattern, an extra dot is added parallel to the oriented axis of each dipole to provide more apparent orientation information by strengthening the correspondence in the orientation axis. We sought to investigate if reinforcing the orientation cues by adding an extra element for each Glass pattern component in our stimuli would facilitate the detection of a Glass pattern for strabismic amblyopes who previously could not detect the dipole Glass pattern. In principle, adding more dots at the same orientation makes the dot sequence look more similar to a line segment which has been used successfully by other studies for the evaluation of form perception in amblyopia. Therefore, employing a tripole Glass pattern would allow the comparison of the current results to that of previous studies using line segment stimuli.

6.3.1 Methods:

6.3.1.1 Stimuli modification

To facilitate the Glass pattern task for the unable strabismic amblyopes, we varied display parameters in the Glass pattern. When the numbers of elements were reduced from 500 to 240 dots, one strabismic amblyope (SS) could reliably detect the structure of the Glass pattern. The number of elements was hence reduced to 240 elements with other parameters remaining constant. The variance threshold was measured at only a single multiple (3x) of the direction/orientation discrimination threshold of the no noise condition. The *high noise* condition was reduced from 2x and 4x (in Experiment 1) to only 3x as theoretically the variance thresholds from 2x, 3x and 4x represent a continuum of the same *TvN* curve and as such should not affect the final analysis in terms of model fits. Additionally, this also reduced the length of the experiment.

The tripole Glass patterns were created by adding an extra dot element to the dipole Glass pattern on the same orientation axis at the same dipole separation (0.266˚) (Figure 6.10). The individual orientations of the tripole elements were generated from the Gaussian distribution with prescribed means and standard deviations. Other physical parameters and data collection methods were the same as described for the dipole Glass pattern.

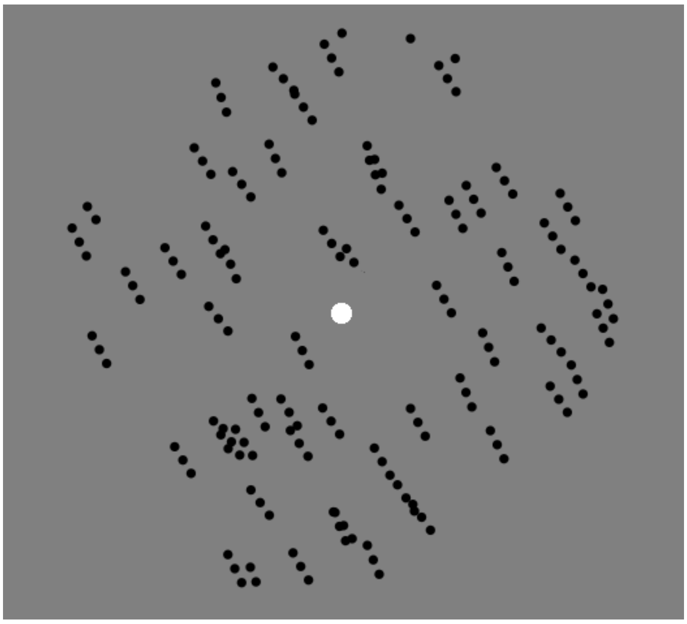

Figure 6.10: Schematic representation of the tripole Glass pattern

The tripole Glass pattern oriented left from the vertical with no added noise.

6.3.1.2 Participants

A total of nine strabismic amblyopes (mean age = 32.55 ±13.82 years) and six visually normal participants (mean age = 27 ±7.10 years) were recruited. All participants performed the task monocularly. As the previous normal controls from experiment 1 did not show a significant difference between the thresholds for dominant eye and non-dominant eye for both RDK and Glass pattern, the normal participants completed the experiment monocularly with a randomly selected eye. The participant details are provided in Table 6.2.

ID	**Age (yr.)**	**Visual Acuity**		**Refraction**		**Binocularity**	**Cover Test**	**Stereo (sec of arc)**	**Treatment history**
Amblyopes		**RE**	**LE**	**RE**	**LE**				
SS	20	-0.01	0.4	+4.50/-0.50*172	+5.75/-1.00*22	Absent	Esotropia	No	Patching
NJ	21	-0.2	0.2	+1.00	+3.00	Absent	Esotropia	No	Patching
CO	20	0	0.34	+4.00/-1.50*175	+4.50/-1.50*90	Intermittent	Int. Esotropia	200	Patching
HQ	34	0	0.5	-1.50/-2.00*5	-1.50/-2.00*5	Absent	Exotropia	No	Patching
JW	57	-0.1	0.14	+0.75/-0.25*25	+3.00/-0.50*25	Absent	Esotropia	No	Patching
KH	22	0.2	0	+8.50/-3.50*25	+9.00/-3.00*170	Absent	Esotropia	No	None
MR	**48**	**0.16**	**-0.1**	**+3.00/-2.50*90**	**+1.50**	**Absent**	**Esotropia**	**No**	**Patching**
SM	**28**	**-0.1**	**0.5**	**+0.50**	**+3.50/-1.50*90**	**Absent**	**Exotropia**	**No**	**Patching**
JR	**43**	**0**	**0.48**	**-2.50**	**-2.50**	**Absent**	**Esotropia**	**No**	**Patching**
Normal									
SS	19	-0.06	-0.04	0.00	0.00	Present	Orthophoria	20	
MS	20	-0.1	-0.1	-5.25	-3.00/-1.00*10	Present	Exophoria	20	
MG	38	-0.02	-0.04	0.00	0.00	Present	Orthophoria	20	
AM	28	0	-0.02	-0.75/-0.50*15	-0.75/-0.50*155	Present	Exophoria	30	
EM	26	0	-0.04	-4.50/-0.50*180	-4.50/-0.75*160	Present	Orthophoria	20	
RB	31	-0.02	-0.04	-0.75	-0.75	Present	Exophoria	20	

Table 6.2: The clinical details of strabismic amblyopes and normal participants.

The highlighted participants represent the strabismic amblyopes who could not complete the Glass pattern experiment.

6.3.2 Results

The orientation discrimination thresholds (Glass pattern) were higher than the direction discrimination thresholds (RDK) for all normal controls at both low and high noise (variance) levels (Figure 6.11).

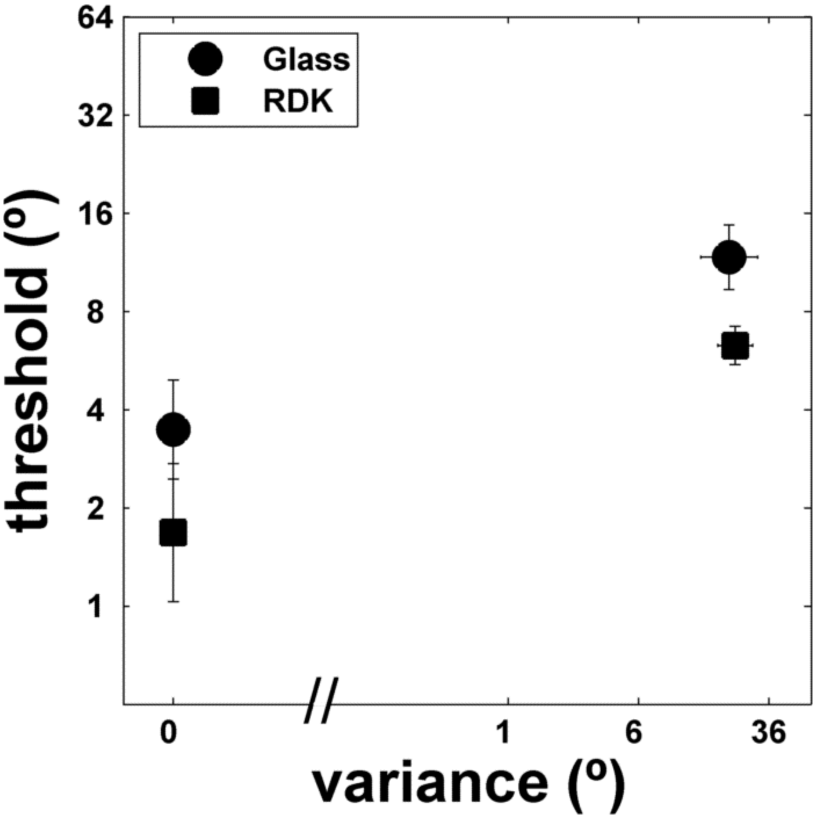

	No Noise	*High Noise*
Glass	**3.65˚ (1.19˚)**	**21.93˚ (7.78˚) at 12.00˚ (3.10˚)**
RDK	**1.83˚ (0.76˚)**	**22.98˚ (5.56˚) at 6.33˚ (0.82˚)**

Figure 6.11: The mean orientation discrimination (Glass) and direction discrimination thresholds (RDK) for normal participants.

The error bar represents ± 1standard deviation. The attached table shows the mean direction/variance thresholds for no noise and high noise condition. The values in parenthesis represent the standard deviation.

The mean direction offset/ direction variance thresholds were higher for the fellow and amblyopic eye compared to the normal at both low noise and high noise levels (Figure 6.12).

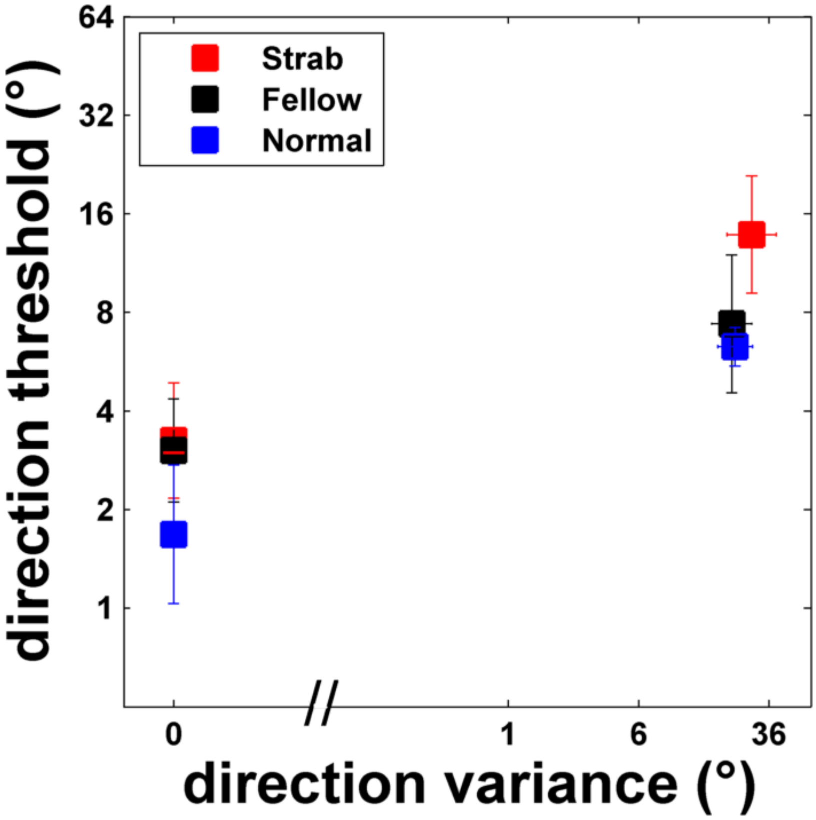

	No Noise	*High Noise (x at y)*
Strab	**3.12˚ (1.40˚)**	**29.98˚ (8.51˚) at 13.82˚ (6.21˚)**
Fellow	**3.03˚ (1.04˚)**	**21.43˚ (6.05˚) at 7.38˚ (4.29˚)**

Figure 6.12: The mean direction offset/ direction variance threshold for strabismic amblyopes and normal controls.

The thresholds are presented for strabismic amblyopic eye (red squares), fellow eye (black squares) and normal eye (blue squares). The error bar represents ± 1standard deviation. The attached table shows the mean direction/variance thresholds for no noise and high noise conditions. The values in parenthesis represent the standard deviation.

Among the nine strabismic amblyopes, only six could detect the structure of the translational Glass pattern. The orientation discrimination thresholds were consistently higher for the amblyopic eye compared to the fellow eye and normal eye (Figure 6.13).

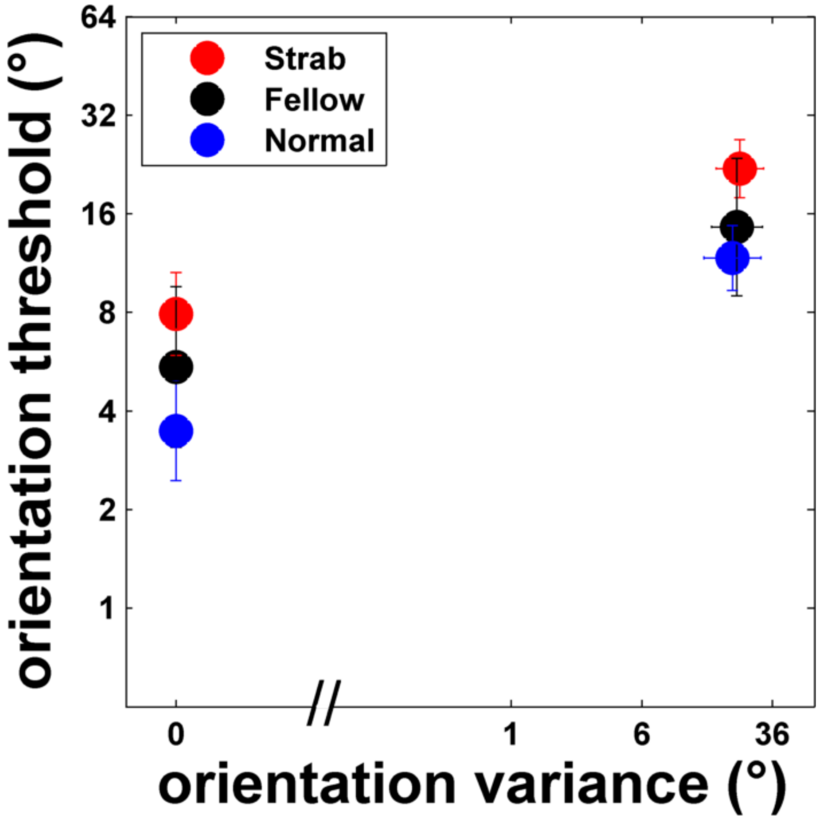

	No Noise	High Noise
Strab	**7.91˚ (2.61˚)**	**22.87˚ (7.57˚) at 21.94˚ (4.59˚)**
Fellow	**5.44˚ (3.78˚)**	**21.98˚ (8.66˚) at 14.57˚ (7.37˚)**

Figure 6.13: The mean orientation offset/ orientation variance threshold for strabismic amblyopes and normal controls.

The thresholds are presented for strabismic amblyopic eye (red circles), fellow eye (black circles) and normal eye (blue circles). The error bar represents ± 1standard deviation. The attached table shows the mean direction/variance thresholds for no noise and high noise conditions. The values in parenthesis represent the standard deviation.

The thresholds for the normal controls and strabismic amblyopes were analysed with a MANOVA. The log values of direction/orientation offset and noise (variance) were treated as dependent variables while *eye* (three levels; normal, fellow and amblyopic) and *stimulus type* (two levels; RDK and Glass) were considered as the between subject factors. The Box's test of equality of covariance matrices showed that covariance of the dependent variable was similar across the groups (M = 13.94, $F = 0.87$, $p > 0.05$). Levene's test of equality of variance showed that the variance of the dependent variable was similar across the groups for both noise [$F(5,78) = 1.35$, $p > 0.05$] and direction/orientation offsets [$F(5,78) = 1.17$, $p > 0.05$]. The between subject tests revealed a significant effect of *eye* on direction/orientation offset [$F(2, 83) = 6.38$, $p < 0.01$] but not on noise [$F(2,83) = 0.004$, $p > 0.05$]. The effect of *stimulus type* was also significant on direction/orientation offsets [$F(1,83) = 17.19$, $p < 0.05$] but not on noise [$F(1,83) = 0.003$, $p > 0.05$]. The interaction of *eye* and *stimulus type* was not significant on both direction/orientation offsets [$F(2,83) = 0.01$, $p > 0.05$] and noise [$F(2,83) = 0.002$, $p > 0.05$].

Pairwise comparison of *eye* after Bonferroni correction showed a significant difference for direction/orientation offset between the normal and amblyopic eyes ($p < 0.01$) but not between the normal and fellow eyes ($p > 0.05$). There was no significant difference in the noise between different eyes ($p > 0.05$). The pairwise analysis of *stimulus type* showed a significantly higher orientation offset thresholds for Glass compared to the direction offset thresholds for RDK ($p < 0.01$) with no significant difference on noise ($p > 0.05$).

6.3.2.1 Equivalent noise fit analysis with nested modelling in strabismic amblyopia

The individual threshold data from amblyopic and normal eyes were then used to fit the linear equivalent noise model. Further, the nested modelling method was used to investigate the differences in performance among the normal and strabismic participants. Figure 6.14 shows the full model and nested models for direction discrimination. The goodness of fit (r^2) for the reduced model with σ_{eq} constrained across the eyes with three independent *Eff* ($r^2 = 0.733$) was most comparable to the full-model ($r^2 = 0.747$) while the other two reduced models resulted in a lower goodness of fit ($r^2 < 0.71$). This was confirmed statistically with the goodness of fit for the reduced model with one σ_{eq} and three independent *Eff* being statistically similar to the full model [$F(2,42) = 1.16$, $p > 0.1$]. The other reduced model with three σ_{eq} and one *Eff* [$F(2,42) = 3.24$, $p < 0.05$] and the simplest model with only two parameters both resulted in a statistically poorer fit [$F(4,42) = 4.32$, $p < 0.01$]. The model with one σ_{eq} and three independent *Eff* was then treated as the full model and again compared to the simplest model (one σ_{eq} and one independent *Eff).* The result showed that the simplest model resulted in poorer fit compared to the selected model (one σ_{eq} and three independent *Eff)* [$F(2,44) = 7.83$, $p < 0.01$]. The result hence showed that the model with one σ_{eq} and three *Eff* best described the threshold data.

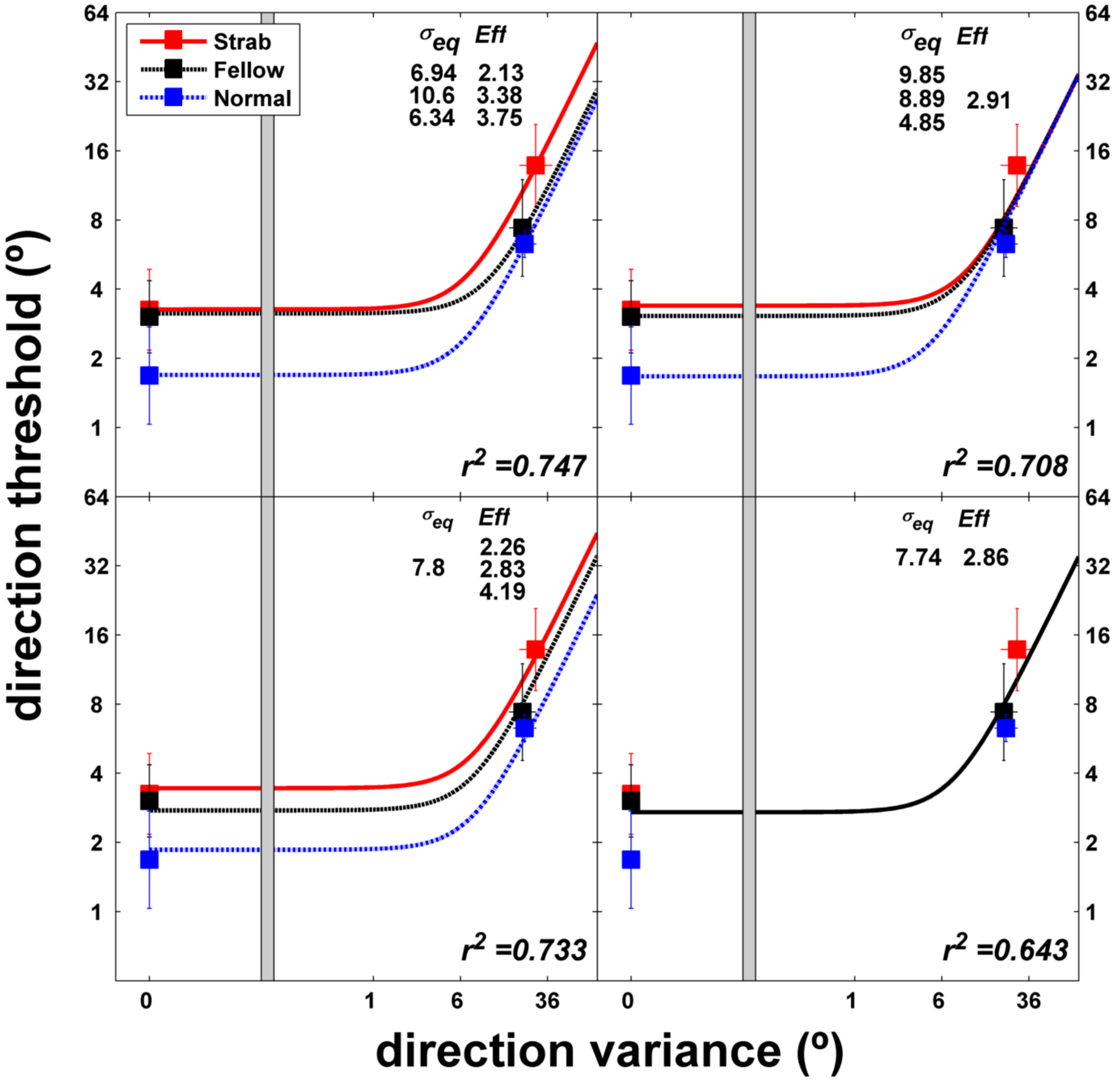

Figure 6.14: Nested models for the individual direction discrimination threshold data for the normal and strabismic eyes.

The models relate the direction offset thresholds and variance to different values of internal noise and sampling efficiency. The model with σ_{eq} *parameter constrained across the amblyopic, fellow and normal eyes (bottom left section) was statistically the best model to represent the threshold data. The best fitting parameters (*σ_{eq} *and Eff) and the goodness of fit (*r^2*) of each model is also provided.*

Similarly for the orientation discrimination, the reduced model with σ_{eq} constrained across the different eyes (r^2 = 0.683) was most identical to the full model (r^2 = 0.687). The model with both parameters constrained resulted in a relatively poorer fit (r^2 = 0.525). The statistical test on goodness of fits showed that two reduced models were similar to the full model; one σ_{eq} and three *Eff* [$F(2,30) = 0.19$, $p > 0.1$], three σ_{eq} and one *Eff* [$F(2,30) = 1.53$, $p > 0.1$] but the simplest model with both σ_{eq} and *Eff* constrained resulted in a statistically poorer fit [$F(4,30) = 3.88$, $p <$

0.01]. Among the reduced models, the model with the better goodness of fit (higher r^2) was chosen as the best fitting model, *i.e.,* the model with one σ_{eq} and three *Eff*. The model with one σ_{eq} and three *Eff* was treated as the full model and further compared against the simplest model (one σ_{eq} and one *Eff*). The results showed that the simplest model resulted in poorer fit compared to the selected best model (one σ_{eq} and three *Eff*) [$F(2,32) = 8.08$, $p < 0.01$]

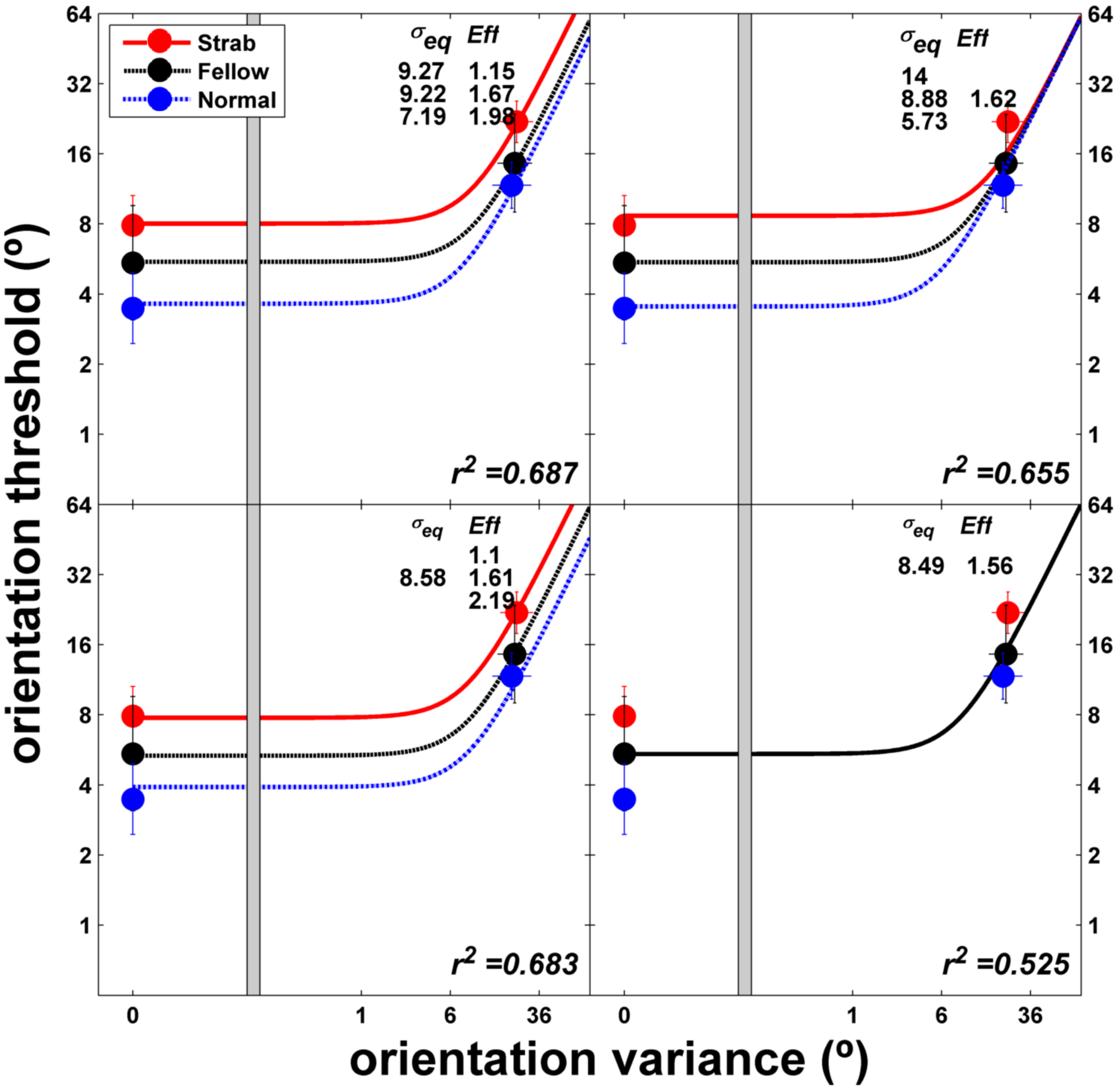

Figure 6.15: Nested models for the individual orientation discrimination threshold data for the normal and strabismic eyes.

The models relate the direction offset thresholds and variance to different values of internal noise and sampling efficiency. The model with σ_{eq} *parameter constrained across the amblyopic, fellow and normal eyes (bottom left section) was statistically the best model to represent the threshold data. The best fitting parameters (*σ_{eq} *and Eff) and the goodness of fit (*r^2*) of each model is also provided.*

6.3.2.2 The perception of tripole Glass pattern in strabismic amblyopia

Two strabismic amblyopes (JR and MR) who could not detect the structure of the Glass pattern also participated in the experiment with the tripole Glass pattern. Both participants could easily complete the experiment on the tripole Glass patterns. The thresholds for both strabismic eyes and fellow eyes were similar to normal (*n* = 2) thresholds at both no noise and high noise conditions (Figure 6.16).

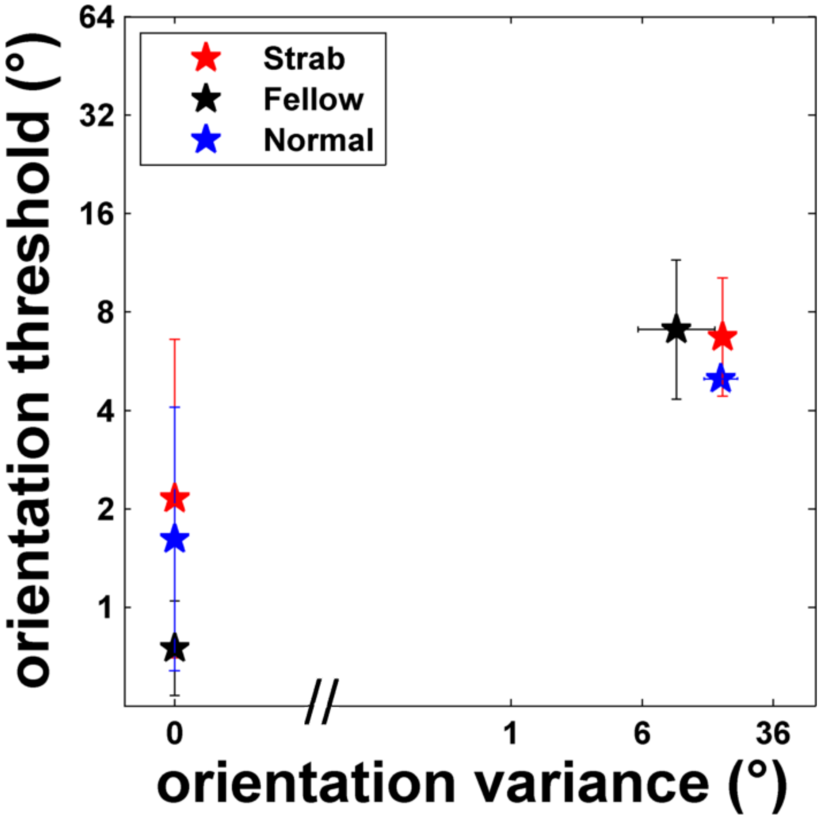

Eyes/Noise	No Noise	High Noise (*x at y*)
Strab	2.15˚ (2.67˚)	17.89˚ (0.31˚) at 7.00˚ (2.83˚)
Fellow	0.75˚ (0.25˚)	10.17˚ (5.11˚) at 7.50˚ (3.53˚)
Normal	1.62˚ (1.61˚)	17.67˚ (3.99˚) at 5.00˚(0.00˚)

Figure 6.16: The mean orientation offset/orientation variance threshold for two strabismic amblyopic and normal participants for the tripole Glass pattern.

The thresholds are presented for strabismic amblyopic eye (red stars), fellow eye (black stars), and normal eye (blue stars). The error bar represents ± 1standard deviation. The attached table shows the mean direction/variance thresholds for no noise and high noise conditions. The values in parenthesis represent the standard deviation.

6.3.2.3 Comparison of motion and form performance in strabismic amblyopia

The model with a single internal noise and independent sampling efficiencies best described the difference in thresholds between strabismic amblyopes and normal participants for both motion and form processing. To directly compare the results from the motion and form domains in individual amblyopes, the threshold data from each amblyopic observer was fit with that of the normal eyes to the model with constrained internal noise. Since the internal noise is constrained across the eyes (amblyopic, fellow, and normal), any difference in performance is only reflected by changes in the efficiency parameter. The values of the internal noise and sampling efficiency for each individual observer are provided in Table 6.3.

Observer	**Eyes**	**RDK**		**Glass**	
		σ_{eq}	***Eff***	σ_{eq}	***Eff***
CO	Amblyopic	7.04	3.77	7.16	0.99
	Fellow		5.24		1.95
	Normal		3.96		1.97
SS	Amblyopic	6.93	2.96	8.17	1.61
	Fellow		2.32		2.69
	Normal		3.93		2.13
NJ	Amblyopic	6.00	1.62	6.90	0.99
	Fellow		2.20		1.95
	Normal		3.63		1.93
HQ	Amblyopic	6.72	2.05	9.26	1.00
	Fellow		1.91		1.70
	Normal		3.87		2.29
JW	Amblyopic	6.36	2.71	7.47	0.95
	Fellow		1.92		0.99
	Normal		3.75		2.02
KH	Amblyopic	6.86	1.98	7.46	0.82
	Fellow		2.35		0.68
	Normal		3.91		2.02
SM	Amblyopic	7.89	1.45		
	Fellow		5.49		
	Normal		4.22		
MR	Amblyopic	7.27	1.84		
	Fellow		3.30		
	Normal		4.03		
JR	Amblyopic	6.12	1.49		
	Fellow		1.36		
	Normal		3.67		

Table 6.3: The internal noise (σ_{eq}) and sampling efficiency (*Eff*) parameters for the reduced model with internal noise constant across the amblyopic eye, fellow eye and normal eye.

The individual differences in the sampling efficiency parameter were further analysed by calculating the log efficiency ratio of amblyopic/fellow eye to normal eye, a value of zero shows that the amblyopic participants have the same efficiency in global processing as the normal controls while a value less than zero shows that the efficiency is poorer in amblyopes. The motion and form ratio of the efficiency parameter for each individual amplyope, amblyopic and fellow eyes, compared to normal is given in figure 6.17. For the motion domain (Figure 6.17, A) all amblyopic participants showed poorer efficiency in the amblyopic eye and five out of seven amblyopes also had poorer efficiency for the fellow eye. For the form domain (Figure 6.17, B), all six amblyopes showed poorer efficiency in the amblyopic eye while three participants had abnormal efficiency in the fellow eye. For the participants (SM, MR, JR) who could not complete the Glass pattern experiment, the difference in efficiency was larger compared to those who could complete the Glass pattern experiment in the motion domain.

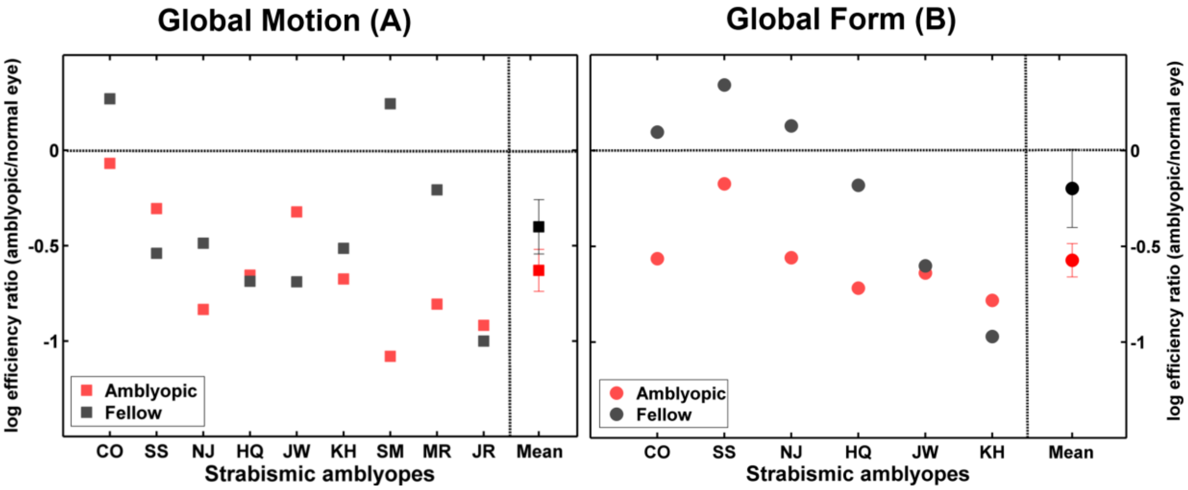

Figure 6.17: The sampling efficiency of the amblyopic and fellow eye compared to normal controls for each strabismic amblyope and the mean data.

The data points represent log values of the ratio of sampling efficiency parameter (amblyopic/normal participant) for global motion domain (A) and global form domain (B). The data points along the negative values represent how deficient the amblyopic participants are with respect to the normal controls.

6.4 Experiment 3: Implied motion perception in strabismic amblyopia

Previous studies that have evaluated sensitivity in amblyopia to tasks that depended on inputs from both the motion and form domains have reported normal thresholds for some tasks such as biological motion perception (Hamm *et al.*, 2014) while abnormal thresholds for other tasks such as structure from motion (Hayward *et al.*, 2011; Husk *et al.*, 2012). As some strabismic amblyopes were unable to complete the Glass pattern task even with the modified stimuli (Experiment 2), we further evaluated strabismic performance on the dynamic Glass pattern. A dynamic Glass pattern is composed of multiple static Glass patterns presented over sequential frames. The pattern stimulates a distinct cortical processing mechanism, which requires information from both the motion and form processing streams (Nankoo *et al.*, 2012; Day and Palomares, 2014; Nankoo *et al.*, 2015) (for details Chapter 4). Such presentation improves the discrimination thresholds in normals, as seen in our previous study (Chapter 4) and reported by other studies (Nankoo *et al.*, 2012; Day and Palomares, 2014; Nankoo *et al.*, 2015).

6.4.1 Methods

6.4.1.1 Stimuli and procedure

All stimuli parameters for dynamic Glass pattern were the same as described for the static Glass pattern except that nine independent frames of static Glass pattern, instead of a single frame in the static Glass pattern, were displayed over the 0.5s. The quick method with two data points (*no noise* and *high noise*) was used for data collection. All procedures were as described for the Glass pattern stimuli for the strabismic amblyopes.

6.4.1.2 Participants

A total of seven strabismic amblyopes (except SM and JW) and six normal controls that participated in experiment 2 were recruited. These seven strabismic amblyopes included two amblyopes (JR and MR) who were unable to detect the static Glass pattern structure even after stimuli modification.

6.4.2 Results

The mean implied motion thresholds in dynamic Glass patterns for the amblyopic eye were higher than that for the fellow eye at the high noise condition but similar at the no noise condition. When the mean thresholds for the dynamic Glass patterns of the amblyopic group were compared with the thresholds from the six normal participants, the mean thresholds were higher for both fellow and amblyopic eyes at both noise levels (Figure 6.18).

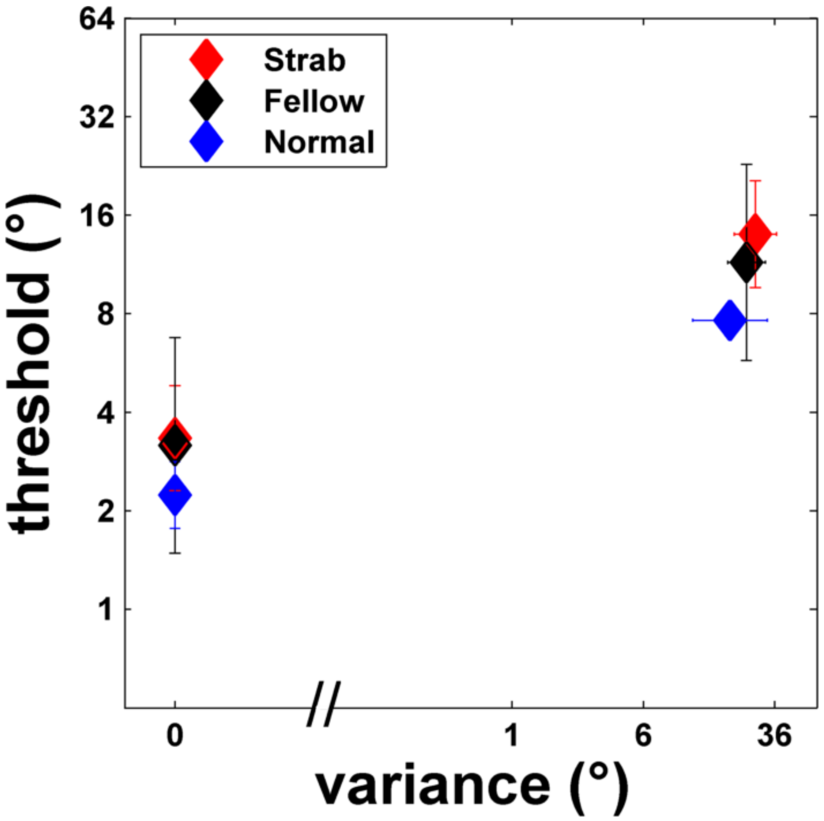

	No Noise	High Noise (*x at y*)
Strab	**3.33˚ (1.17˚)**	**27.47˚ (8.32˚) at 13.98˚ (5.67˚)**
Fellow	**3.17˚ (3.34˚)**	**24.35˚ (6.91˚) at 11.47˚ (7.80˚)**
Normal	**2.23˚ (0.50˚)**	**19.42˚ (9.42˚) at 7.63˚ (0.81˚)**

Figure 6.18: The mean implied motion offset/ implied motion variance threshold for strabismic amblyopes and normal controls.

The thresholds are presented for amblyopic eye (red diamond), fellow eye (black diamond) and normal eye (blue diamond). The error bar represents ± 1standard deviation. The attached table shows the mean direction/variance thresholds for no noise and high noise. The values in parenthesis represent the standard deviation.

The log thresholds were then analysed with a MANOVA. The implied motion offset/variance thresholds were treated as the dependent variable while the *eye* (three levels; amblyopic, fellow and normal) was treated as the between subject variable. The Box's test of equality of covariance matrices showed that covariance of the dependent variable was significantly different between the groups (M = 18.25, F = 2.80, $p < 0.05$). The Pillai's trace statistics (V) however is relatively robust to the violation of this assumption in the case of an equal number of data points across the groups (Tabachnick and Fidell, 2001). Levene's test of equality of variance showed that the variance of the dependent variable was similar across the groups for both the noise [$F(2,37) = 1.67$, $p > 0.05$] and implied motion offsets [$F(2,37) = 0.68$, $p > 0.05$]. The between subject tests then revealed no significant effect of *eye* on both implied motion offset [$F(2, 39) = 1.25$, $p > 0.1$] and noise [$F(2,39) = 0.006$, $p > 0.1$].

6.4.2.1 Equivalent noise fit analysis for implied motion thresholds with nested modelling in strabismic amblyopia

The implied motion/variance thresholds were used to fit the linear equivalent noise model, and the differences between the eyes were evaluated with the nested modelling methods (Figure 6.19). The goodness of fit for all reduced models ($r^2 >$ 0.69) were similar to the full model ($r^2 = 0.72$); one σ_{eq} and three independent *Eff* [$F(2,34) = 0$, $p > 0.1$], three σ_{eq} and one *Eff* [$F(2,34) = 0.79$, $p > 0.1$], and one σ_{eq} and one *Eff* [$F(4,34) = 0.97$, $p > 0.1$]. The model with least parameters *i.e.,* the model with one σ_{eq} and one *Eff* was hence chosen as statistically the best model to represent the threshold data.

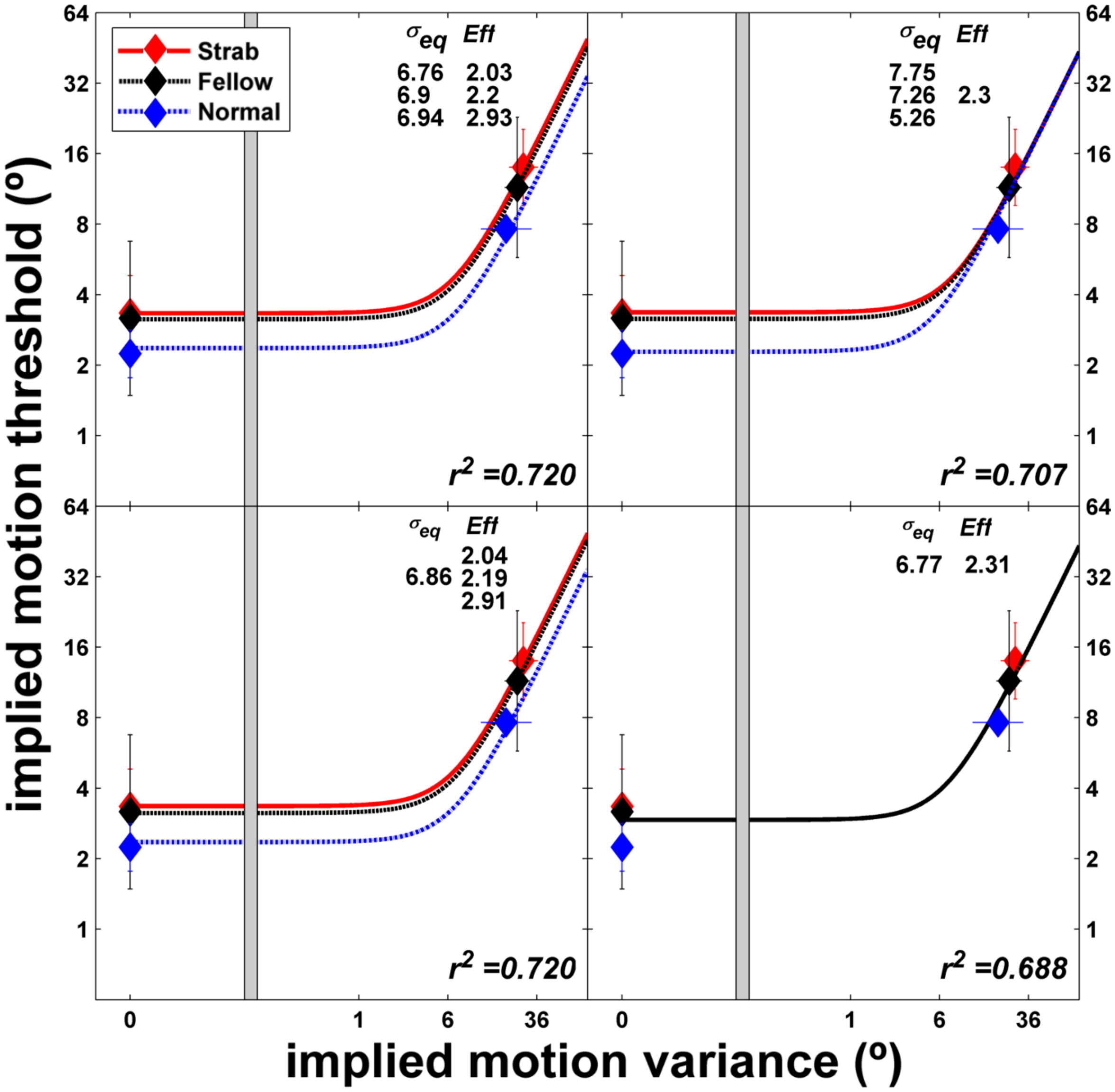

Figure 6.19: Nested models for the individual implied motion discrimination threshold data for dynamic Glass pattern in the normal and strabismic eyes.

The models relate the implied motion offset thresholds and variance to different values of internal noise and sampling efficiency. The model with both parameters constrained across the amblyopic, fellow and normal eyes (bottom right section) was statistically the best model to represent the threshold data. The best fitting parameters (σ_{eq} and Eff) and the goodness of fit (r^2) of each model is also provided.

The thresholds for Glass, dGlass and RDK were compared in normal controls and the amblyopic eye. The mean thresholds for dGlass were closer to the RDK in the amblyopic eye while the thresholds were higher than the RDK for the normal controls (Figure 6.20) as observed in the results from Chapter 4.

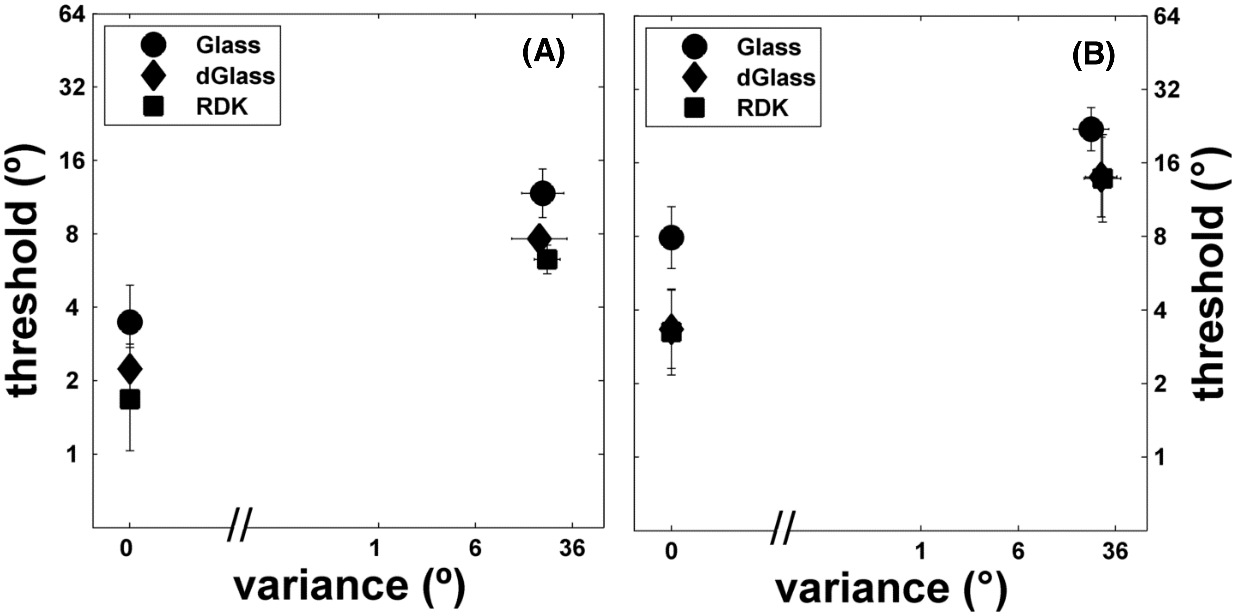

Figure 6.20: Comparison of mean orientation (Glass), mean implied motion (dGlass) and mean direction discrimination (RDK) thresholds for normal (A) and strabismic amblyopic (B) eye.

The error bar represents ±1standard deviation.

6.5 Discussion

This chapter explored global motion and orientation discrimination in amblyopic participants using the comparable stimulus set and quick experimental procedure devised previously in Chapter 5. The results showed that visual function attributed to both the dorsal and ventral stream are affected only in strabismic amblyopia. Contrary to some of the earlier reports (*e.g.,* Simmers *et al.,* 2005), our results indicate that the global form processing may be affected more than the global motion processing in strabismic amblyopia.

6.5.1 Global motion and global form discrimination in normal controls

The fine direction discrimination thresholds (*i.e.,* the direction offset threshold at no noise condition) for the normal controls in experiment 1 (2.4˚ (±1.42˚)) was higher than that in experiment 2 (1.83˚ (±0.76˚)) but the difference was not statistically significant (independent t-test, $t(9) = 0.93$, $p > 0.1$). Similarly, there was no statistically significant difference in the mean fine orientation discrimination thresholds between the normal controls in experiment 1 (5.97˚ (±4.57˚)) and experiment 2 (3.65˚ (±1.19˚)), independent t-test, $t(21) = 1.07$, $p > 0.1$. The mean discrimination thresholds were also similar to that observed in Chapter 3, in which the mean fine direction discrimination and orientation thresholds were 1.55˚ (±1.50˚) and 4.30˚ (±2.31˚) respectively. The orientation discrimination thresholds in both groups of controls were higher than the direction discrimination thresholds as observed in our previous study (Chapter 3).

In the second group of normal controls, we also evaluated the implied motion thresholds using dynamic Glass pattern; the mean threshold for the no noise condition was 2.28˚ (±0.50˚) which was lower than the thresholds we found in chapter 4, 3.55˚ (±2.67˚). Again there was no statistically significant difference between the thresholds among the normal observers from two experiments, independent t-test, t (26) = 1.39, $p > 0.1$. The overall pattern of results when comparing the thresholds for the three stimuli (RDK, Glass pattern, and dynamic Glass pattern) at both no noise and high noise conditions also followed the trend observed in our previous study (Chapter 4); the highest thresholds for the Glass pattern followed by the dynamic Glass pattern and the lowest thresholds for the RDK (Figure 4.21, A). The implications of these findings have been discussed in detail in Chapter 4. The similar findings in this experiment using a modified data collection method and stimulus parameters further confirm the pattern of results obtained in these experiments and validate the robust nature of the quick method used in the current study.

6.5.2 Global motion discrimination in amblyopia

The direction discrimination thresholds were normal in anisometropic amblyopia. We, however, found that the direction discrimination thresholds were elevated in the strabismic amblyopia.

Hess *et al.,* (2006) reported normal direction discrimination thresholds in both anisometropic and strabismic amblyopia using RDK stimuli composed of micro pattern elements with variable directional noise. We also find normal thresholds for the anisometropic amblyopes but not for the strabismic amblyopes. Hess *et al.,* (2006) initially normalised the direction discrimination threshold of a single Gabor micro pattern element between the amblyopic eye and fellow eye by manipulating the stimulus contrast. The local direction discrimination threshold for the amblyopic eye was initially evaluated with a single micro pattern at 50% contrast. For the fellow eye, the stimuli contrast was reduced till the direction discrimination thresholds were equivalent to that of the amblyopic eye (average value of 25% contrast). Global motion discrimination thresholds using multiple micro patterns were then evaluated at the lower stimuli contrast (on average 25%) for the fellow eye and the normal eye while higher stimuli contrast (50%) was used for the amblyopic eye. The local normalised contrast was used in order to filter the local level influences (*i.e.,* equate visibility) from the global thresholds. Using a similar method, Mansouri and Hess (2006) also reported normal thresholds in amblyopia when the directions of motion of individual Gabor micro patterns were derived from the standard Gaussian distribution. However, they reported increased thresholds when another random noise (Gabor micro patterns with random direction) was added to the stimuli. In the current study RDKs with high contrast dot elements (95%) was used to investigate both amblyopic and fellow eye performance independently while the local and global limitations were investigated in terms of internal noise and sampling efficiency respectively. As far as we know no study has evaluated fine motion discrimination in amblyopia using RDKs with broadband dot elements as in the present study. The differences in the experimental stimulus and methods used in these studies might have contributed to the variation in observed results.

Another measure of global motion discrimination capabilities, the motion coherence threshold, has been reported to be abnormal in both anisometropic and strabismic amblyopia (Simmers *et al.*, 2003b; Simmers *et al.*, 2006b; Aaen-Stockdale *et al.*, 2007; Aaen-Stockdale and Hess, 2008). The difference between the motion coherence task and the equivalent noise task used by Hess *et al.,* (2006) and the present study is that in the motion coherence task the noise elements follow a random motion path while the noise in the equivalent noise task is derived from increasing the standard deviation of the distribution from which the directions of motion of all elements are derived. Based on this difference the motion coherence task is defined as mainly a segregation task, *i.e.*, segregating the random noise elements from signals followed by the integration of the signal elements to provide the estimate of the direction (Hess *et al.*, 2006; Mansouri and Hess, 2006). On the other hand, the direction discrimination in the equivalent noise task is reported to be based only on the integration of the local direction of individual elements (Hess *et al.*, 2006; Mansouri and Hess, 2006). The integration of the individual direction of motion might be the best strategy when the external noise is low, however at high noise levels, we speculate that the observer might also rely on segregating the noise elements from the extreme ends of the distribution. Humans are very sensitive in the motion coherence task, only requiring around 5-8% of signal dots for reliable direction discrimination (Blake *et al.*, 2003). So it is plausible that even in the equivalent noise task at high noise levels, the observer may adopt the segregation strategy used in the coherence threshold task. Mansouri and Hess (2006) attempted to reconcile the conflicting results from the equivalent noise task (mainly integration) and coherence threshold task (mainly segregation) using a combination of both tasks. They used RDK stimuli in which the directions of elements were derived from the standard Gaussian distribution (integration elements), then replaced a proportion of these elements with the noise elements generated from a random distribution (pedestal noise) similar to the coherence task (segregation elements). They reported that the thresholds in the amblyopic eye were elevated when the pedestal noise was high compared to normal, suggesting that the difference was only due to the inability of the amblyopic eye to segregate the pedestal noise.

In the current study, the thresholds at the no noise condition were also raised in strabismic amblyopes, suggesting that even pure integration is compromised. The motion coherence task though largely regarded as a segregation task also involves some level of integration. For example, the translational coherence threshold in amblyopia have been reported to be in the range of 25 - 30% at high contrast levels (Simmers *et al.*, 2006b), so in addition to segregating 70 to 75% of local random dot motion, amblyopes must also integrate the direction of motion of the remaining dots to perceive a coherent motion direction. The abnormal motion coherence threshold reported in amblyopia could be due to the combination of compromised integration and segregation mechanisms. Further processing of both motion coherence (defined as segregation) and motion integration occurs in the dorsal stream motion area MT (Newsome and Pare, 1988; Movshon *et al.*, 1995; Blake *et al.*, 2003), hence compromised MT in amblyopia (El-Shamayleh *et al.*, 2010) could potentially result in behavioural deficits in both functions.

The differences in the motion processing capacity observed between the anisometropic and strabismic amblyopia in the current study is similar to the results for other visual functions (Kiorpes and McKee, 1999). Larger deficits in strabismic amblyopes have been reported for optotype acuity (Levi *et al.*, 2011), vernier acuity (Levi and Klein, 1985), and contrast sensitivity (Levi *et al.*, 2011). The neural disarray (Hess and Field, 1994) and undersampling (Levi *et al.*, 1984; Wang *et al.*, 1998) theories have been proposed to account for a wide range of deficits observed in amblyopia. However, both theories have been developed with findings from the strabismic amblyopes and adapted for anisometropic amblyopes. The undersampling theory is based on the findings that vernier acuity in the fovea of strabismic amblyopes shows greater loss compared to the grating acuity, mimicking the normal peripheral retina (Levi *et al.*, 1984; Wang *et al.*, 1998). The theory suggests that the input from the central visual field is processed by the smaller number of neural sensors compared to the normal. But in anisometropia, both vernier and grating acuity are similarly affected; suggesting that the undersampling theory does not apply to the anisometropic amblyopes. The neural disarray theory is based on the mismatch of the visual stimulation due to the input of disparate images from two eyes (Hess and Field, 1994). Again the decorrelated images in strabismus may be more prone to the neural disarray compared to the input of sharp and blurred images in anisometropia. Abnormal hyperacuity in strabismic amblyopia can be explained by a combination of both the undersampling and positional uncertainty due to the neural disarray, but the hyperacuity deficits in anisometropic amblyopia are adequately accounted for by the contrast sensitivity loss at high spatial frequencies (Wilson, 1991). The results suggest that the mechanism of the deficits in the two amblyopic groups may be different, which may account for the larger deficit observed in strabismic amblyopes compared to the anisometropic amblyopes for the motion task in the current study.

Additionally, the severity of the visual deficit may rely on the onset of amblyopia. More severe deficits have been observed in strabismic amblyopia which tends to have an earlier onset during the critical period of visual development in childhood. The later onset of amblyopia in anisometropia during the critical period could result in better maturation of visual functions resulting in less risk of severe deficits compared to strabismics (Levi *et al.*, 2011; Birch, 2013). The normal direction discrimination thresholds in anisometropic but not in strabismic amblyopia observed in this study could be due to the differences in the pathophysiological aspects of each type of amblyopia. The differences in the extent of deficits in strabismic and anisometropic amblyopia have also been reported in various imaging studies. A progressive reduction of neural responses in extra striate cortical areas has been reported for cats with surgically induced strabismic amblyopia (Schröder *et al.*, 2002), but not for anisometropic monkeys (Kiorpes *et al.*, 1998). Motion coherence thresholds have also been found to be reduced in the fellow eyes of strabismic primates but not in anisometropic amblyopia (Kiorpes, 2006), suggesting larger deficits in strabismic than the anisometropic amblyopes for the motion task.

The degree of functional visual deficit observed in anisometropic and strabismic amblyopes has also been attributed to the state of binocular vision rather than the aetiological substrate in amblyopia. For example, Levi and colleagues (2011) showed the non-binocular anisometropic amblyopes exhibited more severe loss of visual functions (mainly acuity, contrast sensitivity, and stereopsis), similar to the levels found in strabismic amblyopia. Similarly, the visual acuity and vernier acuity of the non-binocular amblyopes were poorer than the binocular amblyopes even though the non-binocular amblyopes showed better contrast sensitivity than the binocular amblyopes (McKee *et al.*, 2003). Considering all our anisometropic amblyopes were binocular while the strabismic amblyopes were non-binocular (except CO, who had some residual binocular vision, stereoacuity: 200" of arc), the differences in the performance observed among the two groups could well be due to the lack of the binocularity. However, due to the small sample size and with only one strabismic amblyope having any level of binocularity, it is difficult to correlate the level of binocularity and performance in the motion task. A study with a larger group of anisometropic and strabismic amblyopes with varying degrees of binocular vision could help better understand the impact of binocularity on motion processing. Another reason for the differences in the performance of the two groups of amblyopes could be due to the differences in the severity of amblyopia and consequently low level visibility issues (mean IOD was 0.21 in anisometropic and 0.38 in strabismic). However, anisometropic amblyopes (*e.g.,* LS, IOD = 0.4) with an IOD in the range of strabismic amblyopes did show normal motion discrimination thresholds, suggesting that the IOD alone is not responsible for the pattern of the result.

The difference in performance observed between the two groups could also be due to the influence of treatment history. Most of the strabismic amblyopes (eight out of nine) had a history of treatment with conventional patching therapy but still exhibited motion discrimination deficits. Among the anisometropic amblyopes, five out of eight had undergone patching therapy, while the remainder (RK, HM, HMc) were diagnosed beyond the critical developmental years (> 12 years) and did not undergo the treatment. As all three untreated anisometropic amblyopes exhibited normal performance in the motion task, the history of treatment does not seem to have influenced the normal and abnormal findings observed in the anisometropic and strabismic amblyopes respectively.

6.5.2.1 Local and global limitations in fine motion discrimination

The results from the nested modelling showed that there was no significant difference in local or global parameters between the normal and the anisometropic amblyopes. On the other hand, the increased direction discrimination thresholds in strabismic amblyopes compared to normal controls was well represented by a reduction in sampling efficiency. The lower sampling efficiency in strabismic amblyopia suggests that these amblyopes have a poorer capacity in utilising local properties to form a global precept compared to the normal.

Local motion processing is known to occur in the early visual areas of V1 and V2 (Morrone *et al.*, 1995). Our results suggest that the local motion processing in these early areas are intact in both types of amblyopia, which is in line with other studies (Simmers *et al.*, 2003b; Simmers *et al.*, 2006b; Aaen-Stockdale and Hess, 2008; Thompson *et al.*, 2011). For example, Thompson *et al.,* (2011) reported that strabismic amblyopes show normal local motion processing for drifting Gabor patches at high contrast but not at low contrast levels. Abnormal motion thresholds at low contrast levels were attributed to the loss of contrast sensitivity rather than the motion sensitivity per se. The direction selective cells stimulated by the amblyopic eye in V1 are also reported to be normal in anisometropic and strabismic amblyopes in primate studies (Kiorpes *et al.*, 1998) again suggesting that early or local motion processing is intact.

Other studies, which have employed a coherence threshold paradigm to evaluate motion processing in amblyopia have also reported normal local motion processing in amblyopia with the deficits only evident at a later global integration level (Simmers *et al.*, 2003b; Simmers *et al.*, 2006b; Aaen-Stockdale and Hess, 2008). These studies manipulated a range of stimulus properties to separate the influence of local properties and global properties. For example, Simmers *et al.,* (2003, 2005) manipulated the contrast levels of dot elements and reported that the higher motion coherence thresholds in amblyopia could not be accounted for by the traditional loss in contrast sensitivity, thereby attributing the loss in motion processing to global processing at extra striate areas (MT and MST). Similarly, Aaen-Stockdale and Hess (2008) used RDK stimuli composed of band pass, instead of broadband, dot elements to see whether the pattern of the deficit in a global motion task would be different from, or similar to, the pattern of the contrast sensitivity loss (*i.e.,* low level) deficit in amblyopes. Their results showed that global deficits in motion processing in the amblyopes were constant for a range of spatial frequencies evaluated at a supra-threshold contrast (5x contrast threshold). As amblyopes are known to have specific contrast loss at higher spatial frequencies (Levi *et al.*, 2011), these constant deficits found for the motion coherence thresholds would implicate limitations at the global processing stage (Aaen-Stockdale and Hess, 2008).

Our results are also in line with physiological and imaging studies that reported reduced contribution from the strabismic amblyopic eye to higher extra striate motion areas (MT, MST) (El-Shamayleh *et al.*, 2010; Thompson *et al.*, 2012). The vulnerability of the global processing mechanism in strabismic amblyopia could also be due to the late maturation of visual processing at the global processing stage. The studies that have evaluated the development of fine motion discrimination in the presence of noise showed that the improvement in fine motion discrimination with age (from 5 to 11 years) was not related to the decrease in internal equivalent noise (estimate of local direction uncertainty) but rather due to the improved sampling efficiency (Bogfjellmo *et al.*, 2014; Manning *et al.*, 2014). The local processing mechanism (reflected by internal noise) hence seems to mature much earlier than the global mechanism (sampling efficiency). As functions that mature later would be more vulnerable to amblyogenic damage, it seems plausible that the global processing mechanism could be affected more than the local processing in amblyopia.

In the current study, using high contrast RDK stimuli and the equivalent noise method we showed that both local and global motion processing is normal in anisometropic amblyopia. Meanwhile, strabismic amblyopes showed normal local level processing but a lower efficiency at the global processing stage.

6.5.3 Global form discrimination in amblyopia

Global form perception was normal in anisometropic amblyopia across all noise levels. However, the orientation discrimination thresholds were abnormal for the amblyopic eye compared to both fellow and normal eyes across all strabismics.

As far as we know this is the first study to use Glass patterns to evaluate global orientation discrimination thresholds at variable levels of noise in amblyopia. Others (Mansouri *et al.*, 2004; Mansouri and Hess, 2006) have used stimuli composed of a field of Gabor patches in a similar task, with the orientation of individual Gabor patches derived from the standard Gaussian distribution with a defined mean orientation and standard deviation. For example, Mansouri *et al.,* (2004) employed Gabor patch stimuli in which they initially normalised the local orientation discrimination threshold between the amblyopic and fellow eye by manipulating the stimuli contrast. The local orientation discrimination threshold was first measured using a single Gabor patch for the amblyopic eye at 75% contrast. For the fellow eye, the stimuli contrast was reduced until the local orientation discrimination threshold was equivalent to that of the amblyopic eye (average contrast of 25%). When this normalised contrast was used to determine the global orientation discrimination task with multiple Gabor patches, they found no difference in performance for the amblyopic eye compared to the fellow eye and normal eyes (Mansouri *et al.*, 2004). Similar normal result for amblyopic observers was replicated in a later study by Mansouri and Hess (2006). However, when additional noise with random orientation (pedestal noise) was added to the stimuli, the thresholds for the amblyopic eyes increased. Based on these findings Mansouri and Hess (2006) suggested that the integration of orientation was normal in amblyopia. The increase in thresholds with the addition of pedestal noise was attributed to abnormal segregation. However, other studies using similar Gabor patch stimuli reported elevated fine orientation discrimination thresholds in both anisometropic and strabismic amblyopia (Simmers and Bex, 2004; Husk and Hess, 2013).

Our results are in agreement with the studies that have used Glass patterns and coherence threshold paradigm to investigate global form detection in amblyopia. Rislove *et al.,* (2010) reported increased coherence thresholds for both translational and concentric Glass patterns in strabismic amblyopia, with a larger deficit for the translational pattern. They also reported that some strabismic amblyopes could not reliably detect the structure of a translation Glass pattern. Similar to Rislove *et al.,* (2010), we also found that some strabismic amblyopes could not detect the Glass pattern structure even in the no noise condition. The reduced sensitivity to static translational Glass patterns has also been reported in the macaque with surgically induced strabismic amblyopia with seven out of the twelve monkeys unable to perform the form coherence task at any coherence level below 100% (Kiorpes, 2006). The argument from studies that report normal findings in the mean orientation discrimination tasks (employing Gabor patch stimulus) that this reflects normal form integration seem to be inaccurate in the view of the inability of some strabismic amblyopes to determine the Glass pattern structure even in the absence of noise. Dallala *et al.,* (2010) also reported increased global orientation thresholds in amblyopes using radial frequency patterns, a task which only involves pure integration.

The overall trend of the results from previous studies on orientation discrimination deficiency in amblyopia would also appear to be stimuli specific. Studies that used Gabor patches/ line segments in the mean orientation discrimination task reported rather normal (Mansouri *et al.*, 2004; Mansouri and Hess, 2006) or abnormal (Simmers and Bex, 2004; Husk and Hess, 2013) findings in amblyopia while those that used the Glass pattern and coherence threshold paradigm unanimously reported abnormal thresholds (Lewis *et al.*, 2002; Rislove *et al.*, 2010). This apparent difference could be due to the differences in the processing mechanism associated with these experimental stimuli. The local orientation information extraction in Glass patterns may well be influenced by the local correspondence noise as the Glass pattern detection is based on integrating the corresponding dipole elements in the presence of multiple dot elements. The Gabor patches and line segments meanwhile might be processed as elongated contours (Grinter *et al.*, 2010) with limited influence of correspondence noise. The local orientation cues from all individual dipoles of a Glass pattern are subsequently integrated to provide the global precept. The detection of the global structure of a Glass pattern hence seems a more complex task than that in either the Gabor patches or the line segments. This possible difference in processing is also reflected in better sensitivity to line segments compared to Glass patterns as observed in our first study (Chapter 3) and reported by others in both form coherence tasks (Aspell *et* *al.*, 2006) and global orientation discrimination tasks in the presence of noise (Dakin, 1997). Further, the processing of Gabor patches and line segment stimuli may also be influenced by the local lateral connections in V1 and as such these stimuli are not recommended for the evaluation of a true global orientation process (Grinter *et al.*, 2010). The lateral connections in V1 have minimal influence on the perception of the dipole Glass pattern hence the results from the experiments with Glass patterns are more likely to reflect the findings from a global orientation processing stage (details discussed in Chapter 3). Even with the relative ease in detection for line segment stimuli, Simmers *et al.,* (2005) did report increased coherence thresholds for both anisometropic and strabismic amblyopes.

In the current study, when the length of the Glass pattern was increased from dipole to tripole, the strabismic amblyopes who could not detect the structure of the dipole Glass pattern could easily complete the task. The thresholds for the tripole Glass pattern in strabismic amblyopes were comparable to normal thresholds. In Chapter 3.0, we found that the internal noise associated with the tripole Glass pattern was lower than that of the dipole Glass pattern in normal adults. If this is also the case in strabismic amblyopia, the amblyopic visual system would need to overcome relatively lower internal noise in order to make a global orientation judgement in a tripole Glass pattern, making the task relatively easier than that for the dipole Glass pattern. The finding that the strabismic amblyopes who could not detect the structure of the dipole Glass pattern could however easily complete the experiment on the tripole Glass pattern suggests that reinforcing the local orientation cues makes the task easier for the amblyopes. The orientation cues in Gabor patches and line segments are even more apparent than in the tripole Glass pattern. Therefore, the previously reported normal global orientation thresholds using the Gabor patch stimuli could have been due to the overall task being easier. While we cannot confirm the role lateral connections in early visual areas V1/V2 play in the processing of tripole Glass patterns (as has been suggested for the line segments), improved thresholds for the tripole Glass pattern may well be due to the influence of such local level processing in early visual areas.

The differences between results for anisometropic and strabismic amblyopia in global orientation processing could be due to the pathophysiological differences between each type of amblyopia (as explained previously for the motion mechanism). Similarly, the effect of the magnitude of the amblyopic deficit (IOD) and treatment history discussed for the motion task could also apply for the orientation task. For the strabismic amblyopes, the IOD didn't predict whether they could detect the Glass pattern structure or not. The strabismic amblyopes with the least IOD (MR, 0.26) and largest IOD (SM, 0.6), both failed to detect the Glass pattern structure. Both groups of strabismic amblyopes, those who could detect the Glass pattern and those who couldn't had undergone patching therapy in childhood, ruling out the treatment history effect. Similarly, although one strabismic amblyope with residual BSV (CO) completed the Glass pattern evaluation so did the others with no BSV. Rislove *et al.,* (2010) also reported that IOD or previous history of treatment does not correlate with deficiencies in Glass pattern detection. In their study, a strabismic amblyope who had undergone active vision therapy in childhood and had IOD < 0.2 at the time of evaluation still showed a deficit in Glass pattern detection.

6.5.3.1 Local and global limitation in fine orientation discrimination

Our results showed that while there were no local or global differences in orientation processing in the anisometropic amblyopes as compared to normal, the reduced fine orientation sensitivity in strabismic amblyopes was due to the differences in the efficiency with which the local orientation cues are processed at the global level.

Other studies that have used local orientation discrimination tasks have also reported normal local orientation discrimination thresholds in amblyopia. The local orientation thresholds for simple grating stimuli (Skottun *et al.*, 1986) and Gabor patches (Demanins *et al.*, 1999; Hess and Malin, 2003) have been found to be normal in strabismic amblyopes once the spatial frequency and contrast loss are accounted for. Additionally, studies using global orientation tasks have also reported normal local processing but compromised global processing in amblyopia. Simmers *et al.,* (2004) reported normal local orientation discrimination abilities in both strabismic and anisometropic amblyopes but increased global orientation discrimination thresholds which were proposed to be due to the limitation of processing mechanisms at higher cortical levels. Both local and global orientation processing of radial frequency patterns have also been reported to be abnormal in strabismic amblyopia (Dallala *et al.*, 2010).

The normal local orientation processing observed in the current study is also supported by the findings of physiological studies which have showed that V1 cells from amblyopic eyes in anisometropic and strabismic amblyopes have normal orientation selectivity (Kiorpes *et al.*, 1998). The deficits observed in global orientation processing could then be due to reduced activity at higher cortical areas of the ventral stream as reported by a larger reduction of responses in areas V4 and LO complex compared to V1/V2 in both anisometropic and strabismic amblyopia (Muckli *et al.*, 2006).

6.5.4 Perception of global implied motion (motion from form) in amblyopia

The thresholds for implied motion in the dynamic Glass pattern were normal for the strabismic amblyopes at both low and high noise conditions. Two strabismic amblyopes who could not detect the structure of the static Glass pattern easily completed the task on the dynamic Glass pattern. As far as we know this is the first study to have evaluated implied motion using dynamic Glass patterns in amblyopia. The processing of dynamic Glass patterns combines the inputs from both the motion (dorsal stream) and form (ventral stream) mechanisms, but the extent of the contribution of each stream in the processing is still unclear (Day and Palomares, 2014; Nankoo *et al.*, 2015).

Other studies have also evaluated the ability of amblyopes in integrating form and motion cues, but with a task of extracting form information from motion. For example, biological motion, in which the biological form is only apparent when the motion cues are present, is reported be intact in strabismic amblyopia (Thompson *et al.*, 2008b; Hamm *et al.*, 2014). In another task, where the orientation of a rectangle is only apparent when the constituent dots are in motion, amblyopes require a larger number of coherently moving dots defining the rectangle for reliable form discrimination (Hayward *et al.*, 2011). However, such deficits were limited to very slow dot speeds (0.1˚/s), with only one out of 12 amblyopes showing the deficits at a speed of 5˚/s. In the present study the speed of the dynamic Glass pattern was also relatively fast (18Hz), hence our normal findings are similar to that reported by Hayward *et al.* (2011). However, in another structure from motion task, Husk *et al.,* (2012) reported abnormal thresholds for the detection of structure (depth) from motion using broadband dot stimuli as well as

Gabor patches equated for the contrast deficit in the amblyopic eye. As discussed for form perception, the global deficits in amblyopia for form (structure) from motion also seem to be specific to the stimulus used and the differences in the results could be due to the differences in the processing mechanism of each stimulus. Moreover, directly comparing our results using motion from form (orientation) task with the studies based on structure from motion tasks may not be accurate as the visual processing mechanisms for both types of stimuli are not well understood and may well differ.

When the implied motion discrimination thresholds for the dynamic Glass pattern in strabismic amblyopes were compared to the motion and orientation discrimination thresholds for the RDK and static Glass pattern, the implied motion thresholds were generally closer to the RDK thresholds. In the normal controls, however, thresholds were generally mid-way between the RDK and static Glass pattern (as was observed in Chapter 4). This would suggest that strabismic amblyopes may be more reliant on motion cues when processing the implied motion from dynamic Glass patterns. The implied motion may, therefore, be processed more as a motion stimulus than the static form stimuli in strabismic amblyopes. In the normal controls, the lower thresholds for dynamic Glass patterns compared to static patterns may be due to the processing of the temporal properties (Day and Palomares, 2014). Physiological and imaging studies in normal primates and humans using dynamic Glass patterns have also reported that area MT+ along the dorsal stream is similarly activated by the real motion in RDK's and the implied motion from the dynamic Glass pattern, while the ventral stream areas are differentially activated (Krekelberg *et al.*, 2003; Krekelberg *et al.*, 2005). However, other studies suggest that implied motion processing relies more on form processing mechanisms (Nankoo *et al.*, 2012; Nankoo *et al.*, 2015) (discussed in detail in Chapter 4). Our findings of similar thresholds for implied motion and real motion suggests that at least in amblyopia the processing of implied motion may rely more on the motion cues.

In the strabismic amblyopes deficits were found only for the global motion and global form processing stages, while the local processing mechanisms for both seemed relatively intact. The preserved local and global thresholds for the dynamic Glass pattern suggests that the processing of the motion from orientation in a dynamic Glass pattern utilises the intact local level inputs from both motion and form mechanisms, while global processing may occur independently of both the global motion and global form processing mechanisms.

6.5.5 Comparison of the motion and form deficits in strabismic amblyopia

In the current study, we used physically identical stimuli along the dorsal and ventral stream to concurrently evaluate visual processing deficits in amblyopia. The results showed that motion/form perception in strabismic amblyopia is limited by the processing at the global integration stage while the local processing might be normal. When the results from the motion (RDK) and form (Glass) domain were compared for the strabismic amblyopes, all amblyopic participants showed reduced efficiency in the amblyopic eye. The amblyopes also showed reduced efficiency in the fellow eye (7 out of 9) for the motion domain while three amblyopes (out of 6) had poorer efficiency in the form domain. Interestingly the three amblyopes who could not detect the global structure of the Glass pattern also exhibited larger global deficits for the motion domain (2.2 to 3X normal). Our results showed that both motion and form domains and thereby the dorsal and ventral streams are affected in strabismic amblyopia. The fact that strabismic amblyopes who could not detect the structure of the Glass pattern also had larger global deficits in motion processing suggests that the global processing deficit may be a characteristics feature of amblyopia.

The observed limitation in the global sampling efficiency parameter for both domains in strabismic amblyopia was due to the under sampling of the local inputs, this would suggest that the undersampling theory (Levi *et al.*, 1984; Levi and Klein, 1985; Wang *et al.*, 1998) posited for other visual deficits in strabismic amblyopes could be applicable to the current complex tasks processed at higher cortical areas. Strabismic amblyopes are reported to be generally poor at using available information (Kiorpes and McKee, 1999). In a line bisection task, which is proposed to be processed at the higher cortical areas, anisometropic amblyopes showed normal efficiency in using all available samples for judgement but strabismic amblyopes based their judgement on a fewer number of samples than normal (Wang *et al.*, 1998). Similarly in a feature detection task, strabismic amblyopes undercounted stimuli features compared to the normal controls, and this deficit persisted even when the lower level contributions were controlled for

(Sharma *et al.*, 2000). Hence the inability to use all the available information seems to be a generalised deficiency across different domains in strabismic amblyopia.

Dorsal stream function such as motion perception is reported to be more affected than ventral stream function in various developmental disorders, leading to the assumption of dorsal stream vulnerability (Braddick *et al.*, 2003; Grinter *et al.*, 2010). Our results showed that both dorsal and ventral stream functions are affected in amblyopia. Global motion processing was also affected in the fellow eye more than the global form. We also found that some strabismic amblyopes were unable to even detect the structure of a Glass pattern. These mixed results suggest that the generalisation of dorsal stream vulnerability in amblyopia may not be accurate. Imaging and physiological studies in amblyopia also show reduced activity along both dorsal and ventral processing streams (Lerner *et al.*, 2003; Muckli *et al.*, 2006; El-Shamayleh *et al.*, 2010; Thompson *et al.*, 2012) while a study in amblyopic cats report that the ventral stream is more affected than dorsal stream (Schröder *et al.*, 2002).

Two probable causes for the postulated dorsal stream vulnerability are related to the anatomical aspects and the developmental pattern of dorsal stream (Braddick *et al.*, 2003). The M-cells in retina and LGN, the early processors of dorsal stream inputs, are more susceptible to the damage from pathological changes due to their larger size and smaller population (10% of retinal ganglion cells in the retina). A proportionate deficit for the M cells and P cells in retina and LGN should result in a more obvious functional loss for dorsal stream function, innervated by the smaller number of M-cells. In amblyopia, the deficits at the M-cell level should result in lower sensitivity to local as well as global motion tasks, but a wide range of studies (Simmers *et al.*, 2003b; Simmers *et al.*, 2006b; Aaen-Stockdale and Hess, 2008) and our results suggest that the deficits in the motion domain are restricted to mostly the global processing level. Another explanation for the reported dorsal stream vulnerability in developmental disorders is due to the apparent late development of dorsal stream compared to ventral stream visual function [for review (Braddick *et al.*, 2003; Grinter *et al.*, 2010)]. Indeed, global motion processing mechanisms are known to follow a long and protracted developmental pattern extending beyond 14 years. For example, translational motion coherence thresholds mature to adult levels at 12 to 14 years (Gunn *et al.*, 2002; Hadad *et* *al.*, 2011), while the radial coherence thresholds remain immature even at 16 years of age (Joshi and Falkenberg, 2015). However, other studies have shown that some aspects of global motion and form coherence mature at a similar age (Gordon and McCulloch, 1999b; Parrish *et al.*, 2005).

While dorsal stream vulnerability is proposed as a feature of different neurological developmental disorders (Braddick *et al.*, 2003), more recent studies question the generalisation of this assumption (Grinter *et al.*, 2010). For example, it is argued that most studies that have reported dorsal stream vulnerability were tested with stimuli that might not be compatible for direct comparison between the two processing streams (Grinter *et al.*, 2010). Additionally, as discussed before, the global processing deficits in motion and form processing in developmental disorders including amblyopia appear to be dependent on the task and the stimuli used, hence generalising the results from one task or stimuli as dorsal or ventral stream vulnerability may not be accurate. It follows, that the deficit observed in these tasks may only represent a localised processing deficit along the dorsal stream rather than a generalised vulnerability of the whole stream.

Our results have also shown that fine global motion and orientation discrimination is abnormal in strabismic amblyopia only. Abnormal global motion (Simmers *et al.*, 2003b; Simmers *et al.*, 2006b; Aaen-Stockdale and Hess, 2008) and global form (Lewis *et al.*, 2002; Rislove *et al.*, 2010) deficits have been widely reported in the coherence task. However, other studies employing fine global motion discrimination tasks have reported normal thresholds in amblyopia (Hess *et al.*, 2006; Mansouri and Hess, 2006) while the results for fine orientation discrimination have been inconclusive (Mansouri *et al.*, 2004; Simmers and Bex, 2004; Mansouri and Hess, 2006; Husk and Hess, 2013).

These differences have been explained in terms of the strategy adopted by the amblyopic observer during the task with segregation being the main strategy for the coherence threshold task and integration for fine direction/orientation discrimination tasks (Mansouri and Hess, 2006). The rigid classification of the fine mean orientation task as a global integration task and the coherence task as global segregation task is problematic, as both tasks may rely on segregation as well as integration mechanisms as discussed for the motion domain. Further, the conflicting results of normal and abnormal findings from the fine global orientation tasks suggested that the results may well be reliant on the stimuli used for evaluation. Our results, therefore, suggest that both the dorsal and ventral streams functions are similarly affected in amblyopia, moreover the inability of some amblyopes to simply detect the structure of a translational Glass pattern would suggest that contrary to the perceived dorsal vulnerability, ventral stream function may be more greatly affected.

6.6 Conclusion

- Global motion and global form processing appear normal in anisometropic amblyopia.
- Both global motion and global form processing are impaired in strabismic amblyopia.
- The reduced sensitivity to global motion and global form in strabismic amblyopia can be explained by a reduced efficiency with which the local information is processed at the global processing stage.
- The global form deficit in strabismic amblyopia seems task specific and might not represent a general dysfunction of the ventral visual stream processing.
- The differences in sensitivity to various stimuli aimed at global form processing in strabismic amblyopia suggests that a careful consideration needs to be made on selecting experimental stimuli for concurrent comparison along different domains.
- The processing of implied motion seems normal in strabismic amblyopia.
- The fact that global form perception seemed more affected in strabismic amblyopia suggest that the generalised assumption of dorsal stream dysfunction in developmental disorders may not be present in amblyopia.

A paper based on the results of this study was published in Investigative Ophthalmology and Visual Science Journal.

JOSHI, M. R.; SIMMERS, A. J. and JEON, S. T. 2016. Concurrent Investigation of Global Motion and Form Processing in Amblyopia: An Equivalent Noise Approach. Investigative Ophthalmology & Visual Science, 57, 5015-5022.

The results of this study were presented at the 15th Annual Vision Sciences Society Meeting, Florida, USA, 15-20 May 2015 and the 38th European Conference on Visual Perception, Liverpool, United Kingdom, 23 – 27 August 2015

Joshi M, Simmers A, Jeon S; "Deficits in integration of global motion and form in noise is associated with the severity and type of amblyopia" Journal of Vision 2015; 15(12):193.

Jeon S T, Joshi M R, Simmers A; "Noise reveals abnormal global integration of motion and form in strabismic amblyopia". Perception, 2015; 44: 1-415

7.0 General Conclusions

Chapter 3: Concurrent characterisation of dorsal and ventral stream function with equivalent noise paradigm

A concurrent comparison of motion and form processing has remained difficult due to the differences in stimuli employed to evaluate each stream. The experiments in this chapter used physically similar stimuli embedded in varying levels of external noise to evaluate the motion and form processing in visually normal adults. Using random dots, we created an experimental stimulus of which parameters were manipulated in the same manner regardless of the domain – be it motion or form – under testing, setting a scene for the experiments to follow. Using hierarchical nested modelling, it was found that the higher discrimination thresholds for the global form (dipole Glass pattern) compared to the global motion (RDK) were due to the changes in the sampling efficiency parameter with the equivalent noise remaining constant. This is seen as a relatively more efficient global integration mechanism (modelled as a higher sampling efficiency) at the higher extrastriate cortices along the dorsal stream than those along the ventral streams, with a constant limitation (modelled as a single internal noise) in local processing common to both streams, purportedly from the shared, lower areas such as V1.

The global orientation sensitivity was first evaluated by using the dipole Glass pattern then further evaluated by line segments and extending Glass patterns with “multipoles” (namely, tri- and quadrapoles). As opposed to the motion vs. form difference explained by the difference in sampling efficiency, the differences in the form thresholds between dipole Glass pattern, line segments, and multipole Glass pattern were best described by the changes in the internal equivalent noise with the sampling efficiency remaining constant. The differences in internal noise for different stimuli directed at evaluating global orientation processing suggested that the stimuli with line segments and Glass pattern with more than two elements may be more reliant on local processing, therefore, careful consideration needs to be made when selecting a stimulus to evaluate these global processing stages.

Chapter 4: The processing of implied motion in a normal population

The interactions between motion and form processing mechanisms have been previously studied (Nankoo *et al.*, 2012; Day and Palomares, 2014; Nankoo *et al.*, 2015) by measuring implied motion coherence thresholds with dynamic Glass patterns. However, the coherence threshold paradigm is limited in differentiating if the interactions originate at the local or global processing levels. In this chapter we measured implied motion sensitivity at varying levels of external noise. The results were then compared to that of the global motion (RDK) and global form (Glass pattern) to unravel the interactions at the local vs. global processing levels.

The results showed that the local level processing for all three stimuli types (dynamic Glass pattern, RDK, and static Glass pattern) were similar. The lower thresholds for the implied motion in dynamic Glass patterns compared to the orientation thresholds in static Glass patterns when modelled proved to provide a better sampling efficiency at the global processing stage.

The results suggest that the local processing of the dipole orientation in a dynamic Glass pattern is similar to the processing of static Glass patterns with further global processing most likely occurring along the motion processing areas of MT/MST.

Chapter 5: Modification of the data collection method for the faster application of an equivalent noise paradigm

Unlike the coherence threshold paradigm, the external noise paradigm based on measuring discrimination thresholds at different levels of external noise can unravel the contributions of local and global processing mechanisms. However, employing the equivalent noise paradigm in subjects with various clinical conditions has remained difficult due to the time/effort required to measure thresholds at multiple noise levels. In this chapter we adapted the paradigm to facilitate data collection and validated this method against the traditional method of measuring discrimination thresholds at different noise levels.

The results showed the abridged version measuring tolerable noise thresholds to target high noise points in the *TvN* curve is as reliable as the full classical method of measuring discrimination thresholds at multiple noise levels. Moreover, the new method required almost one third of the time compared to the classical method.

This new method provides an opportunity to employ the equivalent noise paradigm in clinical populations who are less likely to complete experiments with the classical method.

Employing the equivalent noise paradigm in clinical populations will be useful in unravelling the local/global processing limitations which will in turn aid to a better understanding of the disease processes.

Chapter 6: Concurrent investigation of dorsal and ventral stream processing in amblyopia: an equivalent noise approach

Global motion perception is known to be abnormal in amblyopia while global form is reported to be either abnormal or normal depending on the experimental stimuli and method employed. All the problems identified in comparing motion and form perception in a normal control population are not only inherited but exaggerated when studying special population with clinical conditions.

The majority of amblyopia studies have measured motion/form coherence thresholds which cannot separate the local/global processing limitations; the difference in the stimuli used for each domain has also made it difficult to directly compare deficits along each domain. In this chapter we employed physically similar RDK and Glass pattern stimuli adapted to the faster method developed in Chapter 5 to probe local and global motion/form processing in amblyopia. We also evaluated implied motion in amblyopia to understand the interaction between the motion and form processing mechanisms.

The global motion and global form thresholds were found to be normal in anisometropic amblyopia. On the other hand, strabismic amblyopes showed elevated thresholds in both the motion and form domains with some amblyopes unable to even detect the structure of a dipole Glass pattern. The abnormal motion and form thresholds in strabismic amblyopia were related to the deficiency in integration at a global processing stage with the local processing appearing normal. Additionally, the strabismic amblyopes who were unable to detect the dipole Glass pattern could easily detect the tripole Glass pattern within normal threshold limits. The implied motion thresholds in dynamic Glass patterns were meanwhile normal for the strabismic amblyopes.

Our results using physically similar stimuli show that both global motion and global form processing are abnormal only in strabismic amblyopia. The normal local motion/form processing, normal implied motion processing, and abnormal global motion/orientation processing in strabismic amblyopia suggest that the generalised assumption of dorsal stream dysfunction in developmental disorders may be reconsidered at least in the case of amblyopia, with more careful experimental design/consideration required when wishing to compare performance along the two domains.

8.0 Future Studies and preliminary data

8.1 Concurrent evaluation of motion and form processing in dyslexia

Dyslexia is a complex disorder involving different sensory deficits. Various electrophysiological, imaging and behavioural studies have implicated visual deficits along the magnocellular/dorsal visual pathway in dyslexia [for review, (Laycock and Crewther, 2008; Skottun and Skoyles, 2008)]. It has been reported that individuals with dyslexia show significantly reduced fMRI responses in early visual area V1 as well as MT when evaluated with low luminance moving gratings that specifically target the magnocellular pathway (Demb *et al.*, 1997; Demb *et al.*, 1998). Similarly, lower fMRI activation of area MT has been reported when compared to control groups employing a motion coherence task but normal activation is demonstrable along the parvo/ventral stream with a form coherence task in dyslexia (Eden *et al.*, 1996).

Dyslexia is also associated with behavioural deficits in various tasks mediated by the lower and higher subcortical magnocellular pathway. A lower sensitivity to flicker contrast (Edwards *et al.*, 2004; Pellicano and Gibson, 2008) processed at lower subcortical areas of the magnocellular pathway but normal sensitivity on tasks aimed at evaluating parvocellular function such as the detection of slow, isoilluminant Gabor patches and gratings has been reported in dyslexia (Edwards *et al.*, 2004). Differences have also been observed in other cognitive tasks, which are processed along the parvocellular and magnocellular pathways. For example in a rapid processing sequencing task, dyslexics performed better at spatial than temporal sequencing tasks (Conlon *et al.*, 2004). However, other lower magnocellular tasks such as directional motion contrast sensitivity (Slaghuis and Ryan, 2006) and contrast sensitivity to flicker or static patterns (Williams *et al.*, 2003) were reported to be normal.

Similarly, adults and children with dyslexia had deficits in a global motion coherence threshold (MCT) task processed at higher cortical areas along the dorsal stream (Raymond and Sorensen, 1998; Hansen *et al.*, 2001; Pellicano and Gibson, 2008) while the global form coherence thresholds processed along the ventral stream were reported to be normal (Hansen *et al.*, 2001; Conlon *et al.*, 2004). Other studies have suggested that the visual deficits observed in the motion processing pathway were due to the inability of individuals with dyslexia to exclude noise (Sperling *et al.*, 2005; Sperling *et al.*, 2006).

As discussed in the preceding chapters, a major obstacle in attributing any specific developmental disorder to a dorsal or ventral stream processing is the lack of a common stimulus that can be shared by both streams for a fair and transparent comparison. Here we evaluated the global motion and form stream using tasks in which the stimulus parameters are shared as much as possible in the presence of noise. The results provide comparable data along each visual processing stream and parse out the presumed differential effect of noise in dyslexia.

Preliminary results:

Four individuals diagnosed with dyslexia (mean age 19.50 ±0.58 years) discriminated the global motion direction in RDK and the global orientation in Glass pattern. Among the four participants, two were diagnosed by community psychologists while the other two were diagnosed at the Visual Stress Clinic at the Glasgow Caledonian University. The data of controls from the amblyopia study (refer to section 6.3) were used for the comparison. The stimuli, methods and procedure were the same as described for the amblyopia study (Chapter 6).

The direction discrimination thresholds for participants with a reading disorder were elevated in comparison to the normal controls at both noise levels. The orientation discrimination thresholds meanwhile were more similar between the two groups. A MANOVA with the log direction/orientation offset and noise thresholds as the dependent variable and *study group* (two levels; reading disorder and control) and *stimulus type* (two levels; RDK and Glass) as the between subject factors showed no significant effect of *study group* [$V = 0.02$, $F(6,488) = 1.033$, $p > 0.05$] but a significant effect of *stimulus type* [$V = 0.30$, $F(2,243) = 52.49$, $p < 0.001$] with no interaction between *eye* and *stimulus type* [$V = 0.02$, $F(6,488) = 0.76$, $p > 0.05$].

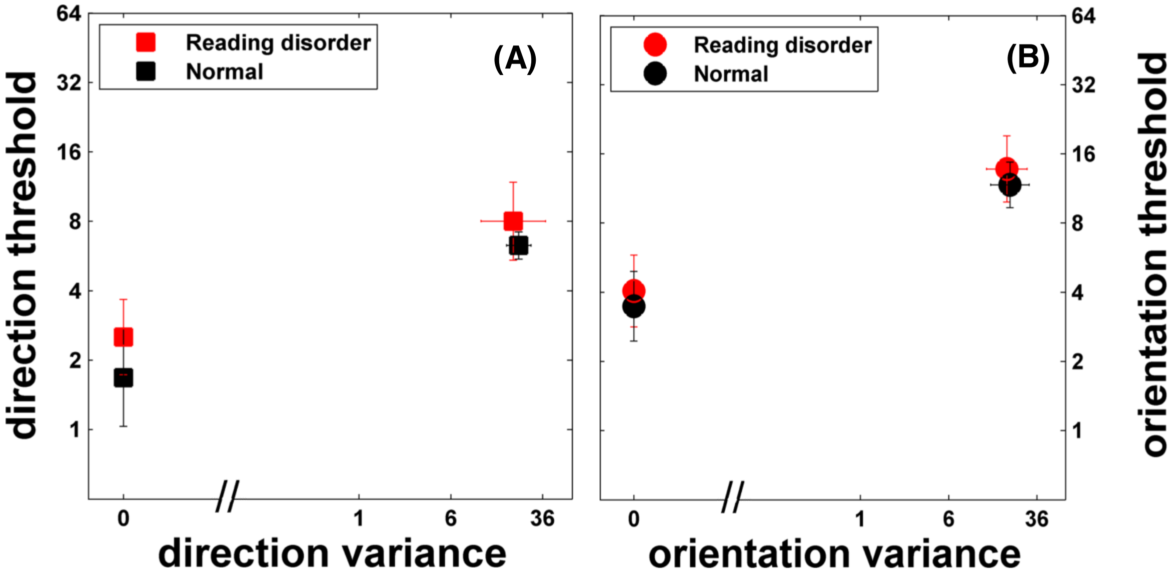

Figure 8.1: The global direction discrimination (A) and orientation discrimination (B) thresholds for individuals with a reading disorder and visually normal controls.

Limitations and future work

Our results showed that while there is a trend for the global motion thresholds to be elevated in the observers with a reading disorder thereby supporting the magno/dorsal stream theory, the thresholds were not significantly different from the visually normal controls. However, our sample group was limited, further to the diagnosis of the reading disorder, additional tests such as reading scores and IQ scores would need to be ascertained. Hence future extension of this work needs to be undertaken with a larger sample and a more refined inclusion criteria is required for an accurate diagnosis of dyslexia.

8.2 The differences in processing of global motion and global form – an ideal observer perspective

In all our experiments we find that the global form thresholds in Glass pattern are elevated compared to the global motion thresholds. This trend was consistent regardless of the type of observers (*i.e.,* normal or amblyopic) and across all external noise levels. On the surface, this might seem unsurprising as motion stimuli (RDK) contain more information/energy compared to the static Glass pattern stimuli, which is shown as a vertical shift across noise levels. However, the picture becomes more complicated when we tested different types of Glass patterns. For example, we find that the thresholds for quadrapole Glass patterns and equivalent line segments are similar to that of RDKs at lower noise levels. In its simplest form, we can hypothesise that it takes as few as four frames to be integrated for the best orientation or direction thresholds at low noise levels, given that Glass patterns can be considered a snapshot of multiple motion frames in sequence. At higher noise levels, however, the direction discrimination thresholds still remained lower than that of the orientation discrimination thresholds for quadrapole Glass patterns and line segments.

We do not know yet from which factors this interaction between the domains (*i.e.,* motion and form) and the level of noise arises. An ideal observer analysis is based on evaluating how a processing system utilises stimulus information available to perform the task bound by the anatomical and physiological limitations. An ideal observer model incorporating the basic stimulus attributes of motion (RDK) and form (various Glass patterns) domains could provide further information on what limits the normal performance along the two domains. Such analysis could also inform more on the interaction of the two visual processing mechanisms.

8.3 Abnormal form processing in strabismic amblyopia – an exploratory study

In Chapter 6, we find that strabismic amblyopes have a deficit in both motion and form processing. We also find that some strabismic amblyopes were unable to detect the Glass pattern stimuli. However, the same amblyopes were able to detect the structure in dynamic Glass patterns and tripole Glass patterns. The difference in performance between various form stimuli could be related to higher internal noise associated with the dipole Glass pattern compared to the tripole Glass pattern. This assumption is also supported by the findings of increased internal noise in dipole Glass pattern compared to tripole, quadrapole, and line segments in a control population (Chapter 3). It would hence be interesting to further explore the form processing pathway in amblyopes with different types of Glass pattern and line segment stimuli to determine if the differences in performance are actually related to local (internal noise) or global (sampling efficiency) limitations. We also investigated the possibility that the deficit was associated with the level of inter-ocular difference in visual acuity but no relationship was found. It would however be interesting to further explore other clinical diagnostic factors such as degree of binocularity, age of onset or duration of previous treatments.

8.4 Development and maturation of motion processing and form processing – an equivalent noise approach

Global motion and global form processing are known to be processed at higher extra cortical areas along the two visual pathways – dorsal and ventral stream. Although infants of 2-3 months show some limited sensitivity to both global motion (Brosseau-Lachaine *et al.*, 2008; Shirai *et al.*, 2008) and global form (Quinn, 2000), the motion and form coherence threshold evaluation has shown that the sensitivity to these global patterns follow a long and protracted development process reaching adult like level at a much later age than other basic visual functions such as visual acuity, stereo acuity, and contrast sensitivity, which are of adult level by 5 to 6 years of age. For example, translational motion coherence thresholds have been reported to reach adult levels at around 11-14 years (Gunn *et al.*, 2002; Parrish *et al.*, 2005; Hadad *et al.*, 2011; Hadad *et al.*, 2015). Similarly, form coherence thresholds employing Glass patterns is reported to be adult like by the age of 9 years (Lewis *et al.*, 2004).

Dorsal stream visual functions (motion) have also been reported to be affected more in a range of developmental disorders [for review (Braddick *et al.*, 2003; Grinter *et al.*, 2010)]. One of the reasons reported for this is due to the late development of dorsal stream function compared to that of the ventral stream (form) (Braddick *et al.*, 2003). However, some studies have reported that both global form and motion mature at a similar age (Gordon and McCulloch, 1999b; Parrish *et al.*, 2005). Similarly, comparing the developmental pattern of dorsal and ventral stream based on physically differing stimulus may be inaccurate as the characterisation of motion and form processing relies heavily on the stimulus and task being used. Hence in this proposed study we would assess development of motion and form processing mechanisms in children using the tasks where as many experimental parameters are shared between the streams for fairer comparison.

8.5 Is the internal noise parameter related to the direction and orientation bandwidth of visual system?

Traditionally the direction and orientation bandwidth has been measured in a single cell analysis (Albright, 1984; Vogels and Orban, 1991; Liu and Newsome, 2003). Behaviourally, the direction/orientation bandwidth has been measured using masking and adaptation paradigms (Phillips and Wilson, 1984; Blake and Holopigian, 1985). In the experiments detailed in this thesis we measured the limits of fine direction/orientation discrimination from the vertical reference in the presence of variable noise.

The internal noise parameter derived from the equivalent noise paradigm may represent the overall noise within the visual system. However, there is much ambiguity on what this value truly represents, with some studies (Beaudot and Mullen, 2006) relating the measure to the overall bandwidth of the system. It would hence be interesting to measure the direction/orientation bandwidth behaviourally using similar stimulus parameters and investigate any relation between the internal equivalent noise and overall direction/orientation bandwidth of the human visual system.

8.6 Limiting factors of speed discrimination – internal noise or sampling efficiency?

Humans have a differential sensitivity to object speed, with higher sensitivity to faster speeds compared to slower speeds (Ahmed *et al.*, 2005; Hadad *et al.*, 2011; Falkenberg *et al.*, 2014; Joshi and Falkenberg, 2015). The better sensitivity to faster speed has again been studied in terms of the spatial and temporal components of motion (Kiorpes *et al.*, 2006; Knox *et al.*, 2013). This difference is present from the very early stages of visual development (Manning *et al.*, 2012; Bogfjellmo *et al.*, 2014; Joshi and Falkenberg, 2015) until senescence (Bogfjellmo *et al.*, 2013). The differences in sensitivity to fast and slow speeds have been explained by the presence of independent processing mechanisms for each speed (Edwards *et al.*, 1998; Khuu and Badcock, 2002) or a single mechanism tuned to different speeds (van Boxtel and Erkelens, 2006). The speed discrimination capability has most commonly been studied with the coherence threshold paradigm. Employing equivalent noise method could separate if the difference in performance is related to a change in internal noise or sampling efficiency. The result would also provide information on whether the slow and fast speed processing mechanisms are related or independent at the local and global visual processing stages.

9.0 Appendices

9.1 Appendix 1: Information Sheets / Consent Forms and Ethics

Information sheet 1

Information Sheet for Adult Participants

Project title: Characterisation of the Dorsal & Ventral Pathways Using External Noise Paradigm in Visually Normal and Abnormal Populations

Investigators: Mahesh Raj Joshi; M.Phil, Ph.D. Candidate
Simon Jeon, Ph.D., Lecturer
Anita J. Simmers, Ph.D., Professor

Introduction and study purpose

You are invited to take part in a study about ‘‘Characterisation of the Dorsal & Ventral Pathways Using External Noise Paradigm’’ in Glasgow Caledonian University. The aim of the study is to investigate how different visual stimulus are perceived by human, specifically we want to understand how normal, typically developing children fare with adults on seeing motion or shape against irrelevant, noisy background information, we will be evaluating 24 adults and around 100 children with normal vision in the study. The study will entail basic testing of your vision and an experiment using computer. Before you decide whether or not to take part, it is important for you to understand what participation in the study will involve for you. Please take time to read the following information carefully and contact us at the address below if you need more information.

What will I have to do if I take part?

If you are interested in taking part, you will be asked to undergo a vision screening which will include testing your visual acuity (how well you can see distant objects) and stereo vision (ability to perceive depth). The visual screening will be followed by completing an experimental task presented on the computer screen.
You will complete two separate tests watching patterns made up of small moving dots many times and respond by pressing appropriate keys on computer keyboard.

Do I have to take part?

No. It is up to you to decide whether or not to take part. You can stop taking part in the study at any time, without giving a reason.

What are the possible disadvantages and risks of taking part?

You may feel uncomfortable or tired after sitting in same position during the experiment. We can pause the experiment at any stage if you wish to take a rest in between.

What are the possible benefits of taking part?

The study likely will not help you directly. However, the results should help our understanding on how humans perceive moving and static objects. This, in turn, is expected to be beneficial to the understanding how the human brain works.

What will happen to the information that you give?

Your results of experiment will be stored anonymously into our database with secured password. All data will be stored anonymously and only the researchers involved in this work will have access to the information. All data will be destroyed after 5 years of completion of the research project.

Will my taking part in this study be kept confidential?

Yes. Ethical and legal practice will be followed, and all of your information will be handled in confidence. The responses that you provide will be treated confidentially. Your rights are protected under the Data Protection Act and any information that might identify you will not be shared outside of the research team. No identifying information will appear in any documents or in the final report.

What will happen to the results of the research study?

The data will be analysed and will be available to a range of people, including scientists and researchers through written reports, presentations and journal publications. However, it will not be possible to identify any individual participant from these reports or publications.

Who has reviewed the study?

This study has been given approval by the School of Health and Life Sciences Ethics committee. Consent to take part in the study will be obtained by the researchers involved.

What happens next?

If you decide you are interested in participating in the study after reading this information sheet, please complete one copy of the consent form. If you would like to find out more about the research before participating please do not hesitate to contact.

Investigator:	Project Supervisor:
Mahesh Raj Joshi	Dr. Simon Jeon, Ph.D
Ph.D candidate	Lecturer
Department of Vision Sciences	Department of Vision Sciences
Glasgow Caledonian University	Glasgow Caledonian University
Email: Mahesh.Joshi@gcu.ac.uk	Email: Simon.Jeon@gcu.ac.uk
Telephone: 01413318316	Telephone: 01412731685

Thank you for taking the time to read this study information sheet.

Consent Form 1

Characterisation of the Dorsal & Ventral Pathways Using External Noise Paradigm in Visually Normal and Abnormal Populations

CONSENT FORM (ADULT)

Please tick box

1. I confirm that I have read and understood the information sheet dated for the above study and have had the opportunity to ask questions and have had these answered satisfactorily. ☐

2. I understand that my participation is voluntary and that I am free to withdraw at any time without giving any reason. ☐

3. I agree to take part in the above study. ☐

4. I understand that the results from this work may be published however this will be completely anonymous. ☐

______________________	__________	______
Name of participant	Date	Signature
______________________	__________	______
Name of person taking consent	Date	Signature

Information Sheet 2

Information Sheet for Adult Participants

Project title: Evaluation of Dorsal and Ventral Stream in Neurodevelopmental Disorders with Equivalent Noise Paradigm

Investigators: Mahesh Raj Joshi; M.Phil, Ph.D. Candidate
Seong Taek Jeon, Ph.D., Lecturer
Anita J. Simmers, Ph.D., Professor
Nadia Northway, Ph.D., Senior Lecturer

Introduction and study purpose

You are invited to take part in a study at Glasgow Caledonian University which aims to the study how human perceive direction of motion (for example, in which direction are the car moving?) and orientation (for example, is the picture on the wall hung straight or tilted?). Specifically we want to understand how different individuals with a known neurodevelopmental disorder are from visually normal adults on seeing motion or orientation of objects against irrelevant, noisy or, 'cluttered' background information.

The study will involve a simple non-invasive computer based experiment. We will measure an individual's sensitivity to different visual patterns, reflecting the different connected pathways between visual brain centres. Before you decide whether or not to take part, it is important for you to understand what participation in the study will involve for you. Please take time to read the following information carefully and contact us at the address below if you need more information.

What will I have to do if I take part?

If you are interested in taking part, we will ask you to watch a computer monitor attentively for a certain visual pattern. You will be required to respond as instructed to the pattern by pressing one of the computer mouse buttons or keypads per presentation of the pattern at a time.Testing will take approximately 45 minutes with as many breaks as you require.

Do I have to take part?

No. It is entirely up to you to decide whether or not to take part. You can stop taking part in the study at any time, without needing to give a reason.

What are the possible disadvantages and risks of taking part?

You may feel uncomfortable or tired after sitting in same position for the duration of the experiment. We can pause the experiment at any stage if you wish to take a rest in between.

What are the possible benefits of taking part?

It is unlikely the study will help you directly. However, the results should help our understanding on how people with neurodevelopmental disorders perceive moving and static objects as compared to normal. This, in turn, is expected to be beneficial to the understanding how the human brain works and may provide a basis for future rehabilitative therapies.

What will happen to the information that you give?

The results of the experiment will be stored anonymously into a database with a secured password. All data will be stored anonymously and only the researchers involved in this work will have access to the information. All data will be destroyed after 5 years of completion of the research project.

Will my taking part in this study be kept confidential?

Yes. Ethical and legal practice will be followed, and all of your information will be handled in confidence. The responses that you provide will be treated confidentially. Your rights are protected under the Data Protection Act and any information that might identify you will not be shared outside of the research team. No identifying information will appear in any documents or in the final report.

What will happen to the results of the research study?

The data will be analysed and will be available to a range of people, including scientists and researchers through written reports, presentations and journal publications. However, it will not be possible to identify any individual participant from these reports or publications.

Who has reviewed the study?

This study has been given ethical approval by the School of Health and Life Sciences departmental committee. Consent to take part in the study will be obtained by the researchers involved.

What happens next?

If you are interested in participating in the study after reading this information sheet, please complete one copy of the consent form. If you would like to find out more about the research before participating please do not hesitate to contact.

Investigator:	Project Supervisor:
Mahesh Raj Joshi	Dr. Seong Taek Jeon, Ph.D
Ph.D candidate	Lecturer
Department of Vision Sciences	Department of Vision Sciences
Glasgow Caledonian University	Glasgow Caledonian University
Email: Mahesh.Joshi@gcu.ac.uk	Email: Simon.Jeon@gcu.ac.uk
Telephone: 01413318316	Telephone: 01412731685

Thank you for taking the time to read this study information sheet.

Consent Form 2

Evaluation of Dorsal and Ventral Stream in Neurodevelopmental Disorders with Equivalent Noise Paradigm

CONSENT FORM

Please tick box

1. I confirm that I have read and understood the information sheet dated for the above study and have had the opportunity to ask questions and have had these answered satisfactorily. ☐

2. I understand that my participation is voluntary and that I am free to withdraw at any time without giving any reason. ☐

3. I agree to take part in the above study. ☐

4. I understand that the results from this work may be published however this will be completely anonymous. ☐

Name of participant	Date	Signature
Name of person taking consent	Date	Signature

Ethics:

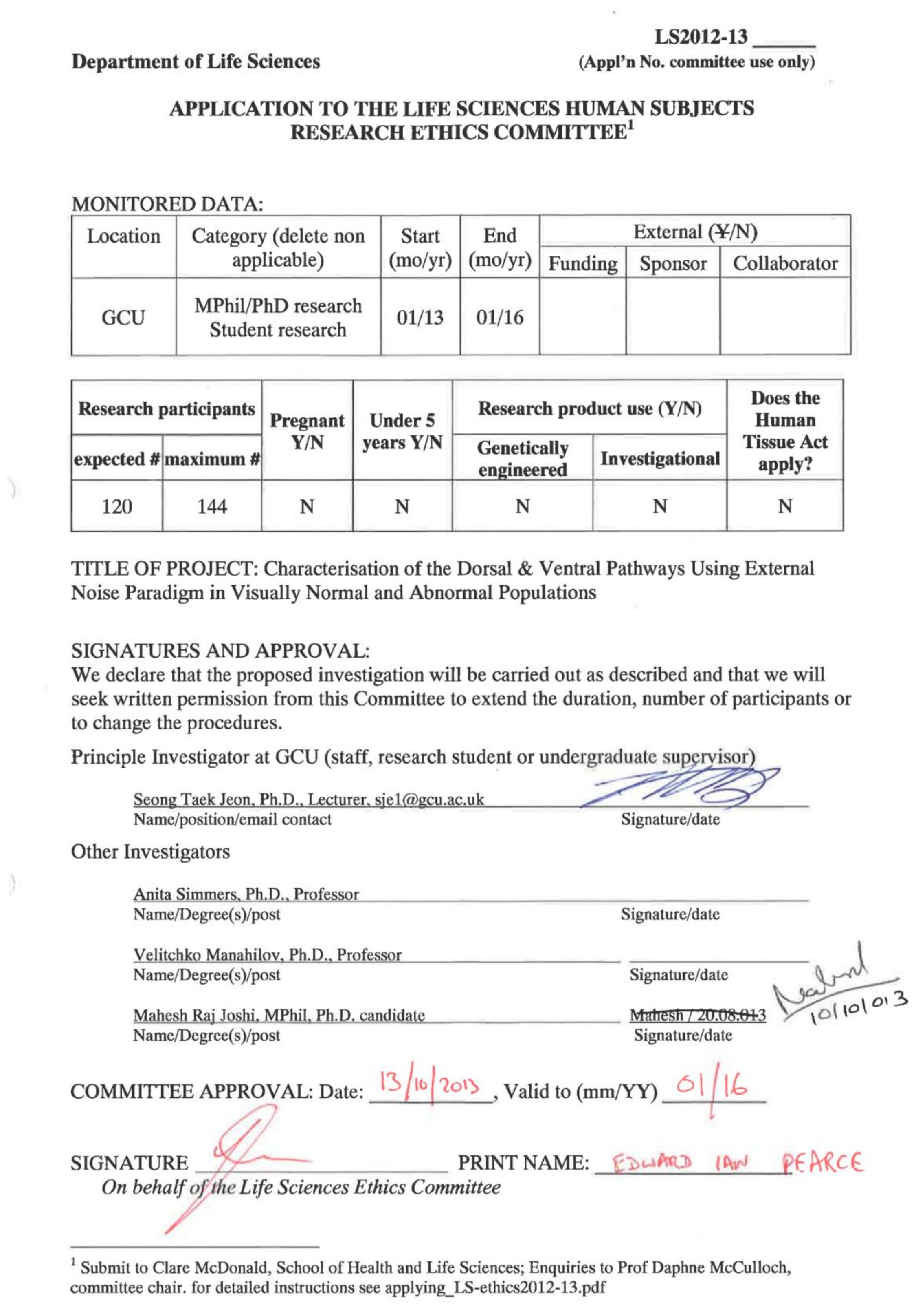

LS2012-13 ______
(Appl'n No. committee use only)

Department of Life Sciences

APPLICATION TO THE LIFE SCIENCES HUMAN SUBJECTS RESEARCH ETHICS COMMITTEE[1]

MONITORED DATA:

Location	Category (delete non applicable)	Start (mo/yr)	End (mo/yr)	External (~~Y~~/N)		
				Funding	Sponsor	Collaborator
GCU	MPhil/PhD research Student research	01/13	01/16			

Research participants		Pregnant Y/N	Under 5 years Y/N	Research product use (Y/N)		Does the Human Tissue Act apply?
expected #	maximum #			Genetically engineered	Investigational	
120	144	N	N	N	N	N

TITLE OF PROJECT: Characterisation of the Dorsal & Ventral Pathways Using External Noise Paradigm in Visually Normal and Abnormal Populations

SIGNATURES AND APPROVAL:
We declare that the proposed investigation will be carried out as described and that we will seek written permission from this Committee to extend the duration, number of participants or to change the procedures.

Principle Investigator at GCU (staff, research student or undergraduate supervisor)

Seong Taek Jeon, Ph.D., Lecturer, sje1@gcu.ac.uk
Name/position/email contact — Signature/date

Other Investigators

Anita Simmers, Ph.D., Professor
Name/Degree(s)/post — Signature/date

Velitchko Manahilov, Ph.D., Professor
Name/Degree(s)/post — Signature/date

Mahesh Raj Joshi, MPhil, Ph.D. candidate — ~~Mahesh / 20.08.013~~ 10/10/013
Name/Degree(s)/post — Signature/date

COMMITTEE APPROVAL: Date: 13/10/2013, Valid to (mm/YY) 01/16

SIGNATURE ______________________ PRINT NAME: EDWARD IAN PEARCE
On behalf of the Life Sciences Ethics Committee

---

[1] Submit to Clare McDonald, School of Health and Life Sciences; Enquiries to Prof Daphne McCulloch, committee chair. for detailed instructions see applying_LS-ethics2012-13.pdf

Department of Life Sciences **LS2012-13** ______

Applicant's name: Mahesh Raj Joshi Supervisor (if applicable): Seong Taek Jeon

TITLE OF PROJECT: Characterisation of the Dorsal & Ventral Pathways Using External Noise Paradigm in Visually Normal and Abnormal Populations

Reviewer Checklist and Feedback

Name of reviewer: EDWARD IAN PEARCE

Reviewer checklist:	NA	Accept	Minor revision	Major amendment
Participant information and consent			✓	
Questionnaire(s)	✓			
Aims, design and methods	--	✓		
Participant and recruitment details		✓		
Study design and procedures		✓		
Pharmaceuticals	✓			
Risk assessment	✓			
Collaborator(s) details	✓			
Letter of support from external agency	✓			
Other (see comments)				

Comments:

Reviewer's decision:

○ *Amendments are required before approval. Please make the changes as advised and return to the Committee for approval

○ *This application requires consideration by the full Life Sciences committee and has been forwarded for this further review.

○ ✓ *There are minor points highlighted on the attached application or communicated by email. To avoid delay, approval is granted from today and you can go forward with all aspects of your data collection2,3. You must make the suggested amendments and submit the revised application (by email to c.mcdonald@gcu.ac.uk)

○ The approval is given with the signature on page 1 of the application proforma, which does not require amendment1,2.

PI or Supervisor, please pass copies to the other investigators and/or project students.

Signed: ______________________ Date: 13/10/2013

---

[2] Any further announcements, emails, posters etc. for recruitment require prior approval

[3] You must file an amendment if you change your protocol or recruit more participants than those stated.

9.2 Appendix 2: Peer Reviewed Papers and Abstracts

Investigative Ophthalmology & Visual Science

Visual Psychophysics and Physiological Optics

Concurrent Investigation of Global Motion and Form Processing in Amblyopia: An Equivalent Noise Approach

Mahesh R. Joshi, Anita J. Simmers, and Seong T. Jeon

Vision Sciences, Department of Life Sciences, Glasgow Caledonian University, Glasgow, United Kingdom

Correspondence: Seong T. Jeon, Vision Sciences, Department of Life Sciences, Glasgow Caledonian University, Glasgow, G4 0BA, United Kingdom;
Simon.Jeon@gcu.ac.uk.

Submitted: November 9, 2015
Accepted: July 19, 2016

Citation: Joshi MR, Simmers AJ, Jeon ST. Concurrent investigation of global motion and form processing in amblyopia: an equivalent noise approach. *Invest Ophthalmol Vis Sci*. 2016;57:5015–5022. DOI:10.1167/iovs.15-18609

Purpose. Directly comparing the motion and form processing in neurologic disorders has remained difficult due to the limitations in the experimental stimulus. In the current study, motion and form processing in amblyopia was characterized using random dot stimuli in different noise levels to parse out the effect of local and global processing on motion and form perception.

Methods. A total of 17 amblyopes (8 anisometropic and 9 strabismic), and 12 visually normal subjects monocularly estimated the global direction of motion and global orientation in random dot kinematograms (RDK) and Glass patterns (Glass), whose directions/orientations were drawn from normal distributions with a range of means and variances that served as external noise. Direction/orientation discrimination thresholds were measured without noise first then variance threshold was measured at the multiples of the direction/orientation threshold. The direction/orientation and variance thresholds were modelled to estimate internal noise and sampling efficiency parameters.

Results. Overall, the thresholds for Glass were higher than RDK for all subjects. The thresholds for both Glass and RDK were higher in the strabismic eyes compared with the fellow and normal eyes. On the other hand, the thresholds for anisometropic amblyopic eyes were similar to the normal eyes. The worse performance of strabismic amblyopes was best explained by relatively low sampling efficiency compared with other groups ($P < 0.05$).

Conclusions. A deficit in global motion and form perception was only evident in strabismic amblyopia. Contrary to the dorsal stream deficiency hypothesis assumed in other developmental disorders, deficits were present in both motion (dorsal) and form (ventral) processing.

Keywords: amblyopia, motion perception, form perception, dorsal stream dysfunction, noise

Amblyopia is a neurodevelopmental disorder characterized by reduction in either monocular or binocular vision without any organic cause. The primary site of the visual deficit in amblyopia is reported to be the striate cortex.[1–3] However, the functional visual deficits in amblyopia seem to spread beyond primary visual cortex to extra striate cortical areas.[4–8]

Global motion direction judgment or perceiving a global orientation from the distribution of locally oriented elements is accomplished in two stages where the local direction and orientation are initially encoded in early visual areas of primary visual cortex/area V2 (V1/V2), after which the global processing is thought to occur at higher extra striate cortical areas; middle temporal area (MT), medial superior temporal (MST) for motion, and V4 for form.[9,10] Behavioral studies in humans have reported reduced sensitivity to both global motion and global form in amblyopia.[11–15] The motion coherence threshold remained elevated even after the local deficits from V1/V2 such as in contrast sensitivity was accounted for.[13,14,16,17] However, other studies have reported normal performance in amblyopes using a different experimental design where the global motion direction judgement was evaluated in varying degrees of local directional noise.[15,18] Global form is also compromised in amblyopes as observed by abnormal global form coherence thresholds for Glass patterns (Glass) and translational/rotational line segments.[12,19,20] However, other studies have reported inconsistent results where discrimination of the mean global orientation from an array of Gabor patches with different orientations is reported to be normal,[15] slightly reduced,[11] or even abnormal.[21]

Several reviews of global motion and form perception in a range of developmental disorders[22–24] including amblyopia[12] indicate that the motion processing is more affected than the form processing. According to the ‘two-streams hypothesis’,[25] the global motion and form perceptions are processed along the dorsal and ventral streams, respectively, bifurcated from early cortical areas.[26–28] There have been a number of attempts to compare these two domains of vision by measuring the outputs from the processing of the corresponding stream using similar stimuli. For example, studies used translational random dot kinematograms (RDK) for motion and oriented streaks for form created by superimposing the multiple still frames from the respective RDK to compare the amblyopic performance in two streams.[12,29] The results showed deficits along both visual processing streams, with a relatively larger deficit in motion processing (dorsal stream) compared with the form processing (ventral stream). The superimposed orientation streaks are considered, however, no different from line segments where the global integration of local elements does not seem necessary to do the task.[22] It is also difficult to ascertain if the deficit observed in either or both streams is purely stream-

Table 1. The Clinical Details of the Amblyopic Participants

Type of Amblyopia	ID	Age, y	IOD	Refraction RE	Refraction LE	Cover Test	Stereo, arc sec
Anisometropic	KW	18	0.1	−6.25/−1.25*170	−6.50/−1.50*180	Exophoria	20
	RK	19	0.22	+1.75/−1.00*180	0.00	Exophoria	85
	LC	18	0.14	+3.75/−1.00*170	+5.25/−1.25*180	Exophoria	36
	HM	18	0.18	−2.75/−3.00*180	−2.25/−1.75*10	Exophoria	75
	MR	20	0.16	+6.00/−3.75*10	+5.00/−3.25*180	Esophoria	100
	LS	19	0.40	+5.25/−0.50*105	+3.50/−0.50*105	Esophoria	No
	MI	19	0.20	−3.50/−0.50*60	−8.50/−1.50*140	Exophoria	40
	HMc	19	0.26	−0.25	+1.00/−1.00*90	Exophoria	20
Strabismic	SS	20	0.41	+4.50/−0.50*172	+5.75/−1.00*22	Esotropia	No
	JR	43	0.48	−2.50	−2.50	Esotropia	No
	CO	20	0.34	+4.00/−1.50*175	+4.50/−1.50*90	Int. Esotropia	200
	HQ	34	0.50	−1.50/−2.00*5	−1.50/−2.00*5	Exotropia	No
	MR	48	0.26	+3.00/−2.50*90	+1.50	Esotropia	No
	SM	28	0.6	+0.50	+3.50/−1.50*90	Exotropia	No
	NJ	21	0.4	+1.00	+3.00	Esotropia	No
	JW	57	0.24	+0.75/−0.25*25	+3.00/−0.50*25	Esotropia	No
	KH	22	0.2	+8.50/−3.50*25	+9.00/−3.00*170	Esotropia	No

IOD, interocular difference; RE, right eye; LE: left eye.

specific, mere collateral damage from the early areas (V1/V2) common to both streams, or a combined effect of both. Direct comparison of the two streams can be made more precise by making stimulus parameters as similar as possible except for the domain specific outputs of interest.

Many psychophysical studies of global processing mechanisms have used coherence tasks where one measures the minimum proportion of coherent elements to random elements needed for a reliable discrimination. However, this paradigm is limited in separating the local influence of the early visual areas (V1/V2) shared by both streams from the global aspect of visual processing by the higher extra striate areas specific to each stream. This limitation can be resolved by measuring outputs in varying levels of noise added to the stimuli.[30]

In the current study, we measured global motion and form discrimination thresholds in normal and amblyopic subjects to probe and compare the differences (or similarities) in their motion and form processing using similar stimulus with and without external noise to investigate how their performance are affected by the local and global parameters of the task.

METHODS

Participants

A total of 17 amblyopes (strabismic = 9, anisometropic = 8, mean age = 26.06 ± 12.09 years) with interocular acuity difference (IOD) of greater than or equal to 0.2 logMAR or past history of amblyopia treatment (Table 1), and 12 normal controls (mean age = 28 ± 5.24 years) were recruited. Viewing was monocular in all cases. The control group had normal binocular vision and normal or corrected-to-normal visual acuity. All experiments were conducted with the best (full) correction after refraction by an optometrist, who is one of the authors (MRJ).

The study was conducted in accordance with The Code of Ethics of the World Medical Association, Declaration of Helsinki, and approved by the Life Sciences Human Subjects Research Ethics Committee of the Glasgow Caledonian University. Informed consent was obtained once the nature and possible consequences of the experiment had been explained.

Stimuli

The experimental stimuli were generated using MATLAB 64 bit version R2013a (The MathWorks, Natick, MA, USA) with Psychophysics Toolbox-3 extensions[31,32] and displayed on a 21" Sony FD Trinitron monitor with a pixel resolution of 1920 × 1440 and refresh rate of 75 Hz (Sony, Tokyo, Japan) powered by an Apple computer with OS X (Apple, Cupertino, CA, USA) and ATI Radeon HD 5770 1024 MB graphics card. Across all the experiments, stimulus parameters across domains (i.e., form and motion) were kept identical except for the tasks specific to each domain (orientation versus direction discrimination). For example, both form and motion stimuli were composed of same number of black dots of the same size (0.166°) and contrast (95% Michelson contrast). They were displayed for 0.5 seconds in a circular aperture of 10° when viewed at 50 cm.

For the anisometropes and six normal controls (Experiment 1), both motion and form stimuli were composed of 500 dot elements with a dot density of 12.81 dots/deg^2. The overall dot speed in the motion stimulus (RDK) was 10°/sec. The dots had a limited lifetime of six frames (0.08 sec), upon completion of which each dot was randomly regenerated within the stimulus area. The form stimulus was a Glass pattern[33] generated by superimposing two identical copies of 250 random dots at the center of the display, with a linear displacement of 0.266° to create a translation Glass pattern. In essence, the dipoles in the Glass pattern are the spatial representation of two snapshots of the RDK stimulus captured in two different time frames. The direction of motion of the individual dot elements in the RDK and the orientation of the dipole elements in the Glass pattern were derived from a Gaussian distribution with a prescribed mean and SD that served as external noise (Fig. 1). The level of external noise was determined by the SD of the distribution with the mean of the distribution centered at different angles from the vertical reference (90°). The overall direction of the RDK and orientation of the Glass pattern (right or left of vertical) was randomized. For the strabismic amblyopes and remaining six normal controls (Experiment 2), both RDK and Glass patterns were composed of a total of 240 dots to facilitate the discrimination of Glass patterns (refer to discussion).

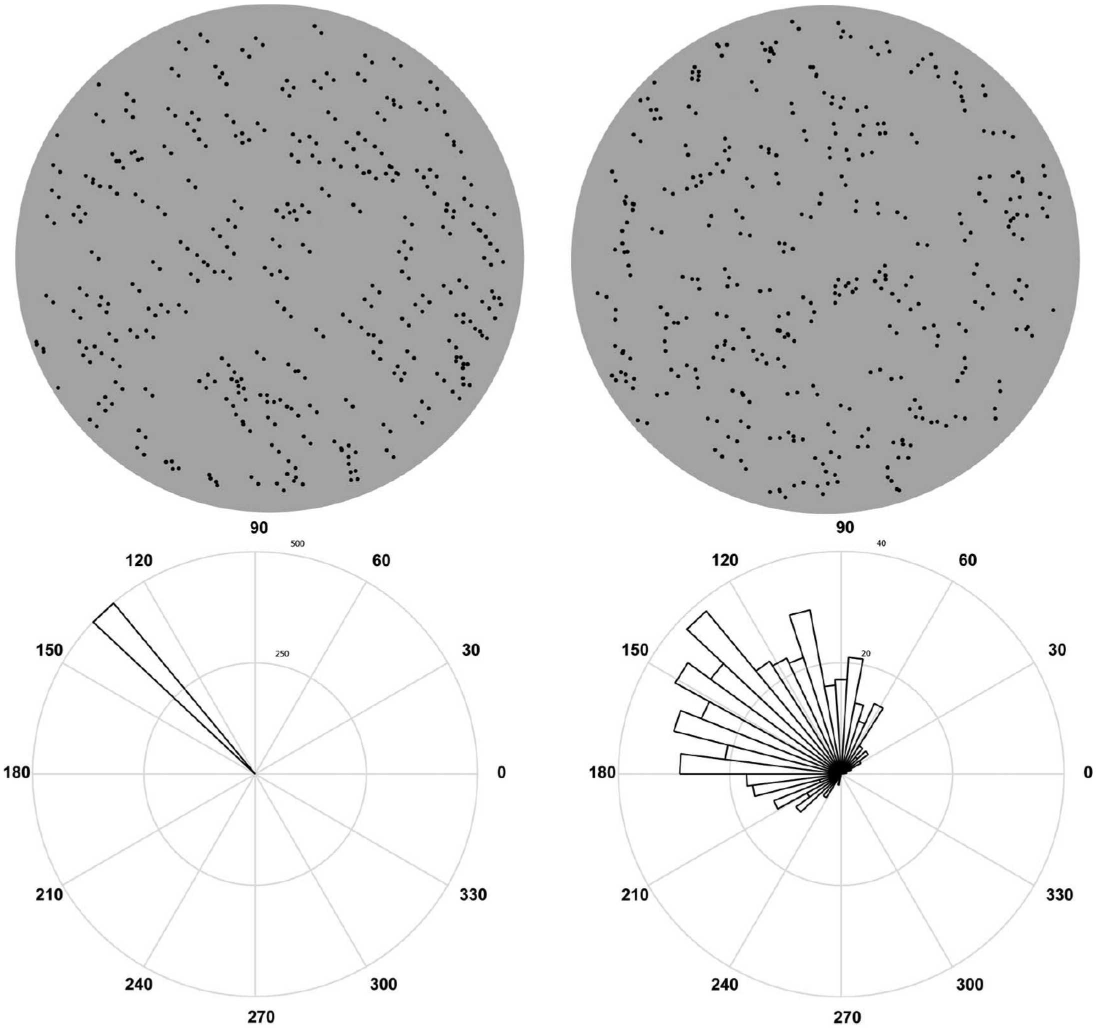

FIGURE 1. (*Top*) Example of Glass pattern stimuli with the same mean orientation and different variances. (*Bottom*) Angle histograms showing the distribution of dipole orientations in each pattern. The orientations of individual dipoles are generated from a Gaussian distribution with the mean (μ) of the distribution representing global orientation of the Glass pattern (*left of the vertical* shown here). The increase in the SD of the distribution (σ) increases the noise in the stimulus (*from left to right*).

Procedure

All participants completed the experiments in a dark room with the computer monitor being the only source of light. The participant's task in each trial was to discriminate the mean direction (RDK) of dots or orientation (Glass) of dipoles from the vertical (90°) reference.

To facilitate the data collection,[34] we first measured fine direction/orientation discrimination threshold at no noise where the overall direction/orientation in each trial was adaptively changed by the 3-down-1-up staircase. Then, the multiples (2× and 4× for anisometropic amblyopes and 3× only for strabismic amblyopes) of the initial direction/orientation thresholds at no noise were used to evaluate the threshold variance with a 3-down-1-up staircase. The staircase in no noise started with the mean direction/orientation of ±10° from vertical. The staircases in high noise condition started from a SD of 10° with the mean fixed at the multiples of direction/orientation threshold determined previously for each subject. All staircases terminated after 10 reversals or 100 trials, whichever was reached first. The thresholds were then calculated as a geometrical mean of the last seven reversals. All participants completed two sessions of 15 practice trials for each noise condition. Upon the satisfactory completion of the practice session, a full experimental session was commenced. The total time for each experiment (RDK or Glass pattern) including practice sessions was approximately 15 to 20 minutes.

The thresholds were modelled by the equation below to relate the direction/orientation offset thresholds to the external noise (σ_{ext}), internal equivalent noise (σ_{eq}) and

TABLE 2. The Table Provides the Mean Thresholds With the Values in Parenthesis Representing the Standard Deviation

Eyes	Glass No Noise	Glass High Noise (y @ x)	RDK No Noise	RDK High Noise (y @ x)
Normal	4.22 (2.19)	11.71 (1.73) @ 19.67 (1.77)	1.99 (1.72)	5.67 (1.50) @ 25.11 (1.45)
Aniso (Fellow)	4.36 (2.17)	14.19 (1.71) @ 16.83 (3.00)	2.55 (1.59)	5.63 (1.52) @19.79 (1.42)
Aniso (Amblyopic)	4.35 (1.98)	15.83 (1.66) @ 23.48 (1.43)	2.69 (1.23)	8.14 (1.50) @ 24.15 (1.66)
Strab (Fellow)	5.45 (1.76)	14.56 (1.62) @ 21.99 (1.14)	3.03 (1.52)	7.38 (1.71) @ 21.43 (1.24)
Strab (Amblyopic)	7.91 (1.34)	21.94 (1.23) @ 22.87 (1.39)	3.13 (1.70)	13.82 (1.45) @ 28.98 (1.35)

The data for the high noise condition represents the mean orientation/direction offset at (@) mean variance thresholds. Anisometropic, Ansio; Strabismic, Strab.

sampling efficiency (*Eff*) parameters.[35]

$$\tau_{obs} = \sqrt{\frac{\sigma_{eq}^2 + \sigma_{ext}^2}{Eff}} \tag{1}$$

For each task (Glass or RDK), the numbers of σ_{eq} & *Eff* needed to model the thresholds can range from two to six given the number of eyes (normal versus fellow versus amblyopic eye for patients). Among all the possible models, here we illustrate only four of them: a full model with six parameters (i.e., three pairs of σ_{eq} & *Eff* for normal, fellow and amblyopic eye); two models with four parameters (one σ_{eq} with three *Eff* or three σ_{eq} with one *Eff*); the most parsimonious model with two parameters (single σ_{eq} and *Eff*). Among the layers of nested models, the best model was selected by testing the goodness of fits between the models hierarchically with the following:

$$F(df_1, df_2) = \frac{(r_{full}^2 - r_{reduced}^2)/df_1}{(1 - r_{full}^2)/df_2} \tag{2}$$

Where, $df_1 = k_{full} - k_{reduced}$ and $df_2 = N - k_{full}$. The k is the number of parameters in each model, and N is the number of predicted data points.

RESULTS

Figure 2 shows the raw thresholds for both Glass and RDK across the experiments 1 and 2. There was no significant difference in the orientation/direction discrimination thresholds for normal controls between experiments 1 and 2 using 500 and 240 dot stimuli ($PS > 0.05$). The thresholds for normal controls were hence collapsed for further data analysis. The thresholds for Glass were higher than RDK for all participants. The thresholds for the strabismic amblyopes were elevated compared to normal for both RDK and Glass. On the other hand, the thresholds for anisometropic amblyopes were similar to normal for both stimuli. Table 2 summarizes the Figure 2 by providing the mean thresholds at different noise levels for normal and amblyopes across tasks.

Experiment 1: Anisometropic Amblyopia

The nested models were statistically tested to determine the influence of internal noise/sampling efficiency on the orientation/direction discrimination. The nested model results for orientation discrimination are provided in Figure 3. All three reduced models (Figs. 3B–D) were similar to the full model (Fig. 3A), 1 σ_{eq} and 3 *Eff* [$F(2,62) = 0.163$, $P > 0.1$], 3 σ_{eq} with 1 *Eff* [$F(2,62) = 0.244$, $P > 0.1$], and 1 σ_{eq} with 1 *Eff* [$F(2,64) = 0.252$, $P > 0.1$]. Hence, the most parsimonious model (1 σ_{eq} and 1 *Eff*) showing no difference in parameters between normal, fellow, and amblyopic eyes was chosen as the best model.

Similar nested model analysis for the direction discrimination among normal, fellow, and amblyopic eyes showed that the simplest model with both σ_{eq} and *Eff* constrained across the eyes best described the threshold data [$F(2,64) = 2.84$, $P > 0.05$] (Fig. 4).

Experiment 2: Strabismic Amblyopia

All nine strabismic amblyopes completed the RDK experiment while only six could detect the Glass pattern structure. The

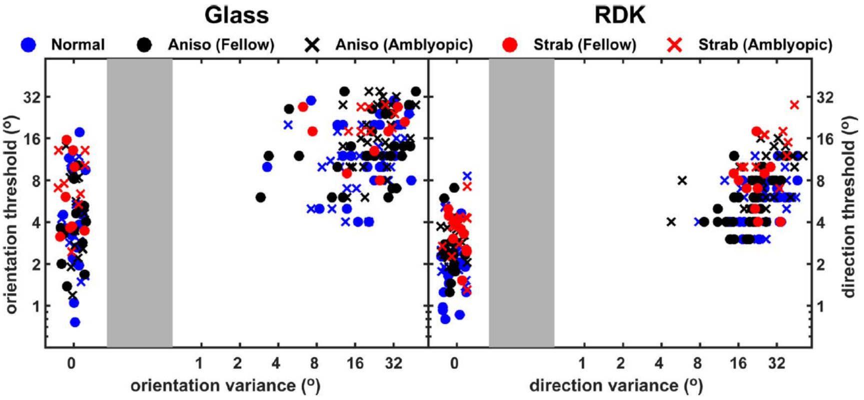

FIGURE 2. A scatterplot of individual thresholds for all participants for Glass and RDK. Small random jitters are added to the thresholds at no noise for better presentation.

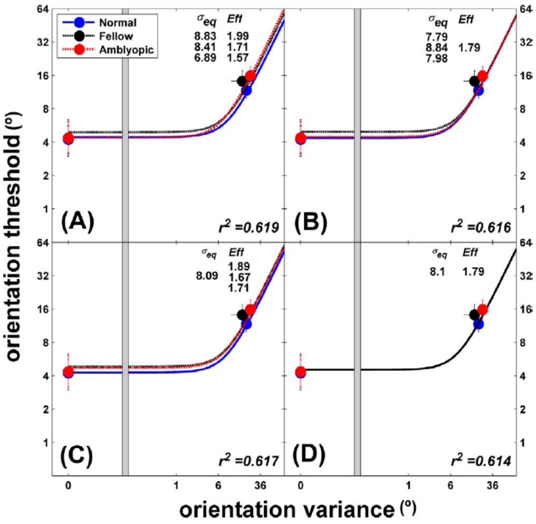

FIGURE 3. Nested models for the mean orientation discrimination data for the anisometropic amblyopes ($n = 8$) and normal controls ($n = 12$), relating the orientation offset and variance thresholds to different values of the internal noise and sampling efficiency; full model (**A**), reduced model with *Eff* constrained (**B**), reduced model with σ_{eq} constrained (**C**), and the simplest model with both σ_{eq} and *Eff* constrained (**D**). The best fitting parameters (σ_{eq} and *Eff*) and the goodness of fit (r^2) of each model are provided. *Error bars*: 95%CI. Two high noise conditions (2× and 4×) are averaged to represent a single high noise point.

orientation and direction discrimination thresholds for the amblyopic eye were higher than both fellow eye and normal eye. The nested model testing (Fig. 5) showed that compared with the full model the reduced model with a single σ_{eq} and independent *Eff* was statistically the best model to describe the participants performance for both orientation discrimination [$F(2,22) = 0.42$, $P > 0.1$] and direction discrimination [$F(2,32) = 0.53$, $P > 0.1$]. The reduced models with σ_{eq} constrained for each domain were treated as the full model and further compared against the simplest model (1 σ_{eq} and 1 *Eff*). The results showed that the simplest model resulted in significantly poorer fits ($PS < 0.05$), confirming that the models with σ_{eq} constrained and independent *Eff* were the statistically the best models for both global orientation and direction discrimination.

The nested modelling showed that the difference in sampling efficiency best described the raised direction/orientation thresholds in strabismic amblyopes. To compare the individual strabismic sampling efficiency against the normal in each domain, the individual strabismic thresholds were fitted to the nested models with normal thresholds. The log sampling efficiency ratio of normal to amblyopic/fellow eye, respectively, (Fig. 6) was then calculated. The sampling efficiency was poorer in the amblyopic eye for both global motion and global form compared with the normal controls. The three amblyopes (SM, MR, and JR; Fig. 5A) who could not detect the Glass pattern structure also showed the poorest efficiency in the global motion task. For the fellow eye, seven of nine amblyopes had poorer efficiency for global motion and three out of six amblyopes showed poorer efficiency for the global form.

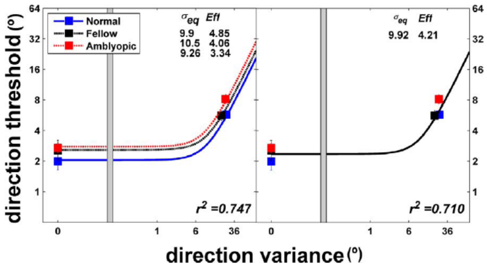

FIGURE 4. Nested models (*full, left panel and statistically chosen, right panel*) for the mean direction discrimination data for the anisometropic amblyopes ($n = 8$) and normal controls ($n = 12$), relating the direction offset and variance thresholds to different values of the internal noise and sampling efficiency. The best fitting parameters (σ_{eq} and *Eff*) and the goodness of fit (r^2) of each model are provided. *Error bars*: 95%CI.

DISCUSSION

Global Motion Discrimination in Amblyopia

Fine global motion discrimination thresholds were normal in anisometropic amblyopia but abnormal in the strabismic amblyopes. This is in contrast to previous studies, which have reported normal thresholds in both types of amblyopia when using RDK composed of micro pattern elements.[15,18] These studies, however, initially normalized the local direction discrimination threshold (angle from vertical reference) of a single micro pattern element between the amblyopic and fellow eye by adjusting stimulus contrast then used the

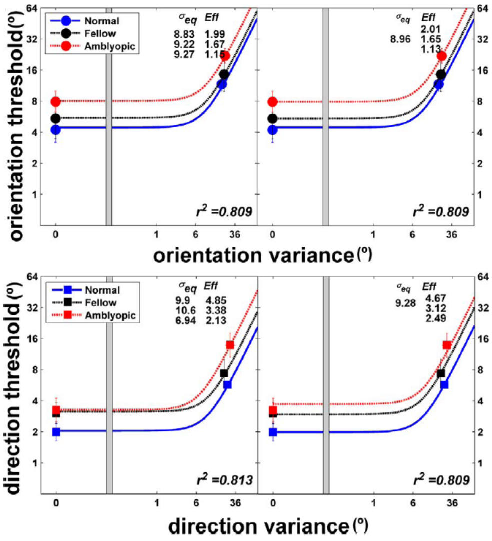

FIGURE 5. Nested models (*full, left panels and statistically chosen, right panels*) for the mean orientation discrimination threshold data for the normal ($n = 12$), fellow ($n = 6$), and amblyopic ($n = 6$) eyes (*upper panels*) and direction discrimination threshold data for the normal ($n = 12$), fellow ($n = 9$), and amblyopic ($n = 9$) eyes (*lower panels*). The orientation/direction offset and variance thresholds are related to different values of the internal noise and sampling efficiency. The best-fitting parameters (σ_{eq} and *Eff*) and the goodness of fit (r^2) of the each model is provided. *Error bars*: 95%CI.

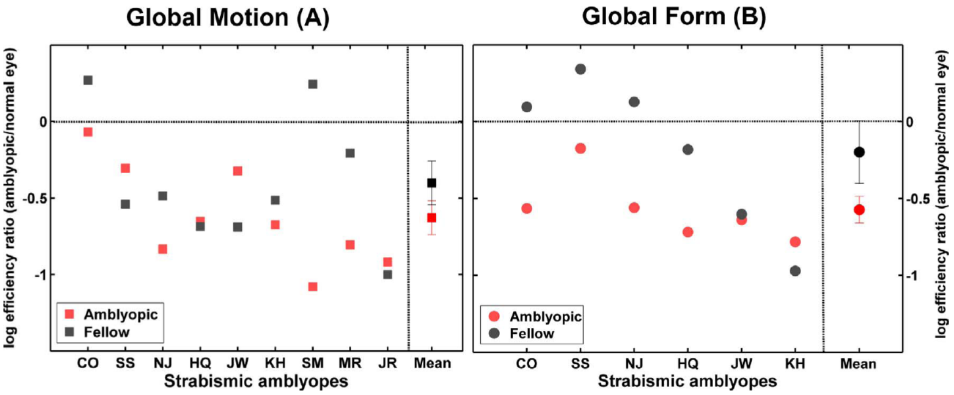

Figure 6. The log efficiency ratio (amblyopic/normal participant) for the global motion (**A**) and global form (**B**) for strabismic amblyopes and mean data. The data point lying above the *horizontal dotted lines* represents no deficiency in comparison to the normal eye; the points along the negative values represent how deficient the amblyopes are with respect to the normal. *Error bars*: 95%CI.

normalized contrast for the global motion discrimination with multiple micro patterns. In the current study, RDKs with high contrast dot elements (95%) were used to study both amblyopic and fellow eye performance. These differences in the stimulus and the experimental procedure may have resulted in different results obtained for strabismic amblyopia. Our results are, however, in line with previous reports of increased motion coherence thresholds in strabismic amblyopes.[13,14,16,17]

Differences in performance between anisometropic and strabismic amblyopia have been reported for a range of visual functions[36] such as optotype acuity,[37] vernier acuity,[38] and contrast sensitivity.[37] Such differences are supported by the results of physiological studies where a progressive reduction of neural responses in extra striate cortical areas has been reported in strabismic but not anisometropic[36] amblyopia.[39,40]

The nested model testing in this study revealed that the higher direction discrimination thresholds in strabismic amblyopes were due to a reduced efficiency at the global processing stage. The normal internal equivalent noise suggests that local motion processing is intact in both types of amblyopia, in agreement with other studies.[13,14,17,41] The direction sensitive cells stimulated by the amblyopic eye in V1 are also reported to be normal in anisometropic and strabismic primates.[40] Our finding of abnormal global processing in strabismic amblyopia is supported by previous physiological and imaging studies that reported a reduced contribution from the amblyopic eye to extra striate motion areas (MT, MST).[4,5] The results suggest that the local direction processing at early visual areas is normal in amblyopia with only the strabismic amblyopes showing a deficit at a later global processing stage.

Global Form Discrimination in Amblyopia

Global form perception in the Glass pattern was found to be normal in anisometropic amblyopia but abnormal in strabismic amblyopia. Notably, the strabismic amblyopes were not able to complete the evaluation for the Glass pattern with 500 dot elements used in the first experiment for anisometropic amblyopia. However, when the number of elements was reduced to 240, six of nine strabismic amblyopes could reliably detect the structure of the Glass pattern. This could have been due to the increase in correspondence noise in a Glass pattern with a higher dipole density. This dependency of performance in amblyopia on the number of elements has been previously reported for a mean orientation discrimination task with Gabor patches.[42] However, even with a reduced number of dipole elements, three strabismic amblyopes could still not reliably detect the Glass pattern structure.

As far as we are aware, this is the first study that used Glass pattern stimuli to determine fine orientation discrimination in amblyopia. Mansouri and Hess[15] reported normal thresholds in both anisometropic and strabismic amblyopes using Gabor patches in a global orientation discrimination task. However, other studies using similar Gabor patch stimuli have reported elevated orientation discrimination thresholds in both anisometropic and strabismic amblyopia.[11,21]

Our results are in agreement with studies that have used Glass patterns to report elevated global form coherence threshold in humans[19] and macaques[43] with amblyopia. Similarly the inability of some strabismic amblyopes to reliably detect the structure of the translational Glass pattern observed in the current study has also been reported previously.[19] This inability does not appear to be related to the severity of the amblyopia as an amblyope (MR) with the least IOD (0.26) and another amblyope (SM) with the largest IOD (0.6) failed to detect the Glass pattern. This is in line with previous report of inability of strabismic amblyope with relatively small IOD to detect the structure of translational Glass pattern.[19]

The apparent difference between these findings could be due to the differences in the processing of the different experimental stimuli (e.g., Gabor patches versus Glass pattern with dot elements). The orientation discrimination in a Glass pattern is based on extracting local orientation cues followed by the global averaging. However, in the line segment and Gabor patches the local orientation extraction does not seem necessary and the stimuli are processed as extended contours.[22] Hence, the discrimination of a Glass pattern is a more complex task than either the Gabor patches or the line segments. This possible difference is also reflected in better sensitivity to the line segments compared with the Glass pattern in visually normal participants.[44,45] Further the averaging in Gabor patches and line segments may be influenced by the local lateral connections in V1, and hence these stimuli are not recommended for the evaluation of a global orientation judgment.[22] Because lateral connections in V1 would be expected to have a minimal influence in the perception of a dipole Glass pattern our results are more likely to reflect true global orientation processing. Even with the relative ease of detection of line segment stimuli, a study reported increased coherence thresholds for both the anisometropic and strabismic amblyopes with a translational line segment stimuli.[12]

The reduced fine orientation sensitivity in strabismic amblyopia appears to be due to the differences in the efficiency with which the local orientation cues are processed at the global level. The local orientation processing is also reported to be normal for simple grating stimuli[46] and Gabor patches,[47,48] once the spatial frequency and contrast deficiencies are accounted for. Simmers et al.[21] also reported normal local orientation discrimination abilities in both strabismic and anisometropic amblyopia with increased orientation coherence thresholds showing limited global processing.[21] Similarly physiological studies have also reported normal orientation selectivity in V1 cells isolated from anisometropic and strabismic amblyopic eyes.[40] The deficits in the global orientation processing meanwhile could be due to the reduced activity at the higher cortical areas of the ventral stream such as V4 and lateral occipital complex.[8]

Comparison of the Global Motion and Form Deficits in Amblyopia

The elevated thresholds for strabismic amblyopes along both domains were due to the under sampling of the local inputs at the global processing stage. This would suggest that the under sampling theory posited for other visual deficits in amblyopia[36,49] could be applicable to global motion and form processing as well. These deficits do not seem to be dependent on the visibility of stimuli as has been reported before for normal participants,[50] as the fellow eyes of strabismic amblyopes which had similar visual acuity to the normal eyes (independent t-test, $t\ (20) = 1.25$, $P > 0.05$) also showed raised thresholds for both motion and form domains.

Dorsal stream functions such as motion perception are reported to be affected in various developmental disorders including amblyopia,[12] leading to the suggestion of dorsal stream vulnerability.[22,23] Our results show that both streams are affected in strabismic amblyopia. However, some strabismic amblyopes were unable to even detect the structure of the Glass pattern, suggesting a more significant deficit for the perception of global form. The imaging and physiological studies also showed that both dorsal and ventral stream activity is reduced in amblyopia[4,5,7,8] while a study using amblyopic cats reported a larger deficit in the ventral stream compared to the dorsal stream.[39]

Two probable causes for a dorsal stream vulnerability are related to the anatomic aspects and the developmental trajectory of the dorsal stream.[23] The M-cells in retina and lateral geniculate nucleus, the early processors of the dorsal stream inputs, are more susceptible to the damage from pathologic changes due to their larger size and smaller population. In amblyopia, the deficits at the M-cell level should result in lower sensitivity at both local and global processing stages. But our results and a wide range of studies[13,14,17,41] suggest that the deficits in the motion domain are restricted mostly to the global processing level. Another explanation for the dorsal stream vulnerability in development disorders is due to the late development of the dorsal stream compared with the ventral stream functions.[23] For example, some studies reported that the global motion processing mechanisms follow a long and protracted developmental pattern extending beyond 14 years.[51–53] However, there are other studies reporting a similar maturation age for both global form and motion processing.[54,55]

Recent studies question the generalizability of dorsal stream vulnerability in neurologic developmental disorders.[22] For example, it is argued that most studies that reported dorsal stream vulnerability used incompatible stimuli to allow for a direct comparison between the visual processing streams.[22] Additionally, the global processing deficits in motion and form processing in developmental disorders including amblyopia seem to be task and stimuli dependent, hence generalizing the results from one task or stimuli as dorsal or ventral stream vulnerability may not be accurate.

Our results using similar random dot stimuli across the motion and form processing pathways suggest that tasks attributed to both the dorsal and ventral streams are affected in strabismic amblyopia with normal thresholds in anisometropic amblyopia. The results seem to suggest that the processing deficit in strabismic amblyopes is specific to the global processing stage along the higher extra striate areas ruling out the direct influence of the lower level deficits. In addition, the inability of some amblyopes to simply detect the structure formed by the Glass pattern would suggest a more profound deficit pertaining to ventral stream processing. This is contrary to the dorsal stream vulnerability previously reported in amblyopia, highlighting the need for further investigation.

Acknowledgements

Supported by the Visual Research Trust Equipment Grant R4304 (Glasgow, UK).

Disclosure: **M.R. Joshi**, None; **A.J. Simmers**, None; **S.T. Jeon**, None

References

1. Hess RF. Amblyopia: site unseen. *Clin Exp Opt*. 2001;84:321–336.
2. Wiesel TN, Hubel DH. Extent of recovery from the effects of visual deprivation in kittens. *J Neurophysiol*.1965;28:1060–1072.
3. Wiesel TN, Hubel DH. Single-Cell response in striate cortex of kittens deprived of vision in one eye. *J Neurophysiol*.1963;26:1003–1017.
4. El-Shamayleh Y, Kiorpes L, Kohn A, Movshon JA. Visual motion processing by neurons in area MT of macaque monkeys with experimental amblyopia. *J Neurosci*. 2010;30:12198–12209.
5. Thompson B, Villeneuve MY, Casanova C, Hess RF. Abnormal cortical processing of pattern motion in amblyopia: evidence from fMRI. *NeuroImage*. 2012;60:1307–1315.
6. Movshon JA, Eggers HM, Gizzi MS, Hendrickson AE, Kiorpes L, Boothe RG. Effects of early unilateral blur on the macaque's visual system. III. Physiological observations. *J Neurosci*. 1987;7:1340–1351.
7. Lerner Y, Pianka P, Azmon B, et al. Area-specific amblyopic effects in human occipitotemporal object representations. *Neuron*. 2003;40:1023–1029.
8. Muckli L, Kieß S, Tonhausen N, Singer W, Goebel R, Sireteanu R. Cerebral correlates of impaired grating perception in individual, psychophysically assessed human amblyopes. *Vision Res*. 2006;46:506–526.
9. Morrone MC, Burr DC, Vaina LM. Two stages of visual processing for radial and circular motion. *Nature*. 1995;376:507–509.
10. Wilkinson F, Wilson HR. Detection of global structure in Glass patterns: implications for form vision. *Vision Res*. 1998;38:2933–2947.
11. Husk JS, Hess RF. Global processing of orientation in amblyopia. *Vision Res*. 2013;82:22–30.
12. Simmers AJ, Ledgeway T, Hess RF. The influences of visibility and anomalous integration processes on the perception of global spatial form versus motion in human amblyopia. *Vision Res*. 2005;45:449–460.

13. Simmers AJ, Ledgeway T, Hess RF, McGraw PV. Deficits to global motion processing in human amblyopia. *Vision Res*. 2003;43:729–738.
14. Simmers AJ, Ledgeway T, Mansouri B, Hutchinson CV, Hess RF. The extent of the dorsal extra-striate deficit in amblyopia. *Vision Res*. 2006;46:2571–2580.
15. Mansouri B, Hess RF. The global processing deficit in amblyopia involves noise segregation. *Vision Res*. 2006;46: 4104–4117.
16. Aaen-Stockdale C, Ledgeway T, Hess RF. Second-order optic flow deficits in amblyopia. *Invest Ophthalmol Vis Sci*. 2007; 48:5532–5538.
17. Aaen-Stockdale C, Hess RF. The amblyopic deficit for global motion is spatial scale invariant. *Vision Res*. 2008;48:1965–1971.
18. Hess RF, Mansouri B, Dakin SC, Allen HA. Integration of local motion is normal in amblyopia. *J Opt Soc Am A*. 2006;23:986–992.
19. Rislove EM, Hall EC, Stavros KA, Kiorpes L. Scale-dependent loss of global form perception in strabismic amblyopia. *J Vis*. 2010;10(12):25.
20. Dallala R, Wang Y-Z, Hess RF. The global shape detection deficit in strabismic amblyopia: Contribution of local orientation and position. *Vision Res*. 2010;50:1612–1617.
21. Simmers AJ, Bex PJ. The representation of global spatial structure in amblyopia. *Vision Res*. 2004;44:523–533.
22. Grinter EJ, Maybery MT, Badcock DR. Vision in developmental disorders: is there a dorsal stream deficit? *Brain Res Bull*. 2010;82:147–160.
23. Braddick O, Atkinson J, Wattam-Bell J. Normal and anomalous development of visual motion processing: motion coherence and 'dorsal-stream vulnerability'. *Neuropsychologia*. 2003;41: 1769–1784.
24. Hamm LM, Black J, Dai S, Thompson B. Global processing in amblyopia: a review. *Front Psychol*. 2014;5:583.
25. Milner AD, Goodale MA. Two visual systems re-viewed. *Neuropsychologia*. 2008;46:774–785.
26. Livingstone M, Hubel D. Psychophysical evidence for separate channels for the perception of form, color, movement, and depth. *J Neurosci*. 1987;7:3416–3468.
27. Braddick OJ, O'Brien JMD, Rees G, Wattam-Bell J, Atkinson J, Turner R. Quantitative neural responses to form coherence in human extrastriate cortex. Paper presentend at: Neuroscience 2002. Washington, DC, November 7, 2002. Society for Neuroscience 32nd Annual Meeting.
28. Braddick OJ, O'Brien JM, Wattam-Bell J, Atkinson J, Hartley T, Turner R. Brain areas sensitive to coherent visual motion. *Perception*. 2001;30:61–72.
29. Simmers AJ, Ledgeway T, Hess RF, McGraw PV. Deficits to global motion processing in human amblyopia. *Vision Res*. 2003;43:729–738.
30. Dakin SC, Mareschal I, Bex PJ. Local and global limitations on direction integration assessed using equivalent noise analysis. *Vision Res*. 2005;45:3027–3049.
31. Brainard DH. The Psychophysics Toolbox. *Spat Vis*. 1997;10: 433–436.
32. Pelli DG. The VideoToolbox software for visual psychophysics: transforming numbers into movies. *Spat Vis*. 1997;10:437–442.
33. Glass L. Moire effect from random dots. *Nature*. 1969;223: 578–580.
34. Tibber MS, Kelly MG, Jansari A, Dakin SC, Shepherd AJ. An inability to exclude visual noise in migraine. *Invest Ophthalmol Vis Sci*. 2014;55:2539–2546.
35. Pelli DG. Effects of Visual Noise. Cambridge: Cambridge University; 1981.
36. Kiorpes L, McKee SP. Neural mechanisms underlying amblyopia. *Curr Opin Neurobiol*. 1999;9:480–486.
37. Levi DM, McKee SP, Movshon JA. Visual deficits in anisometropia. *Vision Res*. 2011;51:48–57.
38. Levi DM, Klein SA. Vernier acuity, crowding and amblyopia. *Vision Res*. 1985;25:979–991.
39. Schröder J-H, Fries P, Roelfsema PR, Singer W, Engel AK. Ocular dominance in extrastriate cortex of strabismic amblyopic cats. *Vision Res*. 2002;42:29–39.
40. Kiorpes L, Kiper DC, O'Keefe LP, Cavanaugh JR, Movshon JA. Neuronal correlates of amblyopia in the visual cortex of Macaque monkeys with experimental strabismus and anisometropia. *J Neurosci*. 1998;18:6411–6424.
41. Thompson B, Richard A, Churan J, Hess RF, Aaen-Stockdale C, Pack CC. Impaired spatial and binocular summation for motion direction discrimination in strabismic amblyopia. *Vision Res*. 2011;51:577–584.
42. Mansouri B, Allen HA, Hess RF, Dakin SC, Ehrt O. Integration of orientation information in amblyopia. *Vision Res*. 2004;44: 2955–2969.
43. Kiorpes L. Visual processing in amblyopia: animal studies. *Strabismus*. 2006;14:3–10.
44. Aspell JE, Wattam-Bell J, Braddick O. Interaction of spatial and temporal integration in global form processing. *Vision Res*. 2006;46:2834–2841.
45. Dakin SC. The detection of structure in glass patterns: psychophysics and computational models. *Vision Res*. 1997; 37:2227–2246.
46. Skottun BC, Bradley A, Freeman RD. Orientation discrimination in amblyopia. *Invest Ophthalmol Vis Sci*. 1986;27:532–537.
47. Demanins R, Hess RF, Williams CB, Keeble DRT. The orientation discrimination deficit in strabismic amblyopia depends upon stimulus bandwidth. *Vision Res*. 1999;39: 4018–4031.
48. Hess RF, Malin SA. Threshold vision in amblyopia: orientation and phase. *Invest Ophthalmol Vis Sci*. 2003;44:4762–4771.
49. Wang H, Levi DM, Klein SA. Spatial uncertainty and sampling efficiency in amblyopic position acuity. *Vision Res*. 1998;38: 1239–1251.
50. Burton EA, Wattam-Bell J, Rubin GS, Atkinson J, Braddick O, Nardini M. The effect of blur on cortical responses to global form and motion. *J Vis*. 2015;15(15):12.
51. Gunn A, Cory E, Atkinson J, et al. Dorsal and ventral stream sensitivity in normal development and hemiplegia. *Neuroreport*. 2002;13:843–847.
52. Hadad BS, Maurer D, Lewis TL. Long trajectory for the development of sensitivity to global and biological motion. *Dev Sci*. 2011;14:1330–1339.
53. Joshi MR, Falkenberg HK. Development of radial optic flow pattern sensitivity at different speeds. *Vision Res*. 2015; 110(part A):68–75.
54. Gordon G, McCulloch D. A VEP investigation of parallel visual pathway development in primary school age children. *Doc Ophthalmol*. 1999;99:1–10.
55. Parrish EE, Giaschi DE, Boden C, Dougherty R. The maturation of form and motion perception in school age children. *Vision Res*. 2005;45:827–837.

36th European Conference on Visual Perception, Bremen, Germany, 25 – 29 August 2013

Joshi M, Jeon S T, 2013; "Characterisation of the Dorsal and Ventral Pathways Using External Noise Paradigm" *Perception*, 42 ECVP Abstract Supplement, page 210

- Poster presentation

Current study evaluated the sensitivity to global motion and form perception which are presumably processed by two distinct visual pathways – dorsal and ventral respectively [Ungerleider and Mishikin, 1982, in: Analysis of Visual Behavior, Cambridge, MIT press] – in varying noise levels. We used Glass pattern [Glass, 1969, Nature, 223, 578-579] and random dot kinematogram (RDK) to evaluate and compare each pathway directly by making the experimental parameters as equivalent as possible in both tasks. Four normal observers discriminated global direction of 500 moving dots or overall orientation of 250 dipoles from 12 o'clock. For each trial, direction/orientation of a dot/dipole was sampled from a normal distribution with one of the eight predetermined direction/orientation variances ranging from ±1° to ±120°, whereas the mean direction/orientation to be discriminated was determined by the 3-down-1-up staircase. When plotted against noise levels, the thresholds remained constant at low variances and started to increase as variance increased. Except for one observer, individual thresholds for Glass pattern were consistently higher than those for RDK across the different variance levels; mean log threshold ratio (Glass/RDK) was 1.503±0.24. In the future, functional mechanisms of both pathways will be quantitatively modelled with consideration of noise.

Concurrent Characterization of Dorsal & Ventral Pathway with Equivalent Noise

Mahesh R. Joshi , Seong T. Jeon and Anita J. Simmers

Dept. of Vision Sciences, Glasgow Caledonian University, United Kingdom
correspondence: Mahesh.Joshi@gcu.ac.uk

Introduction:

- Previously, dorsal and ventral streams have been evaluated separately with respect to their implied functions[1].
- Here, we designed an experiment where one can:
  1. concurrently test and compare how different/similar their performance will be when tested on an (almost) identical dimension.
  2. parse out the influences of local and global constraints on motion and form integration using the equivalent noise approach.

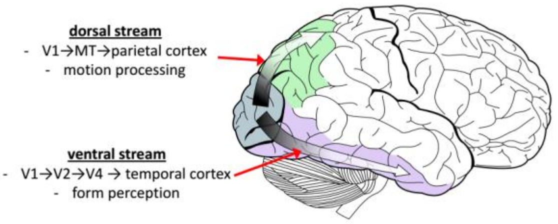

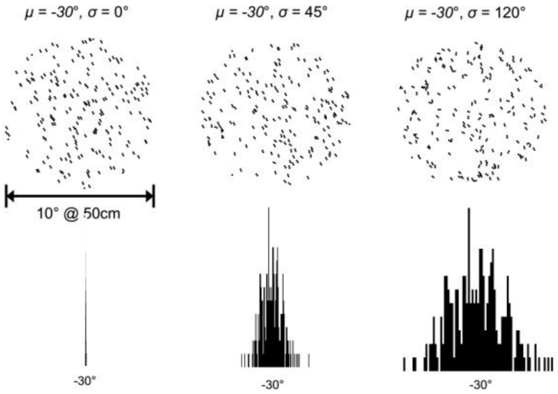

Fig: Example of Glass pattern stimuli to show how they were sampled from the Gaussian distributions with prescribed means & s.d.s

Method:

- Observers: 3 males, 1 female (normal, corrected normal acuity)
- Stimuli:

	RDK	Glass
dot size	0.083°	
number of dots	500	500 (250 dipoles)
dot to dot distance	N/A	0.133°
speed of dots	10°/sec	N/A
duration	500msec	
task	direction discrimination	orientation discrimination
variances (deg)	1, 5, 15, 30, 45, 60, 90, 120	

Results:

- Discrimination threshold for both stimuli were constant at lower variance before increasing proportionately with increased variance level.
- Threshold for Glass pattern was consistently higher than that for RDK at different orientation/direction variance evaluated. [mean (n=4) log threshold ratio (Glass/RDK) = 1.503±0.24]
- Thresholds between Glass and RDK seemed to run parallel across external noise, suggesting the difference in efficiency between the streams. [3]

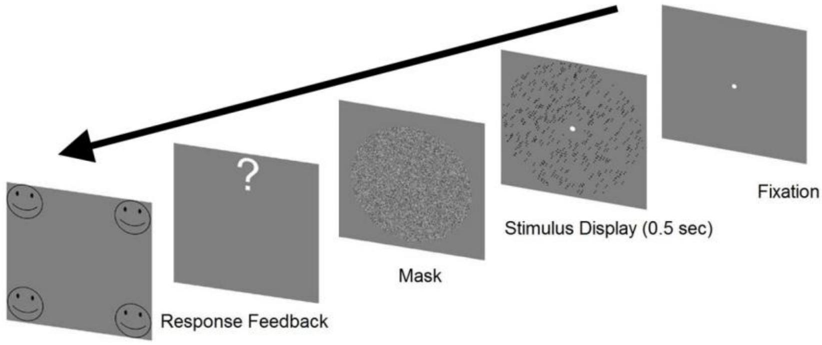

Fig: Schematic representation of a single trial of experiment. Stimulus display shows rightward oriented Glass pattern.

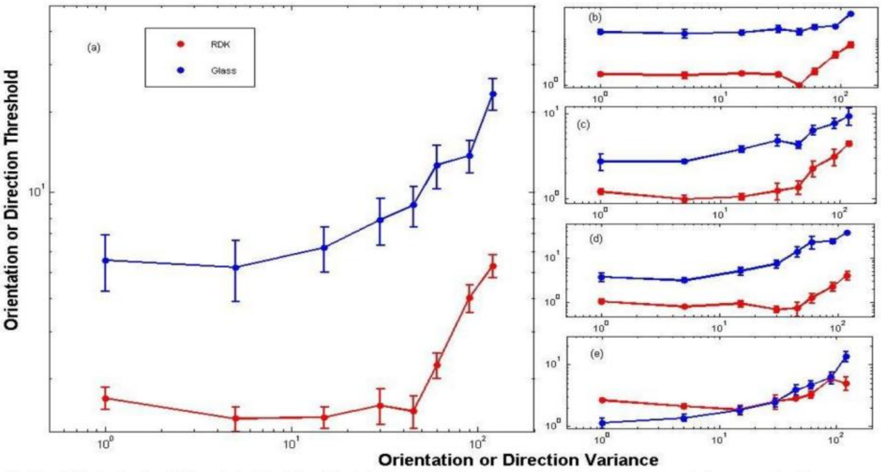

Fig : Thresholds for direction (RDK) and orientation (Glass) discrimination at different variance levels. Each data point represents the mean value of four observers (a) and individual observers (b,c,d,e). Error bars represent ±1 standard error of mean.

Discussion:

- Observers were more efficient at global motion processing in comparison to global form processing at all levels of external noise.
- Both processing stream is limited by similar internal noise.
- In the future, functional mechanisms of both pathways will be quantitatively modelled with consideration of noise.

References:

1. McIntosh, R. D. and T. Schenk (2009). "Two visual streams for perception and action: current trends." Neuropsychologia 47(6): 1391-1396.

2. Glass, L. (1969). "Moire effect from random dots." Nature 223(5206): 578-580.

3. Pelli, D. G. (1990) The quantum efficiency of vision. In: C. Blakemore (Ed.) *Vision: Coding and Efficiency* (pp. 3-24). Cambridge: Cambridge University Press.

14^{th} Annual Vision Sciences Society Meeting, Florida, USA, 16-21 May 2014. — Poster presentation

The British Congress of optometry and Vision Science, Cardiff, UK, 8-9 Sep 2014. — Oral presentation

Joshi M R, Simmers A J, Jeon S T; Limiting Factors in Form and Motion Perception: Shared locally, Differentiated Globally. *Journal of Vision* 2014;14(10):1418.

The visual system is functionally differentiated into dorsal (motion) and ventral (form) pathways, owing to the limitations in previously employed stimuli analogous comparison of the outputs from these two streams has proven difficult. In the current study, we adapted the equivalent noise paradigm to (1) disentangle the effect of local and global limits on motion and form perception and (2) compare how those constraints manifest in the two pathways. Six visually normal observers estimated the mean direction or orientation (clockwise or counter-clockwise of vertical) of a field of moving dots (Random Dot Kinematogram; RDK), static dipoles (Glass Pattern; Glass), or dynamic dipoles (dynamic Glass pattern; dGlass) whose direction/orientations were drawn from normal distributions with a range of direction/orientation variances. Thresholds (τ) obtained after five sessions for each stimulus condition showed a consistent pattern across observers and external variance levels, where τGlass>τdGlass>τRDK. Overall, the average threshold ratios between the tasks were constant (1.13, 0.72, and 0.42 log units across external variance levels for τGlass /τRDK, τdGlass/τRDK, and τGlass/τdGlass, respectively), suggesting a parallel vertical shift in performance. This pattern of result was confirmed by the mixed ANOVA where we found significant effect of the external variance (F6.03, 524.37= 185.33, $p < 0.001$) and the stimulus type (F2, 87 = 33.50, $p < 0.001$), but no interaction between them (F12.05, 524.37= 1.05, $p > 0.1$). Nested model comparisons where the thresholds were related to the external variances, internal noise, and the sampling efficiency revealed that change in performance between the tasks can be best described by the sole change in sampling efficiency with the internal noise remained invariable across tasks. Our findings provide a concurrent framework in which to consider global motion and form integration in human perception. This may prove valuable in diagnosing functional visual deficits in a range of developmental/cognitive disorders.

Limiting Factors in Form and Motion Perception: Shared Locally, Differentiated Globally

Mahesh R. Joshi , Seong T. Jeon and Anita J. Simmers

Vision Sciences, Glasgow Caledonian University, United Kingdom
correspondence: Mahesh.Joshi@gcu.ac.uk

Introduction:

- Previously, dorsal and ventral streams have been evaluated separately with respect to their implied functions.[1] We used physically equivalent stimuli (RDK and Glass pattern[2]) for the concurrent study of both streams by adapting the equivalent noise paradigm to

(1) disentangle the effect of local and global limits and
(2) compare how those constraints manifest in the two pathways.

- Sensitivity to implied motion (motion perceived from the form cues), processed in part along both streams was also evaluated with dynamic Glass pattern (dGlass).[3]

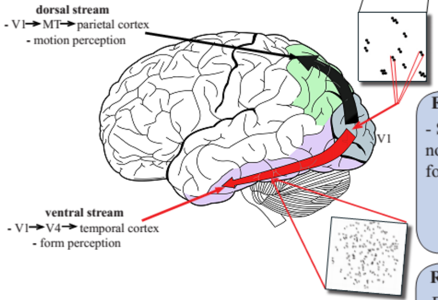

Schematic representation of the bifurcation of the visual pathway into dorsal and ventral streams. As illustrated local processing of Glass pattern occurs in V1 with global representation further down the ventral stream.

Methods:

- Observers: 5 males, 1 female (normal, corrected normal acuity, mean age 31.66 +/-6.86 years)

- Stimuli:

	RDK	Glass/dGlass
dot size	0.083°	
number of dots	500	500 (250 dipoles)
dot to dot distance	N/A	0.133°
speed of dots	10°/sec	N/A
duration	500msec	
task (discrimination)	direction of motion	orientation/implied direction
variances (deg)	0,2,4,8,16,24,32,40	

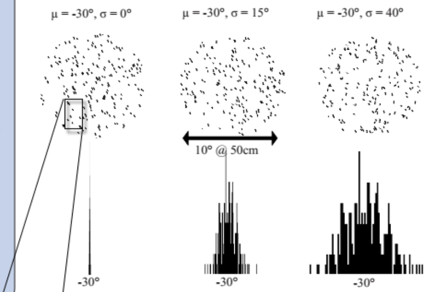

Example of Glass pattern stimuli to show how they were sampled from the Gaussian distributions with prescribed means & s.d.s

Equivalent noise paradigm

- Sensory thresholds were related to the external noise with the linear amplifier model[4] expressed by following equation.

$$\tau_{abs} = \sqrt{\frac{\sigma_{eq}^2+\sigma_{ext}^2}{Eff}}$$

where,
τ_{abs} = threshold
σ_{eq} = equivalent internal noise
σ_{ext} = external noise
Eff = sampling efficiency

Results:

- Discrimination threshold for three stimuli were constant at lower variance before increasing proportionately with variance level. Thresholds(τ) showed a consistent pattern across observers and external variance levels, where τGlass>τdGlass>τRDK.

-The mixed ANOVA with significant effect of the external variance ($F_{6.03, 524.37}$= 185.33, p < .001) and the stimulus type ($F_{2, 87}$ = 33.50, p < .001), but no significant interaction ($F_{12.05, 524.37}$= 1.05, p > .1) confirmed the parallel vertical shift.

- F-test on goodness of fit of nested models showed that sole change in sampling efficiency (*Eff*) with invariable internal noise (σ_{eq}) across the tasks best described the performance for each observer and mean (n=6) data.

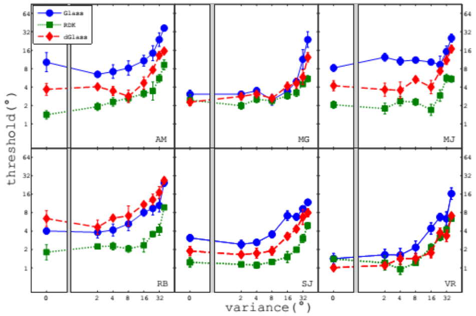

Mean discrimination thresholds (n= 5 sessions) for six observers at different level of variance for each stimulus.

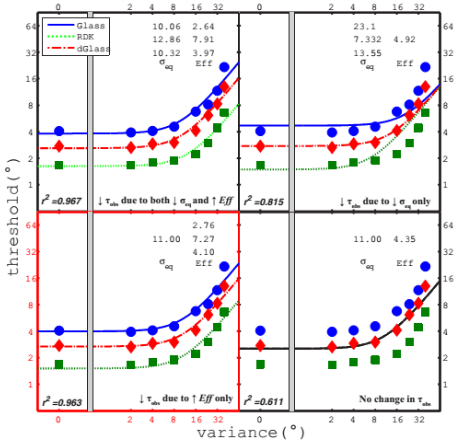

Nested modelling for mean data (n=6) relating the thresholds to the different values for the internal noise and sampling efficiency for each stimulus type. The highlighted box indicates the reduced model which resulted in no significant difference (p>0.05) in the goodness of the fit measure (r^2) compared to the full model.

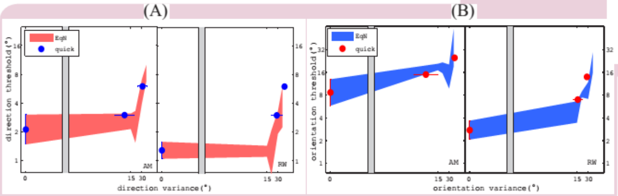

Direction discrimination (A) and orientation discrimination threshold (B) for two observers with EqN and quick method.

Discussion and conclusion:

- Humans seem to be more efficient at discriminating direction of real motion compared to implied motion or orientation at all levels of external noise. This could be attributed to differences in the sampling efficiency with equivalent internal noise remaining constant for different stimulus types.

- The similar levels of internal noise observed in the study suggests that the different visual streams may share a common local processing mechanism before global processing along a more efficient channel for motion cues.

- In future the concurrent study of dorsal and ventral streams will be applied to a range of developmental/cognitive disorders to discern the role of local and global processing mechanisms.

quick (Threshold vs Noise) method

- Evaluating threshold at different noise levels require long experimental sessions, here we report on a faster method (quick) for determination of threshold vs noise curve.

- For the validation of the quick method, five observers completed five sessions of experiments for direction and orientation discrimination with seven interleaved staircases (five conventional EqN method and two quick method).

- For all observers and both functions the thresholds from quick method were similar to those from the EqN method.

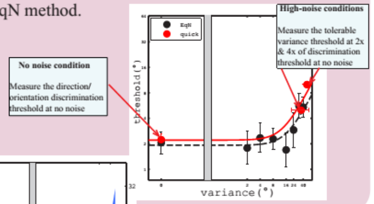

No noise condition

Measure the direction/ orientation discrimination threshold at no noise

High-noise conditions

Measure the tolerable variance threshold at 2x & 4x of discrimination threshold at no noise

References:

1. McIntosh, R. D. and T. Schenk (2009). "Two visual streams for perception and action: current trends." Neuropsychologia 47(6): 1391-1396.
2. Glass, L. (1969). "Moire effect from random dots." Nature 223(5206): 578-580.
3. Nankoo, J. F., C. R. Madan, et al. (2012). "Perception of dynamic glass patterns." Vision Res 72: 55-62.
4. Pelli, D.G., The quantum efficiency of vision, in In C. Blakemore (Ed.) , Vision: Coding and Efficiency. 1990, Cambridge University Press: New York. p. 3-24.

15th Annual Vision Sciences Society Meeting, Florida, USA, 15-20 May 2015.

Joshi M, Simmers A, Jeon S; "Deficits in integration of global motion and form in noise is associated with the severity and type of amblyopia" ***Journal of Vision*** **2015;15(12):193.**

- Oral Presentation

Motion and form processing along the functionally differentiated dorsal and ventral stream is reported to be abnormal in amblyopia; however limitations in previous stimuli have made analogous comparison of the outputs from these two streams difficult. In the current study, we characterise both functions in amblyopia using equivalent stimuli for fine global motion and orientation discrimination in the presence of noise. Anisometropic (n = 6) and strabismic (n = 6) amblyopes, and 12 visually normal subjects monocularly estimated the mean direction of motion of random dot kinematogram (RDK) and orientation of Glass pattern (Glass), whose directions/orientations were drawn from normal distributions with a range of means and variances that served as external noise. Two levels of noise were tested to obtain direction/orientation discrimination threshold in the absence of noise then threshold variance at the multiples of the direction/orientation threshold. For all subjects the thresholds for Glass were higher than RDK. The direction/orientation thresholds were higher for amblyopic eye (AE) in the strabismic group compared to the fixing eye (FE) and normal observers (NE) but not for anisometropic group. The MANOVA for the strabismic group revealed significant effect of both eyes ($p < 0.01$) and stimulus type ($p < 0.01$) but no interaction $p > 0.1$), with thresholds significantly higher for the AE than both FE and NE (ps < 0.05) on pairwise analysis. The MANOVA for the anisometropic group showed no significant effect of eyes $p > 0.1$) but a significant effect of stimulus type ($p < 0.001$) with no interaction $p > 0.1$). Our results show a deficit in motion and form perception only in subjects with dense strabismic amblyopia, irrespective of noise levels. The thresholds will be modelled to parse out the influence of local and global processing mechanisms in the respective streams.

38th European Conference on Visual Perception, Liverpool, United Kingdom, 23 – 27 August 2015

Jeon S T, Joshi M R, Simmers A; "Noise reveals abnormal global integration of motion and form in strabismic amblyopia". *Perception,* 2015; 44: 1-415

- Poster presentation

Abnormal motion and form processing along the dorsal or ventral pathway has been reported in amblyopia. In the current study, we attempted to characterise visual processings in both pathways in amblyopia concurrently using equivalent stimuli in the presence of noise.

Six anisometropes, six strabismics, and 12 visually normal observers monocularly discriminated the global direction of random dot kinematogram (motion) and orientation of Glass pattern (form) where individual direction or orientation of local elements were drawn from normal distributions with a range of variances that served as noise. Direction/orientation discrimination threshold without noise was measured first, followed by threshold variance measured at the multiples of the direction/orientation threshold.

Overall, the form thresholds were higher than motion thresholds for all observers regardless of the noise levels. The thresholds were modelled to separate the effect of local and global processing in the respective pathways. The analyses showed that the anisometropic performance for both form and motion were identical to normal ($p > .5$). The strabismic performance for both form and motion were poorer than the normal eyes ($p < .01$). Nested model testing suggested the poorer performance of the strabismic eyes were due to the deficits in global integration, reflected in the lower efficiency parameter.

9.3 References

AAEN-STOCKDALE, C. and HESS, R. F. 2008. The amblyopic deficit for global motion is spatial scale invariant. *Vision Research,* 48**,** 1965-1971.

AAEN-STOCKDALE, C.; LEDGEWAY, T. and HESS, R. F. 2007. Second-Order Optic Flow Deficits in Amblyopia. *Investigative Ophthalmology & Visual Science,* 48**,** 5532-5538.

ADELSON, E. H. and MOVSHON, J. A. 1982. Phenomenal coherence of moving visual patterns. *Nature,* 300**,** 523-525.

ADELSON, E. H. and MOVSHON, J. A. 1986. The perception of coherent motion in two-dimensional patterns. *Proceedings of the ACM SIGGRAPH/SIGART interdisciplinary workshop on Motion: representation and perception.* Toronto, Ontario, Canada: Elsevier North-Holland, Inc.

AGLIOTI, S.; DESOUZA, J. F. and GOODALE, M. A. 1995. Size-contrast illusions deceive the eye but not the hand. *Current Biology,* 5**,** 679-685.

AHMED, I. J.; LEWIS, T. L.; ELLEMBERG, D. and MAURER, D. 2005. Discrimination of speed in 5-year-olds and adults: are children up to speed? *Vision Research,* 45**,** 2129-2135.

AHUMADA, A. J., JR. and WATSON, A. B. 1985. Equivalent-noise model for contrast detection and discrimination. *Journal of the Optical Society of America A,* 2**,** 1133-1139.

ALBRIGHT, T. D. 1984. Direction and orientation selectivity of neurons in visual area MT of the macaque. *Journal of Neurophysiology,* 52**,** 1106-1130.

ALBRIGHT, T. D. 1993. Cortical processing of visual motion. *Reviews of Oculomotor Research,* 5**,** 177-201.

ALBRIGHT, T. D.; DESIMONE, R. and GROSS, C. G. 1984. Columnar organization of directionally selective cells in visual area MT of the macaque. *Journal of Neurophysiology,* 51**,** 16-31.

ANDERSON, S. J. and SWETTENHAM, J. B. 2006. Neuroimaging in Human Amblyopia. *Strabismus,* 14**,** 21-35.

APTHORP, D.; SCHWARZKOPF, D. S.; KAUL, C.; BAHRAMI, B.; ALAIS, D. and REES, G. 2013. Direct evidence for encoding of motion streaks in human visual cortex. *Proceedings of the Royal Society B: Biological Sciences,* 280**,** 20122339.

ASPELL, J. E.; WATTAM-BELL, J. and BRADDICK, O. 2006. Interaction of spatial and temporal integration in global form processing. *Vision Research,* 46**,** 2834-2841.

ASSAD, J. A. and MAUNSELL, J. H. 1995. Neuronal correlates of inferred motion in primate posterior parietal cortex. *Nature,* 373**,** 518-521.

BAILEY, I. L. and LOVIE, J. E. 1976. New design principles for visual acuity letter charts. *American Journal of Optometry and Physiological Optics,* 53**,** 740-745.

BARLOW, H. B. 1956. Retinal Noise and Absolute Threshold. *Journal of the Optical Society of America,* 46**,** 634-639.

BARNES, G. R.; LI, X.; THOMPSON, B.; SINGH, K. D.; DUMOULIN, S. O. and HESS, R. F. 2010. Decreased Gray Matter Concentration in the Lateral Geniculate Nuclei in Human Amblyopes. *Investigative Ophthalmology & Visual Science,* 51**,** 1432-1438.

BEAUDOT, W. H. A. and MULLEN, K. T. 2006. Orientation discrimination in human vision: Psychophysics and modeling. *Vision Research,* 46**,** 26-46.

BEHRMANN, M.; GENG, J. J. and SHOMSTEIN, S. 2004. Parietal cortex and attention. *Current Opinion in Neurobiology,* 14**,** 212-217.

BENNETT, P. J.; SEKULER, A. B. and OZIN, L. 1999. Effects of aging on calculation efficiency and equivalent noise. *Journal of the Optical Society of America. A, Optics, image science, and vision,* 16**,** 654-668.

BI, H.; ZHANG, B.; TAO, X.; HARWERTH, R. S.; SMITH, E. L. and CHINO, Y. M. 2011. Neuronal Responses in Visual Area V2 (V2) of Macaque Monkeys with Strabismic Amblyopia. *Cerebral Cortex,* 21**,** 2033-2045.

BIRCH, E. E. 2013. Amblyopia and Binocular Vision. *Progress in Retinal and Eye Research,* 33**,** 67-84.

BLAKE, R.; GROSSMAN, E. and SEKULER, R. 2003. Motion Processing in Human Visual Cortex. *The Primate Visual System.* CRC Press.

BLAKE, R. and HOLOPIGIAN, K. 1985. Orientation selectivity in cats and humans assessed by masking. *Vision Research,* 25**,** 1459-1467.

BOCHEVA, N.; ANGELOVA, D. and STEFANOVA, M. 2013. Age-related changes in fine motion direction discriminations. *Experimental Brain Research,* 228**,** 257-278.

BOGFJELLMO, L. G.; BEX, P. J. and FALKENBERG, H. K. 2013. Reduction in Direction Discrimination With Age and Slow Speed Is Due to Both Increased Internal Noise and Reduced Sampling Efficiency. *Investigative Ophthalmology & Visual Science,* 54**,** 5204-5210.

BOGFJELLMO, L. G.; BEX, P. J. and FALKENBERG, H. K. 2014. The development of global motion discrimination in school aged children. *Journal of Vision,* 14**,** 19.

BONHOEFFER, T. and GRINVALD, A. 1991. Iso-orientation domains in cat visual cortex are arranged in pinwheel-like patterns. *Nature,* 353**,** 429-431.

BORN, R. T. and BRADLEY, D. C. 2005. Structure and function of visual area MT. *Annual Review of Neuroscience,* 28**,** 157-189.

BRADDICK, O.; ATKINSON, J. and WATTAM-BELL, J. 2003. Normal and anomalous development of visual motion processing: motion coherence and 'dorsal-stream vulnerability'. *Neuropsychologia,* 41**,** 1769-1784.

BRADDICK, O. J.; O'BRIEN, J.; WATTAM-BELL, J. and ATKINSON, J. 1999. fMRI study of human brain areas activated by form coherence: Dorsal or ventral function? *Investigative ophthalmology & visual science,* 40**,** S2-S2.

BRADDICK, O. J.; O'BRIEN, J. M.; WATTAM-BELL, J.; ATKINSON, J.; HARTLEY, T. and TURNER, R. 2001. Brain areas sensitive to coherent visual motion. *Perception,* 30**,** 61-72.

BRADDICK, O. J.; O'BRIEN, J. M. D.; REES, G.; WATTAM-BELL, J.; ATKINSON, J. and TURNER, R. Year. Quantitative neural responses to form coherence in human extrastriate cortex. *In:* Society for Neuroscience 32nd Annual Meeting, 2002 Washington, DC.

BRADDICK, O. J.; O'BRIEN, J. M. D.; WATTAM-BELL, J.; ATKINSON, J. and TURNER, R. 2000. Form and motion coherence activate independent, but not dorsal/ventral segregated, networks in the human brain. *Current Biology,* 10**,** 731-734.

BRAINARD, D. H. 1997a. The Psychophysics Toolbox. *Spatial Vision,* 10**,** 433-436.

BRAINARD, D. H. 1997b. The Psychophysics Toolbox. *Spatial Vision,* 10**,** 433-436.

BRIGGS, F. and USREY, W. M. 2009. Parallel Processing in the Corticogeniculate Pathway of the Macaque Monkey. *Neuron,* 62**,** 135-146.

BRIGGS, F. and USREY, W. M. 2011. Corticogeniculate feedback and visual processing in the primate. *The Journal of Physiology,* 589**,** 33-40.

BRITTEN, K.; SHADLEN, M.; NEWSOME, W. and MOVSHON, J. 1992. The analysis of visual motion: a comparison of neuronal and psychophysical performance. *The Journal of Neuroscience,* 12**,** 4745-4765.

BROSSEAU-LACHAINE, O.; CASANOVA, C. and FAUBERT, J. 2008. Infant sensitivity to radial optic flow fields during the first months of life. *Journal of Vision,* 8**,** 5 1-14.

BURGESS, A. E. and COLBORNE, B. 1988. Visual signal detection. IV. Observer inconsistency. *Journal of the Optical Society of America A,* 5**,** 617-627.

BURR, D. C. and ROSS, J. 2002. Direct Evidence That “Speedlines” Influence Motion Mechanisms. *The Journal of Neuroscience,* 22**,** 8661-8664.

BURTON, E. A.; WATTAM-BELL, J.; RUBIN, G. S.; ATKINSON, J.; BRADDICK, O. and NARDINI, M. 2015. The effect of blur on cortical responses to global form and motion. *Journal of Vision,* 15**,** 12.

CARDOSO-LEITE, P. and GOREA, A. 2010. On the Perceptual/Motor Dissociation: A Review of Concepts, Theory, Experimental Paradigms and Data Interpretations. *Seeing and Perceiving,* 23**,** 89-151.

CLELAND, B. G.; CREWTHER, D. P.; CREWTHER, S. G. and MITCHELL, D. E. 1982. Normality of spatial resolution of retinal ganglion cells in cats with strabismic amblyopia. *The Journal of Physiology,* 326**,** 235-249.

CONLON, E.; SANDERS, M. and ZAPART, S. 2004. Temporal processing in poor adult readers. *Neuropsychologia,* 42**,** 142-157.

DACEY, D. M. 2000. Parallel pathways for spectral coding in primate retina. *Annual Review of Neuroscience,* 23**,** 743-775.

DACEY, D. M. and PACKER, O. S. 2003. Colour coding in the primate retina: diverse cell types and cone-specific circuitry. *Current Opinion in Neurobiology,* 13**,** 421-427.

DAKIN, S. C. 1997. The detection of structure in glass patterns: Psychophysics and computational models. *Vision Research,* 37**,** 2227-2246.

DAKIN, S. C. 2001. Information limit on the spatial integration of local orientation signals. *Journal of the Optical Society of America. A, Optics, image science, and vision,* 18**,** 1016-1026.

DAKIN, S. C. and BEX, P. J. 2002. Summation of concentric orientation structure: seeing the Glass or the window? *Vision Research,* 42**,** 2013-2020.

DAKIN, S. C.; MARESCHAL, I. and BEX, P. J. 2005. Local and global limitations on direction integration assessed using equivalent noise analysis. *Vision Research,* 45**,** 3027-3049.

DALLALA, R.; WANG, Y.-Z. and HESS, R. F. 2010. The global shape detection deficit in strabismic amblyopia: Contribution of local orientation and position. *Vision Research,* 50**,** 1612-1617.

DAY, A. M. and PALOMARES, M. 2014. How temporal frequency affects global form coherence in Glass patterns. *Vision Research,* 95**,** 18-22.

DE VALOIS, R. L.; MORGAN, H. C.; POLSON, M. C.; MEAD, W. R. and HULL, E. M. 1974. Psychophysical studies of monkey vision—I. Macaque luminosity and color vision tests. *Vision Research,* 14**,** 53-67.

DE VRIES, H. L. 1943. The quantum character of light and its bearing upon threshold of vision, the differential sensitivity and visual acuity of the eye. *Physica,* 10**,** 553-564.

DEAN, H. L.; HAGAN, M. A. and PESARAN, B. 2012. Only coherent spiking in posterior parietal cortex coordinates looking and reaching. *Neuron,* 73**,** 829-841.

DEMANINS, R.; HESS, R. F.; WILLIAMS, C. B. and KEEBLE, D. R. T. 1999. The orientation discrimination deficit in strabismic amblyopia depends upon stimulus bandwidth. *Vision Research,* 39**,** 4018-4031.

DEMB, J. B.; BOYNTON, G. M. and HEEGER, D. J. 1997. Brain activity in visual cortex predicts individual differences in reading performance. *Proceedings of the National Academy of Sciences of the United States of America,* 94**,** 13363-13366.

DEMB, J. B.; BOYNTON, G. M. and HEEGER, D. J. 1998. Functional magnetic resonance imaging of early visual pathways in dyslexia. *The Journal of Neuroscience,* 18**,** 6939-6951.

DESIMONE, R. and SCHEIN, S. J. 1987. Visual properties of neurons in area V4 of the macaque: sensitivity to stimulus form. *The Journal of Neurophysiology,* 57**,** 835-868.

DEYOE, E. A.; FELLEMAN, D. J.; VAN ESSEN, D. C. and MCCLENDON, E. 1994. Multiple processing streams in occipitotemporal visual cortex. *Nature,* 371**,** 151-154.

DIJKERMAN, H. C.; LÊ, S.; DÉMONET, J.-F. and MILNER, A. D. 2004. Visuomotor performance in a patient with visual agnosia due to an early lesion. *Cognitive Brain Research,* 20**,** 12-25.

DITCHFIELD, J. A.; MCKENDRICK, A. M. and BADCOCK, D. R. 2006. Processing of global form and motion in migraineurs. *Vision Research,* 46**,** 141-148.

DUMOULIN, S. O. and HESS, R. F. 2007. Cortical specialization for concentric shape processing. *Vision Research,* 47**,** 1608-1613.

EDEN, G. F.; VANMETER, J. W.; RUMSEY, J. M.; MAISOG, J. M.; WOODS, R. P. and ZEFFIRO, T. A. 1996. Abnormal processing of visual motion in dyslexia revealed by functional brain imaging. *Nature,* 382**,** 66-69.

EDWARDS, M.; BADCOCK, D. R. and SMITH, A. T. 1998. Independent speed-tuned global-motion systems. *Vision Research,* 38**,** 1573-1580.

EDWARDS, M. and CRANE, M. F. 2007. Motion streaks improve motion detection. *Vision Research,* 47**,** 828-833.

EDWARDS, V. T.; GIASCHI, D. E.; DOUGHERTY, R. F.; EDGELL, D.; BJORNSON, B. H.; LYONS, C. and DOUGLAS, R. M. 2004. Psychophysical Indexes of Temporal Processing Abnormalities in Children With Developmental Dyslexia. *Developmental Neuropsychology,* 25**,** 321-354.

EL-SHAMAYLEH, Y.; KIORPES, L.; KOHN, A. and MOVSHON, J. A. 2010. Visual Motion Processing by Neurons in Area MT of Macaque Monkeys with Experimental Amblyopia. *The Journal of Neuroscience,* 30**,** 12198-12209.

ELLEMBERG, D.; LEWIS, T. L.; MAURER, D.; BRAR, S. and BRENT, H. P. 2002. Better perception of global motion after monocular than after binocular deprivation. *Vision Research,* 42**,** 169-179.

ENROTH-CUGELL, C. and ROBSON, J. G. 1966. The contrast sensitivity of retinal ganglion cells of the cat. *The Journal of Physiology,* 187**,** 517-552.

FAISAL, A. A.; SELEN, L. P. and WOLPERT, D. M. 2008. Noise in the nervous system. *Nature Reviews Neuroscience,* 9**,** 292-303.

FALKENBERG, H. K. and BEX, P. J. 2007. Sources of motion-sensitivity loss in glaucoma. *Investigative Ophthalmology & Visual Science,* 48**,** 2913-2921.

FALKENBERG, H. K.; SIMPSON, W. A. and DUTTON, G. N. 2014. Development of sampling efficiency and internal noise in motion detection and discrimination in school-aged children. *Vision Research,* 100**,** 8-17.

FECHNER, G. T. 1860. *Elemente der Psychophysik*, Breitkopf und Härtel.

FELLEMAN, D. J.; XIAO, Y. and MCCLENDON, E. 1997. Modular Organization of Occipito-Temporal Pathways: Cortical Connections between Visual Area 4 and Visual Area 2 and Posterior Inferotemporal Ventral Area in Macaque Monkeys. *The Journal of Neuroscience,* 17**,** 3185-3200.

FERBER, S.; HUMPHREY, G. K. and VILIS, T. 2003. The Lateral Occipital Complex Subserves the Perceptual Persistence of Motion-defined Groupings. *Cerebral Cortex,* 13**,** 716-721.

FERRERA, V. P.; NEALEY, T. A. and MAUNSELL, J. H. 1992. Mixed parvocellular and magnocellular geniculate signals in visual area V4. *Nature,* 358**,** 756-761.

FERRERA, V. P.; NEALEY, T. A. and MAUNSELL, J. H. 1994. Responses in macaque visual area V4 following inactivation of the parvocellular and magnocellular LGN pathways. *The Journal of Neuroscience,* 14**,** 2080-2088.

FERRIS, F. L., 3RD; KASSOFF, A.; BRESNICK, G. H. and BAILEY, I. 1982. New visual acuity charts for clinical research. *American Journal of Ophthalmology,* 94**,** 91-96.

FIELD, D. J. and HAYES, A. 2004. Contour integration and lateral connections of V1 neurons. *In:* CHALUPA, L. M. and WERNER, J. S. (eds.) *The Visual Neurosciences.* Massachusetts: The MIT Press.

FRANZ, V. H. 2001. Action does not resist visual illusions. *Trends in Cognitive Sciences,* 5**,** 457-459.

FRANZ, V. H. and GEGENFURTNER, K. R. 2008. Grasping visual illusions: consistent data and no dissociation. *Cognitive Neuropsychology,* 25**,** 920-950.

FRANZ, V. H.; GEGENFURTNER, K. R.; BULTHOFF, H. H. and FAHLE, M. 2000. Grasping visual illusions: no evidence for a dissociation between perception and action. *Psychological Science,* 11**,** 20-25.

FREEMAN, T. C. and HARRIS, M. G. 1992. Human sensitivity to expanding and rotating motion: effects of complementary masking and directional structure. *Vision Research,* 32**,** 81-87.

FRIIS, H. T. 1944. Noise Figures of Radio Receivers. *Proceedings of the IRE,* 32**,** 419-422.

GALLANT, J. L.; SHOUP, R. E. and MAZER, J. A. 2000. A human extrastriate area functionally homologous to macaque V4. *Neuron,* 27**,** 227-235.

GALLETTI, C.; FATTORI, P.; KUTZ, D. F. and BATTAGLINI, P. P. 1997. Arm Movement-related Neurons in the Visual Area V6A of the Macaque Superior Parietal Lobule. *European Journal of Neuroscience,* 9**,** 410-413.

GANEL, T.; TANZER, M. and GOODALE, M. A. 2008. A double dissociation between action and perception in the context of visual illusions: opposite effects of real and illusory size. *Psychological Science,* 19**,** 221-225.

GARNHAM, L. and SLOPER, J. J. 2006. Effect of age on adult stereoacuity as measured by different types of stereotest. *British Journal of Ophthalmology,* 90**,** 91-95.

GEGENFURTNER, K. R.; KIPER, D. C. and FENSTEMAKER, S. B. 1996. Processing of color, form, and motion in macaque area V2. *Visual Neuroscience,* 13**,** 161-172.

GEISLER, W. S. 1999. Motion streaks provide a spatial code for motion direction. *Nature,* 400**,** 65-69.

GEISLER, W. S.; ALBRECHT, D. G.; CRANE, A. M. and STERN, L. 2001. Motion direction signals in the primary visual cortex of cat and monkey. *Visual Neuroscience,* 18**,** 501-516.

GILAIE-DOTAN, S.; SAYGIN, A. P.; LORENZI, L. J.; EGAN, R.; REES, G. and BEHRMANN, M. 2013. The role of human ventral visual cortex in motion perception. *Brain,* 136**,** 2784-2798.

GILBERT, C. D. and WIESEL, T. N. 1983. Clustered intrinsic connections in cat visual cortex. *The Journal of Neuroscience,* 3**,** 1116-1133.

GILBERT, C. D. and WIESEL, T. N. 1989. Columnar specificity of intrinsic horizontal and corticocortical connections in cat visual cortex. *The Journal of Neuroscience,* 9**,** 2432-2442.

GLASS, L. 1969. Moire effect from random dots. *Nature,* 223**,** 578-580.

GOLD, J. M.; SEKULER, A. B. and BENNETT, P. J. 2004. Characterizing perceptual learning with external noise. *Cognitive Science,* 28**,** 167-207.

GOODALE, M. A. 2011. Transforming vision into action. *Vision Research,* 51**,** 1567-1587.

GOODALE, M. A. and MILNER, A. D. 1992. Separate visual pathways for perception and action. *Trends in Neurosciences,* 15**,** 20-25.

GOODALE, M. A.; MILNER, A. D.; JAKOBSON, L. S. and CAREY, D. P. 1991. A neurological dissociation between perceiving objects and grasping them. *Nature,* 349**,** 154-156.

GOODALE, M. A. and WESTWOOD, D. A. 2004. An evolving view of duplex vision: separate but interacting cortical pathways for perception and action. *Current Opinion in Neurobiology,* 14**,** 203-211.

GORDON, G. and MCCULLOCH, D. 1999a. A VEP investigation of parallel visual pathway development in primary school age children. *Documenta Ophthalmologica,* 99**,** 1-10.

GORDON, G. E. and MCCULLOCH, D. L. 1999b. A VEP investigation of parallel visual pathway development in primary school age children. *Documenta Ophthalmologica,* 99**,** 1-10.

GREEN, D. M. and SWETS, J. A. 1974. *Signal Detection Theory and Psychophysics*, John Wiley & Sons Canada, Limited.

GREENLEE, M. W. 2000. Human cortical areas underlying the perception of optic flow: Brain imaging studies. *In:* LAPPE, M. (ed.) *Neuronal processing of optic flow.* San Diego, Calif. [u.a.]: Acad. Press.

GRINTER, E. J.; MAYBERY, M. T. and BADCOCK, D. R. 2010. Vision in developmental disorders: is there a dorsal stream deficit? *Brain Research Bulletin,* 82**,** 147-160.

GUNN, A.; CORY, E.; ATKINSON, J.; BRADDICK, O.; WATTAM-BELL, J.; GUZZETTA, A. and CIONI, G. 2002. Dorsal and ventral stream sensitivity in normal development and hemiplegia. *Neuroreport,* 13**,** 843-847.

HADAD, B.-S.; SCHWARTZ, S.; MAURER, D. and LEWIS, T. L. 2015. Motion Perception: A review of developmental changes and the role of early visual experience. *Frontiers in Integrative Neuroscience,* 9.

HADAD, B. S.; MAURER, D. and LEWIS, T. L. 2011. Long trajectory for the development of sensitivity to global and biological motion. *Developmental Science,* 14**,** 1330-1339.

HAMM, L. M.; BLACK, J.; DAI, S. and THOMPSON, B. 2014. Global processing in amblyopia: a review. *Frontiers in Psychology,* 5**,** 583.

HANSEN, P. C.; STEIN, J. F.; ORDE, S. R.; WINTER, J. L. and TALCOTT, J. B. 2001. Are dyslexics' visual deficits limited to measures of dorsal stream function? *Neuroreport,* 12**,** 1527-1530.

HAWKEN, M. J.; PARKER, A. J. and LUND, J. S. 1988. Laminar organization and contrast sensitivity of direction-selective cells in the striate cortex of the Old World monkey. *The Journal of Neuroscience,* 8**,** 3541-3548.

HAYWARD, J.; TRUONG, G.; PARTANEN, M. and GIASCHI, D. 2011. Effects of speed, age, and amblyopia on the perception of motion-defined form. *Vision Research,* 51**,** 2216-2223.

HEEGER, D. J.; BOYNTON, G. M.; DEMB, J. B.; SEIDEMANN, E. and NEWSOME, W. T. 1999. Motion Opponency in Visual Cortex. *The Journal of Neuroscience,* 19**,** 7162-7174.

HEGDE, J. and VAN ESSEN, D. C. 2000. Selectivity for complex shapes in primate visual area V2. *The Journal of Neuroscience,* 20**,** RC61.

HESS, R. F. 2001. Amblyopia: site unseen. *Clinical and Experimental Optometry,* 84**,** 321-336.

HESS, R. F. and FIELD, D. J. 1994. Is the spatial deficit in strabismic amblyopia due to loss of cells or an uncalibrated disarray of cells? *Vision Research,* 34**,** 3397-3406.

HESS, R. F.; HAYES, A. and FIELD, D. J. 2003. Contour integration and cortical processing. *Journal of Physiology-Paris,* 97**,** 105-119.

HESS, R. F. and MALIN, S. A. 2003. Threshold vision in amblyopia: orientation and phase. *Investigative Ophthalmology & Visual Science,* 44**,** 4762-4771.

HESS, R. F.; MANSOURI, B.; DAKIN, S. C. and ALLEN, H. A. 2006. Integration of local motion is normal in amblyopia. *Journal of the Optical Society of America A,* 23**,** 986-992.

HOLMES, J. A. and LESKE, D. A. Year. Monocular clues in tests of stereoacuity

In: PRITCHARD, C., ed. International Orthoptic, Congress, June 20-30 1999 Nurnberg, Germany [publisher not identified], 103-106.

HUBEL, D. and LIVINGSTONE, M. 1987. Segregation of form, color, and stereopsis in primate area 18. *The Journal of Neuroscience,* 7**,** 3378-3415.

HUBEL, D. H. 1982. Exploration of the primary visual cortex, 1955-78. *Nature,* 299**,** 515-524.

HUBEL, D. H. 1995. *Eye, Brain, and Vision*, Henry Holt and Company.

HUBEL, D. H. and WIESEL, T. N. 1961. Integrative action in the cat's lateral geniculate body. *The Journal of Physiology,* 155**,** 385-398.

HUBEL, D. H. and WIESEL, T. N. 1968. Receptive fields and functional architecture of monkey striate cortex. *The Journal of Physiology,* 195**,** 215-243.

HUK, A. C.; DOUGHERTY, R. F. and HEEGER, D. J. 2002. Retinotopy and Functional Subdivision of Human Areas MT and MST. *The Journal of Neuroscience,* 22**,** 7195-7205.

HUSK, J. S.; FARIVAR, R. and HESS, R. F. 2012. Amblyopic deficits in processing structure-from-motion. *Journal of Vision,* 12**,** 4.

HUSK, J. S. and HESS, R. F. 2013. Global processing of orientation in amblyopia. *Vision Research,* 82**,** 22-30.

IKEDA, H. 1980. Visual acuity, its development and amblyopia. *Journal of the Royal Society of Medicine,* 73**,** 546-555.

ILG, U. J. and SCHUMANN, S. 2007. Primate Area MST-l Is Involved in the Generation of Goal-Directed Eye and Hand Movements. *Journal of Neurophysiology,* 97**,** 761-771.

ITO, M. and KOMATSU, H. 2004. Representation of Angles Embedded within Contour Stimuli in Area V2 of Macaque Monkeys. *The Journal of Neuroscience,* 24**,** 3313-3324.

JAMES, T. W.; CULHAM, J.; HUMPHREY, G. K.; MILNER, A. D. and GOODALE, M. A. 2003. Ventral occipital lesions impair object recognition but not object-directed grasping: an fMRI study. *Brain,* 126**,** 2463-2475.

JEON, S. T.; LU, Z. L. and DOSHER, B. A. 2009. Characterizing perceptual performance at multiple discrimination precisions in external noise. *Journal of the Optical Society of America. A, Optics, image science, and vision,* 26**,** B43-58.

JOHANSSON, G. 1973. Visual perception of biological motion and a model for its analysis. *Perception & Psychophysics,* 14**,** 201-211.

JOLY, O. and FRANKÓ, E. 2014. Neuroimaging of amblyopia and binocular vision: a review. *Frontiers in Integrative Neuroscience,* 8.

JOSHI, M. R. and FALKENBERG, H. K. 2015. Development of radial optic flow pattern sensitivity at different speeds. *Vision Research,* 110, Part A**,** 68-75.

KANWISHER, N. and YOVEL, G. 2006. The fusiform face area: a cortical region specialized for the perception of faces. *Philosophical Transactions of the Royal Society B: Biological Sciences,* 361**,** 2109-2128.

KAPLAN, E. 2004. The P, M and K Streams of the Primate Visual System: What Do They Do for Vision? *In:* CHALUPA, L. M. and WERNER, J. S. (eds.) *The visual neurosciences.* Cambridge, Mass.: MIT Press.

KAPLAN, E. and SHAPLEY, R. M. 1986. The primate retina contains two types of ganglion cells, with high and low contrast sensitivity. *Proceedings of the National Academy of Sciences of the United States of America,* 83**,** 2755-2757.

KARNATH, H.-O.; RÜTER, J.; MANDLER, A. and HIMMELBACH, M. 2009. The Anatomy of Object Recognition—Visual Form Agnosia Caused by Medial Occipitotemporal Stroke. *The Journal of Neuroscience,* 29**,** 5854-5862.

KASTNER, S.; SCHNEIDER, K. A. and WUNDERLICH, K. 2006. Beyond a relay nucleus: neuroimaging views on the human LGN. *In:* MARTINEZ-CONDE, S.; MACKNIK, S. L.; MARTINEZ, L. M.; ALONSO, J. M. and TSE, P. U. (eds.) *Progress in Brain Research.* Elsevier.

KHUU, S. K. and BADCOCK, D. R. 2002. Global speed processing: evidence for local averaging within, but not across two speed ranges. *Vision Research,* 42**,** 3031-3042.

KIORPES, L. 2006. Visual processing in amblyopia: animal studies. *Strabismus,* 14**,** 3-10.

KIORPES, L.; KIPER, D. C.; O'KEEFE, L. P.; CAVANAUGH, J. R. and MOVSHON, J. A. 1998. Neuronal Correlates of Amblyopia in the Visual Cortex of Macaque Monkeys with Experimental Strabismus and Anisometropia. *The Journal of Neuroscience,* 18**,** 6411-6424.

KIORPES, L. and MCKEE, S. P. 1999. Neural mechanisms underlying amblyopia. *Current Opinion in Neurobiology,* 9**,** 480-486.

KIORPES, L. and MOVSHON, J. A. 1996. Amblyopia: a developmental disorder of the central visual pathways. *Cold Spring Harbor Symposia on Quantitative Biology,* 61**,** 39-48.

KIORPES, L. and MOVSHON, J. A. 2004. Neural limitations on visual development in primates. *In:* WERNER, J. S. and CHALUPA, L. M. (eds.) *The Visual Neurosciences.* MIT Press.

KIORPES, L.; TANG, C. and MOVSHON, J. A. 2006. Sensitivity to visual motion in amblyopic macaque monkeys. *Visual Neuroscience,* 23**,** 247-256.

KNOX, P. J.; LEDGEWAY, T. and SIMMERS, A. J. 2013. The effects of spatial offset, temporal offset and image speed on sensitivity to global motion in human amblyopia. *Vision Research,* 86**,** 59-65.

KOURTZI, Z.; KREKELBERG, B. and VAN WEZEL, R. J. 2008. Linking form and motion in the primate brain. *Trends in Cognitive Sciences,* 12**,** 230-236.

KREKELBERG, B.; DANNENBERG, S.; HOFFMANN, K.-P.; BREMMER, F. and ROSS, J. 2003. Neural correlates of implied motion. *Nature,* 424**,** 674-677.

KREKELBERG, B.; VATAKIS, A. and KOURTZI, Z. 2005. Implied motion from form in the human visual cortex. *Journal of Neurophysiology,* 94**,** 4373-4386.

LACHICA, E. A.; BECK, P. D. and CASAGRANDE, V. A. 1992. Parallel pathways in macaque monkey striate cortex: anatomically defined columns in layer III. *Proceedings of the National Academy of Sciences of the United States of America,* 89**,** 3566-3570.

LAWLESS, H. T. 2013. Psychophysics II. *Quantitative Sensory Analysis.* John Wiley & Sons.

LAYCOCK, R. and CREWTHER, S. G. 2008. Towards an understanding of the role of the 'magnocellular advantage' in fluent reading. *Neuroscience & Biobehavioral Reviews,* 32**,** 1494-1506.

LEE, A. L. and LU, H. 2010. A comparison of global motion perception using a multiple-aperture stimulus. *Journal of Vision,* 10**,** 9 1-16.

LENNIE, P. 1998. Single units and visual cortical organization. *PERCEPTION-LONDON-,* 27**,** 889-936.

LERNER, Y.; HENDLER, T.; MALACH, R.; HAREL, M.; LEIBA, H.; STOLOVITCH, C. and PIANKA, P. 2006. Selective fovea-related deprived activation in retinotopic and high-order visual cortex of human amblyopes. *NeuroImage,* 33**,** 169-179.

LERNER, Y.; PIANKA, P.; AZMON, B.; LEIBA, H.; STOLOVITCH, C.; LOEWENSTEIN, A.; HAREL, M.; HENDLER, T. and MALACH, R. 2003. Area-Specific Amblyopic Effects in Human Occipitotemporal Object Representations. *Neuron,* 40**,** 1023-1029.

LESMES, L. A.; JEON, S.-T.; LU, Z.-L. and DOSHER, B. A. 2006. Bayesian adaptive estimation of threshold versus contrast external noise functions: The quick TvC method. *Vision Research,* 46**,** 3160-3176.

LETTVIN, J. Y.; MATURANA, H. R.; MCCULLOCH, W. S. and PITTS, W. H. 1959. What the Frog's Eye Tells the Frog's Brain. *Proceedings of the IRE,* 47**,** 1940-1951.

LEVI, D. M. 2006. Visual processing in amblyopia: human studies. *Strabismus,* 14**,** 11-19.

LEVI, D. M. and KLEIN, S. A. 1985. Vernier acuity, crowding and amblyopia. *Vision Research,* 25**,** 979-991.

LEVI, D. M.; KLEIN, S. A. and AITSEBAOMO, P. 1984. Detection and discrimination of the direction of motion in central and peripheral vision of normal and amblyopic observers. *Vision Research,* 24**,** 789-800.

LEVI, D. M.; KLEIN, S. A. and CHEN, I. 2008. What limits performance in the amblyopic visual system: seeing signals in noise with an amblyopic brain. *Journal of Vision,* 8**,** 1 1-23.

LEVI, D. M.; MCKEE, S. P. and MOVSHON, J. A. 2011. Visual deficits in anisometropia. *Vision Research,* 51**,** 48-57.

LEVITT, J. B.; KIPER, D. C. and MOVSHON, J. A. 1994. Receptive fields and functional architecture of macaque V2. *Journal of Neurophysiology,* 71**,** 2517-2542.

LEWIS, T. L.; ELLEMBERG, D.; MAURER, D.; DIRKS, M.; WILKINSON, F. and WILSON, H. R. 2004. A window on the normal development of sensitivity to global form in Glass patterns. *Perception,* 33**,** 409-418.

LEWIS, T. L.; ELLEMBERG, D.; MAURER, D.; WILKINSON, F.; WILSON, H. R.; DIRKS, M. and BRENT, H. P. 2002. Sensitivity to global form in glass patterns after early visual deprivation in humans. *Vision Research,* 42**,** 939-948.

LI, C.; CHENG, L.; YU, Q.; XIE, B. and WANG, J. 2012. Relationship of Visual Cortex Function and Visual Acuity in Anisometropic Amblyopic Children. *International Journal of Medical Sciences,* 9**,** 115-120.

LI, P.; ZHU, S.; CHEN, M.; HAN, C.; XU, H.; HU, J.; FANG, Y. and LU, HAIDONG D. 2013. A Motion Direction Preference Map in Monkey V4. *Neuron,* 78**,** 376-388.

LI, W. and GILBERT, C. D. 2002. Global Contour Saliency and Local Colinear Interactions. *Journal of Neurophysiology,* 88**,** 2846-2856.

LI, X.; DUMOULIN, S. O.; MANSOURI, B. and HESS, R. F. 2007. The fidelity of the cortical retinotopic map in human amblyopia. *European Journal of Neuroscience,* 25**,** 1265-1277.

LI, X.; LU, Z.-L.; XU, P.; JIN, J. and ZHOU, Y. 2003. Generating high gray-level resolution monochrome displays with conventional computer graphics cards and color monitors. *Journal of Neuroscience Methods,* 130**,** 9-18.

LIU, J. and NEWSOME, W. T. 2003. Functional Organization of Speed Tuned Neurons in Visual Area MT. *Journal of Neurophysiology,* 89**,** 246-256.

LIVINGSTONE, M. and HUBEL, D. 1987. Psychophysical evidence for separate channels for the perception of form, color, movement, and depth. *The Journal of Neuroscience,* 7**,** 3416-3468.

LIVINGSTONE, M. S. and HUBEL, D. H. 1984. Specificity of intrinsic connections in primate primary visual cortex. *The Journal of Neuroscience,* 4**,** 2830-2835.

LOFFLER, G. 2008. Perception of contours and shapes: Low and intermediate stage mechanisms. *Vision Research,* 48**,** 2106-2127.

LU, H. D.; CHEN, G.; TANIGAWA, H. and ROE, A. W. 2010. A Motion Direction Map in Macaque V2. *Neuron,* 68**,** 1002-1013.

LU, H. D. and ROE, A. W. 2008. Functional organization of color domains in V1 and V2 of macaque monkey revealed by optical imaging. *Cerebral Cortex,* 18**,** 516-533.

LU, Z. L. and DOSHER, B. A. 1998. External noise distinguishes attention mechanisms. *Vision Research,* 38**,** 1183-1198.

LU, Z. L. and DOSHER, B. A. 1999. Characterizing human perceptual inefficiencies with equivalent internal noise. *Journal of the Optical Society of America. A, Optics, image science, and vision,* 16**,** 764-778.

LUND, J. S.; YOSHIOKA, T. and LEVITT, J. B. 1993. Comparison of Intrinsic Connectivity in Different Areas of Macaque Monkey Cerebral Cortex. *Cerebral Cortex,* 3**,** 148-162.

MAJAJ, N. J.; CARANDINI, M. and MOVSHON, J. A. 2007. Motion Integration by Neurons in Macaque MT Is Local, Not Global. *The Journal of Neuroscience,* 27**,** 366-370.

MALACH, R.; AMIR, Y.; HAREL, M. and GRINVALD, A. 1993. Relationship between intrinsic connections and functional architecture revealed by optical imaging and in vivo targeted biocytin injections in primate striate cortex. *Proceedings of the National Academy of Sciences of the United States of America,* 90**,** 10469-10473.

MALACH, R.; REPPAS, J. B.; BENSON, R. R.; KWONG, K. K.; JIANG, H.; KENNEDY, W. A.; LEDDEN, P. J.; BRADY, T. J.; ROSEN, B. R. and TOOTELL, R. B. 1995. Object-related activity revealed by functional magnetic resonance imaging in human occipital cortex. *Proceedings of the National Academy of Sciences,* 92**,** 8135-8139.

MANDELLI, M.-J. F. and KIPER, D. C. 2005. The local and global processing of chromatic Glass patterns. *Journal of Vision,* 5**,** 2-2.

MANNING, C.; AAGTEN-MURPHY, D. and PELLICANO, E. 2012. The development of speed discrimination abilities. *Vision Research,* 70**,** 27-33.

MANNING, C.; DAKIN, S. C.; TIBBER, M. S. and PELLICANO, E. 2014. Averaging, not internal noise, limits the development of coherent motion processing. *Developmental Cognitive Neuroscience,* 10**,** 44-56.

MANNING, C.; TIBBER, M. S.; CHARMAN, T.; DAKIN, S. C. and PELLICANO, E. 2015. Enhanced Integration of Motion Information in Children With Autism. *The Journal of Neuroscience,* 35**,** 6979-6986.

MANSOURI, B.; ALLEN, H. A.; HESS, R. F.; DAKIN, S. C. and EHRT, O. 2004. Integration of orientation information in amblyopia. *Vision Research,* 44**,** 2955-2969.

MANSOURI, B. and HESS, R. F. 2006. The global processing deficit in amblyopia involves noise segregation. *Vision Research,* 46**,** 4104-4117.

MARESCHAL, I.; BEX, P. J. and DAKIN, S. C. 2008. Local motion processing limits fine direction discrimination in the periphery. *Vision Research,* 48**,** 1719-1725.

MARKS, L. E. 1978. *The unity of the senses: interrelations among the modalities*, Academic Press.

MATHER, G.; PAVAN, A.; BELLACOSA, R. M. and CASCO, C. 2012. Psychophysical evidence for interactions between visual motion and form processing at the level of motion integrating receptive fields. *Neuropsychologia,* 50**,** 153-159.

MATLAB 2013. *8.1.0.604 (R2013a),* Natick, Massachusetts, The MathWorks Inc.

MAUNSELL, J. H.; NEALEY, T. A. and DEPRIEST, D. D. 1990. Magnocellular and parvocellular contributions to responses in the middle temporal visual area (MT) of the macaque monkey. *The Journal of Neuroscience,* 10**,** 3323-3334.

MAUNSELL, J. H. and VAN ESSEN, D. C. 1983. Functional properties of neurons in middle temporal visual area of the macaque monkey. I. Selectivity for stimulus direction, speed, and orientation. *Journal of Neurophysiology,* 49**,** 1127-1147.

MCKEE, S. P.; LEVI, D. M. and MOVSHON, J. A. 2003. The pattern of visual deficits in amblyopia. *Journal of Vision,* 3**,** 380-405.

MILNER, A. D. and GOODALE, M. 2006. *The Visual Brain in Action*, Oup Oxford.

MILNER, A. D. and GOODALE, M. A. 1993. Visual pathways to perception and action. *Progress in Brain Research,* 95**,** 317-337.

MILNER, A. D. and GOODALE, M. A. 1996. *The Visual Brain in Action*, Oxford University Press.

MILNER, A. D. and GOODALE, M. A. 2008. Two visual systems re-viewed. *Neuropsychologia,* 46**,** 774-785.

MILNER, A. D.; PERRETT, D. I.; JOHNSTON, R. S.; BENSON, P. J.; JORDAN, T. R.; HEELEY, D. W.; BETTUCCI, D.; MORTARA, F.; MUTANI, R.; TERAZZI, E. and DAVIDSON, D. L. W. 1991. Perception and action in 'visual form agnosia'. *Brain,* 114**,** 405-428.

MILNER, D. and DYDE, R. 2003. Why do some perceptual illusions affect visually guided action, when others don't? *Trends in Cognitive Sciences,* 7**,** 10-11.

MOREL, A. and BULLIER, J. 1990. Anatomical segregation of two cortical visual pathways in the macaque monkey. *Visual Neuroscience,* 4**,** 555-578.

MORRONE, M. C.; BURR, D. C. and VAINA, L. M. 1995. Two stages of visual processing for radial and circular motion. *Nature,* 376, 507-509.

MORRONE, M. C.; TOSETTI, M.; MONTANARO, D.; FIORENTINI, A.; CIONI, G. and BURR, D. C. 2000. A cortical area that responds specifically to optic flow, revealed by fMRI. *Nature Neuroscience,* 3, 1322-1328.

MOVSHON, J. A.; ADELSON, E. H.; GIZZI, M. S. and NEWSOME, W. T. (eds.) 1995. *The analysis of moving visual patterns*: MIT Press.

MOVSHON, J. A.; EGGERS, H. M.; GIZZI, M. S.; HENDRICKSON, A. E.; KIORPES, L. and BOOTHE, R. G. 1987. Effects of early unilateral blur on the macaque's visual system. III. Physiological observations. *The Journal of Neuroscience,* 7, 1340-1351.

MUCKLI, L.; KIEß, S.; TONHAUSEN, N.; SINGER, W.; GOEBEL, R. and SIRETEANU, R. 2006. Cerebral correlates of impaired grating perception in individual, psychophysically assessed human amblyopes. *Vision Research,* 46, 506-526.

NAGARAJA, N. S. 1964. Effect of Luminance Noise on Contrast Thresholds. *Journal of the Optical Society of America,* 54, 950-955.

NAKAMURA, H.; GATTASS, R.; DESIMONE, R. and UNGERLEIDER, L. G. 1993. The modular organization of projections from areas V1 and V2 to areas V4 and TEO in macaques. *The Journal of Neuroscience,* 13, 3681-3691.

NANKOO, J.-F.; MADAN, C. R.; SPETCH, M. L. and WYLIE, D. R. 2012. Perception of dynamic Glass patterns. *Vision Research,* 72, 55-62.

NANKOO, J.-F.; MADAN, C. R.; SPETCH, M. L. and WYLIE, D. R. 2015. Temporal summation of global form signals in dynamic Glass patterns. *Vision Research,* 107, 30-35.

NASSI, J. J. and CALLAWAY, E. M. 2006. Multiple Circuits Relaying Primate Parallel Visual Pathways to the Middle Temporal Area. *The Journal of Neuroscience,* 26, 12789-12798.

NASSI, J. J. and CALLAWAY, E. M. 2007. Specialized Circuits from Primary Visual Cortex to V2 and Area MT. *Neuron,* 55, 799-808.

NEALEY, T. A. and MAUNSELL, J. H. 1994. Magnocellular and parvocellular contributions to the responses of neurons in macaque striate cortex. *The Journal of Neuroscience,* 14, 2069-2079.

NEWSOME, W. and PARE, E. 1988. A selective impairment of motion perception following lesions of the middle temporal visual area (MT). *The Journal of Neuroscience,* 8, 2201-2211.

NISHIDA, S. Y. 2011. Advancement of motion psychophysics: Review 2001–2010. *Journal of Vision,* 11, 11-11.

NORTH, D. O. 1942. The absolute sensitivity of radio receivers. *RCA Review,* 6, 332–344.

O'BRIEN, J.; SPENCER, J.; ATKINSON, J.; BRADDICK, O. and WATTAM-BELL, J. 2002. Form and motion coherence processing in dyspraxia: evidence of a global spatial processing deficit. *Neuroreport,* 13, 1399-1402.

OHLA, K.; BUSCH, N. A.; DAHLEM, M. A. and HERRMANN, C. S. 2005. Circles are different: the perception of Glass patterns modulates early event-related potentials. *Vision Research,* 45, 2668-2676.

OR, C. C.; KHUU, S. K. and HAYES, A. 2007. The role of luminance contrast in the detection of global structure in static and dynamic, same- and opposite-polarity, Glass patterns. *Vision Research,* 47, 253-259.

OTTO-DE HAART, E. G.; CAREY, D. P. and MILNE, A. B. 1999. More thoughts on perceiving and grasping the Müller–Lyer illusion. *Neuropsychologia,* 37**,** 1437-1444.

PACK, C. C. and BORN, R. T. 2001. Temporal dynamics of a neural solution to the aperture problem in visual area MT of macaque brain. *Nature,* 409**,** 1040-1042.

PARDHAN, S.; GILCHRIST, J.; ELLIOTT, D. B. and BEH, G. K. 1996. A comparison of sampling efficiency and internal noise level in young and old subjects. *Vision Research,* 36**,** 1641-1648.

PARKER, A. J. and NEWSOME, W. T. 1998. Sense and the Single Neuron: Probing the Physiology of Perception. *Annual Review of Neuroscience,* 21**,** 227-277.

PARRISH, E. E.; GIASCHI, D. E.; BODEN, C. and DOUGHERTY, R. 2005. The maturation of form and motion perception in school age children. *Vision Research,* 45**,** 827-837.

PASUPATHY, A. and CONNOR, C. E. 2001. Shape representation in area V4: position-specific tuning for boundary conformation. *Journal of Neurophysiology,* 86**,** 2505-2519.

PAVAN, A.; MAROTTI, R. B. and MATHER, G. 2013. Motion-form interactions beyond the motion integration level: Evidence for interactions between orientation and optic flow signals. *Journal of Vision,* 13**,** 16-16.

PAYNE, B. R.; LOMBER, S. G.; VILLA, A. E. and BULLIER, J. 1996. Reversible deactivation of cerebral network components. *Trends in Neurosciences,* 19**,** 535-542.

PELLI, D. G. 1981. *Effects of Visual Noise.* PhD, Cambridge University.

PELLI, D. G. 1997. The VideoToolbox software for visual psychophysics: transforming numbers into movies. *Spatial Vision,* 10**,** 437-442.

PELLI, D. G. and FARELL, B. 1999. Why use noise? *Journal of the Optical Society of America. A, Optics, image science, and vision,* 16**,** 647-653.

PELLI, D. G.; LEVI, D. M. and CHUNG, S. T. 2004. Using visual noise to characterize amblyopic letter identification. *Journal of Vision,* 4**,** 904-920.

PELLICANO, E. and GIBSON, L. Y. 2008. Investigating the functional integrity of the dorsal visual pathway in autism and dyslexia. *Neuropsychologia,* 46**,** 2593-2596.

PHILLIPS, G. C. and WILSON, H. R. 1984. Orientation bandwidths of spatial mechanisms measured by masking. *Journal of the Optical Society of America A,* 1**,** 226-232.

PIANO, M. E. F. and O'CONNOR, A. R. 2013. The Effect of Degrading Binocular Single Vision on Fine Visuomotor Skill Task Performance. *Investigative Ophthalmology & Visual Science,* 54**,** 8204-8213.

PRIEBE, N. J.; LISBERGER, S. G. and MOVSHON, J. A. 2006. Tuning for Spatiotemporal Frequency and Speed in Directionally Selective Neurons of Macaque Striate Cortex. *The Journal of Neuroscience,* 26**,** 2941-2950.

QUINN, P. 2000. Perceptual reference points for form and orientation in young infants: Anchors or magnets? *Perception & Psychophysics,* 62**,** 1625-1633.

RADHAKRISHNAN, H. and PARDHAN, S. 2006. Contrast detection in noise with positive and negative defocus in myopes. *Vision Research,* 46**,** 2949-2955.

RAYMOND, J. E. and SORENSEN, R. E. 1998. Visual Motion Perception in Children with Dyslexia: Normal Detection but Abnormal Integration. *Visual Cognition,* 5**,** 389-404.

RISLOVE, E. M.; HALL, E. C.; STAVROS, K. A. and KIORPES, L. 2010. Scale-dependent loss of global form perception in strabismic amblyopia. *Journal of Vision,* 10**,** 25-25.

RODMAN, H. R.; GROSS, C. G. and ALBRIGHT, T. D. 1989. Afferent basis of visual response properties in area MT of the macaque. I. Effects of striate cortex removal. *The Journal of Neuroscience,* 9**,** 2033-2050.

RODMAN, H. R.; GROSS, C. G. and ALBRIGHT, T. D. 1990. Afferent basis of visual response properties in area MT of the macaque. II. Effects of superior colliculus removal. *The Journal of Neuroscience,* 10**,** 1154-1164.

ROE, A. and TS'O, D. 1997. The Functional Architecture of Area V2 in the Macaque Monkey. *In:* ROCKLAND, K.; KAAS, J. and PETERS, A. (eds.) *Extrastriate Cortex in Primates.* Springer US.

ROSS, J. 2004. The perceived direction and speed of global motion in Glass pattern sequences. *Vision Research,* 44**,** 441-448.

ROSS, J.; BADCOCK, D. R. and HAYES, A. 2000. Coherent global motion in the absence of coherent velocity signals. *Current Biology,* 10**,** 679-682.

SALZMAN, C. D.; BRITTEN, K. H. and NEWSOME, W. T. 1990. Cortical microstimulation influences perceptual judgements of motion direction. *Nature,* 346**,** 174-177.

SCHEIN, S. J.; MARROCCO, R. T. and DE MONASTERIO, F. M. 1982. Is there a high concentration of color-selective cells in area V4 of monkey visual cortex? *Journal of Neurophysiology,* 47**,** 193-213.

SCHRÖDER, J.-H.; FRIES, P.; ROELFSEMA, P. R.; SINGER, W. and ENGEL, A. K. 2002. Ocular dominance in extrastriate cortex of strabismic amblyopic cats. *Vision Research,* 42**,** 29-39.

SECEN, J.; CULHAM, J.; HO, C. and GIASCHI, D. 2011. Neural correlates of the multiple-object tracking deficit in amblyopia. *Vision Research,* 51**,** 2517-2527.

SHARMA, V.; LEVI, D. M. and KLEIN, S. A. 2000. Undercounting features and missing features: evidence for a high-level deficit in strabismic amblyopia. *Nature Neuroscience,* 3**,** 496-501.

SHIPP, S. and ZEKI, S. 2002. The functional organization of area V2, I: Specialization across stripes and layers. *Visual Neuroscience,* 19**,** 187-210.

SHIRAI, N.; KANAZAWA, S. and YAMAGUCHI, M. K. 2008. Early development of sensitivity to radial motion at different speeds. *Experimental Brain Research,* 185**,** 461-467.

SIEGEL, R. M. and READ, H. L. 1997. Analysis of optic flow in the monkey parietal area 7a. *Cerebral Cortex,* 7**,** 327-346.

SIMMERS, A. J. and BEX, P. J. 2004. The representation of global spatial structure in amblyopia. *Vision Research,* 44**,** 523-533.

SIMMERS, A. J.; LEDGEWAY, T. and HESS, R. F. 2005. The influences of visibility and anomalous integration processes on the perception of global spatial form versus motion in human amblyopia. *Vision Research,* 45**,** 449-460.

SIMMERS, A. J.; LEDGEWAY, T.; HESS, R. F. and MCGRAW, P. V. 2003a. Deficits to global motion processing in human amblyopia. *Vision Res,* 43**,** 729-738.

SIMMERS, A. J.; LEDGEWAY, T.; HESS, R. F. and MCGRAW, P. V. 2003b. Deficits to global motion processing in human amblyopia. *Vision Research,* 43**,** 729-738.

SIMMERS, A. J.; LEDGEWAY, T.; MANSOURI, B.; HUTCHINSON, C. V. and HESS, R. F. 2006a. The extent of the dorsal extra-striate deficit in amblyopia. *Vision Res,* 46**,** 2571-2580.

SIMMERS, A. J.; LEDGEWAY, T.; MANSOURI, B.; HUTCHINSON, C. V. and HESS, R. F. 2006b. The extent of the dorsal extra-striate deficit in amblyopia. *Vision Research,* 46**,** 2571-2580.

SINCICH, L. C. and HORTON, J. C. 2005. The circuitry of V1 and V2: integration of color, form, and motion. *Annual Review of Neuroscience,* 28**,** 303-326.

SKOTTUN, B. C.; BRADLEY, A. and FREEMAN, R. D. 1986. Orientation discrimination in amblyopia. *Investigative Ophthalmology & Visual Science,* 27**,** 532-537.

SKOTTUN, B. C. and SKOYLES, J. R. 2008. Coherent motion, magnocellular sensitivity and the causation of dyslexia. *International Journal of Neuroscience,* 118**,** 185-190.

SLAGHUIS, W. L. and RYAN, J. F. 2006. Directional motion contrast sensitivity in developmental dyslexia. *Vision Research,* 46**,** 3291-3303.

SLOAN, L. L. 1959. New test Charts for the Measurement of Visual Acuity at far and Near Distances. *American Journal of Ophthalmology,* 48**,** 807-813.

SMITH, A. T.; GREENLEE, M. W.; SINGH, K. D.; KRAEMER, F. M. and HENNIG, J. 1998. The processing of first- and second-order motion in human visual cortex assessed by functional magnetic resonance imaging (fMRI). *The Journal of Neuroscience,* 18**,** 3816-3830.

SMITH, A. T.; WALL, M. B.; WILLIAMS, A. L. and SINGH, K. D. 2006. Sensitivity to optic flow in human cortical areas MT and MST. *European Journal of Neuroscience,* 23**,** 561-569.

SMITH, M. A.; BAIR, W. and MOVSHON, J. A. 2002. Signals in Macaque Striate Cortical Neurons that Support the Perception of Glass Patterns. *The Journal of Neuroscience,* 22**,** 8334-8345.

SMITH, M. A.; KOHN, A. and MOVSHON, J. A. 2007. Glass pattern responses in macaque V2 neurons. *Journal of Vision,* 7**,** 5-5.

SNOWDEN, R. J.; TREUE, S. and ANDERSEN, R. A. 1992. The response of neurons in areas V1 and MT of the alert rhesus monkey to moving random dot patterns. *Experimental Brain Research,* 88**,** 389-400.

SNYDER, L. H.; BATISTA, A. P. and ANDERSEN, R. A. 1997. Coding of intention in the posterior parietal cortex. *Nature,* 386**,** 167-170.

SPENCER, J.; O'BRIEN, J.; RIGGS, K.; BRADDICK, O.; ATKINSON, J. and WATTAM-BELL, J. 2000. Motion processing in autism: evidence for a dorsal stream deficiency. *Neuroreport,* 11**,** 2765-2767.

SPENCER, J. V. and O'BRIEN, J. M. 2006. Visual form-processing deficits in autism. *Perception,* 35**,** 1047-1055.

SPERLING, A. J.; LU, Z. L.; MANIS, F. R. and SEIDENBERG, M. S. 2005. Deficits in perceptual noise exclusion in developmental dyslexia. *Nature Neuroscience,* 8**,** 862-863.

SPERLING, A. J.; LU, Z. L.; MANIS, F. R. and SEIDENBERG, M. S. 2006. Motion-perception deficits and reading impairment: it's the noise, not the motion. *Psychological Science,* 17**,** 1047-1053.

SUBRAMANIAN, V.; MORALE, S. E.; WANG, Y.-Z. and BIRCH, E. E. 2012. Abnormal Radial Deformation Hyperacuity in Children with Strabismic Amblyopia. *Investigative Ophthalmology & Visual Science,* 53**,** 3303-3308.

TABACHNICK, B. G. and FIDELL, L. S. 2001. *Using Multivariate Statistics*, Allyn and Bacon.

TANAKA, K. 1993. Neuronal mechanisms of object recognition. *Science,* 262**,** 685-688.

TANG, M. F.; DICKINSON, J. E.; VISSER, T. A. W. and BADCOCK, D. R. 2015. The broad orientation dependence of the motion streak aftereffect reveals interactions between form and motion neurons. *Journal of Vision,* 15**,** 4-4.

TANIGAWA, H.; LU, H. D. and ROE, A. W. 2010. Functional organization for color and orientation in macaque V4. *Nature Neuroscience,* 13**,** 1542-1548.

TELLER, D. Y. 1984. Linking propositions. *Vision Research,* 24**,** 1233-1246.

THOMPSON, B.; AAEN-STOCKDALE, C. R.; MANSOURI, B. and HESS, R. F. 2008a. Plaid perception is only subtly impaired in strabismic amblyopia. *Vision Research,* 48**,** 1307-1314.

THOMPSON, B.; RICHARD, A.; CHURAN, J.; HESS, R. F.; AAEN-STOCKDALE, C. and PACK, C. C. 2011. Impaired spatial and binocular summation for motion direction discrimination in strabismic amblyopia. *Vision Research,* 51**,** 577-584.

THOMPSON, B.; TROJE, N. F.; HANSEN, B. C. and HESS, R. F. 2008b. Amblyopic perception of biological motion. *Journal of Vision,* 8**,** 22-22.

THOMPSON, B.; VILLENEUVE, M. Y.; CASANOVA, C. and HESS, R. F. 2012. Abnormal cortical processing of pattern motion in amblyopia: Evidence from fMRI. *NeuroImage,* 60**,** 1307-1315.

TIBBER, M. S.; KELLY, M. G.; JANSARI, A.; DAKIN, S. C. and SHEPHERD, A. J. 2014. An Inability to Exclude Visual Noise in Migraine. *Investigative Ophthalmology & Visual Science,* 55**,** 2539-2546.

TOHYAMA, K. and FUKUSHIMA, K. 2005. Neural network model for extracting optic flow. *Neural Networks,* 18**,** 549-556.

TREUTWEIN, B. and STRASBURGER, H. 1999. Fitting the psychometric function. *Perception & Psychophysics,* 61**,** 87-106.

TS'O, D. Y.; ROE, A. W. and GILBERT, C. D. 2001. A hierarchy of the functional organization for color, form and disparity in primate visual area V2. *Vision Research,* 41**,** 1333-1349.

TSE, P. U.; SMITH, M. A.; AUGATH, M.; TRINATH, T.; LOGOTHETIS, N. K. and MOVSHON, J. A. 2002. Using Glass Patterns and fMRI to identify areas that process global form in macaque visual cortex. *Journal of Vision,* 2**,** 285.

TSERMENTSELI, S.; O'BRIEN, J. and SPENCER, J. 2008. Comparison of Form and Motion Coherence Processing in Autistic Spectrum Disorders and Dyslexia. *Journal of Autism and Developmental Disorders,* 38**,** 1201-1210.

UNGERLEIDER, L. G. and MISHKIN, M. 1982. Two Cortical Visual Systems. *In:* INGLE, D. J.; GOODALE, M. and MANSFIELD, R. J. W. (eds.) *Analysis of Visual Behaviour.*

URBANSKI, M.; COUBARD, O. A. and BOURLON, C. 2014. Visualizing the blind brain: brain imaging of visual field defects from early recovery to rehabilitation techniques. *Frontiers in Integrative Neuroscience,* 8**,** 74.

VAN BOXTEL, J. J. and ERKELENS, C. J. 2006. A single motion system suffices for global-motion perception. *Vision Research,* 46**,** 4634-4645.

VOGELS, R. and ORBAN, G. A. 1991. Quantitative study of striate single unit responses in monkeys performing an orientation discrimination task. *Experimental Brain Research,* 84**,** 1-11.

VON DER HEYDT, R.; PETERHANS, E. and BAUMGARTNER, G. 1984. Illusory contours and cortical neuron responses. *Science,* 224**,** 1260-1262.

VUL, E.; BERGSMA, J. and MACLEOD, D. 2010. Functional Adaptive Sequential Testing. *Seeing and Perceiving,* 23**,** 483-515.

WAGNER, D.; MANAHILOV, V.; LOFFLER, G.; GORDON, G. E. and DUTTON, G. N. 2010. Visual noise selectively degrades vision in migraine. *Investigative Ophthalmology & Visual Science,* 51**,** 2294-2299.

WALLACE, D. K.; LAZAR, E. L.; MELIA, M.; BIRCH, E. E.; HOLMES, J. M.; HOPKINS, K. B.; KRAKER, R. T.; KULP, M. T.; PANG, Y.; REPKA, M. X.; TAMKINS, S. M. and WEISE, K. K. 2011. Stereoacuity in children with anisometropic amblyopia. *Journal of American Association for Pediatric Ophthalmology and Strabismus,* 15**,** 455-461.

WANG, H.; LEVI, D. M. and KLEIN, S. A. 1998. Spatial uncertainty and sampling efficiency in amblyopic position acuity. *Vision Research,* 38**,** 1239-1251.

WARDLE, S. G.; BEX, P. J.; CASS, J. and ALAIS, D. 2012. Stereoacuity in the periphery is limited by internal noise. *Journal of Vision,* 12**,** 12.

WATAMANIUK, S. N. and HEINEN, S. J. 1999. Human smooth pursuit direction discrimination. *Vision Research,* 39**,** 59-70.

WATAMANIUK, S. N. and SEKULER, R. 1992. Temporal and spatial integration in dynamic random-dot stimuli. *Vision Research,* 32**,** 2341-2347.

WATAMANIUK, S. N. J. 1993. Ideal observer for discrimination of the global direction of dynamic random-dot stimuli. *Journal of the Optical Society of America A,* 10**,** 16-28.

WELBERG, L. 2013. Visual processing: Area V4 in motion. *Nature Reviews Neuroscience,* 14**,** 379-379.

WERNER, J. S. and CHALUPA, L. M. 2004. *The Visual Neurosciences*, MIT Press.

WETHERILL, G. B. and LEVITT, H. 1965. Sequential estimation of points on a psychometric function. *British Journal of Mathematical and Statistical Psychology,* 18**,** 1-10.

WICHMANN, F. A. and HILL, N. J. 2001. The psychometric function: I. Fitting, sampling, and goodness of fit. *Perception & Psychophysics,* 63**,** 1293-1313.

WIESEL, T. N. and HUBEL, D. H. 1963a. Single-Cell response in striate cortex of kittens deprived of vision in one eye. *Journal of Neurophysiology,* 26**,** 1003-1017.

WIESEL, T. N. and HUBEL, D. H. 1963b. SINGLE-CELL RESPONSES IN STRIATE CORTEX OF KITTENS DEPRIVED OF VISION IN ONE EYE. *Journal of Neurophysiology,* 26**,** 1003-1017.

WIESEL, T. N. and HUBEL, D. H. 1965. Extent of recovery from the effects of visual deprivation in kittens. *Journal of Neurophysiology,* 28**,** 1060-1072.

WILKINSON, F.; JAMES, T. W.; WILSON, H. R.; GATI, J. S.; MENON, R. S. and GOODALE, M. A. 2000. An fMRI study of the selective activation of human extrastriate form vision areas by radial and concentric gratings. *Current Biology,* 10**,** 1455-1458.

WILKINSON, F. and WILSON, H. R. 1998. Detection of global structure in Glass patterns: implications for form vision. *Vision Research,* 38**,** 2933-2947.

WILKINSON, F.; WILSON, H. R. and HABAK, C. 1998. Detection and recognition of radial frequency patterns. *Vision Research,* 38**,** 3555-3568.

WILLIAMS, M. J.; STUART, G. W.; CASTLES, A. and MCANALLY, K. I. 2003. Contrast sensitivity in subgroups of developmental dyslexia. *Vision Research,* 43**,** 467-477.

WILSON, H. R. 1991. Model of peripheral and amblyopic hyperacuity. *Vision Research,* 31**,** 967-982.

WILSON, H. R. and WILKINSON, F. 1998. Detection of global structure in Glass patterns: implications for form vision. *Vision Research,* 38**,** 2933-2947.

WILSON, H. R. and WILKINSON, F. 2003. Further evidence for global orientation processing in circular Glass patterns. *Vision Research,* 43**,** 563-564; author reply 565-566.

WILSON, H. R.; WILKINSON, F. and ASAAD, W. 1997. Concentric orientation summation in human form vision. *Vision Research,* 37**,** 2325-2330.

WILSON, J. A.; SWITKES, E. and DE VALOIS, R. L. 2004. Glass pattern studies of local and global processing of contrast variations. *Vision Research,* 44**,** 2629-2641.

WUERGER, S.; SHAPLEY, R. and RUBIN, N. 1996. On the visually perceived direction of motion by Hans Wallach: 60 years later. *PERCEPTION-LONDON-,* 25**,** 1317-1368.

YOUNG, M. P. 1992. Objective analysis of the topological organization of the primate cortical visual system. *Nature,* 358**,** 152-155.

ZEKI, S. 2015. Area V5 - A Microcosm of the visual brain. *Frontiers in Integrative Neuroscience,* 9.

ZIHL, J. and HEYWOOD, C. 2015. The contribution of LM to the neuroscience of movements vision. *Frontiers in Integrative Neuroscience,* 9.

ZIHL, J.; VON CRAMON, D. and MAI, N. 1983. Selective disturbance of movement vision after bilateral brain damage. *Brain,* 106 (Pt 2)**,** 313-340.